

Automatic Face Recognition from Video

Images removed to fit arXive's size requirements

For complete version see

https://www.researchgate.net/profile/Ognjen_Arandjelovic/

Ognjen Arandjelović

Trinity College



This dissertation is submitted for
the degree of Doctor of Philosophy

Abstract

The objective of this work is to automatically recognize faces from video sequences in a realistic, unconstrained setup in which illumination conditions are extreme and greatly changing, viewpoint and user motion pattern have a wide variability, and video input is of low quality. At the centre of focus are face appearance manifolds: this thesis presents a significant advance of their understanding and application in the sphere of face recognition. The two main contributions are the *Generic Shape-Illumination Manifold* recognition algorithm and the *Anisotropic Manifold Space* clustering.

The *Generic Shape-Illumination Manifold* algorithm shows how video sequences of unconstrained head motion can be reliably compared in the presence of greatly changing imaging conditions. Our approach consists of combining *a priori* domain-specific knowledge in the form of a photometric model of image formation, with a statistical model of generic face appearance variation. One of the key ideas is the *reillumination* algorithm which takes two sequences of faces and produces a third, synthetic one, that contains the same poses as the first in the illumination of the second.

The *Anisotropic Manifold Space* clustering algorithm is proposed to automatically determine the cast of a feature-length film, without any dataset-specific training information. The method is based on modelling coherence of dissimilarities between appearance manifolds: it is shown how inter- and intra-personal similarities can be exploited by mapping each manifold into a single point in the *manifold space*. This concept allows for a useful interpretation of classical clustering approaches, which highlights their limitations. A superior method is proposed that uses a mixture-based generative model to hierarchically grow class boundaries corresponding to different individuals.

The *Generic Shape-Illumination Manifold* is evaluated on a large data corpus acquired in real-world conditions and its performance is shown to greatly exceed that of state-of-the-art methods in the literature and the best performing commercial software. Empirical evaluation of the *Anisotropic Manifold Space* clustering on a popular situation comedy is also described with excellent preliminary results.

Contents

I Preliminaries	21
1 Introduction	23
1.1 Problem statement	25
1.2 Applications	25
1.3 A case for face recognition from video	27
1.4 Basic premises and synopsis	28
1.4.1 List of publications	29
2 Background	33
2.1 Introduction	35
2.2 Face detection	35
2.3 Face recognition	38
2.3.1 Statistical, appearance-based methods	39
2.3.2 Model-based methods	45
2.3.3 Image set and video-based methods.	48
2.3.4 Summary.	49
2.4 Performance evaluation	50
2.4.1 Data	51
2.5 Summary and conclusions	52
II Access Control	59
3 Manifold Density Divergence	61
3.1 Introduction	63
3.2 Modelling face manifold densities	64
3.2.1 Manifold density model	64

3.2.2	Kullback-Leibler divergence	66
3.2.3	Gaussian mixture models	66
3.2.4	Estimating KL divergence	67
3.3	Empirical evaluation	69
3.3.1	Results	70
3.4	Summary and conclusions	71
4	Unfolding Face Manifolds	73
4.1	Dissimilarity between manifolds	75
4.1.1	Resistor-Average distance.	75
4.2	Estimating RAD for nonlinear densities	78
4.3	Kernel PCA	78
4.4	Combining RAD and kernel PCA	79
4.5	Synthetically repopulating manifolds	80
4.5.1	Outlier rejection	81
4.6	Empirical evaluation	82
4.6.1	Results	84
4.7	Summary and conclusions	86
5	Fusing Visual and Thermal Face Biometrics	89
5.1	Face recognition in the thermal spectrum	91
5.1.1	Multi-sensor based techniques	92
5.2	Method details	93
5.2.1	Matching image sets	93
5.2.2	Data preprocessing & feature extraction	95
5.2.3	Single modality-based recognition	96
5.2.4	Fusing modalities	97
5.2.5	Prescription glasses	99
5.3	Empirical evaluation	100
5.3.1	Results	100
5.4	Summary and conclusions	101
6	Illumination Invariance using Image Filters	113
6.1	Adapting to data acquisition conditions	115
6.1.1	Adaptive framework	117
6.2	Empirical evaluation	121
6.2.1	Results	123

6.2.2	Failure modes	123
6.3	Summary and conclusions	125
7	Boosted Manifold Principal Angles	127
7.1	Manifold illumination invariants	129
7.2	Boosted principal angles	131
7.3	Nonlinear subspaces	134
7.4	Empirical evaluation	135
7.4.1	BoMPA implementation	136
7.4.2	Results	136
7.5	Summary and conclusions	139
8	Pose-Wise Linear Illumination Manifold Model	141
8.1	Overview	143
8.2	Face registration	143
8.3	Pose-invariant recognition	145
8.3.1	Defining pose clusters	146
8.3.2	Finding pose clusters	146
8.4	Illumination-invariant recognition	148
8.4.1	Gamma intensity correction	148
8.4.2	Pose-specific illumination subspace normalization	150
8.5	Comparing normalized pose clusters	156
8.6	Empirical evaluation	159
8.6.1	Results	161
8.7	Summary and conclusions	164
9	Generic Shape-Illumination Manifold	165
9.1	Synthetic reillumination of face motion manifolds	167
9.1.1	Stage 1: pose matching	168
9.1.2	Stage 2: fine reillumination	172
9.2	The shape-illumination manifold	172
9.2.1	Offline stage: learning the generic SIM (gSIM)	175
9.3	Novel sequence classification	176
9.4	Empirical evaluation	177
9.4.1	Results	180
9.5	Summary and conclusions	186

III	Multimedia Organization and Retrieval	189
10	Film Character Retrieval	191
10.1	Introduction	193
10.1.1	Previous work	194
10.2	Method details	195
10.2.1	Facial feature detection	196
10.2.2	Registration	200
10.2.3	Background removal	202
10.2.4	Compensating for changes in illumination	204
10.2.5	Comparing signature images	205
10.3	Empirical evaluation	207
10.3.1	Evaluation methodology	207
10.3.2	Results	207
10.4	Summary and conclusions	208
11	Automatic Cast Listing in Films	213
11.1	Introduction	215
11.2	Method details	216
11.2.1	Automatic data acquisition	216
11.2.2	Appearance manifold discrimination	219
11.2.3	The manifold space	223
11.3	Empirical evaluation	226
11.3.1	Results	227
11.4	Summary and conclusions	228
IV	Conclusions, Appendices and Bibliography	233
12	Conclusion	235
12.1	Contributions	237
12.2	Future work	239
A	Incremental Learning of Temporally-Coherent GMMs	243
A.1	Introduction	245
A.1.1	Related previous work	246
A.2	Incremental GMM estimation	247
A.2.1	Temporally-coherent GMMs	247

A.2.2	Method overview	247
A.2.3	GMM update for fixed complexity	248
A.2.4	Model splitting	250
A.2.5	Component merging	251
A.3	Empirical evaluation	253
A.4	Summary and conclusions	254
B	Maximally Probable Mutual Modes	259
B.1	Introduction	261
B.1.1	Maximally probably mutual modes	261
B.1.2	Numerical and implementation issues	264
B.2	Experimental evaluation	265
B.3	Summary and conclusions	265
C	The <i>CamFace</i> data set	267
C.1	Description	269
C.2	Automatic extraction of faces	271

List of Figures

1.1	Effects of imaging conditions.	26
1.2	Security applications.	26
1.3	Content-based data organization applications.	27
1.4	Face recognition revenues.	28
2.1	Face recognition system components.	35
2.2	Face detection example.	36
2.3	Neural network face detection.	37
2.4	Eigenfaces and PCA.	40
2.5	Fisherfaces and LDA.	42
2.6	Bottleneck neural network.	42
2.7	Elastic Graph Matching.	44
2.8	Gabor wavelets.	44
2.9	Lambertian reflectance.	46
2.10	Spatial frequency-based generative model.	53
2.11	AAM mesh fitting.	54
2.12	3D Morphable Model	54
2.13	Summary of face recognition approaches.	55
2.14	Matching paradigms.	55
2.15	Receiver-Operator Characteristic curve.	56
2.16	Frames from our video databases.	57
2.17	Illuminations in <i>CamFace</i> and <i>ToshFace</i> data sets	58
3.1	Appearance manifolds.	65
3.2	GMM description lengths.	66
3.3	Training and test manifold models.	68
3.4	Appearance variations captured by the manifold model.	68
3.5	Training data and the manifold model in 3PC space.	69

4.1	KL divergence asymmetry and RAD.	76
4.2	Example appearance manifolds.	77
4.3	Nonlinear manifold unfolding.	80
4.4	Stochastic manifold repopulation.	82
4.5	False positive face detections.	82
4.6	RANSAC KPCA algorithm.	83
4.7	Robust Kernel RAD algorithm.	84
4.8	Dimensionality reduction by nonlinear unfolding.	85
4.9	ROC curves and recognition difficulties.	87
5.1	System overview.	94
5.2	Principal vectors between linear subspaces.	105
5.3	Facial feature localization and registration.	106
5.4	Performance changes with filtering in visual and thermal spectra.	106
5.5	Filtered examples in visual and thermal spectra.	106
5.6	Local features.	107
5.7	Learnt weighting function for modality fusion.	107
5.8	Optimal fusion algorithm.	108
5.9	Glasses detection: training data.	108
5.10	Prescription glasses detector response.	109
5.11	Data set examples.	110
5.12	Number of training images across the data set.	110
5.13	ROC curves: local features	111
5.14	ROC curves: holistic representations	111
6.1	Image filtering paradox.	116
6.2	Filtering effects on signal energy distribution.	116
6.3	Class separation with simple decision-level fusion.	117
6.4	Fusion algorithm.	119
6.5	Iterative density estimate.	120
6.6	Learning the α -function.	121
6.7	Evaluated filters.	122
6.8	Principal vectors using different filters.	124
6.9	Recognition results.	126
7.1	Manifold illumination invariant.	130
7.2	MSM, Boosted Principal Angles and BoMPA.	132
7.3	Weak classifier weights and performance improvement with boosting.	133

7.4	Finding stable tangent planes.	135
7.5	ROC curves.	138
8.1	Affine-registered faces – manifold and poses.	144
8.2	Face registration and cropping.	145
8.3	Motion parallax.	147
8.4	Distributions of faces across pose clusters.	148
8.5	Two-stage illumination normalization algorithm.	149
8.6	Region-based gamma intensity correction.	151
8.7	Seamless vs. smoothed region-based GIC.	152
8.8	Pose-specific illumination subspaces.	153
8.9	Illumination normalization effects in the image space.	156
8.10	Learnt pose-specific likelihood ratios.	160
8.11	Joint likelihood ratio.	161
8.12	Separation of intra- and inter-personal manifold distances.	162
9.1	Appearance and albedo-free appearance manifolds.	168
9.2	Pose matching.	169
9.3	Sequence reillumination example.	169
9.4	Pose matching as genetic algorithm-based optimization.	171
9.5	Appearance and pose-signature manifold structures.	173
9.6	Computing fine reillumination coefficients.	173
9.7	Generic SIM: example of learnt illumination effects.	176
9.8	Inter-personal “reillumination” results.	178
9.9	Robust likelihood.	178
9.10	Generic SIM model learning algorithm.	179
9.11	Recognition algorithm based on the learnt Generic SIM model.	179
9.12	Face representations used in evaluation.	181
9.13	Generic SIM ROC curves.	182
9.14	Failure modes.	184
9.15	Theoretical and measured computational demands.	185
10.1	Faces in films.	194
10.2	Appearance variations in films.	195
10.3	Proposed face matching algorithm.	196
10.4	Signature image cascade.	197
10.5	Appearance context importance for feature detection.	198
10.6	SVM training data.	198

10.7	Fast, coarse-to-fine SVM-based feature detection.	199
10.8	Feature detection examples.	200
10.9	Coarse feature-based face registration and false positive detection removal.	201
10.10	Affine registration examples.	202
10.11	Markov chain-based face outline fitting.	203
10.12	Background removal stages.	204
10.13	Background clutter removal example.	204
10.14	Appearance-based pose refinement.	206
10.15	“Fawlty Towers” ROC curves.	209
10.16	“Fawlty Towers” rank ordering scores.	210
10.17	“Pretty Woman” data set.	210
10.18	“Fawlty Towers” data set.	210
10.19	“Groundhog Day” data set.	211
11.1	Sources and extent of appearance variations in “Yes, Minister” data set.	216
11.2	Cast clustering algorithm overview.	217
11.3	Edge Change Ratio response.	218
11.4	Connecting face detections with tracks.	218
11.5	Typical face track.	219
11.6	Data-specific discrimination algorithm summary.	220
11.7	Illumination normalization and background suppression.	221
11.8	PCA, LDA and Constraint subspaces.	222
11.9	MSM ROC, estimated offline.	224
11.10	Distributions of appearance manifolds in the “manifold space”.	225
11.11	Distance threshold-based clustering: manifold space interpretation.	225
11.12	“Yes, Minister” data set.	227
11.13	Isotropic clustering results.	229
11.14	Anisotropic manifold space clustering results.	230
11.15	Examples of “Sir Humphrey” cluster tracks.	231
12.1	Thesis contributions.	238
A.1	Temporally-coherent GMMs.	248
A.2	Incremental TC-GMM algorithm.	249
A.3	Fixed complexity update.	249
A.4	Dynamic model order selection.	252
A.5	Evaluation: synthetic data.	255
A.5	Evaluation: synthetic data.	256

A.6	Evaluation: face motion data.	257
B.1	Piece-wise manifolds.	261
B.2	Maximally Probable Mutual Mode illustration.	263
B.3	Example face sequences.	263
B.4	Maximally probable mutual mode as image.	264
B.5	MPMM Receiver-Operator Characteristics curve.	265
C.1	<i>CamFace</i> ages distribution.	269
C.2	<i>CamFace</i> illuminations	270
C.3	<i>CamFace</i> acquisition setup.	270
C.4	Typical <i>CamFace</i> sequence.	271
C.5	Face preprocessing pipeline.	272
C.6	Typical <i>CamFace</i> detections.	272
C.7	Number of face detections across the <i>CamFace</i> data set.	273
C.8	False positive face detections.	273
C.9	Face “frontality” measure.	274
C.10	Face and background colour models.	275
C.11	Preprocessing cascade.	276

List of Tables

2.1	Detection approaches overview.	36
2.2	State-of-the-art detection performance.	38
2.3	Recognition approaches overview.	39
2.4	Appearance and model-based approach comparison.	49
3.1	Recognition results.	70
4.1	Recognition results.	86
5.1	Recognition results summary.	102
5.2	Verification results summary.	102
5.3	Verification results: local features.	103
5.4	Verification results: hybrid representations.	103
5.5	Verification results: glasses detection.	103
7.1	Recognition results.	137
8.1	Recognition results.	161
8.2	Discriminative power of different poses.	163
8.3	Comparison with algorithms in the literature.	163
9.1	Recognition results.	182
B.1	MPMM and MSM evaluation results.	265
C.1	<i>CamFace</i> gender distribution.	269
C.2	<i>CamFace</i> statistics.	271

I

Preliminaries

1

Introduction



Michelangelo. *Genesis*
1509-1512, Fresco
Sistine Chapel, Vatican

This chapter sets up the main premises of the thesis. We start by defining the problem of automatic face recognition and explain why this is an extremely challenging task, followed by an overview of its practical significance. An argument for the advantages of face recognition, in the context of other biometrics, is presented. Finally, the main assumptions and claims of the thesis are stated, followed by a synopsis of the remaining chapters.

1.1 Problem statement

This thesis addresses the problem of automatic face recognition from video in realistic imaging conditions. While in some previous work the term “face recognition” has been used for any face-based biometric identification, we will operationally define face recognition as classification of persons by their identity using images acquired in the visible electromagnetic spectrum.

Humans seemingly effortlessly recognize faces on a daily basis, yet the same task has so far proved to be of formidable difficulty to automatic methods [Bri04, Bos02, Cha03, Zha04]. A number of factors other than one’s identity influence the way an imaged face appears. Lighting conditions, and especially light angle, can drastically change the appearance of a face. Facial expressions, including closed or partially closed eyes, also complicate the problem, just as head pose and scale changes do. Background clutter and partial occlusions, be they artifacts in front of the face (such as glasses), or resulting from hair style change, growing a beard or a moustache all pose problems to automatic methods. Invariance to the aforementioned factors is a major research challenge, see Figure 1.1.

1.2 Applications

The most popularized use of automatic face recognition is in a broad range of security applications. These can be typically categorized under either (i) voluntary authentication, such as for the purpose of accessing a building or a computer system, or for passport control, or (ii) surveillance, for example for identifying known criminals at airports or offenders from CCTV footage, see Figure 1.2.

In addition to its security uses, the rapid technological development we are experiencing has created a range of novel promising applications for face recognition. Mobile devices, such as PDAs and mobile phones with cameras, together with freely available software for video-conferencing over the Internet, are examples of technologies that manufacturers are trying to make “aware” of their environment for the purpose of easier, more intuitive interaction with the human user. Cheap and readily available imaging devices, such as

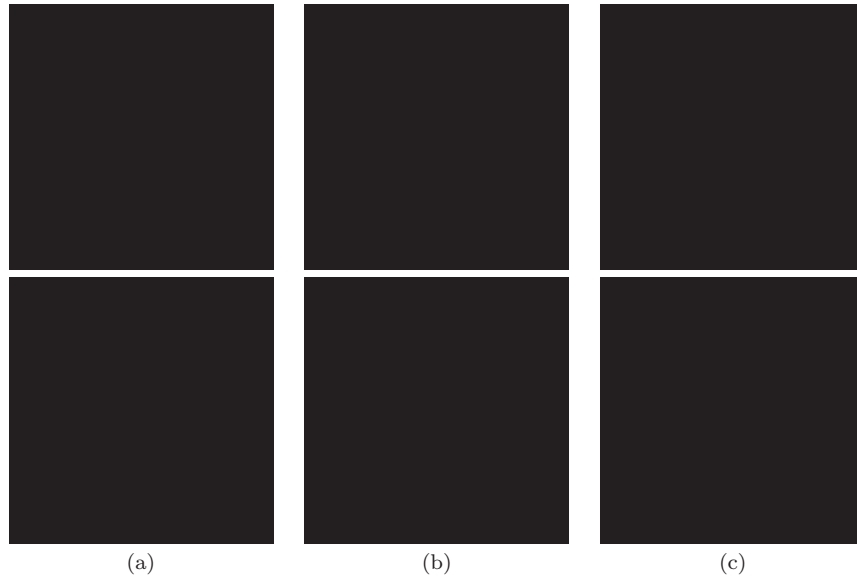


Figure 1.1: *The effects of imaging conditions – illumination (a), pose (b) and expression (c) – on the appearance of a face are dramatic and present the main difficulty to automatic face recognition methods.*



Figure 1.2: *The two most common paradigms for security applications of automatic face recognition are (a) authentication and (b) surveillance. It is important to note the drastically different data acquisition conditions. In the authentication setup, the imaging conditions are typically milder, more control over the illumination setup can be exercised and the user can be asked to cooperate to a degree, for example by performing head motion. In surveillance environment, the viewpoint and illumination are largely uncontrolled and often extreme, face scale can have a large range and image quality is poor.*



Figure 1.3: *Data organization applications of face recognition are rapidly gaining in importance. Automatic organization and retrieval of (a) amateur photographs or (b) video collections are some of the examples. Face recognition is in both cases extremely difficult, with large and uncontrolled variations in pose, illumination and expression, further complicated by image clutter and frequent partial occlusions of faces.*

cameras and camcorders, and storage equipment (such as DVDs, flash memory and HDDs) have also created a problem in organizing large volumes of visual data. Given that humans (and faces) are often at the centre of interest in images and videos, face recognition can be employed for content-based retrieval and organization, or even synthesis of imagery, see Figure 1.3.

The increasing commercial interest in face recognition technology is well witnessed by the trend of the relevant market revenues, as shown in Figure 1.4.

1.3 A case for face recognition from video

Over the years, a great number of biometrics have been proposed and found their use for the task of human identification. Examples are fingerprint [Jai97, Mal03], iris [Dau92, Wil94] or retinal scan-based methods. Some of these have achieved impressively high identification rates [Gra03] (e.g. retinal scan $\sim 10^{-7}$ error rate [Nat]).

However, face recognition has a few distinct advantages. In many cases, face information may be the only cue available, such as in the increasingly important content-based multimedia retrieval applications [Ara06a, Ara05c, Ara06i, Le06, Siv03]. In others, such as in some surveillance environments, bad imaging conditions render any single cue insufficient and a fusion of several may be needed (e.g. see [Bru95a, Bru95b, Sin04]). Even for access-control applications, when more reliable cues are available [Nat], face recognition has the attractive property of being very intuitive to humans as well as non-invasive, making it readily acceptable by wider audiences. Finally, face recognition does not require user cooperation.



Figure 1.4: *Total face recognition market revenues in the period 2002–2007 (\$m) [Int].*

Video. The nature of many practical applications is such that more than a single image of a face is available. In surveillance, for example, the face can be tracked to provide a temporal sequence of a moving face. For access-control use of face recognition the user may be assumed to be cooperative and hence be instructed to move in front of a fixed camera. This is important as a number of technical advantages of using video exist: person-specific dynamics can be learnt, or more effective face representations be obtained (e.g. super-resolution images or a 3D face model) than in the single-shot recognition setup. Regardless of the way in which multiple images of a face are acquired, this abundance of information can be used to achieve greater robustness of face recognition by resolving some of the inherent ambiguities (shape, texture, illumination etc.) of single-shot recognition.

1.4 Basic premises and synopsis

The first major premise of work in this thesis is:

Premise 1 *Neither purely discriminative nor purely generative approaches are very successful for face recognition in realistic imaging conditions.*

Hence, the development of an algorithm that in a principle manner combines (i) a generative model of well-understood stages of image formation with, (ii) data-driven machine learning, is one of our aims. Secondly:

Premise 2 *Face appearance manifolds provide a powerful way of representing video sequences (or sets) of faces and allow for a unified treatment of illumination, pose and face motion pattern changes.*

Thus, the structure of this work is as follows. In Chapter 2 we review the existing literature on face recognition and highlight the limitations of state-of-the-art methods, motivating the aforementioned premises. Chapter 3 introduces the notion of appearance manifolds and proposes a solution to the simplest formulation of the recognition problem addressed in this thesis. The subsequent chapters build up on this work, relaxing assumptions about the data from which recognition is performed, culminating with the *Generic Shape-Illumination* method in Chapter 9. The two chapters that follow apply the introduced concepts on the problem of face-driven content-based video retrieval and propose a novel framework for making further use of the available data. A summary of the thesis and its major conclusions are presented in Chapter 12.

1.4.1 List of publications

The following publications have directly resulted from the work described in this thesis:

Journal publications

1. O. Arandjelović and R. Cipolla. An information-theoretic approach to face recognition from face motion manifolds. *Image and Vision Computing (special issue on Face Processing in Video Sequences)*, 24(6):639–647, 2006.
2. M. Johnson, G. Brostow, J. Shotton, O. Arandjelović and R. Cipolla. Semantic photo synthesis. *Computer Graphics Forum*, 3(25):407–413, 2006.
3. O. Arandjelović and R. Cipolla. Incremental learning of temporally-coherent Gaussian mixture models. *Society of Manufacturing Engineers (SME) Technical Papers*, 2, 2006.
4. T-K. Kim, O. Arandjelović and R. Cipolla. Boosted manifold principal angles for image set-based recognition. *Pattern Recognition*, 40(9):pages 2475–2484, 2007.
5. O. Arandjelović and R. Cipolla. A pose-wise linear illumination manifold model for face recognition using video. *Computer Vision and Image Understanding*, 113(1):113–125, 2009.
6. O. Arandjelović and R. Cipolla. A methodology for rapid illumination-invariant face recognition using image processing filters. *Computer Vision and Image Understanding*, 113(2):159–171, 2009.

7. O. Arandjelović, R. Hammoud and R. Cipolla. Thermal and reflectance based personal identification methodology in challenging variable illuminations. *Pattern Recognition*, 43(5):1801–1813, 2010.
8. O. Arandjelović and R. Cipolla. Achieving robust face recognition from video by combining a weak photometric model and a learnt generic face invariant. *Pattern Recognition*, 46(1):9–23, January 2013.

Conference proceedings

1. O. Arandjelović and R. Cipolla. Face recognition from face motion manifolds using robust kernel resistor-average distance. In *Proc. IEEE Workshop on Face Processing in Video*, 5:88, 2004.
2. O. Arandjelović and R. Cipolla. An illumination invariant face recognition system for access control using video. In *Proc. British Machine Vision Conference*, pages 537–546, 2004.
3. O. Arandjelović, G. Shakhnarovich, J. Fisher, R. Cipolla, and T. Darrell. Face recognition with image sets using manifold density divergence. In *Proc. IEEE Conference on Computer Vision and Pattern Recognition*, 1:581–588, 2005.
4. O. Arandjelović and A. Zisserman. Automatic face recognition for film character retrieval in feature-length films. In *Proc. IEEE Conference on Computer Vision and Pattern Recognition*, 1:860–867, 2005.
5. T-K. Kim, O. Arandjelović and R. Cipolla. Learning over sets using boosted manifold principal angles (BoMPA). In *Proc. British Machine Vision Conference*, 2:779–788, 2005.
6. O. Arandjelović and R. Cipolla. Incremental learning of temporally-coherent Gaussian mixture models. In *Proc. British Machine Vision Conference*, 2:759–768, 2005.
7. O. Arandjelović and R. Cipolla. A new look at filtering techniques for illumination invariance in automatic face recognition. In *Proc. IEEE Conference on Automatic Face and Gesture Recognition*, pages 449–454, 2006.
8. O. Arandjelović and R. Cipolla. Face recognition from video using the generic shape-illumination manifold. In *Proc. European Conference on Computer Vision*, 4:27–40, 2006.
9. O. Arandjelović and R. Cipolla. Automatic cast listing in feature-length films with anisotropic manifold space. In *Proc. IEEE Conference on Computer Vision Pattern Recognition*, 2:1513–1520, 2006.

10. G. Brostow, M. Johnson, J. Shotton, O. Arandjelović and R. Cipolla. Semantic photo synthesis. In *Proc. Eurographics*, 2006.
11. O. Arandjelović, R. Hammoud and R. Cipolla. Multi-sensory face biometric fusion (for personal identification). In *Proc. IEEE Workshop on Object Tracking and Classification Beyond the Visible Spectrum*, pages 128–135, 2006.
12. O. Arandjelović and R. Cipolla. Face set classification using maximally probable mutual modes. In *Proc. IAPR International Conference on Pattern Recognition*, pages 511–514, 2006.
13. O. Arandjelović, R. Hammoud and R. Cipolla. On face recognition by fusing visual and thermal face biometrics. In *Proc. IEEE International Conference on Advanced Video and Signal Based Surveillance*, pages 50–56, 2006.

Book chapters

1. O. Arandjelović and A. Zisserman. On film character retrieval in feature-length films. Chapter in *Interactive video: Algorithms and Technologies*, Springer-Verlag, ISBN 978-3-540-33214-5, 2006.
2. O. Arandjelović, R. Hammoud and R. Cipolla. Towards person authentication by fusing visual and thermal face biometrics. Chapter in *Multi-Sensory Multi-Modal Face Biometrics for Personal Identification*, Springer-Verlag, ISBN 978-3-540-49344-0, 2007.
3. O. Arandjelović, R. Hammoud and R. Cipolla. A person authentication system based on visual and thermal face biometrics. Chapter in *Object Tracking and Classification Beyond the Visible Spectrum*, Springer-Verlag, ISBN 978-3-540-49344-0, 2007.
4. O. Arandjelović and R. Cipolla. Achieving Illumination Invariance using Image Chapter in *Face Recognition*, Advanced Robotic Systems, ISBN 978-3-902613-03-5, 2007.

2

Background



Paul Gauguin. *The Swineherd*
1888, Oil on canvas, 74 x 93 cm
Los Angeles County Museum of Art, Los Angeles



Figure 2.1: *The main stages of an automatic face recognition system. (i) A face detector is used to detect (localize in space and scale) faces in a cluttered scene; this is followed by (ii) extraction of features used to represent faces and, finally (iii) extracted features are compared to those stored in a training database to associate novel faces to known individuals.*

Important practical applications of automatic face recognition have made it a very popular research area of computer vision. This is evidenced by a vast number of face recognition algorithms developed over the last three decades and, in recent years, the emergence of a number of commercial face recognition systems. This chapter: (i) presents an account of the face detection and recognition literature, highlighting the limitations of the state-of-the-art, (ii) explains the performance measures used to gauge the effectiveness of the proposed algorithms, and (iii) describes the data sets on which algorithms in this thesis were evaluated.

2.1 Introduction

At the coarsest level, the task of automatic, or computer-based, face recognition inherently involves three stages: (i) detection/localization of faces in images, (ii) feature extraction and (iii) actual recognition, as shown in Figure 2.1. The focus of this thesis, and consequently the literature review, is on the last of the three tasks. However, it is important to understand the difficulties of the two preceding steps. Any inaccuracy injected in these stages impacts the data a system must deal with in the recognition stage. Additionally, the usefulness of the overall system in practice ultimately depends on the performance of the entire cascade. For this reason we first turn our attention to the face detection literature and review some of the most influential approaches.

2.2 Face detection

Unlike recognition which concerns itself with discrimination of objects in a category, the task of detection is that of discerning the entire category. Specifically, face detection deals with



Figure 2.2: An input image and the result using the popular Viola-Jones face detector [Vio04]. Detected faces are shown with green square bounding boxes, showing their location and scale. One missed detection (i.e. a false negative) is shown with a red bounding box. There are no false detections (i.e. false positives).

Table 2.1: An overview of face detection approaches.

	Face detection approaches				
Input data	Still images			Sequences	
Approach	Ensemble			Cascade	
Cues	Greyscale	Colour	Motion	Depth	Other
Representation	Holistic		Feature-based		Hybrid
Search	Greedy		Exhaustive		Focus of attention

the problem of determining the presence of and localizing faces in images. Much like face recognition, this is complicated by in-plane rotation of faces, occlusion, expression changes, pose (out-of-plane rotation) and illumination, see Figure 2.2.

Face detection technology is fairly mature and a number of reliable face detectors have been built. Here we summarize state-of-the-art approaches – for a higher level of detail the reader may find it useful to refer to a general purpose review [Hje01, Yan02c].

State-of-the-art methods. Most of the current state-of-the-art face detection methods are holistic in nature, as opposed to part-based. While part-based (also know as constellation of features) approaches were proposed for their advantage of exhibiting greater viewpoint robustness [Hei00], they have largely been abandoned for complex, cluttered scenes in favour of multiple view-specific detectors that treat the face as a whole. Henceforth this should be assumed when talking about holistic methods, unless otherwise stated. One such successful algorithm was proposed by Rowley *et al.* [Row98]. An input image is scanned at multiple



Figure 2.3: A diagram of the method of Rowley *et al.* [Row98]. This approach is representative of the group of neural network-based face detection approaches: (i) input image is scanned at different scales and locations, (ii) features are extracted from the current window and are (iii) fed into an MLP classifier.

scales with a neural network classifier which is fed filtered appearance of the current patch, see Figure 2.3. Sung and Poggio [Sun98] also employ a Multi-Layer Perceptron (MLP), but in a statistical framework, learning “face” and “non-face” appearances as Gaussian mixtures embedded in the 361-dimensional image space (19×19 pixels). Classification is then performed based on the “difference” vector between the appearance of the current patch and the learnt statistical models. Much like in [Row98], an exhaustive search over the location/scale space is performed. The method of Schneiderman and Kanade [Sch00] moves away from greyscale appearance, proposing to use histograms of wavelet coefficients instead. An extension to video sequence-based detections was proposed by Mikolajczyk *et al.* in [Mik01] – a dramatic reduction of the search space between consecutive frames was achieved by propagating temporal information using the Condensation tracking algorithm [Isa98].

While achieving good accuracy – see Table 2.2 – the described early approaches suffer from tremendous computational overhead. More recent methods have focused on online detector efficiency, with attention-based rather than exhaustive search over an entire image. The key observation is that the number of face patches in a typical image is usually much smaller than the number of non-faces. A hierarchical search that quickly eliminate many unpromising candidates was proposed in [Fer01]. Simplest and fastest filters are applied first, greatly reducing the workload of the subsequent, gradually slower and more complex classifiers. The same principle using support Vector Machines was employed by Romdhani *et al.* [Rom03a]. In [Fer01] Féraud *et al.* used a variety of cues including colour and motion-based filters. A cascaded approach was also employed in the breakthrough method of Viola and Jones [Vio04]. This detector, including a number of extensions proposed thereafter, is the fastest one currently available (the authors report a speedup of a factor of 15 over [Row98]). This is achieved by several means: (i) the attention cascade mentioned previously reduces

Table 2.2: A performance summary of state-of-the-art face detection algorithms. Shown is the % of detected faces (i.e. true positives), followed by a number of incorrect detections (i.e. false positives).

Method	Data set	
	CMU (130 images, 507 faces)	MIT (23 images, 57 faces)
Féraud <i>et al.</i> [Fer01]	86.0% / 8	
Garcia-Delakis [Gar04]	90.3% / 8	90.1% / 7
Li <i>et al.</i> [Li02]	90.2% / 31	
Rowley <i>et al.</i> [Row98]	86.2% / 23	84.5% / 8
Sung-Poggio [Sun98]		79.9% / 5
Schneiderman-Kanade [Sch00]	90.5% / 33	91.1% / 12
Viola-Jones [Vio04]	85.2% / 5	77.8% / 31

the number of computationally heavy operations, (ii) it is based on boosting fast weak learners [Fre95], and (iii) the proposed integral image representation eliminates repeated computation of Haar feature-responses. Improvements to the original detector have since been proposed, e.g. by using a pyramidal structure [Hua05, Li02] for multi-view detection and rotation invariance [Hua05, Wu04], or joint low-level features [Mit05] for reducing the number of false positive detections.

2.3 Face recognition

There are many criterions by which one may decide to cluster face recognition algorithms, depending on the focus of discussion, see Table 2.3. For us it will be useful to start by talking about the type of data available as input and the conditions in which such data was acquired. As was mentioned in the previous chapter, the main sources of changes in one's appearance are the illumination, head pose, image quality, facial expressions and occlusions. In *controlled* imaging conditions, some of or all these variables are fixed so as to simplify recognition, and this is known *a priori*. This is a possible scenario in the acquisition of passport photographs, for example.

Historically, the first attempts at automatic face recognition date back to the early 1970s and were able to cope with some success with this problem setup only. These pioneering

Table 2.3: *An overview of face recognition approaches.*

	Face recognition approaches		
Acquisition conditions	Controlled	“Loosely” controlled	Extreme
Input data	Still images	Image sets	Sequences
Modality	Optical data	Other (IR, range etc.)	Hybrid
Representation	Holistic	Feature-based	Hybrid
Approach	Appearance-based	Model-based	

methods relied on predefined geometric features for recognition [Kel70, Kan73]. Distances [Bru93] or angles between locations of characteristic facial features (such as the eyes, the nose etc.) were used to discriminate between individuals, typically using a Bayes classifier [Bru93]. In [Kan73] Kanade reported correct identification of only 15 out of 20 individuals under controlled pose. Later Goldstein *et al.* [Gol72] and, Kaya and Kobayashi [Kay72] (also see work by Bledsoe *et al.* [Ble66, Cha65]) showed geometric features to be sufficiently discriminatory if facial features are manually selected.

Most obviously, geometric feature-based methods are inherently very sensitive to head pose variation, or equivalently, the camera angle. Additionally, these methods also suffer from sensitivity to noise in the stage of localization of facial features. While geometric features themselves are insensitive to illumination changes, the difficulty of their extraction is especially prominent in extreme lighting conditions and when the image resolution is low.

2.3.1 Statistical, appearance-based methods

In sharp contrast to the geometric, feature-based algorithms are appearance-based methods. These revived research interest in face recognition in the early 1990s and to this day are dominant in number in the literature. Appearance-based methods, as their name suggests, perform recognition directly from the way faces appear in images, interpreting them as ordered collections of pixels. Faces are typically represented as vectors in the D -dimensional *image space*, where D is the number of image pixels (and hence usually large). Discrimination between individuals is then performed by employing statistical models that explain inter- and/or intra- personal appearance changes.

The *Eigenfaces* algorithm of Turk and Pentland [Tur91a, Tur91b] is the most famous algorithm of this group. Its approach was motivated by previous work by Kohonen [Koh77] on auto-associative memory matrices for storage and retrieval of face images, and by Kirby



(a) Conceptual drawing



(b) Face space basis as images

Figure 2.4: (a) A conceptual picture of the Eigenfaces method. All data is projected and then classified in the linear subspace corresponding to the dominant modes of variation across the entire data set, estimated using PCA. (b) The first 10 dominant modes of the Cam-Face data, shown as images. These are easily interpreted as corresponding to the main modes of illumination-affected appearance changes (brighter/darker face, strong light from the left/right etc.) and pose.

and Sirovich [Sir87, Kir90]. It uses Principal Component Analysis (PCA) to construct the so-called *face space* – a space of dimension $d \ll D$ that explains appearance variations of human faces, see Figure 2.4. Recognition is performed by projecting all data onto the face space and classifying a novel face to the closest class. The most common norms used in the literature are the Euclidean (also known as L_2), L_1 and Mahalanobis [Dra03, Bev01], in part dictated by the availability of training data.

By learning what appearance variations one can expect across the corpus of *all* human faces and then by effectively *reconstructing* any novel data using the underlying subspace model, the main advantage of Eigenfaces is that of suppressing noise in data [Wan03a]. By interlacing the subspace projection with RANSAC [Fis81], occlusion detection and removal are also possible [Bla98, Ara05c]. However, inter- and intra-personal appearance variations are not learnt separately. Hence, the method is recognized as more suitable for detection and compression tasks [Mog95, Kin97] than recognition.

A Bayesian extension of Eigenfaces, proposed by Moghaddam *et al.* [Mog98], improves on the original method by learning the mean intra-personal subspace. Recognition decision is again cast using the assumption that appearance for each person follows a Gaussian distribution, with also Gaussian, but isotropic image noise.

To address the lack of discriminative power of Eigenfaces, another appearance-based subspace method was proposed – the *Fisherfaces* [Yam00, Zha00], named after Fisher’s Linear Discriminant Analysis (LDA) that it employs. Under the assumption of isotropically Gaussian class data, LDA constructs the optimally discriminating subspace in terms of maximizing the between to within class scatter, as shown in Figure 2.5. Given sufficient training data, Fisherfaces typically perform better than Eigenfaces [Yam00, Wen93] with further invariance to lighting conditions when applied to Fourier transformed images [Aka91]. One of the weaknesses of Fisherfaces is that the estimate of the optimal projection subspace is sensitive to a particular choice of training images [Bev01]. This finding is important as it highlights the need for more extensive use of domain specific information. It is therefore not surprising that limited improvements were achieved by applying other purely statistical techniques on the face recognition task: Independent Component Analysis (ICA) [Bae02, Dra03, Bar98c, Bar02]; Singular Value Decomposition (SVD) [Pre92]; Canonical Correlation Analysis (CCA) [Sun05]; Non-negative Matrix Factorization (NNMF) [Wan05]. Simple linear extrapolation techniques, such as the Nearest Feature Line (NFL) [Li99], Nearest Feature Plane (NFS) or Nearest Feature Space (NFS) also failed to achieve significant performance increase using holistic appearance.

Nonlinear approaches. Promising results of the early subspace methods and new research challenges they uncovered, motivated a large number of related approaches. Some of these focused on relaxing the crude assumption that the appearance of a face conforms to a Gaussian distribution. The most popular direction employed the kernel approach [Sch99, Sch02] with methods such as *Kernel Eigenfaces* [Yan00, Yan02b], *Kernel Fisherfaces* [Yan00], *Kernel Principal Angles* [Wol03], *Kernel RAD* [Ara04b, Ara06e], *Kernel ICA* [Yan05] and others (e.g. see [Zho03]). As an alternative to Kernel Eigenfaces, a multi-layer perceptron (MLP) neural network with a bottleneck architecture [deM93, Mal98], shown in Figure 2.6, was proposed to implement nonlinear PCA projection of faces [Mog02], but has since been largely abandoned due to the difficulty to optimally train [Che97]¹. The recently proposed Isomap [Ten00] and Locally Linear Embedding (LLE) [Row01] algorithms were successfully applied to unfolding nonlinear appearance manifolds [Bai05, Kim05b, Pan06, Yan02a], as were piece-wise linear models [Ara05b, Lee03, Pen94].

¹The reader may be interested in the following recent paper that proposes an automatic way of initializing the network weights so that they are close to a good solution [Hin06].



(a) Conceptual drawing



(b) LDA basis as images

Figure 2.5: (a) A conceptual picture of the Fisherfaces method. All data is projected and then classified in the linear subspace that best separates classes, which are assumed to be isotropic and Gaussian. (b) The first 10 most discriminative modes of the CamFace data, shown as images. To the human eye these are not as meaningful as face space basis, see Figure 2.4.



Figure 2.6: The feed-forward bottleneck neural network structure, used to implement nonlinear projection of faces. Functionality-wise, two distinct parts of the network can be identified: (i) layers 1-3 perform compression of data by exploiting the inherently low-dimensional nature of facial appearance variations; (ii) layers 4-5 perform classification of the projected data.

Local feature-based methods. While the above-mentioned methods improve on the linear subspace approaches by more accurately modelling appearance variations *seen in*

training, they fail to significantly improve on the limited ability of the original methods in *generalizing* appearance to unseen imaging conditions (i.e. illumination, pose and so on) [Bae02, Bar98a, Gro01, Nef96, Sha02b].

Local feature-based methods were proposed as an alternative to holistic appearance algorithms, as a way of achieving a higher degree of viewpoint invariance. Due to the smoothness of faces, a local surface patch is nearly planar and its appearance changes can be expected to be better approximated by a linear subspace than those of an entire face. Furthermore, their more limited spatial extent and the consequent lower subspace dimensionality have both computational benefits and are less likely to suffer from the so-called *curse of dimensionality*.

Trivial extensions such as *Eigenfeatures* [Abd98, Pen94] and *Eigeneyes* [Cam00] demonstrated this, achieving recognition rates better than those of the original Eigenfaces [Cam00]. Even better results were obtained using hybrid methods i.e. combinations of holistic and local patch-based appearances [Pen94].

An influential group of local features-based methods are the *Local Feature Analysis* (LFA) (or elastic graph matching) algorithms, the most acclaimed of these being *Elastic Bunch Graph Matching* (EBGM) [Arc03, Bol03, Pen96, Wis97, Wis99b]². LFA methods have proven to be amongst the most successful in the literature [Heo03b] and are employed in commercial systems such as FaceIt[®] by Identix [Ide03] (the best performing commercial face recognition software in the 2003 Face Recognition Vendor Test [Phi03]).

The common underlying idea behind these methods is that they combine in a unified manner holistic with local features, and appearance information with geometric structure. Each face is represented by a graph overlaid on the appearance image. Its nodes correspond to the locations of features used to describe local face appearance, while its edges constrain the holistic geometry by representing feature adjacency, as shown in Figure 2.7. To establish the similarity between two faces, their elastic graph representations are compared by measuring the distortion between their topological configurations and the similarities of feature appearances.

Various LFA methods primarily differ: (i) in how local feature appearances are represented and (ii) in the way two elastic graphs are compared. In Elastic Bunch Graph Matching [Bol03, Sen99, Wis97, Wis99b], for example, Gabor wavelet [Gab88] jets are used to characterize local appearance. In part, their use is attractive in this context because the functional form of Gabor wavelets closely resembles the response of receptive fields of the visual cortex [Dau80, Dau88, Jon87, Mar80], see Figure 2.8. They also provide powerful means of extracting *local* frequency information, which has been widely employed in various

²The reader should note that LFA-based algorithms are sometimes categorized as model-based. In this thesis the term model-based is used for algorithms that explain the entire observed face appearance.



Figure 2.7: *An elastic graph successfully fitted to an input image. Its nodes correspond to fiducial points, which are used to characterize local, discriminative appearance. Graph topology (i.e. fiducial point adjacency constraints) is typically used only in the fitting stage, but is discarded for recognition as it is greatly distorted by viewpoint variations.*



Figure 2.8: *A 2-dimensional Gabor wavelet, shown as a surface and a corresponding intensity image. The wavelet closely resembles the response of receptive fields of the visual cortex and provides a trade-off between spatial and frequency localization of the signal (i.e. appearance).*

branches of computer vision for characterizing texture [Hon04, Lee96, Mun05, Pun04]. Local responses to multi-scale morphological operators (dilation and erosion) were also successfully used as fiducial point descriptors [Kot98, Kot00a, Kot00b, Kot00c].

Unlike any of the previous methods, LFA algorithms generalize well in the presence of facial expression changes [Phi95, Wis99a]. On the other hand, much like the early geometric-feature based methods, significant viewpoint changes pose problems in both the graph fitting stage, as well as in recognition, as the projected topological layout of fiducial features changes dramatically with out-of-plane head rotation. Furthermore, both wavelet-based and morphological response-based descriptors show little invariance to illumination changes, causing a sharp performance decay in realistic imaging conditions (an Equal Error Rate of 25-35% was reported in [Kot00c]) and, importantly for the work presented in this thesis, with low resolution images [Ste06].

Appearance-based methods – a summary. In closing, purely appearance-based recognition approaches can achieve good generalization to unseen (i) poses and (ii) facial expressions by using local or hybrid local and holistic features. However, they all poorly generalize in the presence of large illumination changes.

2.3.2 Model-based methods

The success of LFA in recognition across pose and expression can be attributed to the shift away from purely statistical pattern classification to the use of models that exploit *a priori* knowledge about the very specific instance of classification that face recognition is. Model-based methods take this approach further. They formulate models of image formation with the intention of recovering (i) mainly person-specific (e.g. face albedo or shape) and (ii) extrinsic, nuisance variables (e.g. illumination direction, or head yaw). The key challenge lies in coming up with models for which the parameter estimation problem is not ambiguous or ill-conditioned.

2D illumination models. The simplest generative models in face recognition are used for illumination normalization of raw images, as a preprocessing step cascaded with, typically, appearance-based classification that follows it. Considering the previously-discussed observation that the face surface, as well as albedo, are largely smooth, and assuming a Lambertian reflectance model, illumination effects on appearance are for the most part slowly spatially varying, see Figure 2.9. On the other hand, discriminative person-specific information is mostly located around facial features such as the eye, the mouth and the nose, which contain discontinuities and give rise to appearance changes of high frequency, as illustrated in Figure 2.10 (a).

It has been applied in the forms of high-pass and band-pass filters [Ara05c, Ara06a, Buh94, Fit02], Laplacian-of-Gaussian filters [Adi97, Ara06f], edge maps [Adi97, Ara06f, Gao02, Tak98] and intensity derivatives [Adi97, Ara06f], to name the few most popular approaches, see Figure 2.10 (b) (also see Chapter 6). Although widely used due to its simplicity, numerical efficiency and the lack of assumptions on head pose, the described spatial frequency model is universally regarded as insufficiently sophisticated in all but mild illumination conditions, struggling with cast shadows and specularities, for example. Various modifications have thus been proposed. In the *Self-Quotient Image* (SQI) method [Wan04a], the mid-frequency, discriminative band is also scaled with local image intensity, thus normalizing edge strengths in weakly and strongly illuminated regions of the face.

A principled treatment of illumination invariant recognition for Lambertian faces, the *Illumination Cones* method, was proposed in [Geo98]. In [Bel96] it was shown that the



Figure 2.9: (a) A conceptual drawing of the Lambertian reflectance model. Light is reflected isotropically, the reflected intensity being proportional to the cosine between the incident light direction \mathbf{l} and the surface normal \mathbf{n} . (b) The appearance of a face rendered as a texture-free Lambertian surface.

set of images of a convex, Lambertian object, illuminated by an arbitrary number of point light sources at infinity, forms a polyhedral cone in the image space with dimension equal to the number of distinct surface normals. Georghiades *et al.* successfully used this result by reilluminating images of frontal faces. The key limitations of their method are (i) the requirement of at least 3 images for each novel face, illuminated from linearly independent directions and in the same pose, (ii) lack of accounting non-Lambertian effects. These two limitations are separately addressed in [Nis06] and [Wol03]. In [Nis06], a simple model of diffuse reflections of a generic face is used to iteratively classify face regions as ‘Lambertian, no cast shadows’, ‘Lambertian, cast shadow’ and ‘specular’, applying SQI-based normalization to each separately. It is important to observe that the success of this method which uses a model of only a *single* (generic) face demonstrates that shape and reflectance similarities across individuals can also be exploited so as to improve recognition. The *Quotient Image* (QI) method [Wol03] makes use of this by making the assumption that all human faces have the same shape. Using a small (~ 10) bootstrap set of individuals, each in 3 different illuminations, it is shown how pure albedo and illumination effects can approximately be separated from a single image of a novel face. However, unlike the method of Nishiyama and Yamaguchi [Nis06], QI does not deal well with non-Lambertian effects or cast shadows.

2D combined shape and appearance models. The *Active Appearance Model* (AAM) [Coo98] was proposed for modelling objects that vary in shape and appearance. It has a lot of similarity to the older *Active Contour Model* [Kas87] and the *Active Shape Model* [Coo95, Ham98a, Ham98b] (also see [Scl98]) that model shape only.

In AAM a deformable triangular (c.f. EBGM) mesh is fitted to an image of a face, see

Figure 2.11 (a). This is guided by combined statistical models of shape and shape-free appearance, so as to best explain the observed image. In [Coo98] linear, PCA models are used, see Figure 2.11 (b). Still, AAM parameter estimation is a difficult optimization problem. However, given that faces do not vary a lot in either shape or appearance, the structure of the problem is similar whenever the minimization is performed. In [Coo98] and [Coo99b], this is exploited by learning a linear relationship between the current reconstruction error and the model parameter perturbation required to correct it (for variations on the basic algorithm also see [Coo02, Sco03]).

AAMs have been successfully used for face recognition [Edw98b, Fag06], tracking [Dor03] and expression recognition [Saa06]. The main limitations of the original method are: (i) the sensitivity to illumination changes in the recognition stage, and (ii) occlusion (including self-occlusion, due to 3D rotation for example). The latter problem was recently addressed by Gross *et al.* [Gro06], a modification to the original algorithm demonstrating good fitting results with extreme pose changes and occlusion.

3D combined shape and illumination models. The most recent and complex generative models used for face recognition are largely based on the *3D Morphable Model* introduced in [Bla99] which builds up on the previous work on 3D modelling and animation of faces [DeC98, DiP91, MT89, Par75, Par82, Par96]. The model consists of albedo values at the nodes of a 3-dimensional triangular mesh describing face geometry. Model fitting is performed by combining a Gaussian prior on the shape and texture of human faces with photometric information from an image [Wal99b]. The priors are estimated from training data acquired with a 3D scanner and densely registered using a regularized 3D optical flow algorithm [Bla99]. 3D model recovery from an input image is performed using a gradient descent search in an analysis-by-synthesis loop. Linear [Rom02] or quadratic [Rom03b] error functions have been successfully used.

An attractive feature of the 3D Morphable Model is that it explicitly models both intrinsic and extrinsic variables, respectively: face shape and albedo, and pose and illumination parameters, see Figure 2.12 (a). On the other hand, it suffers from convergence problems in the presence of background clutter or facial occlusions (glasses or facial hair). Furthermore and importantly for the work presented in this thesis, the 3D Morphable Model requires high quality image input [Eve04] and struggles with non-Lambertian effects or multiple light sources. Finally, nontrivial user intervention is required (localization of up to seven facial landmarks and the dominant light direction, see Figure 2.12 (b)), the fitting procedure is slow [Vet04] and can get stuck in local minima [Lee04].

2.3.3 Image set and video-based methods.

Both appearance and model-based methods have been applied to face recognition using image set or video sequence matching. In principle, evidence from multiple shots can be used to optimize model parameter recovery in model-based methods and reduce the problem of local minima [Edw99]. However, an important limitation lies in the computational demands of model fitting. Specifically, it is usually too time consuming to optimize model parameters over an entire sequence. If, on the other hand, parameter constraints are merely propagated from the first frame, the fitting can experience steady deterioration over time, the so-called *drift*.

More variability in the manner in which still-based algorithms are extended to deal with multi-image input is seen amongst appearance-based methods. We have stated that the main limitation of purely appearance-based recognition is that of limited generalization ability, especially in the presence of greatly varying illumination conditions. On the other hand, a promising fact is that data collected from video sequences often contains some variability in these parameters.

Eigenfaces, for example, have been used on a per-image basis, with recognition decision cast using majority vote [Ara06e]. A similar voting approach was also successfully used with local features in [Cam00], which were extracted by tracking a face using a Gabor Wavelet Network [Cam00, Krü00, Krü02]. In [Tor00] video information is used only in the training stage to construct person-specific PCA spaces, *self-eigenfaces*, while verification was performed from a single image using the Distance from Feature Space criterion. Classifiers using different eigenfeature spaces were used in [Pri01] and combined using the sum rule [Kit98]. Better use of training data is made with various discriminative methods such as Fisherfaces, which can be used to estimate *database-specific* optimal projection [Edw97].

An interesting extension of appearance correlation-based recognition to matching sets of faces was proposed by Yamaguchi *et al.* [Yam98]. The so-called Mutual Subspace Method (MSM) has since gained considerable attention in the literature. In MSM, linear subspaces describing appearance variations within sets or sequences are matched using canonical correlations [Git85, Hot36, Kai74, Oja83]. It can be shown that this corresponds to finding the most similar modes of variation between subspaces [Kim07] (see Chapters 6 and 7, and Appendix B for more detail and criticism of MSM). A discriminative heuristic extension was proposed in [Fuk03] and a more rigorous framework in [Kim06]. This group of methods typically performs well when some appearance variation between training and novel input is shared [Ara05b, Ara06e], but fail to generalize in the presence of large illumination changes, for example [Ara06b]. The same can be said of the methods that use the temporal component to enforce prior knowledge on likely appearance changes between consecutive frames.

Table 2.4: A qualitative comparison of advantages and disadvantages of the two main groups of face recognition methods in the literature.

	Appearance-based	Model-based
Advantages	<ul style="list-style-type: none"> • Well-understood statistical methods can be applied. • Can be used for poor quality and low resolution input. 	<ul style="list-style-type: none"> • Explicit modelling and recovery of personal and extrinsic variables. • Prior, domain-specific knowledge is used.
Disadvantages	<ul style="list-style-type: none"> • Lacking generalization to unseen pose, illumination etc. • No (or little) use of domain-specific knowledge. 	<ul style="list-style-type: none"> • High quality input is required. • Model parameter recovery is time-consuming. • Fitting optimization can get stuck in a local minimum. • User intervention is often required for initialization. • Difficult to model complex illumination effects – fitting becomes as ill-conditioned problem.

In the algorithm of Zhou *et al.* [Zho03] the joint probability distribution of identity and motion is modelled using sequential importance sampling, yielding the recognition decision by marginalization. Lee *et al.* [Lee03] approximate face manifolds by a finite number of infinite extent subspaces and use temporal information to robustly estimate the operating part of the manifold.

2.3.4 Summary.

Amongst a great number of developed face recognition algorithms, we've seen that two drastically different groups of approaches can be identified: appearance-based and model-based, see Figure 2.13. The preceding section described the rich variety of methods within each group and highlighted their advantages and disadvantages. In closing, we summarize these in Table 2.4.

2.4 Performance evaluation

To motivate different performance measures used across the literature, it is useful to first consider the most common paradigms in which face matching is used. These are

- recognition – 1-to-N matching,
- verification – 1-to-1 matching, and
- retrieval.

In this context by the term “matching” we mean that the result of a comparison of two face representations yields a scalar, numerical score d that measures their dissimilarity.

Paradigm 1: 1-to-N matching. In this setup novel input is matched to each of the individuals in a database of known persons and classified to – *recognized* as – the closest, most similar one. One and only one correct correspondence is assumed to exist. This is illustrated in Figure 2.14 (a).

When 1-to-N matching is considered, the most natural and often used performance measure is the *recognition rate*. We define it as the ratio of the number of correctly assigned to the total number of test persons.

Paradigm 2: 1-to-1 matching. In 1-to-1 matching, only a single comparison is considered at a time and the question asked is if two people are the same. This is equivalent to thresholding the dissimilarity measure d used for matching, see Figure 2.14 (b).

Given a particular distance threshold d^* , the *true positive rate* (TPR) $p_t(d^*)$ is the proportion of intra-personal comparisons that yields distances within the threshold. Similarly, the *false positive rate* (FPR) $p_f(d^*)$ is the proportion of inter-personal comparisons that yields distances within the threshold. As d^* is varied, the changes in $p_t(d^*)$ and $p_f(d^*)$ are often visualized using the so-called *Receiver-Operator Characteristic* (ROC) curve, see Figure B.5.

The *Equal Error Rate* (EER) point of the ROC curve is sometimes used for brevity:

$$EER = p_f(d_{EER}), \text{ where: } p_f(d_{EER}) = 1 - p_t(d_{EER}), \quad (2.1)$$

see Figure B.5.

Paradigm 3: retrieval. In the retrieval paradigm the novel person is now a query to the database, which may contain several instances of any individual. The result of a query

is an *ordering* of the entire database using the dissimilarity measure d , see Figure 2.14 (c). More successful orderings have instances of the query individual first (i.e. with a lower recall index).

From the above, it can be seen that the normalized sum of indexes corresponding to in-class faces is a meaningful measure of the recall accuracy. We call this the rank ordering score and compute it as follows:

$$\rho = 1 - \frac{S - m}{M}, \quad (2.2)$$

where S is the sum of indexes of retrieved in-class faces, and m and M , respectively, the minimal and maximal values S and $(S - m)$ can take.

The score of $\rho = 1.0$ corresponds to orderings which correctly cluster all the data (all the in-class faces are recalled first), 0.0 to those that invert the classes (the in-class faces are recalled last), while 0.5 is the expected score of a random ordering. The *average normalized rank* [Sal83] is equivalent to $1 - \rho$.

2.4.1 Data

Most algorithms in this thesis were evaluated on three large data sets of video sequences – the *CamFace*, *ToshFace* and *Face Video Database*. These are briefly described next. Other data, used only in a few specific chapters, is explained in the corresponding evaluation sections. The algorithm we used to automatically extract faces from video is described in Appendix C.2.

The *CamFace* dataset. This database contains 100 individuals of varying age and ethnicity, and equally represented genders. For each person in the database there are 7 video sequences of the person in arbitrary motion (significant translation, yaw and pitch, negligible roll), each in a different illumination setting, see Fig. 2.16 (a) and 2.17, for 10s at 10fps and 320×240 pixel resolution (face size ≈ 60 pixels). For more information see Appendix C in which this database is thoroughly described.

The *ToshFace* dataset. This database was kindly provided to us by Toshiba Corporation. It contains 60 individuals of varying age, mostly male Japanese, and 10 sequences per person. Each 10s sequence corresponds to a different illumination setting, acquired at 10fps and 320×240 pixel resolution (face size ≈ 60 pixels), see Fig. 2.16 (b).

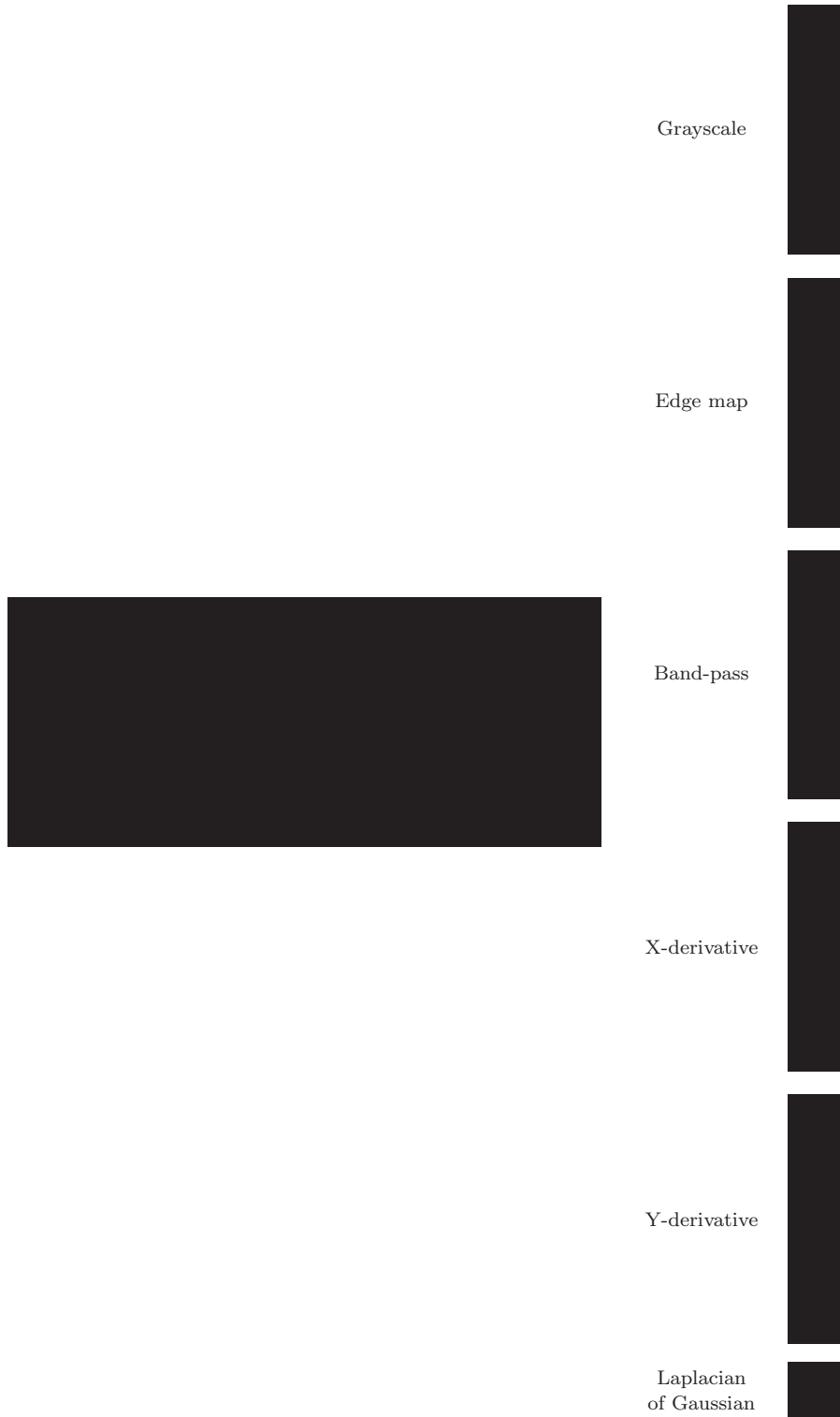
The *Face Video Database*. This database is freely available and described in [Gor05]. Briefly, it contains 11 individuals and 2 sequences per person, little variation in illumination,

but extreme and uncontrolled variations in pose, acquired for 10-20s at 25fps and 160×120 pixel resolution (face size ≈ 45 pixels), see Fig. 2.16 (c).

2.5 Summary and conclusions

This chapter finished laying out the foundations for understanding the novelty of this thesis. The challenges of face recognition were explored by presenting a detailed account of previous research attempts at solving the problem at hand. It was established that both major methodologies, discriminative model-based and generative model-based, suffer from serious limitations when dealing with data acquired in realistic, practical conditions.

The second part of the chapter addressed the issue of evaluating and comparing face recognition algorithms. We described a number of useful performance measures and three large data sets that will be used extensively throughout this work.



(a)

(b)

Figure 2.10: (a) The simplest generative model used for face recognition: images are assumed to consist of the low-frequency band that mainly corresponds to illumination changes, mid-frequency band which contains most of the discriminative, personal information and white noise. (b) The results of several most popular image filters operating under the assumption of the frequency model.



Figure 2.11: (a) Two input images with correct adaptation (top) and the corresponding geometrically normalized images (bottom). [Dor03]. (b) First three modes of the AAM appearance model in ± 3 standard deviations [Kan02]

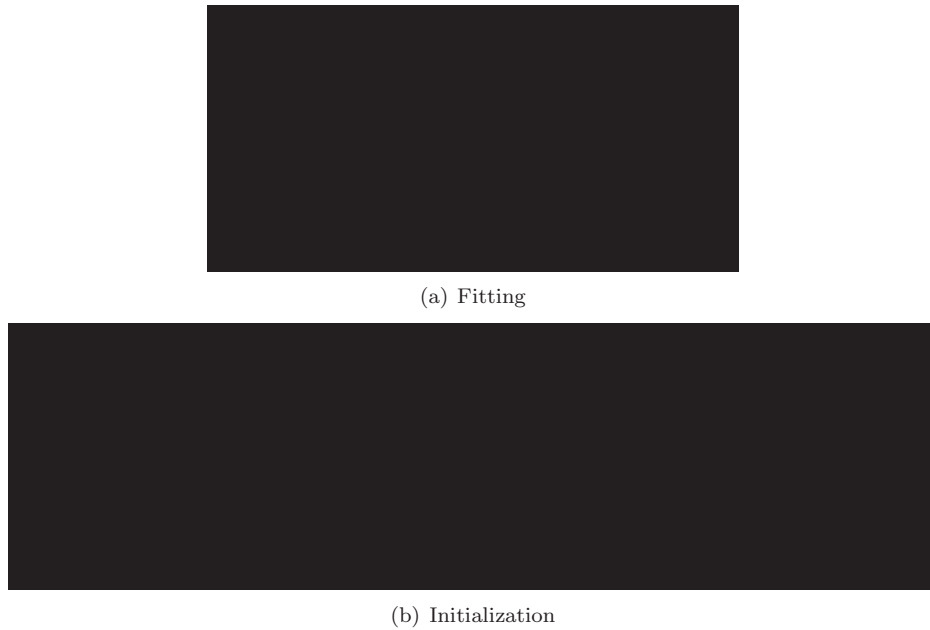


Figure 2.12: (a) Simultaneous reconstruction of 3D shape and texture of a new face from two images taken under different conditions. In the centre row, the 3D face is rendered on top of the input images [Bla99]. (b) 3D Morphable Model Initialization: seven landmarks for front and side views and eight for the profile view are manually labelled for each input image [Li04].



Figure 2.13: *A summary of reviewed face recognition trends in the literature. Also see Table 2.4 for a comparative summary.*



(a) 1-to-N



(b) 1-to-N



(c) Retrieval

Figure 2.14: *Three matching paradigms give rise to different performance measures for face recognition algorithms.*



Figure 2.15: *The variations in the true positive and false positive rates, as functions of the distance threshold, are often visualized using the Receiver-Operator Characteristic (ROC) curve, by plotting them against each other. Shown is a family of ROC curves and the Equal Error Rate (EER) line. Better performing algorithms have ROC curves closer to the 100% true positive and 0% false positive rate.*



(a) *CamFace*



(b) *ToshFace*



(c) *Face Video DB*

Figure 2.16: *Frames from typical video sequences from the 3 databases used for evaluation of most recognition algorithms in this thesis.*



(a) FaceDB100



(b) FaceDB60

Figure 2.17: (a) *Illuminations 1–7 from CamFace data set* and (b) *illuminations 1–10 from ToshFace data set.*

II

Access Control

3

Manifold Density Divergence



Albrecht Dürer. *Melancholia*
1514, Engraving, 24.1 x 18.8 cm
Albright-Knox Art Gallery, Buffalo

The preceding two chapters introduced the problem of face recognition from video, placed it into the context of biometrics-based identification methods and current practical demands on them, in broad strokes describing relevant research with its limitations. In this chapter we adopt the *appearance-based* recognition approach and set up the grounds for most of the material in the chapters that follow by formalizing the face manifold model. The first contribution of this thesis is also introduced – the *Manifold Density Divergence (MDD)* algorithm.

Specifically, we address the problem of matching a novel face video sequence to a set of faces containing typical, or expected, appearance variations. We propose a flexible, semi-parametric model for learning probability densities confined to highly non-linear but intrinsically low-dimensional manifolds. The model leads to a statistical formulation of the recognition problem in terms of minimizing the divergence between densities estimated on these manifolds. The proposed method is evaluated on the *CamFace* data set and is shown to match the best and outperform other state-of-the-art algorithms in the literature, achieving 94% recognition rate on average.

3.1 Introduction

Training a system in certain imaging conditions (single illumination, pose and motion pattern) and being able to recognize under arbitrary changes in these conditions can be considered to be the hardest problem formulation for automatic face recognition. However, in many practical applications this is too strong of a requirement. For example, it is often possible to ask a subject to perform random head motion under varying illumination conditions. It is often not reasonable, however, to request that the user perform a strictly defined motion, assume strictly defined poses or illuminate the face with lights in a specific setup. We therefore assume that the training data available to an AFR system is organized in a database where a *set* of images for each individual represents significant (typical) variability in illumination and pose, but does not exhibit temporal coherence and is not obtained in scripted conditions.

The test data – that is, the input to an AFR system – also often consist of a *set* of images, rather than a single image. For instance, this is the case when the data is extracted from surveillance videos. In such cases the recognition problem can be formulated as taking a set of face images from an unknown individual and finding the best matching set in the database of labelled sets. This is the recognition paradigm we are concerned with in this chapter.

We approach the task of recognition with image sets from a statistical perspective, as an

instance of the more general task of measuring similarity between two probability density functions that generated two sets of observations. Specifically, we model these densities as Gaussian Mixture Models (GMMs) defined on low-dimensional nonlinear manifolds embedded in the image space, and evaluate the similarity between the estimated densities via the Kullback-Leibler divergence. The divergence, which for GMMs cannot be computed in closed form, is efficiently evaluated by a Monte Carlo algorithm.

In the next section, we introduce our model and discuss the proposed method for learning and comparing face appearance manifolds. Extensive experimental evaluation of the proposed model and its comparison to state-of-the-art methods are reported in Section 3.3, followed by discussion of the results and a conclusion.

3.2 Modelling face manifold densities

Under the standard representation of an image as a raster-ordered pixel array, images of a given size can be viewed as points in a Euclidean *image space*. The dimensionality, D , of this space is equal to the number of pixels. Usually D is high enough to cause problems associated with the *curse of dimensionality* in learning and estimation algorithms. However, surfaces of faces are mostly smooth and have regular texture, making their appearance quite constrained. As a result, it can be expected that face images are confined to a *face space*, a manifold of lower dimension $d \ll D$ embedded in the image space [Bic94]. We next formalize this notion and propose an algorithm for comparing estimated densities on manifolds.

3.2.1 Manifold density model

The assumption of an underlying manifold subject to additive sensor noise leads to the following statistical model: An image \mathbf{x} of subject i 's face is drawn from the probability density function (*pdf*) $p_F^{(i)}(\mathbf{x})$ within the face space, and embedded in the image space by means of a mapping function $f^{(i)} : \mathbb{R}^d \rightarrow \mathbb{R}^D$. The resulting point in the D -dimensional space is further perturbed by noise drawn from a noise distribution p_n (note that the noise operates in the image space) to form the observed image \mathbf{X} . Therefore the distribution of the observed face images of the subject i is given by:

$$p^{(i)}(\mathbf{X}) = \int p_F^{(i)}(\mathbf{x}) p_n(f^{(i)}(\mathbf{x}) - \mathbf{X}) d\mathbf{x} \quad (3.1)$$

Note that both the manifold embedding function f and the density p_F on the manifold are subject-specific, as denoted by the superscripts, while the noise distribution p_n is assumed to be common for all subjects. Following accepted practice, we model p_n by an isotropic,

zero-mean Gaussian. Figure 3.1 shows an example of a face image set projected onto a few principal components estimated from the data, and illustrates the validity of the manifold notion.



(a) First three PCs



(b) Second three PCs

Figure 3.1: *A typical manifold of face images in a training (small blue dots) and a test (large red dots) set. Data used come from the same person and shown projected to the first three (a) and second three (b) principal components. The nonlinearity and smoothness of the manifolds are apparent. Although globally quite dissimilar, the training and test manifolds have locally similar structures.*

Let the training database consist of sets S_1, \dots, S_K , corresponding to K individuals. S_i is assumed to be a set of independent and identically distributed (i.i.d.) observations drawn from $p^{(i)}$ (3.1). Similarly, the input set S_0 is assumed to be i.i.d. drawn from the test subject’s face image density $p^{(0)}$. The recognition task can then be formulated as selecting one among K hypotheses, the k -th hypothesis postulating that $p^{(0)} = p^{(k)}$. The Neyman-Pearson lemma [Dud00] states that the optimal solution for this task consists of choosing the model under which S_0 has the highest likelihood. Since the underlying densities are unknown, and the number of samples is limited, relying on direct likelihood estimation is problematic. Instead, we use Kullback-Leibler divergence as a “proxy” for the likelihood statistic needed in this K -ary hypothesis test [Sha02a].



Figure 3.2: *Description lengths for varying numbers of GMM components for training (solid) and test (dashed) sets. The lines show the average plus/minus one standard deviation across sets.*

3.2.2 Kullback-Leibler divergence

The Kullback-Leibler (KL) divergence [Cov91] quantifies how well a particular pdf $q(\mathbf{x})$ describes samples from another pdf $p(\mathbf{x})$:

$$D_{KL}(p||q) = \int p(\mathbf{x}) \log \left(\frac{p(\mathbf{x})}{q(\mathbf{x})} \right) d\mathbf{x} \quad (3.2)$$

It is nonnegative and equal to zero iff $p \equiv q$. Consider the integrand in (3.2). It can be seen that the regions of the image space with a large contribution to the divergence are those in which $p(\mathbf{x})$ is significant and $p(\mathbf{x}) \gg q(\mathbf{x})$. On the other hand, regions in which $p(\mathbf{x})$ is small contribute comparatively little. We expect the sets in the training data to be significantly more extensive than the input set, and as a result $p^{(i)}$ to have broader support than $p^{(0)}$. We therefore use $D_{KL}(p^{(0)}||p^{(i)})$ as a “distance measure” between training and test sets. This expectation is confirmed empirically, see Figure 3.2. The novel patterns not represented in the training set are heavily penalized, but there is no requirement that all variation seen during training should be present in the novel distribution.

We have formulated recognition in terms of minimizing the divergence between densities on face manifolds. Two problems still remain to be solved. First, since the analytical form for neither the densities nor the embedding functions is known, these must be estimated from the data. Second, the KL divergence between the estimated densities must be evaluated. In the remainder of this section, we describe our solution for these two problems.

3.2.3 Gaussian mixture models

Our goal is to estimate the density defined on a complex nonlinear manifold embedded in a high-dimensional image space. Global parametric models typically fail to adequately

capture such manifolds. We therefore opt for a more flexible mixture model for $p^{(i)}$: the Gaussian Mixture Model (GMM). This choice has a number of advantages:

- It is a flexible, semi-parametric model, yet simple enough to allow efficient estimation.
- The model is generative and offers interpolation and extrapolation of face pattern variation based on local manifold structure.
- Principled model order selection is possible.

The multivariate Gaussian components of a GMM in our method need not be semantic (corresponding to a specific view or illumination) and can be estimated using the Expectation Maximization (EM) algorithm [Dud00]. The EM is initialized by K-means clustering, and constrained to diagonal covariance matrices. As with any mixture model, it is important to select an appropriate number of components in order to allow sufficient flexibility while avoiding overfitting. This can be done in a principled way with the Minimal Description Length (MDL) criterion [Bar98b]. Briefly, MDL assigns to a model a cost related to the amount of information necessary to encode the model and the data *given* the model. This cost, known as the description length, is proportional to the likelihood of the training data under that model penalized by the model complexity, measured as the number of free parameters in the model.

Average description lengths for different numbers of components for the data sets used in this chapter are shown in Figure 3.2. Typically, the optimal (in the MDL sense) number of components for a training manifold was found to be 18, while 5 was typical for the manifolds used for recognition. This is illustrated in Figures 3.3, 3.4 and 3.5.

3.2.4 Estimating KL divergence

Unlike in the case of Gaussian distributions, the KL divergence cannot be computed in a closed form when $\hat{p}(\mathbf{x})$ and $\hat{q}(\mathbf{x})$ are GMMs. However, it is straightforward to sample from a GMM. The KL divergence in (3.2) is the expectation of the log-ratio of the two densities w.r.t. the density p . According to the law of large numbers [Gri92], this expectation can be evaluated by a Monte-Carlo simulation. Specifically, we can draw a sample \mathbf{x}_i from the estimated density \hat{p} , compute the log-ratio of \hat{p} and \hat{q} , and average this over M samples:

$$D_{KL}(\hat{p}||\hat{q}) \approx \frac{1}{M} \sum_{i=1}^M \log \left(\frac{\hat{p}(\mathbf{x}_i)}{\hat{q}(\mathbf{x}_i)} \right) \quad (3.3)$$

Drawing from \hat{p} involves selecting a GMM component and then drawing a sample from the corresponding multi-variate Gaussian. Figure 3.4 shows a few examples of samples drawn



(a)



(b)

Figure 3.3: *Centres of the MDL GMM approximation to a typical training face manifold, displayed as images (a) (also see Figure 3.5). These appear to correspond to different pose/illumination combinations. Similarly, centres for a typical face manifold used for recognition are shown in (b). As this manifold corresponds to a video in fixed illumination, the number of Gaussian clusters is much smaller. In this case clusters correspond to different poses only: frontal, looking down, up, left and right.*



Figure 3.4: *Synthetically generated images from a single Gaussian component in a GMM of a training image set. It can be seen that local manifold structure, corresponding to varying head pose in fixed illumination, is well captured.*



Figure 3.5: A training face manifold (blue dots) and the centres of Gaussian clusters of the corresponding MDL GMM model of the data (circles), projected on the first three principal components.

in this manner. In summary, we use the following approximation for the KL divergence between the test set and the k -th subject's training set:

$$D_{KL}(\hat{p}^{(0)} \parallel \hat{p}^{(k)}) \approx \frac{1}{M} \sum_{i=1}^M \log \left(\frac{\hat{p}^{(0)}(\mathbf{x}_i)}{\hat{p}^{(k)}(\mathbf{x}_i)} \right) \quad (3.4)$$

In our experiments we used $M = 1000$ samples.

3.3 Empirical evaluation

We compared the performance of our recognition algorithm on the *CamFace* data set to that of:

- KL divergence-based algorithm of Shakhnarovich et al. (Simple KLD) [Sha02a],
- Mutual Subspace Method (MSM) [Yam98],
- Constrained MSM (CMSM) [Fuk03] which projects the data onto a linear subspace before applying MSM,
- Nearest Neighbour (NN) in the set distance sense; that is, achieving $\min_{\mathbf{x} \in S_0} \min_{\mathbf{y} \in S_i} d(\mathbf{x}, \mathbf{y})$.

In Simple KLD, we used a principal subspace that captured 90% of the data variance. In MSM, the dimensionality of PCA subspaces was set to 9 [Fuk03], with the first three principal angles used for recognition. The constraint subspace dimensionality in CMSM (see [Fuk03]) was chosen to be 70. All algorithms were preceded with PCA performed on the entire dataset, which resulted in dimensionality reduction to 150 (while retaining 95% of the variance).

Table 3.1: *Recognition accuracy (%) of the various methods using different training/testing illumination combinations.*

Method		MDD	Simple KLD	MSM	CMSM	Set NN
Recognition rate	mean	94	69	83	92	89
	std	8	5	10	7	9

In each experiment we used all of the sets from one illumination setup as test inputs and the remaining sets as training data, see Appendix C.

3.3.1 Results

A summary of the experimental results is shown in Table 3.1. Notice the relatively good performance of the simple NN classifier. This supports our intuition that for training, even random illumination variation coupled with head motion is sufficient for gathering a representative set of samples from the illumination-pose face manifold.

Both MSM-based methods scored relatively well, with CMSM achieving the best performance of all of the algorithms besides the proposed method. That is an interesting result, given that this algorithm has not received significant attention in the AFR community; to the best of our knowledge, this is the first report of CMSM’s performance on a data set of this size, with such illumination and pose variability. On the other hand, the lack of a probabilistic model underlying CMSM may make it somewhat less appealing.

Finally, the performance of the two statistical methods evaluated, the Simple KLD method and the proposed algorithm, are very interesting. The former performed worst, while the latter produced the highest recognition rates out of the methods compared. This suggests several conclusions. Firstly, that the approach to statistical modelling of manifolds of faces is a promising research direction. Secondly, it is confirmed that our flexible GMM-based model captures the modes of the data variation well, producing good generalization results even when the test illumination is not present in the training data set. And lastly, our argument in Section 3.2 for the choice of the direction of KL divergence is empirically confirmed, as our method performs well even when the subject’s pose is only very loosely controlled.

3.4 Summary and conclusions

In this chapter we introduced a new statistical approach to face recognition with image sets. Our main contribution is the formulation of a flexible mixture model that is able to accurately capture the modes of face appearance under broad variation in imaging conditions. The basis of our approach is the semi-parametric estimate of probability densities confined to intrinsically low-dimensional, but highly nonlinear face manifolds embedded in the high-dimensional image space. The proposed recognition algorithm is based on a stochastic approximation of Kullback-Leibler divergence between the estimated densities. Empirical evaluation on a database with 100 subjects has shown that the proposed method, integrated into a practical automatic face recognition system, is successful in recognition across illumination and pose. Its performance was shown to match the best performing state-of-the-art method in the literature and exceed others.

Related publications

The following publications resulted from the work presented in this chapter:

- O. Arandjelović, G. Shakhnarovich, J. Fisher, R. Cipolla, and T. Darrell. Face recognition with image sets using manifold density divergence. In *Proc. IEEE Conference on Computer Vision and Pattern Recognition (CVPR)*, **1**:pages 581–588, June 2005. [Ara05b]

4

Unfolding Face Manifolds



Athanadoros, Hagesandros, and Polydoros of Rhodes. *Laocoön and His Sons*
Early 1st century, Marble
Museo Pio Clementino, Vatican

In the previous chapter we addressed the problem of matching a novel face video sequence to a set of faces containing typical, or expected, appearance variations. In this chapter we move away from the assumption of having available such a large training corpus and instead match a novel sequence against a database which too contains only a single sequence per known individual. To solve the problem we propose the *Robust Kernel RAD* algorithm.

Following the adopted appearance-based approach, we motivate the use of the Resistor-Average Distance (RAD) as a dissimilarity measure between densities corresponding to appearances of faces in a single sequence. We then introduce a kernel-based algorithm that makes use of the simplicity of the closed-form expression for RAD between two Gaussian densities, while allowing for modelling of complex but intrinsically low-dimensional face manifolds. Additionally, it is shown how geodesically local appearance manifold structure can be modelled, naturally leading to a stochastic algorithm for generalizing to unseen modes of data variation. On the *CamFace* data set our method is demonstrated to exceed the performance of state-of-the-art algorithms achieving the correct recognition rate of 98% in the presence of mild illumination variations.

4.1 Dissimilarity between manifolds

Consider the Kullback-Leibler $D_{KL}(p||q)$ divergence employed in Chapter 3. As previously discussed, the regions of the observation space that produce a large contribution to $D_{KL}(p||q)$ are those that are well explained by $p(\mathbf{x})$, but not by $q(\mathbf{x})$. The asymmetry of the KL divergence makes it suitable in cases when it is known a priori that one of the densities $p(\mathbf{x})$ or $q(\mathbf{x})$ describes a wider range of data variation than the other. This is conceptually illustrated in Figure 4.1 (a).

However, in the proposed recognition framework, this is not the case – pitch and yaw changes of a face are expected to be the dominant modes of variation in both training and novel data, see Figure 4.2. Additionally, exact head poses assumed by the user are expected to somewhat vary from sequence to sequence and the robustness to variations not seen in either is desired. This motivates the use of a symmetric “distance” measure.

4.1.1 Resistor-Average distance.

We propose to use the Resistor-Average distance (RAD) as a measure of dissimilarity between two probability densities. It is defined as:

$$D_{RAD}(p, q) \doteq [D_{KL}(p||q)^{-1} + D_{KL}(q||p)^{-1}]^{-1} \quad (4.1)$$



(a)



(b)

Figure 4.1: A 1D illustration of the asymmetry of the KL divergence (a). $D_{KL}(q||p)$ is an order of magnitude greater than $D_{KL}(p||q)$ – the “wider” distribution $q(\mathbf{x})$ explains the “narrower” $p(\mathbf{x})$ better than the other way round. In (b), $D_{RAD}(p, q)$ is plotted as a function of $D_{KL}(p||q)$ and $D_{KL}(q||p)$.

Much like the KL divergence from which it is derived, it is nonnegative and equal to zero iff $p(\mathbf{x}) \equiv q(\mathbf{x})$, but unlike it, it is symmetric. Another important property of the Resistor-Average distance is that when two classes of patterns \mathcal{C}_p and \mathcal{C}_q are distributed according to, respectively, $p(\mathbf{x})$ and $q(\mathbf{x})$, $D_{RAD}(p, q)$ reflects the error rate of the Bayes-optimal classifier between \mathcal{C}_p and \mathcal{C}_q [Joh01].

To see in what manner RAD differs from the KL divergence, it is instructive to consider two special cases: when divergences in both directions between two pdfs are approximately equal and when one of them is much greater than the other:

- $D_{KL}(p||q) \approx D_{KL}(q||p) \equiv D$

$$D_{RAD}(p, q) \approx D/2 \tag{4.2}$$

- $D_{KL}(p||q) \gg D_{KL}(q||p)$ or

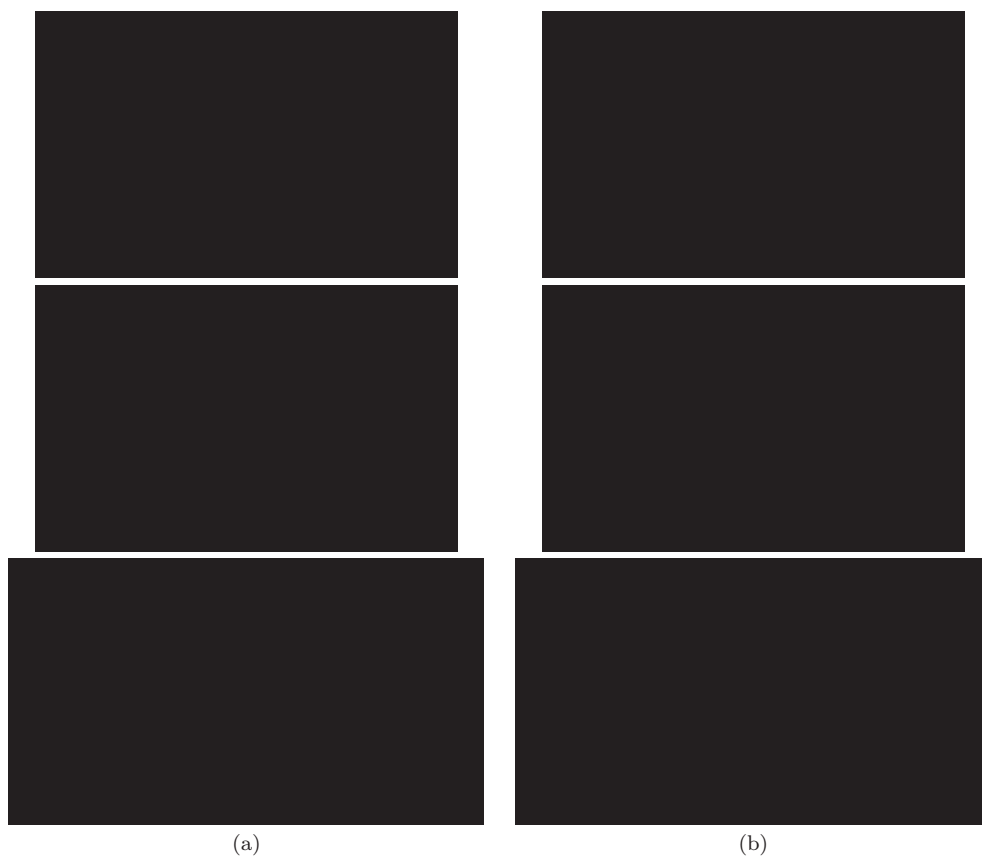


Figure 4.2: A subset of 10 samples from two typical face sets used to illustrate concepts addressed in this chapter (top) and the corresponding patterns in the 3D principal component subspaces (bottom), estimated from data. The sets capture appearance changes of faces of two different individuals as they performed unconstrained head motion in front of a fixed camera. The corresponding pattern variations (blue circles) are highly nonlinear, with a number of outliers present (red stars).

$$D_{KL}(p||q) \ll D_{KL}(q||p)$$

$$D_{RAD}(p, q) \approx \min(D_{KL}(p||q), D_{KL}(q||p)) \quad (4.3)$$

It can be seen that RAD very much behaves like a smooth min of $D_{KL}(p||q)$ and $D_{KL}(q||p)$ (up to a multiplicative constant), also illustrated in Figure 4.1 (b).

4.2 Estimating RAD for nonlinear densities

Following the choice of the Resistor-Average distance as a means of quantifying the similarity of manifolds, we turn to the question of estimating this distance for two arbitrary, nonlinear face manifolds. For a general case there is no closed-form expression for RAD. However, when $p(\mathbf{x})$ and $q(\mathbf{x})$ are two normal distributions [Yos99]:

$$D_{KL}(p||q) = \frac{1}{2} \log_2 \left(\frac{|\Sigma_q|}{|\Sigma_p|} \right) + \frac{1}{2} \text{Tr} \left[\Sigma_p \Sigma_q^{-1} + \Sigma_q^{-1} (\bar{\mathbf{x}}_q - \bar{\mathbf{x}}_p) (\bar{\mathbf{x}}_q - \bar{\mathbf{x}}_p)^T \right] - \frac{D}{2} \quad (4.4)$$

where D is the dimensionality of data, $\bar{\mathbf{x}}_p$ and $\bar{\mathbf{x}}_q$ data means, and Σ_p and Σ_q the corresponding covariance matrices.

To achieve both expressive modelling of nonlinear manifolds as well as an efficient procedure for comparing them, in the proposed method a nonlinear projection of data using Kernel Principal Component Analysis (Kernel PCA) is performed first. We show that with an appropriate choice of the kernel type and bandwidth, the assumption of normally distributed face patterns in the projection space produces good KL divergence estimates. With a reference to our generative model in (3.1), an appearance manifold is effectively unfolded from the embedding image space.

4.3 Kernel PCA

PCA is a technique in which an orthogonal basis transformation is applied such that the data covariance matrix $\mathbf{C} = \langle (\mathbf{x}_i - \langle \mathbf{x}_j \rangle) (\mathbf{x}_i - \langle \mathbf{x}_j \rangle)^T \rangle$ is diagonalized. When data $\{\mathbf{x}_i\}$ lies on a linear manifold, the corresponding linear subspace is spanned by the dominant (in the eigenvalue sense) eigenvectors of \mathbf{C} . However, in the case of nonlinearly distributed data, PCA does not capture the true modes of variation well.

The idea behind KPCA is to map data into a high-dimensional space in which it is approximately linear – then the true modes of data variation can be found using standard PCA. Performing this mapping explicitly is prohibitive for computational reasons and inherently problematic due to the “curse of dimensionality”. This is why a technique widely known as the “kernel trick” is used to implicitly realize the mapping. Let function Φ map the original data from input space to a high-dimensional feature space in which it is (approximately) linear, $\Phi : \mathbb{R}^D \rightarrow \mathbb{R}^\Delta$, $\Delta \gg D$. In KPCA the choice of mappings Φ is restricted to the set such that there is a function k (the kernel) for which:

$$\Phi(\mathbf{x}_i)^T \Phi(\mathbf{x}_j) = k(\mathbf{x}_i, \mathbf{x}_j) \quad (4.5)$$

In this case, the principal components of the data in \mathbb{R}^Δ space can be found by performing computations in the input, \mathbb{R}^D space only.

Assuming zero-centred data in the feature space (for information on centring data in the feature space as well as a more detailed treatment of KPCA see [Sch99]), the problem of finding principal components in this space is equivalent to solving the eigenvalue problem:

$$\mathbf{K}\mathbf{u}_i = \lambda_i \mathbf{u}_i \quad (4.6)$$

where \mathbf{K} is the kernel matrix:

$$\mathbf{K}_{j,k} = k(\mathbf{x}_j, \mathbf{x}_k) = \Phi(\mathbf{x}_j)^T \Phi(\mathbf{x}_k) \quad (4.7)$$

The projection of a data point \mathbf{x} to the i -th kernel principal component is computed using the following expression [Sch99]:

$$a_i = \sum_{m=1}^N u_i^{(m)} k(\mathbf{x}_m, \mathbf{x}) \quad (4.8)$$

4.4 Combining RAD and kernel PCA

The variation of face patterns is highly nonlinear (see Figure 4.3 (a)), making the task of estimating RAD between two sparsely sampled face manifolds in the image space difficult. The approach taken in this work is that of mapping the data from the input, image space into a space in which it lies on a nearly linear manifold. As before, we would not like to compute this mapping explicitly. Also, note that the inversions of data covariance matrices and the computation of their determinants in the expression for the KL divergence between two normal distributions (4.4) limit the maximal practical dimensionality of the feature space.

In our method both of these problems are solved using Kernel PCA. The key observation is that regardless of how high the feature space dimensionality is, the data has covariance in at most N directions, where N is the number of data points. Therefore, given two data sets of faces, each describing a smooth manifold, we first find the kernel principal components of their union. After dimensionality reduction is performed by projecting the data onto the first M kernel principal components, the RAD between the two densities, each now assumed Gaussian, is computed. Note that the implicit nonlinear map is different for each data set pair. The importance of this can be seen by noticing that the intrinsic dimensionality of the manifold that *both* sets lie on is lower than of the manifold that all data in a database lies

on, resulting in its more accurate “unfolding”, see Figure 4.3 (b).

We estimate covariance matrices in the Kernel PCA space using probabilistic PCA (PPCA) [Tip99b]. In short, probabilistic PCA is an extension of the traditional PCA that recovers parameters of a linear generative model of data (i.e. the full corresponding covariance matrix), with the assumption of isotropic Gaussian noise: $\mathbf{C} = \mathbf{V}\mathbf{\Lambda}\mathbf{V}^T + \sigma\mathbf{I}$. Note the model of noise density in (3.1) that this assumption implies: $g^{(i)}(p_n(\mathbf{x})) \sim \mathcal{N}(\mathbf{0}, \sigma\mathbf{I})$, where $g^{(i)}(f^{(i)}(\mathbf{x})) = \mathbf{x}$.



(a)



(b)

Figure 4.3: A typical face motion manifold in the input, image space exhibits high nonlinearity (a). The “unfolded” manifold is shown in (b). It can be seen that Kernel PCA captures the modes of data variation well, producing a Gaussian-looking distribution of patterns, confined to a roughly 2-dimensional space (corresponding to the intrinsic dimensionality of the manifold). In both (a) and (b) shown are projections to the first three principal components.

4.5 Synthetically repopulating manifolds

In most applications, due to the practical limitations in the data acquisition process, AFR algorithms have to work with sparsely populated face manifolds. Furthermore, some modes of data variation may not be present in full. Specifically, in the AFR for authentication setup considered in this work, the practical limits on how long the user can be expected to wait for verification, as well as how controlled his motion can be required to be, limit the

possible variations that are seen in both training and novel video sequences. Finally, noise in the face localization process increases the dimensionality of the manifolds faces lie on, effectively resulting in even less densely populated manifolds. For a quantitative insight, it is useful to mention that the face appearance variations present in a typical video sequence used in evaluation in this chapter typically lie on a manifold of intrinsic dimensionality of 3-7, with 85 samples on average.

In this work, appearance manifolds are synthetically repopulated in a manner that achieves both higher manifold sample density, as well as some generalization to unseen modes of variation (see work by Martinez [Mar02], and Sung and Poggio [Sun98] for related approaches). To this end, we use domain-specific knowledge to learn face transformations in a more sophisticated way than could be realized by simple interpolation and extrapolation.

Given an image of a face, \mathbf{x} , we stochastically repopulate its geodesic neighbourhood by a set of novel images $\{\mathbf{x}_j^S\}$. Under the assumption that the embedding function $f^{(i)}$ in (3.1) is smooth, geodesically close images correspond to small changes in the imaging parameters (e.g. yaw or pitch). Therefore, using the first-order Taylor approximation of the effects of a projective camera, the face motion manifold is locally similar to the *affine warp* manifold of \mathbf{x} . The proposed algorithm then consists of random draws of a face image \mathbf{x} from the data, stochastic perturbation of \mathbf{x} by a set of affine warps $\{\mathbf{A}_j\}$ and finally, the augmentation of data by the warped images – see Figure 4.6. Writing the affine warp matrix decomposed to rotation and translation, skew and scaling:

$$\mathbf{A} = \begin{pmatrix} \cos \theta & -\sin \theta & t_x \\ \sin \theta & \cos \theta & t_y \\ 0 & 0 & 1 \end{pmatrix} \begin{pmatrix} 1 & k & 0 \\ 0 & 1 & 0 \\ 0 & 0 & 1 \end{pmatrix} \begin{pmatrix} 1 + s_x & 0 & 0 \\ 0 & 1 + s_y & 0 \\ 0 & 0 & 1 \end{pmatrix} \quad (4.9)$$

in the proposed method, affine transformation parameters θ , t_x and t_y , k , and s_x and s_y are drawn from zero-mean Gaussian densities.

4.5.1 Outlier rejection

In most cases, automatic face detection in cluttered scenes will result in a considerable number of incorrect localizations – *outliers*. Typical outliers produced by the Viola-Jones face detector employed in this chapter are reproduced from Appendix C in Figure 4.5.

Note that due to the complexity of face manifolds, outliers cannot be easily removed in the input space. On the other hand, outlier rejection after Kernel PCA-based manifold “unfolding” is trivial. However, a way of computing the kernel matrix robust to the presence of outliers is needed. To this end, our algorithm uses RANSAC [Fis81] with an underlying Kernel PCA model. The application of RANSAC in the proposed framework is summarized



Figure 4.4: *The original, input data (dots) and the result of stochastically repopulating the corresponding manifold (circles). A few samples from the dense result are shown as images, demonstrating that the proposed method successfully captures and extrapolates the most significant modes of data variation.*



Figure 4.5: *Typical false face detections identified by our algorithm.*

in Figure 4.6. Finally, the Robust Kernel RAD algorithm proposed in this chapter is in its entirety shown in Figure 4.7.

4.6 Empirical evaluation

We compared the recognition performance of the following methods¹ on the *CamFace* data set:

- KL divergence-based algorithm of Shakhnarovich et al. (Simple KLD) [Sha02a],
- Simple RAD (based on Simple KLD),
- Kernelized Simple KLD algorithm (Kernel KLD),
- Kernel RAD,

¹Methods were reimplemented through consultation with authors.

Input: set of observations $\{\mathbf{x}_i\}$,
KPCA space dimensionality D .
Output: kernel principal components $\{\mathbf{u}_i\}$.

1: Initialize best minimal sample
 $\mathcal{B} = \emptyset$

2: RANSAC iteration
for $it = 0$ to $LIMIT$

3: Random sample draw
 $\{y_i\} \stackrel{D}{\leftarrow} \{x_i\}$

4: Kernel PCA
 $\{u_i\} = \text{KPCA}(\{y_i\})$

5: Nonlinear projection
 $\{x_i^P\} \stackrel{\{u_i\}}{\leftarrow} \{x_i\}$

6: Consistent data
 $\mathcal{B}_{it} = |\text{filter}(D_{MAH}(x_i, 0) < T)|$

7: Update best minimal sample
 $|\mathcal{B}_{it}| > |\mathcal{B}| ? \mathcal{B} = \mathcal{B}_{it}$

8: Kernel PCA using best minimal sample
 $\{u_i\} = \text{KPCA}(\mathcal{B})$

Figure 4.6: *RANSAC Kernel PCA algorithm for unfolding face appearance manifolds in the presence of outliers.*

- Robust Kernel RAD,
- Mutual Subspace Method (MSM) [Yam98],
- Majority vote using Eigenfaces, and
- Nearest Neighbour (NN) in the set distance sense; that is, achieving $\min_{\mathbf{x} \in S_0} \min_{\mathbf{y} \in S_i} \|\mathbf{x} - \mathbf{y}\|_2$.

In all KLD and RAD-based methods, 85% of data energy was explained by the principal subspaces. In non-kernelized algorithms this typically resulted in the principal subspace

Input: sets of observations $\{\mathbf{a}_i\}, \{\mathbf{b}_i\}$.
 KPCA space dimensionality D .
Output: inter-manifold distance $D_{RAD}(\{\mathbf{a}_i\}, \{\mathbf{b}_i\})$.

1: Inliers with RANSAC

$$\mathcal{V} = \{\mathbf{a}_i^V\}, \{\mathbf{b}_i^V\} = \text{RANSAC}(\{\mathbf{a}_i\}, \{\mathbf{b}_i\})$$

2: Synthetic data

$$\mathcal{S} = \{\mathbf{a}_i^S\}, \{\mathbf{b}_i^S\} = \text{perturb}(\langle \mathbf{a}^V \rangle, \langle \mathbf{b}^V \rangle)$$

3: RANSAC Kernel PCA

$$\{\mathbf{u}_i\} = \text{KPCA}(\mathcal{V} \cup \mathcal{S})$$

4: Nonlinear projection

$$\{\mathbf{a}_i^P\}, \{\mathbf{b}_i^P\} \xleftarrow{\{\mathbf{u}_i\}} (\mathcal{V}, \mathcal{S})$$

7: Closed-form RAD

$$D_{RAD}(\{\mathbf{a}_i^P\}, \{\mathbf{b}_i^P\})$$

Figure 4.7: *Robust Kernel RAD algorithm summary.*

dimensionality of 16, see Figure 4.8. In MSM, first 3 principal angles were used for recognition, while the dimensionality of PCA subspaces describing the data was set to 9 [Yam98]. In the Eigenfaces method, the 150-dimensional principal subspace used explained $\sim 95\%$ of data energy. A 20-dimensional nonlinear projection space was used in all kernel-based methods with the RBF kernel $k(\mathbf{x}_i, \mathbf{x}_j) = \exp -\gamma(\mathbf{x}_i - \mathbf{x}_j)^T(\mathbf{x}_i - \mathbf{x}_j)$. The optimal value of the parameter γ was learnt by optimizing the recognition performance on a 20 person training data set. Note that people from this set were not included in the evaluation reported in Section 4.6.1. We used $\gamma = 0.380$ for greyscale images normalized to have pixel values in the range $[0.0, 1.0]$.

In each experiment we used sets in a single illumination setup, with test and training sets corresponding to sequences acquired in two different sessions, see Appendix C.

4.6.1 Results

The performance of the evaluated recognition algorithms is summarized in Table 4.1. The results suggest a number of conclusions.

Firstly, note the relatively poor performance of the two nearest neighbour-type methods – the Set NN and the Majority vote using Eigenfaces. These can be considered as a proxy for



Figure 4.8: *Histograms of the dimensionality of the principal subspace in kernelized (dotted line) and non-kernelized (solid line) KL divergence-based methods, across the evaluation data set. The corresponding average dimensionalities were found to be ~ 4 and ~ 16 . The large difference illustrates the extent of nonlinearity of face motion manifolds.*

gauging the difficulty of the recognition task, seeing that both can be expected to perform relatively well if the imaging conditions are not greatly different between training and test data sets. An inspection of the incorrect recognitions of these methods offered an interesting insight in one of their particular weaknesses, see Figure 4.9 (a). This reaffirms the conclusion of [Sim04], showing that it is not only *changes* in the data acquisition conditions that are challenging but also that there are certain intrinsically difficult imaging configurations.

The Simple KLD method consistently achieved the poorest results. We believe that the likely reason for this is the high nonlinearity of face manifolds corresponding to the training sets used, caused by near, office lighting used to vary the illumination conditions. This is supported by the dramatic and consistent increase in the recognition performance with kernelization. This result confirms the first premise of this work, showing that sophisticated face manifold modelling is indeed needed to accurately describe variations that are expected in realistic imaging conditions. Furthermore, the improvement observed with the use of Resistor-Average distance suggests its greater robustness with respect to unseen variations in face appearance, compared to the KL divergence. The performance of Kernel RAD was comparable to that of MSM, which ranked second-best in our experiments. The best performing algorithm was found to be Robust Kernel RAD. Synthetic manifold repopulation produced a significant improvement in the recognition rate (of about 10%), the proposed method correctly recognizing 98% of individuals. ROC curves corresponding to the methods that best illustrate the contributions of this chapter are shown in Figure 4.9 (b), with Robust Kernel RAD achieving an Equal Error Rate of 2%.

Table 4.1: Results of the comparison of our novel algorithm with existing methods in the literature. Shown is the identification rate in %.

Method	Robust Kernel RAD	MSM	Kernel RAD	Kernel KLD	Set Nearest Neighbour	Majority Vote w/ Eigenfaces	Simple KLD
Recognition rate	98	89	88	79	72	71	52

4.7 Summary and conclusions

In this chapter we introduced a novel method for face recognition from face appearance manifolds due to head motion. In the proposed algorithm the Resistor-Average distance computed on nonlinearly mapped data using Kernel PCA is used as a dissimilarity measure between distributions of face appearance, derived from video. A data-driven approach to generalization to unseen modes of variation was described, resulting in stochastic manifold repopulation. Finally, the proposed concepts were empirically evaluated on a database with 100 individuals and mild illumination variation. Our method consistently achieved a high recognition rate, on average correctly recognizing in 98% of the cases and outperforming state-of-the-art algorithms in the literature.

Related publications

The following publications resulted from the work presented in this chapter:

- O. Arandjelović and R. Cipolla. Face recognition from face motion manifolds using robust kernel resistor-average distance. In *Proc. IEEE Workshop on Face Processing in Video*, **5**:page 88, June 2004. [Ara04b]
- O. Arandjelović and R. Cipolla. An information-theoretic approach to face recognition from face motion manifolds. *Image and Vision Computing (special issue on Face Processing in Video Sequences)*, **24**(6):pages 639–647, June 2006. [Ara06e]

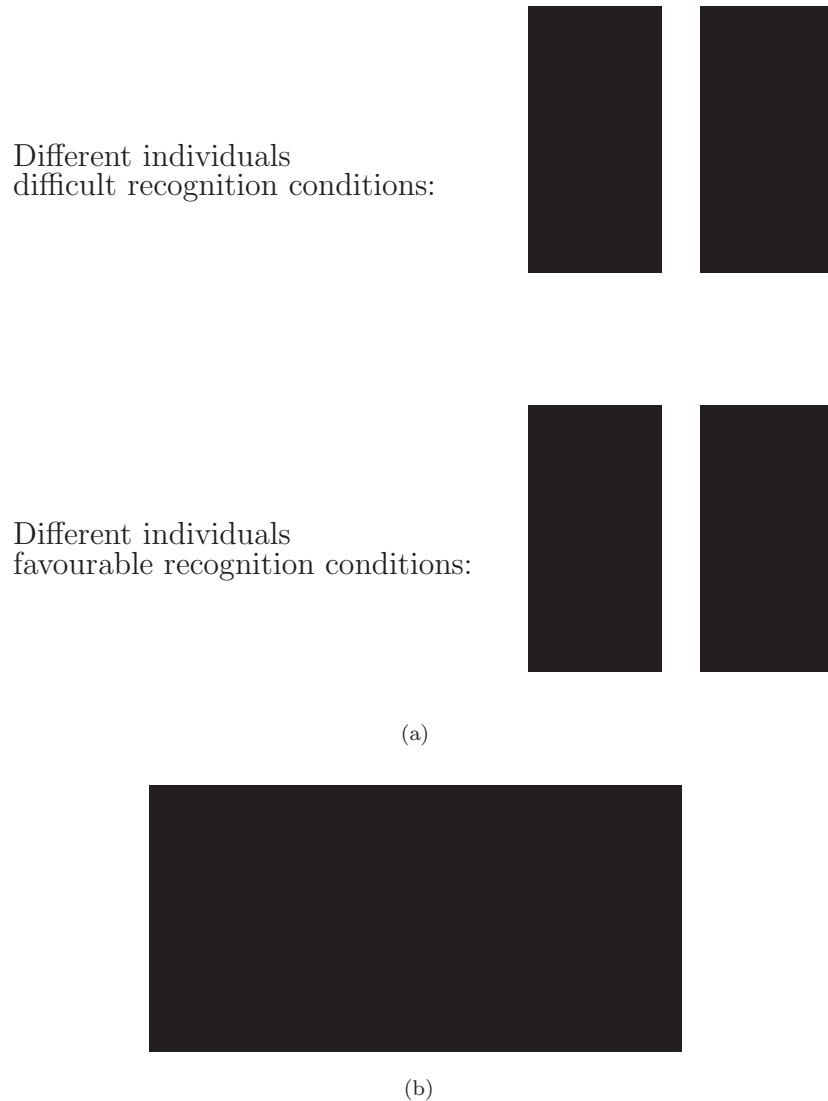


Figure 4.9: (a) The most common failure mode of NN-type recognition algorithms is caused by “hard” illumination conditions and head poses. The two top images show faces that due to severe illumination conditions and semi-profile head orientation look very similar in spite of different identities (see [Sim04]) – the Set NN algorithm incorrectly classified these faces as belonging to the same person. Information from other frames (e.g. the two bottom images) is not used to achieve increased robustness. (b) Receiver Operator Characteristic (ROC) curves of the Simple KLD, MSM, Kernel KLD and the proposed Robust Kernel RAD methods. The latter exhibits superior performance, achieving an Equal Error Rate of 2%.

5

Fusing Visual and Thermal Face Biometrics



Claude Monet, Haystack
Oil on canvas, 73.3 x 92.6 cm
Museum of Fine Arts, Boston

In the preceding chapters we dealt with increasingly difficult formulations of the face recognition problem. As restrictions on both training and novel data were relaxed, more generalization was required. So far we addressed robustness to pose changes of the user, noise contamination and low spatiotemporal resolution of video. In this chapter we start exploring the important but difficult problem of recognition in the presence of changing illumination conditions in which faces are imaged.

In practice, the effects of changing pose are usually least problematic and can often be overcome by acquiring data over a time period e.g. by tracking a face in a surveillance video. As before, we assume that the training image set for each individual contains some variability in pose, but is not obtained in scripted conditions or in controlled illumination.

In contrast, illumination is much more difficult to deal with: the illumination setup is in most cases not practical to control and its physics is difficult to accurately model. Biometric imagery acquired in the thermal, or near-infrared electromagnetic spectrum, is useful in this regard as it is virtually insensitive to illumination changes. On the other hand, it lacks much of the individual, discriminating facial detail contained in visual images. In this sense, the two modalities can be seen as complementing each other. The key idea behind the system presented in this chapter is that robustness to extreme illumination changes can be achieved by fusing the two. This paradigm will further prove useful when we consider the difficulty of recognition in the presence of occlusion caused by prescription glasses.

5.1 Face recognition in the thermal spectrum

A number of recent studies suggest that face recognition in the thermal spectrum offers a few distinct advantages over the visible spectrum, including invariance to ambient illumination changes [Wol01, Soc03, Pro00, Soc04]. This is due to the fact that a thermal infrared sensor measures the heat energy radiation emitted by the face rather than the light reflectance. In outdoor environments, and particularly in direct sunlight, illumination invariance only holds true to good approximation for the Long-Wave Infrared (LWIR: 8–14 μm) spectrum, which is fortunately measured by the less expensive uncooled thermal infrared camera technology. Human skin has high emissivity in the Long-Wave Infrared (MWIR: 3–5 μm) spectrum and even higher emissivity in the LWIR spectrum making face imagery by and large invariant to illumination variations in these spectra.

Appearance-based face recognition algorithms applied to thermal infrared imaging consistently performed better than when applied to visible imagery, under various lighting conditions and facial expressions [Kon05, Soc02, Soc03, Sel02]. Further performance improvements were achieved using decision-based fusion [Soc03]. In contrast to other techniques,

Srivastana and Liu [Sri03], performed face recognition in the space of Bessel function parameters. First, they decompose each infrared face image using Gabor filters. Then, they represent the face by modelling the marginal density of the Gabor filter coefficients using Bessel functions. This approach has further been improved by Buddharaju *et al.* [Bud04]. Recently, Friedrich and Yeshurun [Fri03] showed that IR-based recognition is less sensitive to changes in 3D head pose and facial expression.

A thermal sensor generates imaging features that uncover thermal characteristics of the face pattern. Another advantage of thermal infrared imaging in face recognition is the existence of a direct relationship to underlying physical anatomy such as vasculature. Indeed, thermal face recognition algorithms attempt to take advantage of such anatomical information of the human face as unique signatures. The use of vessel structure for human identification has been studied during recent years using traits such as hand vessel patterns [Lin04, Im03], finger vessel patterns [Shi04, Miu04] and vascular networks from thermal facial images [Pro98]. In [Bud05] a novel methodology that consists of a statistical face segmentation and a physiological feature extraction algorithm, and a matching procedure of the vascular network from thermal facial imagery has been proposed.

The downside of employing near infrared and thermal infrared sensors is that glare reflections and opaque regions appear in presence of subjects wearing prescription glasses, plastic and sun glasses. For a large proportion of individuals the regions around the eyes – that is an area of high interest to face recognition systems – become occluded and therefore less discriminant [Ara06h, Li07].

5.1.1 Multi-sensor based techniques

In the biometric literature several classifiers have been used to concatenate and consolidate the match scores of multiple independent matchers of biometric traits [Cha99] [BY98, Big97, Ver99, Wan03b]. In [Bru95a] a HyperBF network is used to combine matchers based on voice and face features. Ross and Jain [Ros03] use decision tree and linear discriminant classifiers for classifying the match scores pertaining to the face, fingerprint and hand geometry modalities. In [Ros05] three different colour channels of a face image are independently subjected to LDA and then combined.

Recently, several successful attempts have been made to fuse the visual and thermal infrared modalities to increase the performance of face recognition [Heo04, Gya04, Soc04, Wan04b, Che05, Kon05, Bru95a, Ros03, Che03, Heo03a]. Visible and thermal sensors are well-matched candidates for image fusion as limitations of imaging in one spectrum seem to be precisely the strengths of imaging in the other. Indeed, as the surface of the face and its temperature have nothing in common, it would be beneficial to extract and fuse cues from

both sensors that are not redundant and yet complementary.

In [Heo04] two types of visible and thermal fusion techniques have been proposed. The first fuses low-level data while the second fuses matching distance scores. Data fusion was implemented by applying pixel-based weighted averaging of co-registered visual and thermal images. Decision fusion was implemented by combining the matching scores of individual recognition modules.

The fusion at the score level is the most commonly considered approach in the biometric literature [Ros06]. Cappelli et al. [Cap00] use a *double sigmoid function* for score normalization in a multi-biometric system that combines different fingerprint matchers. Once the match scores output by multiple matchers are transformed into a common domain they can be combined using simple fusion operators such as the sum of scores, product of scores or order statistics (e.g., maximum/minimum of scores or median score). Our proposed method falls into this category of multi-sensor fusion at the score level. To deal with occlusions caused by eyeglasses in thermal imagery, Heo et al. [Heo04] used a simple ellipse fitting technique to detect the circle-like eyeglass regions in the IR image and replaced them with an average eye template. Using a commercial face recognition system, FaceIt [Ide03], they demonstrated improvements in face recognition accuracy. Our method differs both in the glasses detection stage, which uses a principled statistical model of appearance variation, and in the manner it handles detected occlusions. Instead of using the average eye template, which carries no discriminative information, we segment out the eye region from the infrared data, effectively placing more weight on the discriminative power of the same region extracted from the filtered, visual imagery.

5.2 Method details

In the sections that follow we explain our system in detail, the main components of which are conceptually depicted in Figure 5.1.

5.2.1 Matching image sets

As before, in this chapter too we deal with face recognition from sets of images, both in the visual and thermal spectrum. We will show how to achieve illumination invariance using a combination of simple data preprocessing (Section 5.2.2), a combination of holistic and local features (Section 5.2.3) and the fusion of two modalities (see Section 5.2.4). These stages normalize for the bulk of appearance changes caused by extrinsic (non person-specific) factors. Hence, the requirements for our basic set-matching algorithm are those of (i) some pose generalization and (ii) robustness to noise. We compare two image sets by modelling



Figure 5.1: *Our system consists of three main modules performing (i) data preprocessing and registration, (ii) glasses detection and (iii) fusion of holistic and local face representations using visual and thermal modalities.*

the variations within a set using a linear subspace and comparing two subspaces by finding the most similar modes of variation within them.

The face appearance modelling step is a simple application of Principal Component Analysis (PCA) without mean subtraction. In other words, given a data matrix \mathbf{d} (each column representing a rasterized image), the corresponding subspace is spanned by the eigenvectors of the matrix $\mathbf{C} = \mathbf{d}\mathbf{d}^T$ corresponding to the largest eigenvalues; we used 5D subspaces, as sufficiently expressive to on average explain over 90% of data variation within intrinsically low-dimensional face appearance changes in a set.

We next formally introduce the concept of principal angles and motivate their application for face image set comparison. We show that they can be used to efficiently extract the most similar appearance variation modes within two sets.

Principal angles

Principal, or canonical, angles $0 \leq \theta_1 \leq \dots \leq \theta_D \leq (\pi/2)$ between two D -dimensional linear subspaces U_1 and U_2 are recursively uniquely defined as the minimal angles between any two vectors of the subspaces [Hot36]:

$$\rho_i = \cos \theta_i = \max_{\mathbf{u}_i \in U_1} \max_{\mathbf{v}_i \in U_2} \mathbf{u}_i^T \mathbf{v}_i \quad (5.1)$$

subject to the orthonormality condition:

$$\mathbf{u}_i^T \mathbf{u}_i = \mathbf{v}_i^T \mathbf{v}_i = 1, \quad \mathbf{u}_i^T \mathbf{u}_j = \mathbf{v}_i^T \mathbf{v}_j = 0, \quad j = 1, \dots, i-1 \quad (5.2)$$

We will refer to \mathbf{u}_i and \mathbf{v}_i as the i -th pair of *principal vectors*, see Figure 5.2 (a). The quantity ρ_i is also known as the i -th canonical correlation [Hot36]. Intuitively, the first pair

of principal vectors corresponds to the most similar modes of variation within two linear subspaces; every next pair to the most similar modes orthogonal to all previous ones. We quantify the similarity of subspaces U_1 and U_2 , corresponding to two face sets, by the cosine of the smallest angle between two vectors confined to them i.e. ρ_1 .

This interpretation of principal vectors motivates the suitability of canonical correlations as a similarity measure when subspaces U_1 and U_2 correspond to face images. First, the empirical observation that face appearance varies smoothly as a function of camera viewpoint [Ara06b, Bic94] is implicitly exploited: since the computation of the most similar modes of appearance variation between sets can be seen as an efficient “search” over entire subspaces, *generalization* by means of linear pose interpolation and extrapolation is inherently achieved. This concept is further illustrated in Figure 5.2 (b,c). Furthermore, by being dependent on only a single (linear) direction within a subspace, by employing the proposed similarity measure the bulk of data in each set, deemed not useful in a specific set-to-set comparison, is thrown away. In this manner *robustness to missing data* is achieved.

An additional appealing feature of comparing two subspaces in this manner is contained in its computational efficiency. If \mathbf{B}_1 and \mathbf{B}_2 are orthonormal basis matrices corresponding to U_1 and U_2 , then writing the Singular Value Decomposition (SVD) of the matrix $\mathbf{B}_1^T \mathbf{B}_2$:

$$\mathbf{M} = \mathbf{B}_1^T \mathbf{B}_2 = \mathbf{U} \mathbf{\Sigma} \mathbf{V}^T. \quad (5.3)$$

The i -th canonical correlation ρ_i is then given by the i -th singular value of \mathbf{M} i.e. $\Sigma_{i,i}$, and the i -th pair of principal vectors \mathbf{u}_i and \mathbf{v}_i by, respectively, $\mathbf{B}_1 \mathbf{U}$ and $\mathbf{B}_2 \mathbf{V}$ [Bjö73]. Seeing that in our case \mathbf{M} is a 5×5 matrix and that we only use the largest canonical correlation, ρ_1 can be rapidly computed as the largest eigenvalue of $\mathbf{M} \mathbf{M}^T$ [Pre92].

5.2.2 Data preprocessing & feature extraction

The first stage of our system involves coarse normalization of pose and illumination. Pose changes are accounted for by in-plane registration of images, which are then passed through quasi illumination-invariant image filters.

We register all faces, both in the visual and thermal domain, to have the salient facial features aligned. Specifically, we align the eyes and the mouth due to the ease of detection of these features (e.g. see [Ara05c, Ber04, Cri04, Fel05, Tru05]). The 3 point correspondences, between the detected and the canonical features’ locations, uniquely define an affine transformation which is applied to the original image. Faces are then cropped to 80×80 pixels, as shown in Figure 5.3.

Coarse brightness normalization is performed by band-pass filtering the images [Ara05c,

Fit02]. The aim is to reduce the amount of high-frequency noise as well as extrinsic appearance variations confined to a low-frequency band containing little discriminating information. Most obviously, in visual imagery, the latter are caused by illumination changes, owing to the smoothness of the surface and albedo of faces [Adi97].

We consider the following type of a band-pass filter:

$$\mathbf{I}_F = \mathbf{I} * \mathbf{G}_{\sigma=W_1} - \mathbf{I} * \mathbf{G}_{\sigma=W_2}, \quad (5.4)$$

which has two parameters - the widths W_1 and W_2 of isotropic Gaussian kernels. These are estimated from a small training corpus of individuals in different illuminations. Figure 5.4 shows the recognition rate across the corpus as the values of the two parameters are varied. The optimal values were found to be 2.3 and 6.2 for visual data; the optimal filter for thermal data was found to be a *low-pass* filter with $W_2 = 2.8$ (i.e. W_1 was found to be very large). Examples are shown in Figure 5.5. It is important to note from Figure 5.4 that the recognition rate varied smoothly with changes in kernel widths, showing that the method is not very sensitive to their exact values, which is suggestive of good generalization to unseen data.

The result of filtering visual data is further scaled by a smooth version of the original image:

$$\hat{\mathbf{I}}_F(x, y) = \mathbf{I}_F(x, y) ./ (\mathbf{I} * \mathbf{G}_{\sigma=W_2}), \quad (5.5)$$

where $./$ represents element-wise division. The purpose of local scaling is to equalize edge strengths in dark (weak edges) and bright (strong edges) regions of the face; this is similar to the Self Quotient Image of Wang *et al.* [Wan04a]. This step further improves the robustness of the representation to illumination changes, see Section 5.3.

5.2.3 Single modality-based recognition

We compute the similarity of two individuals using only a single modality (visual or thermal) by combining the holistic face representation described in Section 5.2.2 and a representation based on local image patches. These have been shown to benefit recognition in the presence of large pose changes [Siv05].

As before, we use the eyes and the mouth as the most discriminative regions, by extracting rectangular patches centred at the detections, see Figure 5.6. The overall similarity score is obtained by weighted summation:

$$\rho_{v/t} = \underbrace{\omega_h \cdot \rho_h}_{\text{Holistic contribution}} + \underbrace{\omega_m \cdot \rho_m + (1 - \omega_h - \omega_m) \cdot \rho_e}_{\text{Local features contribution}}, \quad (5.6)$$

where ρ_m , ρ_e and ρ_h are the scores of separately matching, respectively, the mouth, the eyes and the entire face regions, and ω_h and ω_m the weighting constants.

The optimal values of the weights were estimated from the offline training corpus. As expected, eyes were shown to carry a significant amount of discriminative information, as for the visual spectrum we obtained $\omega_e = 0.3$. On the other hand, the mouth region, highly variable in appearance in the presence of facial expression changes, was found not to improve recognition (i.e. $\omega_m \approx 0.0$).

The relative magnitudes of the weights were found to be different in the thermal spectrum, both the eye and the mouth region contributing equally to the overall score: $\omega_m = 0.1$, $\omega_h = 0.8$. Notice the rather insignificant contribution of individual facial features. This is most likely due to inherently spatially slowly varying nature of heat radiated by the human body.

5.2.4 Fusing modalities

Until now we have focused on deriving a similarity score between two individuals given sets of images in either thermal or visual spectrum. A combination of holistic and local features was employed in the computation of both. However, the greatest power of our system comes from the fusion of the two modalities.

Given ρ_v and ρ_t , the similarity scores corresponding to visual and thermal data, we compute the joint similarity as:

$$\rho_f = \underbrace{\omega_v(\rho_v) \cdot \rho_v}_{\text{Optical contribution}} + \underbrace{[1 - \omega_v(\rho_v)] \cdot \rho_t}_{\text{Thermal contribution}}. \quad (5.7)$$

Notice that the weighting factors are no longer constants, but *functions*. The key idea is that if the visual spectrum match is very good (i.e. ρ_v is close to 1.0), we can be confident that illumination difference between the two images sets compared is mild and well compensated for by the visual spectrum preprocessing of Section 5.2.2. In this case, visual spectrum should be given relatively more weight than when the match is bad and the illumination change is likely more drastic. The value of $\omega_v(\rho_v)$ can then be interpreted as statistically the optimal choice of the mixing coefficient ω_v given the visual domain similarity ρ_v . Formalizing this we can write

$$\omega_v(\rho_v) = \arg \max_{\omega} p(\omega | \rho_v), \quad (5.8)$$

or, equivalently

$$\omega_v(\rho_v) = \arg \max_{\omega} \frac{p(\omega, \rho_v)}{p(\rho_v)}. \quad (5.9)$$

Under the assumption of a uniform prior on the degree of visual similarity, $p(\rho_v)$

$$p(\alpha|\rho_v) \propto p(\alpha, \rho_v), \quad (5.10)$$

and

$$\omega_v(\rho_v) = \arg \max_{\omega} p(\omega, \rho_v). \quad (5.11)$$

Learning the weighting function

The function $\omega_v \equiv \omega_v(\rho_v)$ is estimated in three stages: first (i) we estimate $p(\omega_v, \rho_v)$, then (ii) compute $\omega(\rho_v)$ using (5.11) and finally (iii) make an analytic fit to the obtained marginal distribution. Step (i) is challenging and we describe it next.

Iterative density estimate The principal difficulty of estimating $p(\omega_v, \rho_v)$ is of practical nature: in order to obtain an accurate estimate (i.e. a well-sampled distribution), a prohibitively large training database is needed. Instead, we employ a heuristic alternative. Much like before, the estimation is performed using the offline training corpus.

Our algorithm is based on an iterative incremental update of the density, initialized as uniform over the domain $\omega_v, \rho_v \in [0, 1]$. We iteratively simulate matching of an unknown person against a set gallery individuals. In each iteration of the algorithm, these are randomly drawn from the offline training database. Since the ground truth identities of all persons in the offline database are known, for each $\omega_v = k\Delta\omega_v$ we can compute (i) the initial visual spectrum similarity $\rho_v^{p,p}$ of the novel and the corresponding gallery sequences, and (ii) the resulting separation $\delta(k\Delta\omega_v)$ i.e. the difference between the similarities of the test set and the set corresponding to it in identity, and that between the test set and the most similar set that does *not* correspond to it in identity. This gives us information about the usefulness of a particular value of ω_v for observed $\rho_v^{p,p}$. Hence, the density estimate $\hat{p}(\omega_v, \rho_v)$ is then updated at $(k\Delta\omega_v, \rho^{p,p})$, $k = 1 \dots$. We increment it proportionally to $\delta(k\Delta\omega_v)$ after passing through a y -axis shifted sigmoid function:

$$\hat{p}(k\Delta\omega_v, \rho_v^{p,p})_{[n+1]} = \hat{p}(k\Delta\omega_v, \rho_v^{p,p})_{[n]} + \left[\text{sig}(C \cdot \delta(k\Delta\omega_v)) - 0.5 \right], \quad (5.12)$$

where subscript $[n]$ signifies the n -th iteration step and

$$\text{sig}(x) = \frac{1}{1 + e^{-x}}, \quad (5.13)$$

as shown in Figure 5.7 (a). The sigmoid function has the effect of reducing the overly confident weight updates for the values of ω_v that result in extremely good or bad separations $\delta(k\Delta\omega_v)$. The purpose of this can be seen by noting that we are using separation as a proxy for the statistical goodness of ω_v , while in fact attempting to maximize the average recognition rate (i.e. the average number of cases for which $\delta(k\Delta\omega_v) > 0$).

Figure 6.4 summarizes the proposed offline learning algorithm. An analytic fit to $\omega_v(\rho_v)$ in the form $(1 + e^a)/(1 + e^{a/\rho_v})$ is shown in Figure 5.7 (b).

5.2.5 Prescription glasses

The appeal of using the thermal spectrum for face recognition stems mainly from its invariance to illumination changes, in sharp contrast to visual spectrum data. The exact opposite is true in the case of prescription glasses, which appear as dark patches in thermal imagery, see Figure 5.5. The practical importance of this can be seen by noting that in the US in 2000 roughly 96 million people, or 34% of the total population, wore prescription glasses [Wal01].

In our system, the otherwise undesired, gross appearance distortion that glasses cause in thermal imagery is used to help recognition by detecting their presence. If the subject is not wearing glasses, then both holistic and all local patches-based face representations can be used in recognition; otherwise the eye regions in thermal images are ignored as they contain no useful recognition (discriminative) information.

Glasses detection. We detect the presence of glasses by building representations for the left eye region (due to the symmetry of faces, a detector for only one side is needed) with and without glasses, in the thermal spectrum. The foundations of our classifier are laid out in §5.2.1. Appearance variations of the eye region with out without glasses are represented by two 6D linear subspaces estimated from the training data corpus, see Fig. 5.9 for examples of training data used for subspace estimations. The linear subspace corresponding to eye region patches extracted from a set of thermal imagery of a novel person is then compared with “glasses on” and “glasses off” subspaces using principal angles. The presence of glasses is deduced when the corresponding subspace results in a higher similarity score. We obtain close to flawless performance on our data set (also see §5.3 for description), as shown in Fig. 5.10 (a,b). Good discriminative ability of principal angles in this case is also supported

by visual inspection of the “glasses on” and “glasses off” subspaces; this is illustrated in Fig. 5.10 (c) which shows the first two dominant modes of each, embedded in the 3D principal subspace.

The presence of glasses severely limits what can be achieved with thermal imagery, the occlusion heavily affecting both the holistic face appearance as well as that of the eye regions. This is the point at which our method heavily relies on decision fusion with visual data, limiting the contribution of the thermal spectrum to matching using mouth appearance only i.e. setting $\omega_m = 1.0$ in (5.6).

5.3 Empirical evaluation

We evaluated the described system on the “*Dataset 02: IRIS Thermal/Visible Face Database*” subset of the *Object Tracking and Classification Beyond the Visible Spectrum (OTCBVS)* database¹, freely available for download at <http://www.cse.ohio-state.edu/OTCBVS-BENCH/>. Briefly, this database contains 29 individuals, 11 roughly matching poses in visual and thermal spectra and large illumination variations (some of these are exemplified in Figure 5.11). Images were acquired using the Raytheon Palm-IR-Pro camera in the thermal and Panasonic WV-CP234 camera in the visual spectrum, in the resolution of 240×320 pixels.

Our algorithm was trained using all images in a single illumination in which all 3 salient facial features could be detected. This typically resulted in 7-8 images in the visual and 6-7 in the thermal spectrum, see Figure 5.12, and roughly $\pm 45^\circ$ yaw range, as measured from the frontal face orientation.

The performance of the algorithm was evaluated both in 1-to-N and 1-to-1 matching scenarios. In the former case, we assumed that test data corresponded to one of people in the training set and recognition was performed by associating it with the closest match. Verification (or 1-to-1 matching, “*is this the same person?*”) performance was quantified by looking at the true positive admittance rate for a threshold that corresponds to 1 admitted intruder in 100.

5.3.1 Results

A summary of 1-to-N matching results is shown in Table 11.14.

Firstly, note the poor performance achieved using both raw visual as well as raw thermal data. The former is suggestive of challenging illumination changes present in the OTCBVS

¹IEEE OTCBVS WS Series Bench; DOE University Research Program in Robotics under grant DOE-DE-FG02-86NE37968; DOD/TACOM/NAC/ARC Program under grant R01-1344-18; FAA/NSSA grant R01-1344-48/49; Office of Naval Research under grant #N000143010022.

data set. This is further confirmed by significant improvements gained with both band-pass filtering and the Self-Quotient Image which increased the average recognition rate for, respectively, 35% and 47%. The same is corroborated by the Receiver-Operator Characteristic curves in Figure 5.14 and 1-to-1 matching results in Table 5.2.

On the other hand, the reason for low recognition rate of raw thermal imagery is twofold: it was previously argued that the two main limitations of this modality are the inherently lower discriminative power and occlusions caused by prescription glasses. The addition of the glasses detection module is of little help at this point - some benefit is gained by steering away from misleadingly good matches between any two people wearing glasses, but it is limited in extent as a very discriminative region of the face is lost. Furthermore, the improvement achieved by optimal band-pass filtering in thermal imagery is much more modest than with visual data, increasing performance respectively by 35% and 8%. Similar increase was obtained in true admittance rate (42% vs. 8%), see Table 5.14.

Neither the eyes or the mouth regions, in either the visual or thermal spectrum, proved very discriminative when used in isolation, see Figure 5.13. Only 10-12% true positive admittance was achieved, as shown in Table 5.3. However, the proposed fusion of holistic and local appearance offered a consistent and statistically significant improvement. In 1-to-1 matching the true positive admittance rated increased for 4-6%, while the average correct 1-to-N matching improved for roughly 2-3%.

The greatest power of the method becomes apparent when the two modalities, visual and thermal, are fused. In this case the role of the glasses detection module is much more prominent, drastically decreasing the average error rate from 10% down to 3%, see Table 11.14. Similarly, the true admission rate increases to 74% when data is fused without special handling of glasses, and to 80% when glasses are taken into account.

5.4 Summary and conclusions

In this chapter we described a system for personal identification based on a face biometric that uses cues from visual and thermal imagery. The two modalities are shown to complement each other, their fusion providing good illumination invariance and discriminative power between individuals. Prescription glasses, a major difficulty in the thermal spectrum, are reliably detected by our method, restricting the matching to non-affected face regions. Finally, we examined how different preprocessing methods affect recognition in the two spectra, as well as holistic and local feature-based face representations. The proposed method was shown to achieve a high recognition rate (97%) using only a small number of training images (5-7) in the presence of large illumination changes.

Table 5.1: *Shown is the average rank-1 recognition rate using different representations across all combinations of illuminations. Note the performance increase with each of the main features of our system: image filtering, combination of holistic and local features, modality fusion and prescription glasses detection.*

Representation		Recognition
Visual	Holistic raw data	0.58
	Holistic, band-pass	0.78
	Holistic, SQI filtered	0.85
	Mouth+eyes+holistic	0.87
	data fusion, SQI filtered	
Thermal	Holistic raw data	0.74
	Holistic raw w/ glasses detection	0.77
	Holistic, low-pass filtered	0.80
	Mouth+eyes+holistic	0.82
	data fusion, low-pass filtered	
Proposed thermal + visual fusion	w/o glasses detection	0.90
	w/ glasses detection	0.97

Table 5.2: *A summary of the comparison of different image processing filters for 1 in 100 intruder acceptance rate. Both the simple band-pass filter, and even further its locally-scaled variant, greatly improve performance. This is most significant in the visual spectrum, in which image intensity in the low spatial frequency is most affected by illumination changes.*

Representation	Visual	Thermal
1% intruder acceptance		
Unprocessed/raw	0.2850	0.5803
Band-pass filtered (BP)	0.4933	0.6287
Self-quotient image (SQI)	0.6410	0.6301

Table 5.3: *A summary of the results for 1 in 100 intruder acceptance rate. Local features in isolation perform very poorly.*

Representation	Visual (SQI)	Thermal (BP)
1% intruder acceptance		
Eyes	0.1016	0.2984
Mouth	0.1223	0.3037

Table 5.4: *Holistic & local features – a summary of 1-to-1 matching (verification) results.*

Representation	Visual (SQI)	Thermal (BP)
1% intruder acceptance		
Holistic + Eyes	0.6782	0.6499
Holistic + Mouth	0.6410	0.6501
Holistic + Eyes + Mouth	0.6782	0.6558

Table 5.5: *Feature and modality fusion – a summary of the 1-to-1 matching (verification) results.*

Representation	True admission rate
1% intruder acceptance	
Without glasses detection	0.7435
With glasses detection	0.8014

Related publications

The following publications resulted from the work presented in this chapter:

- O. Arandjelović, R. Hammoud and R. Cipolla. Multi-sensory face biometric fusion (for personal identification). In *Proc. IEEE Workshop on Object Tracking and Classification Beyond the Visible Spectrum (OTCBVS)*, page 52, June 2006. [Ara06h]
- O. Arandjelović, R. Hammoud and R. Cipolla. *Face Biometrics for Personal Identification*, chapter Towards person authentication by fusing visual and thermal face biometrics. Springer-Verlag, 2007. ISBN 978-3-540-49344-0. [Ara07b]
- O. Arandjelović, R. Hammoud and R. Cipolla. On face recognition by fusing visual and thermal face biometrics. In *Proc. IEEE International Conference on Advanced Video and Signal Based Surveillance (AVSS)*, pages 50–56, November 2006. [Ara06g]
- O. Arandjelović, R. Hammoud and R. Cipolla. Thermal and reflectance based personal identification methodology in challenging variable illuminations, *Pattern Recognition*, **43**(5):pages 1801–1813, May 2010. [Ara10]

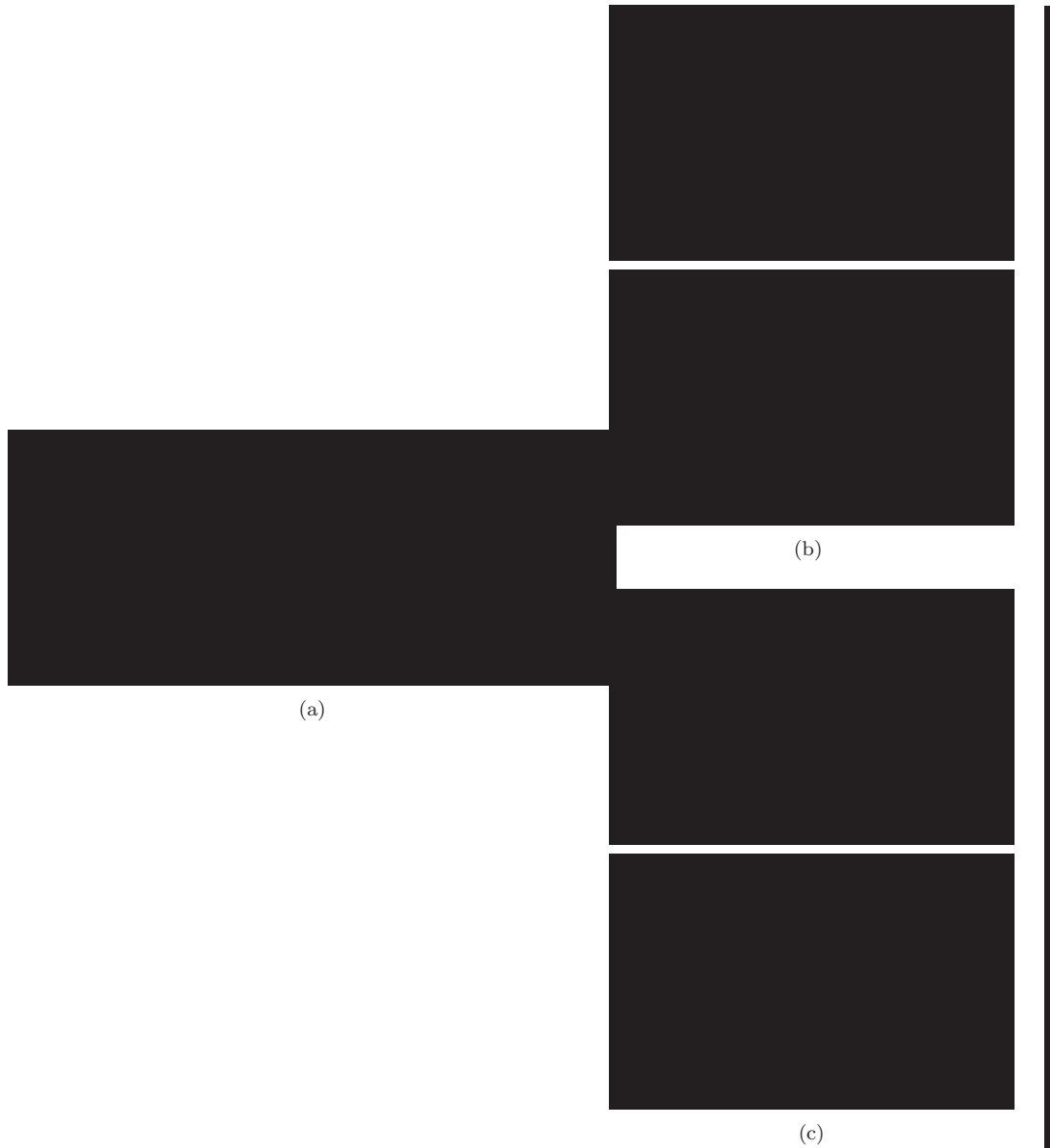


Figure 5.2: An illustration of the concept of principal angles and principal vectors in the case of two 2D subspaces embedded in a 3D space. As two such subspaces necessarily intersect, the first pair of principal vectors is the same (i.e. $\mathbf{u}_1 = \mathbf{v}_1$). However, the second pair is not, and in this case forms the second principal angle of $\cos^{-1} \rho_2 = \cos^{-1}(0.8084) \approx 36^\circ$. The top three pairs of principal vectors, displayed as images, when the subspaces correspond to image sets of the same and different individuals are displayed in (b) and (c) (top rows corresponds to \mathbf{u}_i , bottom rows to \mathbf{v}_i). In (b), the most similar modes of pattern variation, represented by principal vectors, are very much alike in spite of different illumination conditions used in data acquisition.



Figure 5.3: *Shown is the original image in the visual spectrum with detected facial features marked by yellow circles (left), the result of affine warping the image to the canonical frame (centre) and the final registered and cropped facial image.*



Figure 5.4: *The optimal combination of the lower and upper band-pass filter thresholds is estimated from a small training corpus. The plots show the recognition rate using a single modality, (a) visual and (b) thermal, as a function of the widths W_1 and W_2 of the two Gaussian kernels in (5.4). It is interesting to note that the optimal band-pass filter for the visual spectrum passes a rather narrow, mid-frequency band, whereas the optimal filter for the thermal spectrum is in fact a low-pass filter.*



Figure 5.5: *The effects of the optimal band-pass filters on registered and cropped faces in (a) visual and (b) thermal spectra.*



Figure 5.6: *In both the visual and the thermal spectrum our algorithm combines the similarities obtained by matching the holistic face appearance and the appearance of three salient local features – the eyes and the mouth.*



(a) *y*-axis shifted sigmoid function

(b) Weighting function

Figure 5.7: *The contribution of visual matching, as a function of the similarity of visual imagery. A low similarity score between image sets in the visual domain is indicative of large illumination changes and consequently our algorithm leans that more weight should be placed on the illumination-invariant thermal spectrum.*

Input: visual data $d_v(\text{person}, \text{illumination})$,
thermal data $d_t(\text{person}, \text{illumination})$.
Output: density estimate $\hat{p}(\omega_v, \rho_v)$.

1: Initialization

$$\hat{p}(\omega_v, \rho_v) = 0,$$

2: Iteration

for all illuminations i, j and persons p

3: Iteration

for all $k = 0, \dots, 1/\Delta\omega_v$, $\omega_v = k\Delta\omega_v$

5: Separation given ω

$$\delta(k\Delta\omega_v) = \min_{q \neq p} [\omega_v \rho_v^{p,p} + (1 - \omega_v) \rho_t^{p,p} - \omega_v \rho_v^{p,q} + (1 - \omega_v) \rho_t^{p,q}]$$

6: Update density estimate

$$\hat{p}(k\Delta\omega_v, \rho_v^{p,p}) = \hat{p}(k\Delta\omega_v, \rho_v^{p,p}) + \left[\text{sig}(C \cdot \delta(k\Delta\omega_v)) - 0.5 \right]$$

7: Smooth the output

$$\hat{p}(\omega_v, \rho_v) = \hat{p}(\omega_v, \rho_v) * \mathbf{G}_{\sigma=0.05}$$

8: Normalize to unit integral

$$\hat{p}(\omega_v, \rho_v) = \hat{p}(\omega_v, \rho_v) / \int_{\omega_v} \int_{\rho_v} \hat{p}(\omega_v, \rho_v) d\rho_v d\omega_v$$

Figure 5.8: *The proposed fusion learning algorithm, used offline.*



Figure 5.9: *Shown are examples of glasses-on (top) and glasses-off (bottom) thermal data used to construct the corresponding appearance models for our glasses detector.*

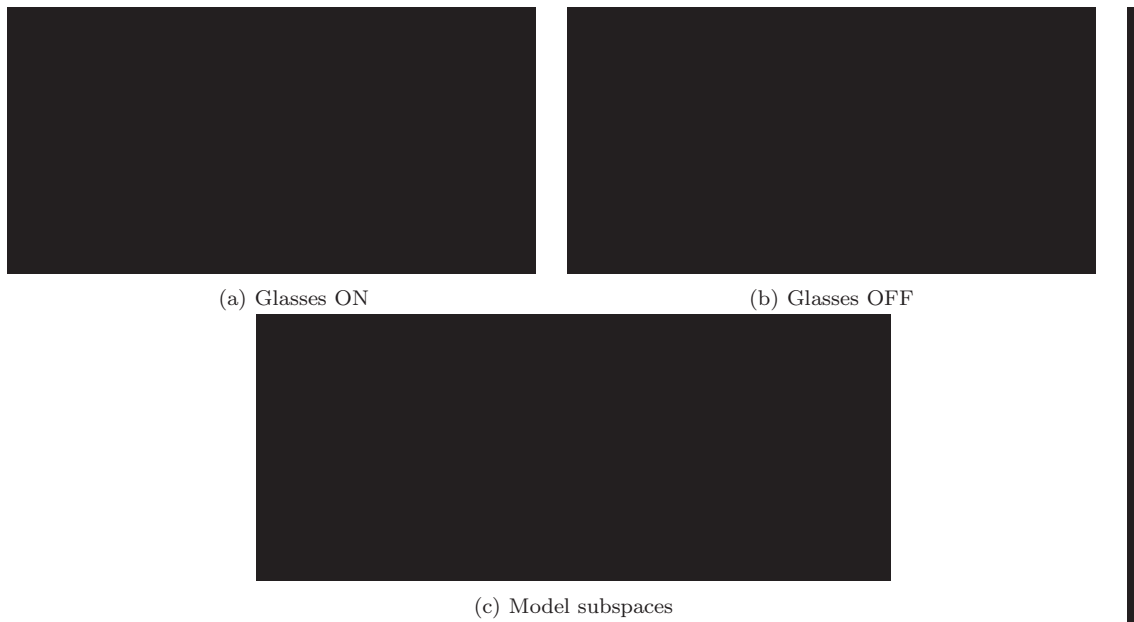


Figure 5.10: (a) *Inter-* and (b) *intra-* class (glasses on and off) similarities across our data set. (c) Good discrimination by principal angles is also motivated qualitatively as the subspaces modelling appearance variations of the eye region with and without glasses on show very different orientations even when projected to the 3D principal subspace. As expected, the “glasses off” subspace describes more appearance variation, as illustrated by the larger extent of the linear patch representing it in the plot.

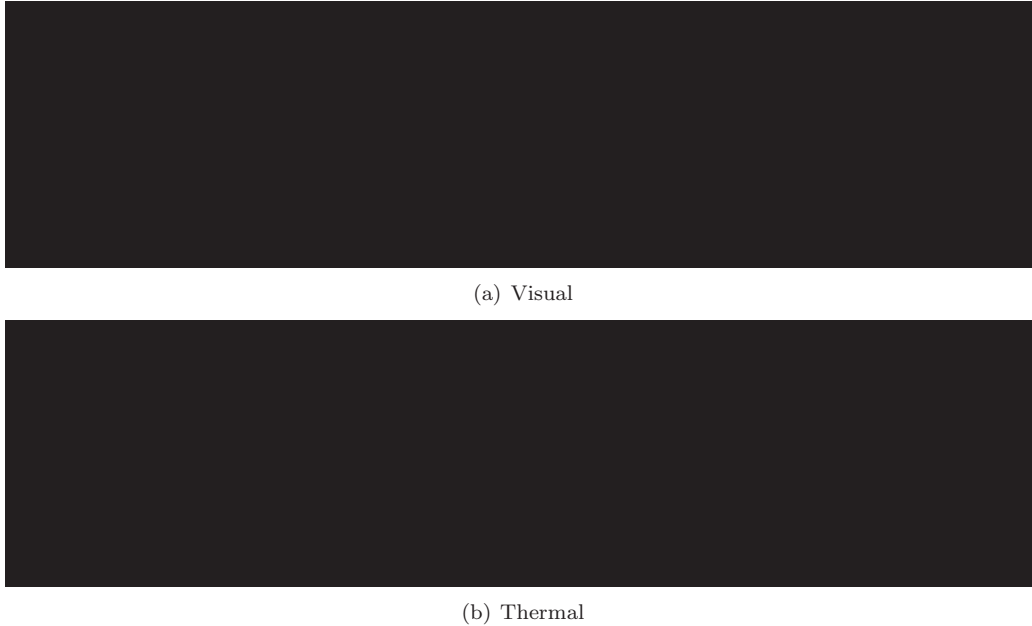


Figure 5.11: *Each row corresponds to an example of a single training (or test) set of images used for our algorithm in the (a) visual and (b) thermal spectrum. Note the extreme changes in illumination, as well as that in some sets the user is wearing glasses and in some not.*

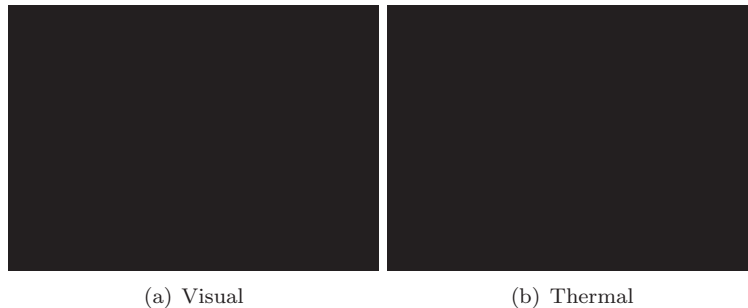


Figure 5.12: *Shown are histograms of the number of images per person used to train our algorithm. Depending on the exact head poses assumed by the user we typically obtained 7-8 visual spectrum images and typically a slightly lower number for the thermal spectrum. The range of yaw angles covered is roughly $\pm 45^\circ$ measured from the frontal face orientation.*



Figure 5.13: *Isolated local features Receiver-Operator Characteristics (ROC): for visual (blue) and thermal (red) spectra.*

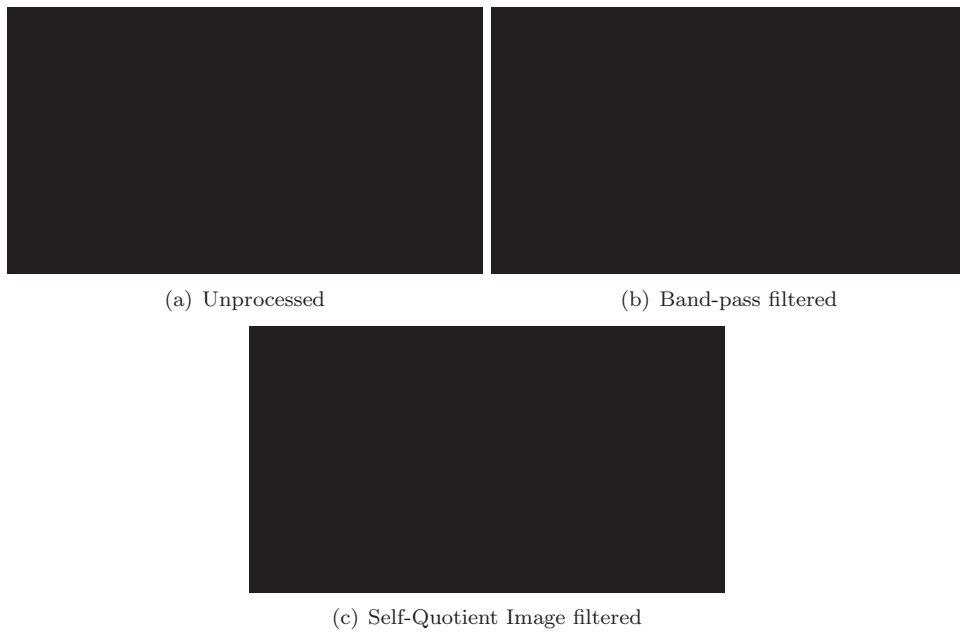


Figure 5.14: *Holistic representations Receiver-Operator Characteristics (ROC) for visual (blue) and thermal (red) spectra.*

6

Illumination Invariance using Image Filters



El Greco. *The Purification of the Temple*
1571-76, Oil on canvas, 117 x 150 cm
Institute of Arts, Minneapolis

In the previous chapter recognition the invariance to illumination condition was achieved by fusing face biometrics acquired in the visual and thermal spectrum. While successful, in practice this approach suffers from the limited availability and high cost of thermal imagers. We wish to achieve the same using visual data only, acquired with an inexpensive and readily available optical camera.

In this chapter we show that image processed visual data can be used to much the same effect as we used thermal data, fusing it with raw visual data. The framework is based on simple image processing filters that compete with unprocessed greyscale input to yield a single matching score between individuals. It is shown how the discrepancy between illumination conditions between novel input and the training data set can be estimated and used to weigh the contribution of two competing representations. Evaluated on *CamFace*, *ToshFace* and *Face Video* databases, our algorithm consistently demonstrated a dramatic performance improvement over traditional filtering approaches. We demonstrate a reduction of 50–75% in recognition error rates, the best performing method-filter combination correctly recognizing 96% of the individuals.

6.1 Adapting to data acquisition conditions

The framework proposed in this chapter is most closely motivated by the findings first reported in [Ara06b]. In that paper several face recognition algorithms were evaluated on a large database using (i) raw greyscale input, (ii) a high-pass (HP) filter and (iii) the Self-Quotient Image (QI) [Wan04a]. Both the high-pass and even further Self Quotient Image representations produced an improvement in recognition for all methods over raw grayscale, which is consistent with previous findings in the literature [Adi97, Ara05c, Fit02, Wan04a]. Of importance to this work is that it was also examined in which cases these filters help and how much depending on the data acquisition conditions. It was found, consistently over different algorithms, that recognition rates using greyscale and either the HP or the QI filter negatively correlated (with $\rho \approx -0.7$), as illustrated in Figure 6.1.

This is an interesting result: it means that while on average both representations increase the recognition rate, they actually *worsen* it in “easy” recognition conditions when no normalization is needed. The observed phenomenon is well understood in the context of energy of intrinsic and extrinsic image differences and noise (see [Wan03a] for a thorough discussion). Higher than average recognition rates for raw input correspond to small changes in imaging conditions between training and test, and hence lower energy of extrinsic variation. In this case, the two filters decrease the signal-to-noise ratio, worsening the performance. On the other hand, when the imaging conditions between training and test are



Figure 6.1: *A plot of the performance improvement with HP and QI filters against the performance of unprocessed, raw imagery across different illumination combinations used in training and test. The tests are shown in the order of increasing raw data performance for easier visualization.*

very different, normalization of extrinsic variation is the dominant factor and performance is improved, see Figure 6.2 (b).



(a) Similar acquisition conditions between sequences



(b) Different acquisition conditions between sequences

Figure 6.2: *A conceptual illustration of the distributions of intrinsic, extrinsic and noise signal energies across frequencies in the cases when training and test data acquisition conditions are (a) similar and (b) different, before (left) and after (right) band-pass filtering.*



Figure 6.3: *Distances (0 – 1) between sets of faces – interpersonal and intrapersonal comparisons are shown respectively as large red and small blue dots. Individuals are poorly separated.*

This is an important observation: it suggests that the performance of a method that uses either of the representations can be increased further by detecting the difficulty of recognition conditions. In this chapter we propose a novel learning framework to do exactly this.

6.1.1 Adaptive framework

Our goal is to implicitly learn how similar the novel and training (or *gallery*) illumination conditions are, to appropriately emphasize either the raw input guided face comparisons or of its filtered output. Figure 6.3 shows the difficulty of this task: different classes (i.e. persons) are not well separated in the space of 2D feature vectors obtained by stacking raw and filtered similarity scores.

Let $\{\mathcal{X}_1, \dots, \mathcal{X}_N\}$ be a database of known individuals, \mathcal{X} novel input corresponding to one of the gallery classes and $\rho()$ and $F()$, respectively, a given similarity function and a quasi illumination-invariant filter. We then express the degree of belief η that two face sets \mathcal{X} and \mathcal{X}_i belong to the same person as a weighted combination of similarities between the corresponding unprocessed and filtered image sets:

$$\eta = (1 - \alpha^*)\rho(\mathcal{X}, \mathcal{X}_i) + \alpha^*\rho(F(\mathcal{X}), F(\mathcal{X}_i)) \quad (6.1)$$

In the light of the previous discussion, we want α^* to be small (closer to 0.0) when novel and the corresponding gallery data have been acquired in similar illuminations, and large (closer to 1.0) when in very different ones. We show that α^* can be learnt as a function:

$$\alpha^* = \alpha^*(\mu), \quad (6.2)$$

where μ is the *confusion margin* – the difference between the similarities of the two \mathcal{X}_i most similar to \mathcal{X} . As in Chapter 5, we compute an estimate of $\alpha^*(\mu)$ in a maximum a posteriori sense:

$$\alpha^*(\mu) = \arg \max_{\alpha} p(\alpha|\mu), \quad (6.3)$$

which, under the assumption of a uniform prior on the confusion margin μ , reduces to:

$$\alpha^*(\mu) = \arg \max_{\alpha} p(\alpha, \mu), \quad (6.4)$$

where $p(\alpha, x)$ is the probability that α is the optimal value of the mixing coefficient. The proposed offline learning algorithm entirely analogous to the algorithm described in Section 5.2.4, so here we just summarize it in Figure 6.4 with a typical evolution of $p(\alpha, \mu)$ shown in Figure 6.5. The final stage of the offline learning in our method involves imposing the monotonicity constraint on $\alpha^*(\mu)$ and smoothing of the result, see Figure 6.6.

Input: training data $D(\text{person}, \text{illumination})$,
 filtered data $F(\text{person}, \text{illumination})$,
 similarity function ρ ,
 filter F .

Output: estimate $\hat{p}(\alpha, \mu)$.

1: Init

$$\hat{p}(\alpha, \mu) = 0,$$

2: Iteration

for all illuminations i, j and persons p

3: Initial separation

$$\delta_0 = \min_{q \neq p} [\rho(D(p, i), D(q, j)) - \rho(D(p, i), D(p, j))]$$

4: Iteration

for all $k = 0, \dots, 1/\Delta\alpha$, $\alpha = k\Delta\alpha$

5: Separation given α

$$\begin{aligned} \delta(k\Delta\alpha) = \min_{q \neq p} [& \alpha\rho(F(p, i), F(q, j)) \\ & - \alpha\rho(F(p, i), F(p, j)) \\ & + (1 - \alpha)\rho(D(p, i), D(q, j)) \\ & - (1 - \alpha)\rho(D(p, i), D(p, j))] \end{aligned}$$

6: Update density estimate

$$\hat{p}(k\Delta\alpha, \delta_0) = \hat{p}(k\Delta\alpha, \delta_0) + \delta(k\Delta\alpha)$$

7: Smooth the output

$$\hat{p}(\alpha, \mu) = \hat{p}(\alpha, \mu) * \mathbf{G}_{\sigma=0.05}$$

8: Normalize to unit integral

$$\hat{p}(\alpha, \mu) = \hat{p}(\alpha, \mu) / \int_{\alpha} \int_x \hat{p}(\alpha, x) dx d\alpha$$

Figure 6.4: *Offline training algorithm.*

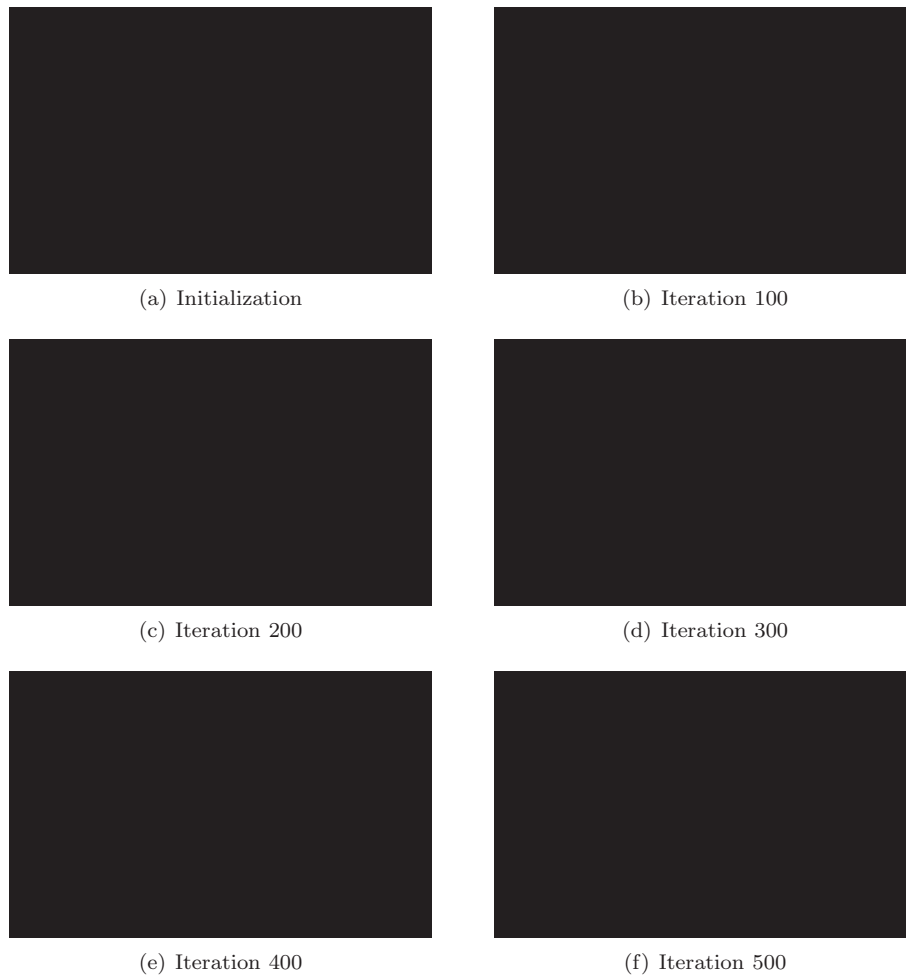


Figure 6.5: *The estimate of the joint density $p(\alpha, \mu)$ through 500 iterations for a band-pass filter used for the evaluation of the proposed framework in Section 6.2.1.*

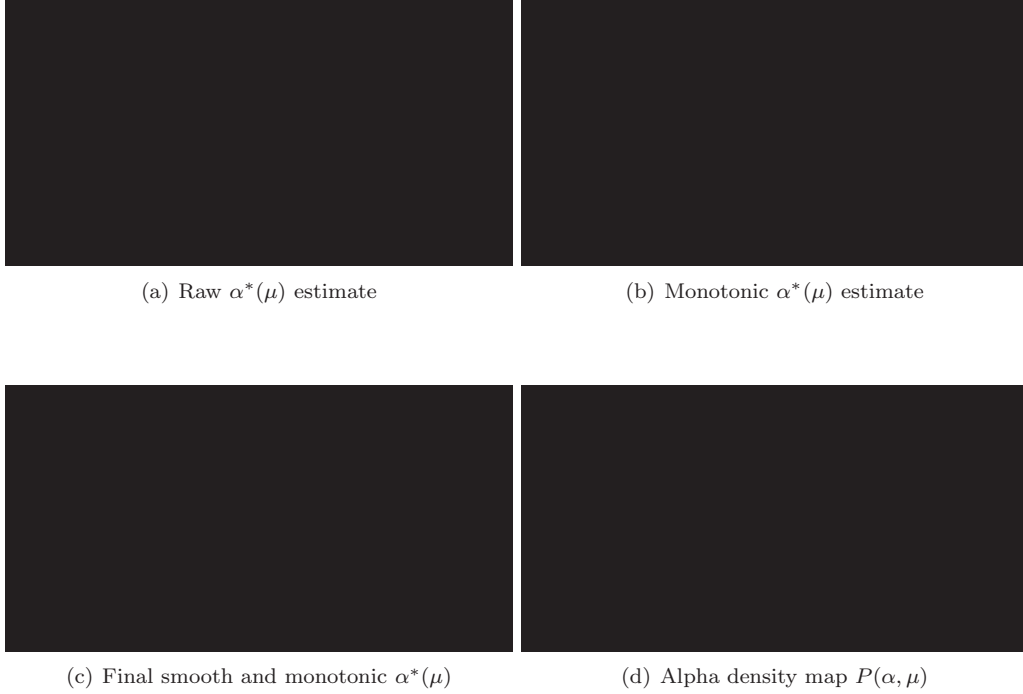


Figure 6.6: *Typical estimates of the α -function plotted against confusion margin μ (a–c). The estimate shown was computed using 40 individuals in 5 illumination conditions for a Gaussian high-pass filter. As expected, α^* assumes low values for small confusion margins and high values for large confusion margins (see (7.8)). Learnt probability density $p(\alpha, \mu)$ (greyscale surface) and a superimposed raw estimate of the α -function (solid red line) for a high-pass filter are shown in (d).*

6.2 Empirical evaluation

The proposed framework was evaluated using the following filters (illustrated in Figure 6.7):

- Gaussian high-pass filtered images [Ara05c, Fit02] (HP):

$$\mathbf{X}_H = \mathbf{X} - (\mathbf{X} * \mathbf{G}_{\sigma=1.5}), \quad (6.5)$$

- local intensity-normalized high-pass filtered images – similar to the Self-Quotient Image [Wan04a] (QI):

$$\mathbf{X}_Q = \mathbf{X}_H ./ \mathbf{X}_L \equiv \mathbf{X}_H ./ (\mathbf{X} - \mathbf{X}_H), \quad (6.6)$$



Figure 6.7: *An example of the original image and the 6 corresponding filtered representations we evaluated.*

the division being element-wise,

- distance-transformed edge map [Ara06b, Can86] (ED):

$$\mathbf{X}_{ED} = \text{DistanceTransform}[\mathbf{X}_E] \quad (6.7)$$

$$\equiv \text{DistanceTransform}[\text{Canny}(\mathbf{X})], \quad (6.8)$$

- Laplacian-of-Gaussian [Adi97] (LG):

$$\mathbf{X}_L = \mathbf{X} * \nabla \mathbf{G}_{\sigma=3}, \quad (6.9)$$

where $*$ denotes convolution, and

- directional grey-scale derivatives [Adi97, Eve04] (DX, DY):

$$\mathbf{X}_x = \mathbf{X} * \frac{\partial}{\partial x} \mathbf{G}_{\sigma_x=6} \quad (6.10)$$

$$(6.11)$$

$$\mathbf{X}_y = \mathbf{X} * \frac{\partial}{\partial y} \mathbf{G}_{\sigma_y=6}. \quad (6.12)$$

To demonstrate the contribution of the proposed framework, we evaluated it with two well-established methods in the literature:

- Constrained MSM (CMSM) [Fuk03] used in a state-of-the-art commercial system FacePass[®] [Tos06], and
- Mutual Subspace Method (MSM) [Fuk03].

In all tests, both training data for each person in the gallery, as well as test data, consisted of only a single sequence. Offline training of the proposed algorithm was performed using

40 individuals in 5 illuminations from the *CamFace* data set. We emphasize that these were not used as test input for the evaluations reported in this section.

6.2.1 Results

We evaluated the performance of CMSM and MSM using each of the 7 face image representations (raw input and 6 filter outputs). Recognition results for the 3 databases are shown in blue in Figure 6.9 (the results on *Face Video* data set are tabulated in Figure 6.9 (c), for the ease of visualization). Confirming the first premise of this work as well as previous research findings, all of the filters produced an improvement in average recognition rates. Little interaction between method/filter combinations was found, Laplacian-of-Gaussian and the horizontal intensity derivative producing the best results and bringing the best and average recognition errors down to 12% and 9% respectively.

In the last set of experiments, we employed each of the 6 filters in the proposed data-adaptive framework. Recognition results for the 3 databases are shown in red in Figure 6.9. The proposed method produced a dramatic performance improvement in the case of all filters, reducing the average recognition error rate to only 4% in the case of CMSM/Laplacian-of-Gaussian combination. An improvement in the robustness to illumination changes can also be seen in the significantly reduced standard deviation of the recognition. Finally, it should be emphasized that the demonstrated improvement is obtained with a negligible increase in the computational cost as all time-demanding learning is performed offline.

6.2.2 Failure modes

In the discussion of failure modes of the described framework, it is necessary to distinguish between errors introduced by a *particular* image processing filter used, and the fusion algorithm itself. As generally recognized across literature (e.g. see [Adi97]), qualitative inspection of incorrect recognitions using filtered representations indicates that the main difficulties are posed by those illumination effects which most significantly deviate from the underlying frequency model (see Section 2.3.2) such as: cast shadows, specularities (especially commonly observed for users with glasses) and photo-sensor saturation.

On the other hand, any failure modes of our fusion framework were difficult to clearly identify, due to such a low frequency of erroneous recognition decisions. Even these were in virtually all of the cases due to overly confident decisions in the filtered pipeline. Overall, this makes the methodology proposed in this chapter extremely promising as a robust and efficient way of matching face appearance image sets, and suggests that future work should concentrate on developing appropriately robust image filters that can deal with more complex illumination effects.



Figure 6.8: (a) The first pair of principal vectors (top and bottom) corresponding to the sequences (b) and (c) (every 4th detection is shown for compactness), for each of the 7 representations used in the empirical evaluation described in this chapter. A higher degree of similarity between the two vectors indicates a greater degree of illumination invariance of the corresponding filter.

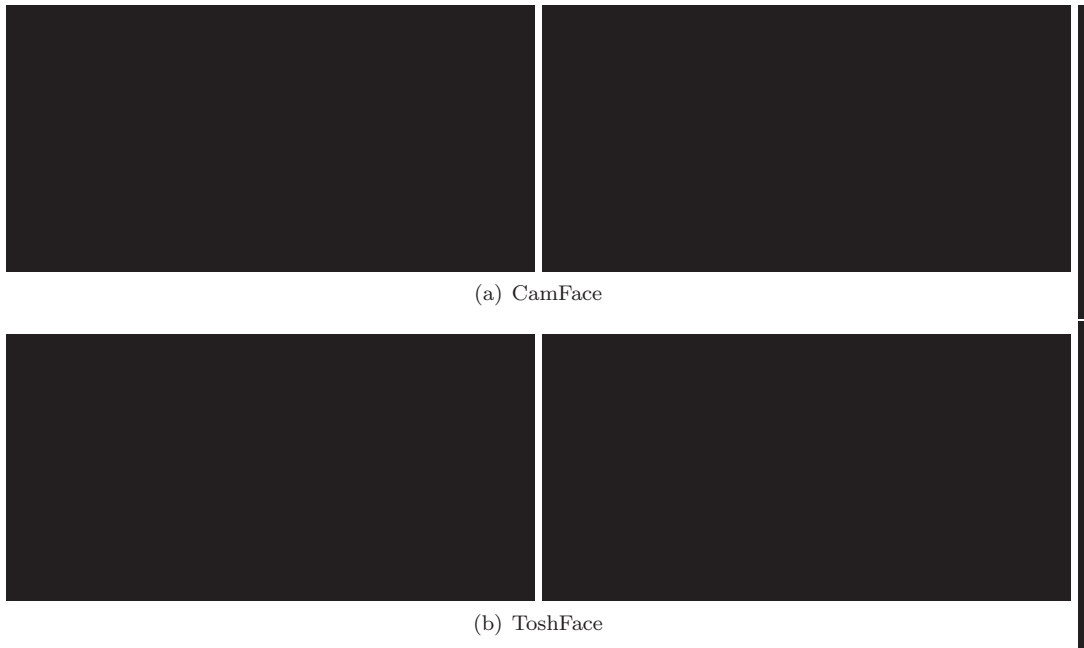
6.3 Summary and conclusions

In this chapter we described a novel framework for increasing the robustness of simple image filters for automatic face recognition in the presence of varying illumination. The proposed framework is general and is applicable to matching face sets or sequences, as well as single shots. It is based on simple image processing filters that compete with unprocessed greyscale input to yield a single matching score between individuals. By performing all numerically consuming computation offline, our method both (i) retains the matching efficiency of simple image filters, but (ii) with a greatly increased robustness, as all online processing is performed in the closed-form. Evaluated on a large, real-world data corpus, the proposed method was shown to dramatically improve video-based recognition across a wide range of illumination, pose and face motion pattern changes.

Related publications

The following publications resulted from the work presented in this chapter:

- O. Arandjelović and R. Cipolla. A new look at filtering techniques for illumination invariance in automatic face recognition. In *Proc. IEEE Conference on Automatic Face and Gesture Recognition (FGR)*, pages 449–454, April 2006. [Ara06f]
- G. Brostow, M. Johnson, J. Shotton, O. Arandjelović, V. Kwatra and R. Cipolla. Semantic photo synthesis. In *Proc. Eurographics*, September 2006. [Bro06]



	RW	HP	QI	ED	LG	DX	DY
MSM	0.00	0.00	0.00	0.00	9.09	0.00	0.00
MSM-AD	0.00	0.00	0.00	0.00	0.00	0.00	0.00
CMSM	0.00	9.09	0.00	0.00	0.00	0.00	0.00
CMSM-AD	0.00	0.00	0.00	0.00	0.00	0.00	0.00

(c) Face Video Database, mean error (%)

Figure 6.9: *Error rate statistics. The proposed framework (-AD suffix) dramatically improved recognition performance on all method/filter combinations, as witnessed by the reduction in both error rate averages and their standard deviations.*

7

Boosted Manifold Principal Angles



Joseph M. W. Turner. *Snow Storm: Steamboat off a Harbour's Mouth*
1842, Oil on Canvas, 91.4 x 121.9 cm
Tate Gallery, London

The method introduced in the previous chapter suffers from two major drawbacks. Firstly, the image formation model implicit in the derivation of the employed quasi-illumination invariant image filters is too simplistic. Secondly, illumination normalization is performed on a frame-by-frame basis, not exploiting in fullness all the available data from a head motion sequence.

In this chapter we focus on the latter problem. We return to considering face appearance manifolds and identify a manifold illumination invariant. We show that under the assumption of a commonly used illumination model by which illumination effects on the appearance are slowly spatially varying, tangent planes of the manifold retain their orientation under the set of transformations caused by face illumination changes. To exploit the invariant, we propose a novel method based on comparisons between linear subspaces corresponding to linear patches, piece-wise approximating appearance manifolds. In particular, there are two main areas of novelty: (i) we extend the concept of principal angles between linear subspaces to manifolds with arbitrary nonlinearities; (ii) it is demonstrated how boosting can be used for application-optimal principal angle fusion.

7.1 Manifold illumination invariants

Let us start by formalizing our recognition framework. Let \mathbf{x} be an image of a face and $\mathbf{x} \in \mathbb{R}^D$, where D is the number of pixels in the image and \mathbb{R}^D the corresponding image space. Then $\mathbf{f}(\mathbf{x}, \Theta)$ is an image of the same face after the rotation with parameter $\Theta \in \mathbb{R}^3$ (yaw, pitch and roll). Function \mathbf{f} is a generative function of the corresponding face motion manifold, obtained by varying Θ ¹.

Rotation affected appearance changes. Now, consider the appearance change of a face due to small rotation $\Delta\Theta$:

$$\Delta\mathbf{x} = \mathbf{f}(\mathbf{x}, \Delta\Theta) - \mathbf{x}. \quad (7.1)$$

For small rotations, geodesic neighbourhood of \mathbf{x} is linear and using Taylor's theorem we get:

$$\mathbf{f}(\mathbf{x}, \Delta\Theta) - \mathbf{x} \approx \mathbf{f}(\mathbf{x}, \mathbf{0}) + \nabla\mathbf{f}|_{(\mathbf{x}, \mathbf{0})} \cdot \Delta\Theta - \mathbf{x}. \quad (7.2)$$

¹As a slight digression, note that strictly speaking, \mathbf{f} should be *person-specific*. Due to self-occlusion of parts of the face, \mathbf{f} cannot produce plausible images of rotated faces simply from a single image \mathbf{x} . However, in our work, the range of head rotations is sufficiently restricted that under the standard assumption of face symmetry [Ara05c], \mathbf{f} can be considered generic.



Figure 7.1: Under the assumption that illumination effects on the appearance faces are spatially slowly varying, appearance manifold tangent planes retrain their orientation in the image space with changes in lighting conditions.

where $\nabla \mathbf{f}|_{(\mathbf{x}, \Theta)}$ is the Jacobian matrix evaluated at (\mathbf{x}, Θ) . Noting that $\mathbf{f}(\mathbf{x}, \mathbf{0}) = \mathbf{x}$ and writing \mathbf{x} as a sum of its low and high frequency components $\mathbf{x} = \mathbf{x}_L + \mathbf{x}_H$:

$$\Delta \mathbf{x} \approx \nabla \mathbf{f}|_{\mathbf{x}, \mathbf{0}} \cdot \Delta \Theta = \nabla \mathbf{f}|_{\mathbf{x}_L, \mathbf{0}} \cdot \Delta \Theta + \nabla \mathbf{f}|_{\mathbf{x}_H, \mathbf{0}} \cdot \Delta \Theta \quad (7.3)$$

But \mathbf{x}_L is by definition slowly spatially varying and therefore:

$$\|\nabla \mathbf{f}|_{\mathbf{x}_L, \mathbf{0}} \cdot \Delta \Theta\| \ll \|\nabla \mathbf{f}|_{\mathbf{x}_H, \mathbf{0}} \cdot \Delta \Theta\|, \quad (7.4)$$

and

$$\Delta \mathbf{x} \approx \nabla \mathbf{f}|_{\mathbf{x}_H, \mathbf{0}} \cdot \Delta \Theta. \quad (7.5)$$

It can be seen that $\Delta \mathbf{x}$ is a function of the person-specific \mathbf{x}_H but not the illumination affected \mathbf{x}_L . Hence, the directions (in \mathbb{R}^D) of face appearance changes due to small head rotations form a *local manifold invariant* with respect to illumination variation, see Figure 7.1.

The manifold illumination invariant we identified explicitly motivates the use of principal angles between tangent planes as a similarity measure between manifolds. We now address two questions that remain:

- given principal angles between two tangent planes, what contribution should each principal angle have, and
- given similarities between different tangent planes of two manifolds, how to obtain a similarity measure between the manifolds themselves.

We now turn to the first of these problems.

7.2 Boosted principal angles

In general, each principal angle θ_i carries some information for discrimination between the corresponding two subspaces. We use this to build simple weak classifiers $\mathcal{M}(\theta_i) = \text{sign}[\cos(\theta_i) - C]$. In the proposed method, these are combined using the now acclaimed AdaBoost algorithm [Fre95]. In summary, AdaBoost learns a weighting $\{w_i\}$ of decisions cast by weak learners to form a classifier $\mathcal{M}(\Theta)$:

$$\mathcal{M}(\Theta) = \text{sign} \left[\sum_{i=1}^N w_i \mathcal{M}(\theta_i) - \frac{1}{2} \sum_{i=1}^N w_i \right] \quad (7.6)$$

In an iterative update scheme classifier performance is optimized on training data which consists of in-class and out-of-class features (i.e. principal angles). Let the training database consist of sets $S_1, \dots, S_K \equiv \{S_i\}$, corresponding to K classes. In the framework described, the $K(K-1)/2$ out-of-class principal angles are computed between pairs of linear subspaces corresponding to training data sets $\{S_i\}$, estimated using Principal Component Analysis (PCA). On the other hand, the K in-class principal angles are computed between a pair of randomly drawn subsets for each S_i .

We use the learnt weights $\{w_i\}$ for computing the following similarity measure between two linear subspaces:

$$f(\Theta) = \frac{1}{N} \frac{\sum_{i=1}^N w_i \cos(\theta_i)}{\sum_{i=1}^N w_i} \quad (7.7)$$

A typical set of weights $\{w_i\}$ we obtained is shown graphically in Figure 7.3 (a). The plot shows an interesting result: the weight corresponding to the first principal angle is not the greatest. Rather it is the second principal angle that is most discriminating, followed by the third one. This shows that the most similar mode of variation across two subspaces can indeed be due an extrinsic factor. Figure 7.2 (b) shows the 3 most discriminating principal vector pairs selected by our algorithm for data incorrectly classified by MSM – the most weighted principal vectors are now much less similar. The gain achieved with boosting is also apparent from Figure 7.3 (b). A significant improvement can be seen both for a small and a large number of principal angles. In the former case this is because our algorithm chooses not the first but the most discriminating set of angles. The latter case is practically more important – as more principal angles are added to MSM, its performance first improves, but after a certain point it starts *worsening*. This highly undesirable behaviour is caused by effectively equal weighting of base classifiers in MSM. In contrast, the performance of our algorithm never decreases as more information is added. As a consequence, no special provision for choosing the optimal number of principal angles is needed.

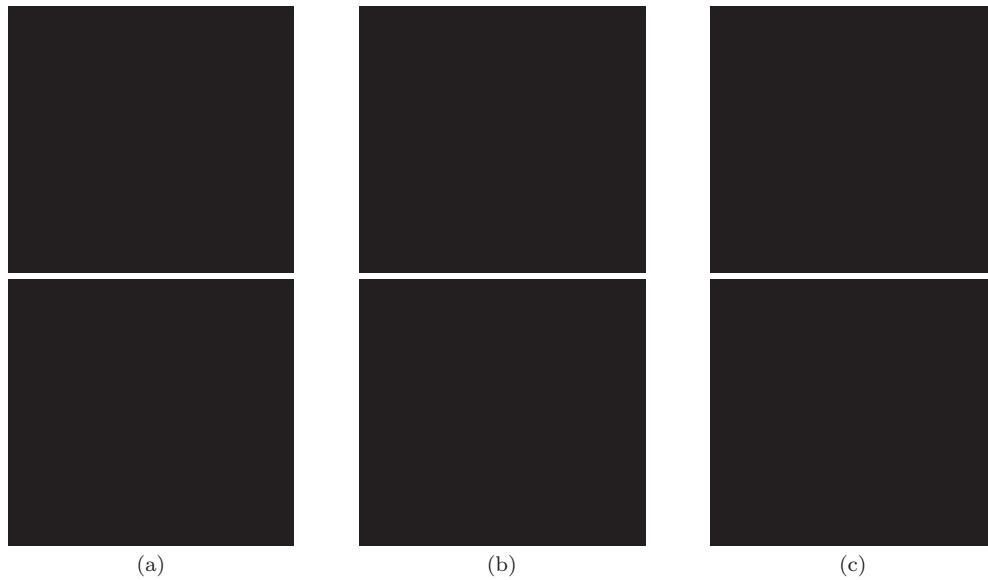


Figure 7.2: (a) The first 3 principal vectors between two linear subspaces which MSM incorrectly classifies as corresponding to the same person. In spite of different identities, the most similar modes of variation are very much alike and can be seen to correspond to especially difficult illuminations. (b) Boosted Principal Angles (BPA), on the other hand, chooses different principal vectors as the most discriminating – these modes of variation are now less similar between the two sets. (c) Modelling of nonlinear manifolds corresponding to the two image sets produces a further improvement. Shown are the most similar modes of variation amongst all pairs of linear manifold patches. Local information is well captured and even these principal vectors are now very dissimilar.



(a) Optimal angle weighting



(b) Performance improvement

Figure 7.3: (a) A typical set of weights corresponding to weak principal angle-based classifiers, obtained using AdaBoost. This figure confirms our criticism of MSM-based methods for (i) their simplistic fusion of information from different principal angles and (ii) the use of only the first few angles. (b) The average performance of a simple MSM classifier and our boosted variant.

At this point it is worthwhile mentioning the work of Maeda *et al.* [Mae04] in which the third principal angle was found to be useful for discriminating between sets of images of a face and its photograph. Much like in MSM and CMSM, the use of a single principal angle was motivated only empirically – the framework described in this chapter can be used for a more principled feature selection in this setting as well.

7.3 Nonlinear subspaces

Our aim is to extend the described framework of boosted principal angles to being able to effectively capture nonlinear data behaviour. We propose a method that combines *global* manifold variations with more subtle, *local* ones.

Without the loss of generality, let S_1 and S_2 be two sets of face appearance images and Θ the set of principal angles between two linear subspaces. We derive a measure of similarity ρ between S_1 and S_2 by comparing the corresponding linear subspaces $U_{1,2}$ and locally linear patches $L_{1,2}^{(i)}$ corresponding to piece-wise linear approximations of manifolds of S_1 and S_2 :

$$\rho(S_1, S_2) = \underbrace{(1 - \alpha) f_G [\Theta(U_1, U_2)]}_{\text{Global manifold similarity contribution}} + \underbrace{\alpha \max_{i,j} f_L [\Theta(L_1^{(i)}, L_2^{(j)})]}_{\text{Local manifold similarity contribution}} \quad (7.8)$$

where f_G and f_L have the same functional form as f in (7.7), but separately learnt base classifier weights $\{w_i\}$. Put in words, the proximity between two manifolds is computed as a weighted average of the similarity between global modes of data variation and the best matching local behaviour. The two terms complement each other: the former provides (i) robustness to noise, whereas the latter ensures (ii) graceful performance degradation with missing data (e.g. unseen poses) and (iii) illumination invariance, see Figure 7.2 (c).

Finding stable locally linear patches

In the proposed framework, stable locally linear manifold patches are found using Mixtures of Probabilistic PCA (PPCA) [Tip99a]. The main difficulty in fitting of a PPCA mixture is the requirement for the local principal subspace dimensionality to be set *a priori*. We solve this problem by performing the fitting in two stages. In the first stage, a Gaussian Mixture Model (GMM) constrained to diagonal covariance matrices is fitted first. This model is crude as it is insufficiently expressive to model local variable correlations, yet too complex (in terms of free parameters) as it does not encapsulate the notion of intrinsic manifold dimensionality and additive noise. However, what it is useful for is the *estimation* of the intrinsic manifold dimensionality d , from the eigenspectra of its covariance matrices,

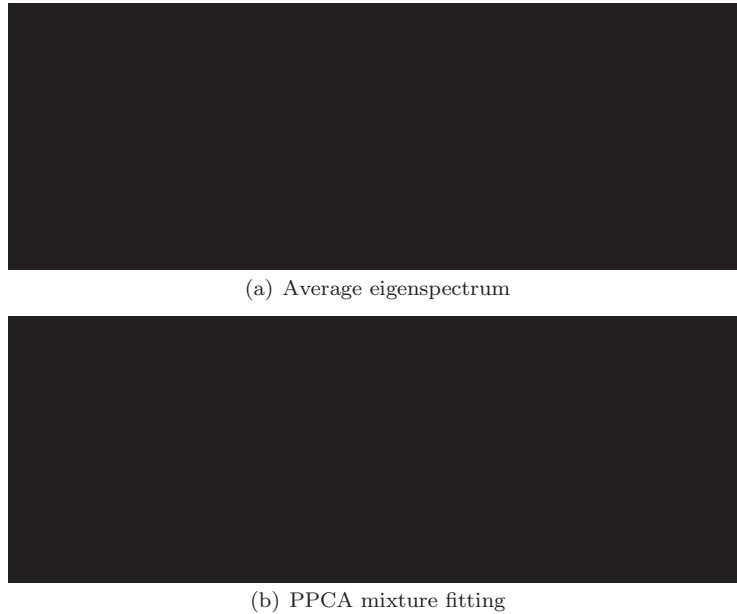


Figure 7.4: (a) Average eigenspectrum of diagonal covariance matrices in a typical intermediate GMM fit. The approximate intrinsic manifold dimensionality can be seen to be around 10. (b) Description length as a function of the number of Gaussian components in the intermediate and final, PPCA-based GMM fitting on a typical data set. The latter results in fewer components and a significantly lower MDL.

see Figure 7.4 (a). Once d is estimated (typically $d \ll D$), the fitting is repeated using a Mixture of PPCA.

Both the intermediate diagonal and the final PPCA mixtures are estimated using the Expectation Maximization (EM) algorithm [Dud00] which is initialized by K-means clustering. Automatic model order selection is performed using the well-known Minimum Description Length (MDL) criterion [Dud00], see Figure 7.4 (b). Typically, the optimal (in the MDL sense) number of components for face data sets used in Section 8.6 was 3.

7.4 Empirical evaluation

Methods in this chapter were evaluated on the *CamFace* data set, see Appendix C. We compared the performance of our algorithm, without and with boosted feature selection (respectively MPA and BoMPA), to that of:

- KL divergence algorithm (KLD) of Shakhnarovich *et al.* [Sha02a]²,
- Mutual Subspace Method (MSM) of Yamaguchi *et al.* [Yam98]²,
- Kernel Principal Angles (KPA) of Wolf and Shashua [Wol03]³, and
- Nearest Neighbour (NN) in the Hausdorff distance sense in (i) LDA [Bel97] and (ii) PCA [Tur91a] subspaces, estimated from data.

In KLD 90% of data energy was explained by the principal subspace used. In MSM, the dimensionality of PCA subspaces was set to 9 [Fuk03]. A sixth degree monomial expansion kernel was used for KPA [Wol03]. In BoMPA, we set the value of parameter α in (7.8) to 0.5. All algorithms were preceded with PCA estimated from the entire training dataset which, depending on the illumination setting used for training, resulted in dimensionality reduction to around 150 (while retaining 95% of data energy).

In each experiment we used performed training using sequences in a single illumination setup and tested recognition with sequences in each different illumination setup in turn.

7.4.1 BoMPA implementation

From a practical stand, there are two key points in the implementation of the proposed method: (i) the computation of principal angles between linear subspaces and (ii) time efficiency. These are now briefly summarized for the implementation used in the evaluation reported in this chapter. We compute the cosines of principal angles using the method of Björck and Golub [Bjö73], as singular values of the matrix $B_1^T B_2$ where $B_{1,2}$ are orthonormal basis of two linear subspaces. This method is numerically more stable than the eigenvalue decomposition-based method used in [Yam98] and with roughly the same computational demands, see [Bjö73] for a thorough discussion on numerical issues pertaining to the computation of principal angles. A computationally far more demanding stage of the proposed method is the PPCA mixture estimation. In our implementation, a significant improvement was achieved by dimensionality reduction using the incremental PCA algorithm of Hall *et al.* [Hal00]. Finally, we note that the proposed model of pattern variation within a set inherently places low demands on storage space.

7.4.2 Results

The performance of evaluated recognition algorithms is summarized in Table 7.1. Firstly, note the relatively poor performance of the two nearest neighbour-type methods – the Haus-

²The algorithm was reimplemented through consultation with the authors.

³We used the original authors' implementation.

Table 7.1: *The mean recognition rate and its standard deviation across different training/test illuminations (in %). The last row shows the average time in seconds for 100 set comparisons.*

Method		KLD	NN-LDA	NN-PCA	MSM	KPA	MPA	BoMPA
	mean	19.8	40.7	44.6	84.9	89.1	89.7	92.6
Recognition	std	9.7	6.6	7.9	6.8	10.1	5.5	4.3
	time	7.8	11.8	11.8	0.8	45	7.0	7.0

dorff NN in PCA and LDA subspaces. These can be considered as proxies for gauging the difficulty of the recognition task, seeing that both can be expected to perform relatively well if the imaging conditions do not greatly differ between training and test data sets. Specifically, LDA-based methods have long been established in the single-shot face recognition literature, e.g. see [Bel97, Zha98, Sad04, Wan04c, Kim05b]. The KL-divergence based method achieved by far the worst recognition rate. Seeing that the illumination conditions varied across data and that the face motion was largely unconstrained, the distribution of intra-class face patterns was significant making this result unsurprising. This is consistent with results reported in the literature [Ara05b].

The performance of the four principal angle-based methods confirms the premises of our work. Basic MSM performed well, but worst of the four. The inclusion of nonlinear manifold modelling, either by using the “kernel trick” or a mixture of linear subspaces, achieved an increase in the recognition rate of about 5%. While the difference in the average performance of MPA and the KPA methods is probably statistically insignificant, it is worth noting the greater robustness to specific imaging conditions of our MPA, as witnessed by a much lower standard deviation of the recognition rate. Further performance increase of 3% is seen with the use of boosted angles, the proposed BoMPA algorithm correctly recognizing 92.6% of the individuals with the lowest standard deviation of all methods compared. An illustration of the improvement provided by each novel step in the proposed algorithm is shown in Figure 7.5. Finally, its computational superiority to the best performing method in the literature, Wolf and Shashua’s KPA, is clear from a 7-fold difference in the average recognition time.

(a) Per-case rank- N performance(b) Average rank- N performance

Figure 7.5: *Shown is the improvement in rank- N recognition accuracy of the basic MSM, MPA and BoMPA algorithms for (a) each training/test combination and (b) on average. A consistent and significant improvement is seen with nonlinear manifold modelling, which is further increased using boosted principal angles.*

7.5 Summary and conclusions

In this chapter we showed how appearance manifolds can be used to integrate information across a face motion video sequence to achieve illumination invariance. This was done by combining (i) an illumination model, and (ii) observed appearance changes, to derive a manifold illumination invariant. A novel method, the *Boosted Manifold Principal Angles* (BoMMPA), was proposed to exploit the invariant. We used a boosting framework by which focus is put on the most discriminative regions of invariant tangent planes and introduced a method for fusing their similarities to obtain the overall manifold similarity. The method was shown to be successful in recognition across large changes in illumination.

Related publications

The following publications resulted from the work presented in this chapter:

- T-K. Kim, O. Arandjelović and R. Cipolla. Learning over Sets using Boosted Manifold Principal Angles (BoMMPA). In *Proc. IAPR British Machine Vision Conference (BMVC)*, **2**:pages 779–788, September 2005. [Kim05a]
- O. Arandjelović and R. Cipolla. Face set classification using maximally probable mutual modes. In *Proc. IEEE International Conference on Pattern Recognition (ICPR)*, pages 511-514, August 2006. [Ara06c]
- T-K. Kim, O. Arandjelović and R. Cipolla. Boosted manifold principal angles for image set-based recognition. *Pattern Recognition*, **40**(9):2475–2484, September 2007. [Kim07]

8

Pose-Wise Linear Illumination Manifold Model



Pablo Picasso. *Bull, 11th State*
1946, Lithograph, 29 x 37.5 cm
Musée Picasso, Paris

In the proceeding chapters, illumination invariance was achieved largely by employing *a priori* domain knowledge, such as the smoothness of faces and their largely Lambertian reflectance properties. Subtle, yet important effects of the underlying complex photometric process were not captured, cast shadows and specularities both causing incorrect recognition decisions. In this chapter we take a further step towards the goal of combining models stemming from our understanding of image formation and learning from available data.

In particular there are two major areas of novelty: (i) illumination generalization is achieved using a two-stage method, combining coarse region-based gamma intensity correction with normalization based on a pose-specific illumination subspace, learnt offline; (ii) pose robustness is achieved by decomposing each appearance manifold into semantic Gaussian pose clusters, comparing the corresponding clusters and fusing the results using an RBF network. On the *ToshFace* data set, the proposed algorithm consistently demonstrated a very high recognition rate (95% on average), significantly outperforming state-of-the-art methods from the literature.

8.1 Overview

A video sequence of a moving face carries information about its 3D shape and texture. In terms of recognition, this information can be used either explicitly, by recovering parameters of a generative model of the face (e.g. as in [Bla03]), or implicitly by modelling face appearance and trying to achieve invariance to extrinsic causes of its variation (e.g. as in [Ara05c]). In this chapter we employ the latter approach, as more suited for low-resolution input data (see Section 8.6 for typical data quality) [Eve04].

In the proposed method, manifolds [Ara05b, Bic94] of face appearance are modelled using at most three Gaussian pose clusters describing small face motion around different head poses. Given two such manifolds, first (i) the pose clusters are determined, then (ii) those corresponding in pose are compared and finally, (iii) the results of pairwise cluster comparisons are combined to give a unified measure of similarity of the manifolds themselves. Each of the steps, aimed at achieving robustness to a specific set of nuisance parameters, is described in detail next.

8.2 Face registration

Using the standard appearance representation of a face as a raster-ordered pixel array, it can be observed that the corresponding variations due to head motion, i.e. pose changes, are highly nonlinear, see Figure 8.1 (a,b). A part of the difficulty of recognition from appearance

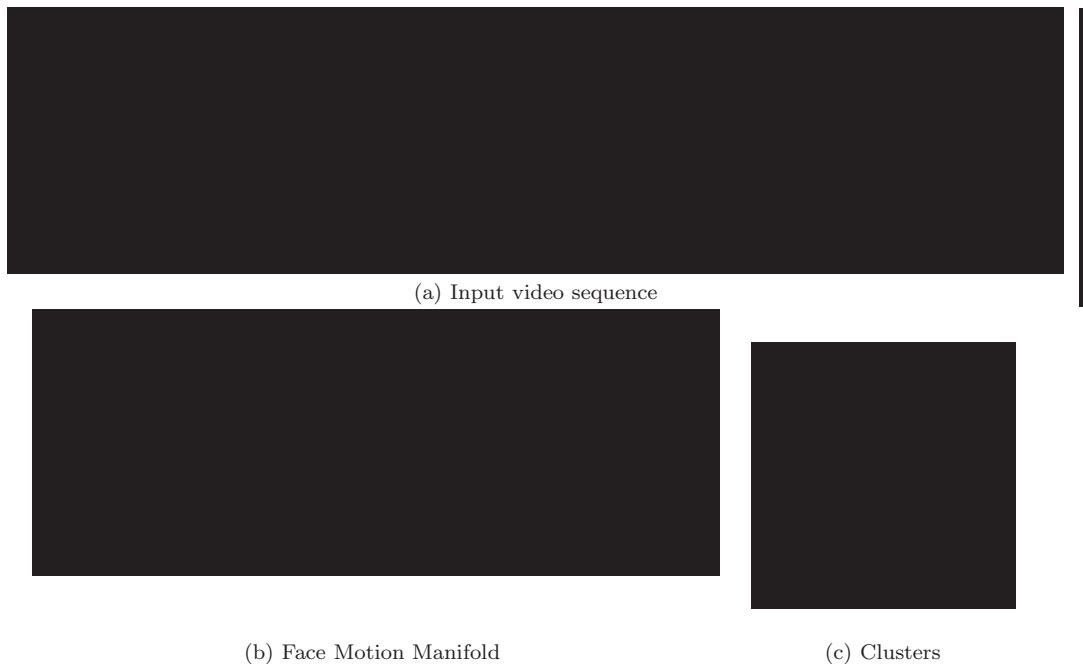


Figure 8.1: A typical input video sequence of random head motion performed by the user (a) and the corresponding face appearance manifold (b). Shown is the projection of affine-registered data (see Section 8.2) to the first three linear principal components. Note that while highly nonlinear, the manifold is continuous and smooth. Different poses are marked in different styles (red stars, blue dots and green squares). Examples of faces from the three clusters can be seen in (b) (also affine-registered and cropped).

manifolds is then contained in the problem of what is an appropriate way of representing them, in a way suitable for the analysis of the effects of varying illumination or pose.

In the proposed method, face appearance manifolds are represented in piece-wise linear manner, by a set of semantic Gaussian *pose clusters*, see Figure 8.1 (b,c). Seeing that each cluster describes a locally linear mode of variation, this approach to modelling manifolds becomes increasingly difficult as their intrinsic dimensionality is increased. Therefore, it is advantageous to normalize the raw, input frames as much as possible so as to minimize this dimensionality. In this first step of our method, this is done by *registering* faces i.e. by warping them to have a set of salient facial features aligned. For related approaches see [Ara05c, Ber04].

We compute warps that align each face with a canonical frame using four point correspondences: the locations of pupils (2) and nostrils (2). These are detected using a two-stage

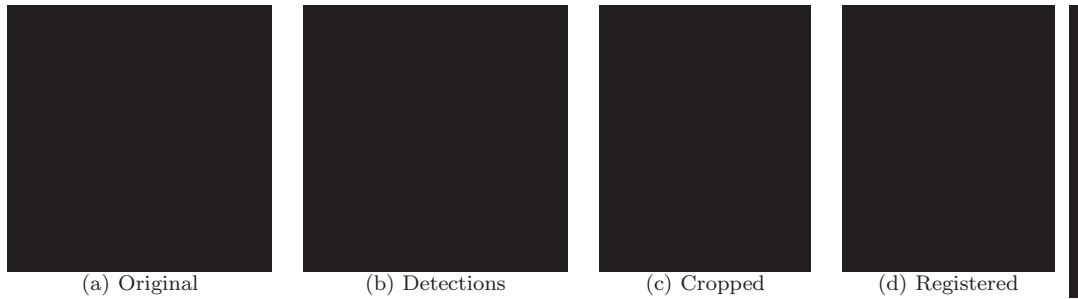


Figure 8.2: (a) Original input frame (resolution 320×240 pixels), (b) superimposed detections of the two pupils and nostrils (as white circles), (c) cropped face regions with background clutter removed, and (d) the final affine registered and cropped image of the face (resolution 30×30 pixels).

feature detector of Fukui and Yamaguchi [Fuk98]¹. Briefly, in the first stage, shape matching is used to rapidly remove a large number of locations in the input image that do not contain features of interest. Out of the remaining, ‘promising’ features, true locations are chosen using the appearance-based, distance from feature space criterion. We found that the described method reliably detected pupils and nostrils across a wide variation in illumination conditions and pose.

From the four point correspondences between the locations of the facial features and their canonical locations (we chose canonical locations to be the mean values of true feature locations) we compute optimal affine warps on a per-frame basis. Since four correspondences over-determine the affine transformation parameters (8 equations with 6 unknown parameters), we estimate them in the minimum L_2 error sense. Finally, the resulting images are cropped, so as to remove background clutter, and resized to the uniform scale of 30×30 pixels. An example of a face registered and cropped in the described manner is shown in Figure 8.2 (also see Figure 8.1 (c)).

8.3 Pose-invariant recognition

Achieving invariance to varying pose is one of the most challenging aspects of face recognition and yet a prerequisite condition for most practical applications. This problem is complicated further by variations in illumination conditions, which inevitably occur due to movement of the user relative to the light sources.

We propose to handle changing pose in two, complementary stages: (i) in the first stage

¹We thank the authors for kindly providing us with the original code of their algorithm.

an appearance manifold is *decomposed* to Gaussian pose clusters, effectively reducing the problem to recognition under a small variation in pose parameters; (ii) in the second stage, fixed-pose recognition results are *fused* using a neural network, trained offline. The former stage is addressed next, while the latter is the topic of Section 8.5.

8.3.1 Defining pose clusters

Inspection of manifolds of registered faces in random motion around the fronto-parallel face shows that they are dominated by the first nonlinear principal component. This principal component corresponds to lateral head rotation, i.e. changes in the face yaw, see Figure 8.1 (a,b). The reason for this lies in the greater smoothness of the face surface in the vertical than in the horizontal direction – pitch changes (“nodding”) are largely compensated for by using the affine registration described in Section 8.2. This is not the case with significant changes, when self-occlusion occurs.

Therefore, the centres of Gaussian clusters used to linearize an appearance manifold correspond to different yaw angle values. In this work we describe the manifolds using three Gaussian clusters, corresponding to the frontal face orientation, face left and face right, see Figure 8.1 (a,b).

8.3.2 Finding pose clusters

As the extent of lateral rotation, as well as the number of frames corresponding to each cluster, can vary between video sequences, a generic clustering algorithm, such as the k-means algorithm, is unsuitable for finding the three Gaussians.

With the prior knowledge of the semantics of clusters, we decide on a single face image membership on a frame-by-frame basis. We show that this can be done in a very simple and rapid manner from already detected locations of the four characteristic facial features: the pupils and nostrils, see Section 8.2.

The proposed method relies on motion parallax based on inherent properties of the shape of faces. Consider the anatomy of a human head shown in profile view in Figure 8.3 (a). It can be seen that the pupils are further away than the nostrils from the vertical axis defined by the neck. Hence, assuming no head roll takes place, as the head rotates laterally, nostrils travel a longer projected path in the image. Using this observation, we define the quantity η as follows:

$$\eta = x_e^c - x_n^c \tag{8.1}$$



Figure 8.3: (a) A schematic illustration of the motion parallax used for coarse pose clustering of input faces (the diagram is based on a figure taken from [Gra18]). (b) The distributions of the scale-normalized parallax measure $\hat{\eta}$ defined in (8.3) for the three pose clusters on the offline training data set. Good separation is demonstrated.

where x_e^c and x_n^c are the mid-points between, respectively, the eyes and the nostrils:

$$x_e^c = \frac{x_{e1} + x_{e2}}{2} \quad x_n^c = \frac{x_{n1} + x_{n2}}{2}. \quad (8.2)$$

It can now be understood that η approximates the discrepancy between distances travelled by the mid-points between the eyes and nostrils, measured from the frontal face orientation. Finally, we normalize η by dividing it with the distance between the eyes, to obtain $\hat{\eta}$, the scale-invariant parallax measure:

$$\hat{\eta} = \frac{\eta}{\|x_{e1} - x_{e2}\|} = \frac{x_e^c - x_n^c}{\|x_{e1} - x_{e2}\|} \quad (8.3)$$

Learning the parallax model. In our method, discrete poses used for linearizing appearance manifolds are automatically learnt from a small training corpus of video sequences of faces in random motion. To learn the model, we took 20 sequences of 100 frames each, acquired at 10fps, and computed the value of $\hat{\eta}$ for each registered face. We then applied the k-means clustering algorithm [Dud00] on the obtained set of parallax measure values and fitted a 1D Gaussian to each, see Figure 8.3 (b).

To apply the learnt model, a frame in our method is classified to the maximal likelihood pose. In other words, when a novel face is to be classified to one of the three pose clusters (i.e. head poses), we evaluate pose likelihood given each of the learnt distributions and classify it to the one giving the highest probability of the observation. Figure 8.4 shows the proportions of faces belonging to each pose cluster.



Figure 8.4: *Histograms of the number of correctly registered faces using four point correspondences between detected facial features (pupils and nostrils) for each of the three discrete poses and in total for each sequence.*

8.4 Illumination-invariant recognition

Illumination variation of face patterns is extremely complex due to varying surface reflectance properties, face shape, and type and distance of lighting sources. Hence, in such a general setup, this is a difficult problem to approach in a purely discriminative fashion.

Our method for compensating for illumination changes is based on the observation that on the coarse level most of the variation can be described by the *dominant light* direction e.g. ‘strong light from the left’. Such variations are addressed much easier. We will also demonstrate that it is the case that *once normalized* at this, coarse level, the learning of residual illumination changes is significantly simplified as well. This motivates the two-stage, per-pose illumination normalization employed in the proposed method:

1. **Coarse level:** Region-based gamma intensity correction (GIC), followed by
2. **Fine level:** Illumination subspace normalization.

The algorithm is summarized in Figure 8.5 while its details are explained in the sections that follow.

8.4.1 Gamma intensity correction

Gamma Intensity Correction (GIC) is a well-known image intensity histogram transformation technique that is used to compensate for global brightness changes [Gon92]. It transforms pixel values (normalized to lie in the range $[0.0, 1.0]$) by exponentiation so as to best match a *canonically illuminated image*. This form of the operator is motivated by non-linear exposure-image intensity response of the photographic film that it approximates well over a wide range of exposure. Formally, given an image I and a canonically illuminated

Input: pose clusters $\mathcal{C}_1 = \{\mathbf{x}_i^{(1)}\}$, $\mathcal{C}_2 = \{\mathbf{x}_i^{(2)}\}$,
face regions mask \mathbf{r} ,
mean face (for pose) \mathbf{m} ,
pose illumination subspace basis matrix \mathbf{B}_I .

Output: pose cluster $\hat{\mathcal{C}}_1$ normalized to \mathcal{C}_2 .

1: Per-frame region-based GIC, sequence 1

$$\forall i. \mathbf{x}_i^{(1)} = \text{region_GIC}(\mathbf{r}, \mathbf{m}, \mathbf{x}_i^{(1)})$$

2: Per-frame region-based GIC, sequence 2

$$\forall i. \mathbf{x}_i^{(2)} = \text{region_GIC}(\mathbf{r}, \mathbf{m}, \mathbf{x}_i^{(2)})$$

3: Per-frame illumination subspace compensation

$$\forall i. \hat{\mathbf{x}}_i^{(1)} = \mathbf{B}_I \mathbf{a}_i^* + \mathbf{x}_i^{(1)}$$

where $\mathbf{a}_i^* = \arg \min_{\mathbf{a}_i} D_{MAH} [\mathbf{B}_I \mathbf{a}_i + \mathbf{x}_i^{(1)} - \langle \mathcal{C}_2 \rangle; \mathcal{C}_2]$

4: The result is the normalized cluster $\hat{\mathcal{C}}_1$

$$\hat{\mathcal{C}}_1 = \{\hat{\mathbf{x}}_i^{(1)}\}$$

Figure 8.5: *Proposed illumination normalization algorithm. Coarse appearance changes due to illumination variation are normalized using region-based gamma intensity correction, while the residual variation is modelled using a linear, pose-specific illumination subspace, learnt offline. Local manifold shape is employed as a constraint in the second, ‘fine’ stage of normalization in the form of Mahalanobis distance for the computation of the optimal additive illumination subspace component.*

image I_C , the gamma intensity corrected image I^* is defined as follows:

$$I^*(x, y) = I(x, y)^{\gamma^*}, \quad (8.4)$$

where γ^* is the optimal gamma value and is computed using

$$\gamma^* = \arg \min_{\gamma} \|\mathbf{I}^{\gamma} - \mathbf{I}_C\| = \quad (8.5)$$

$$\arg \min_{\gamma} \sum_{x,y} [I(x, y)^{\gamma} - I_C(x, y)]^2. \quad (8.6)$$

This is a nonlinear optimization problem in 1D. In our implementation of the proposed method it is solved using the Golden Section search with parabolic interpolation, see [Pre92] for details.

Region-based gamma intensity correction. Gamma intensity correction can be used across a wide range of types of input to correct for *global* brightness changes. However, in the case of objects with a highly variable surface normal, such as faces, it is unable to correct for the effects of side lighting. This is recognized as one of the most difficult problems in face recognition [Adi97].

Region-based GIC proposes to overcome this problem by dividing the image (and hence implicitly the imaged object/face as well) into regions corresponding to surfaces with near-constant surface normal. Regular gamma intensity correction is then applied to each region separately, see Figure 8.6.

An undesirable result of this method is that it tends to produce artificial intensity discontinuities at region boundaries [Sha03]. This occurs due to discontinuities in the computed gamma values between neighbouring regions. We propose to first Gaussian-blur the obtained gamma value map image $\mathbf{\Gamma}^*$:

$$\mathbf{\Gamma}_S^* = \mathbf{\Gamma}^* * \mathbf{G}_{\sigma=2}, \quad (8.7)$$

before applying it to an input image to give the final, region-based gamma corrected output \mathbf{I}_S^* :

$$\forall x, y. I_S^*(x, y) = I(x, y)^{\mathbf{\Gamma}_S^*(x, y)} \quad (8.8)$$

This method almost entirely remedies the problem with boundary artefacts, as illustrated in Figure 8.6. Note that because smoothing is performed on the gamma map, not the processed image, the artefacts are removed without any loss of discriminative, high frequency detail, see Figure 8.7.

8.4.2 Pose-specific illumination subspace normalization

After region-based GIC is applied to all images, for each of the pose clusters, it is assumed that the lighting variation can be modelled using a linear, *pose illumination subspace*. Given a reference and a novel cluster corresponding to the same pose, each frame of the novel cluster is normalized for the illumination change. This is done by adding a vector from the pose illumination subspace to the frame so that its distance from the reference cluster’s centre is minimal.

Learning the model. We define a pose-specific illumination subspace to be a linear manifold that explains *intra-personal* appearance variations due to illumination changes

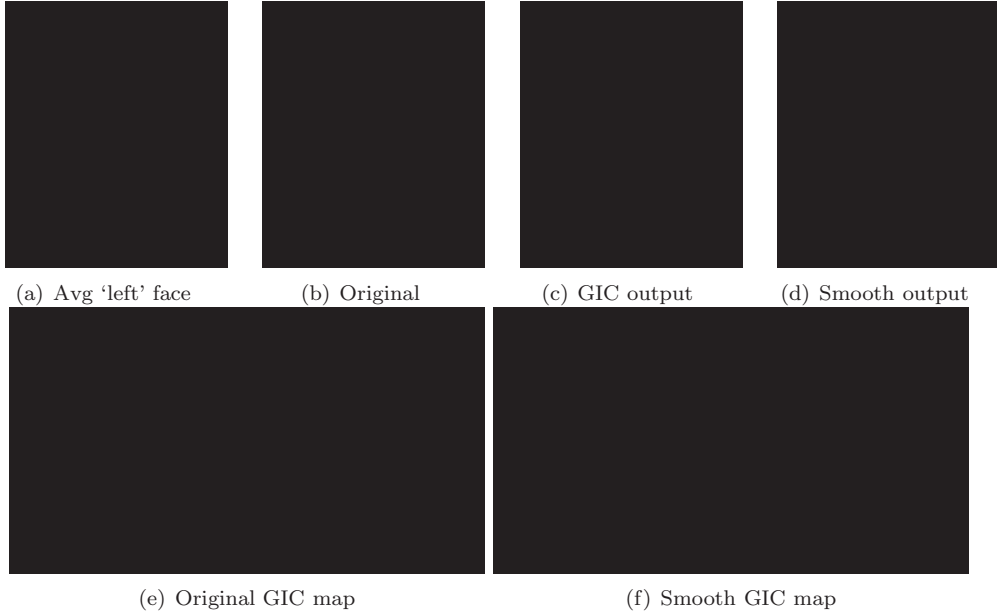


Figure 8.6: *Canonical illumination image and the regions used in region-based GIC (a), original unprocessed face image (b), region-based GIC corrected image without smoothing (c), and region-based GIC corrected image with smoothing (d), gamma value map (e), smoothed gamma value map (f). Notice artefacts at region boundaries in the gamma corrected image (c). The output of the proposed smooth region-based GIC in (d) does not have the same problem. Finally, note that the coarse effects of the strong side lighting in (b) have been greatly removed. Gamma value maps corresponding to the original and the proposed methods is shown under, respectively, (e) and (f).*

across a narrow range of poses. In other words, this is the principal subspace of the within-class scatter.

Formalizing the definition above, given that $\mathbf{x}_{i,j}^k$ is the k -th of $N_f(i,j)$ frames of person i under the illumination j (out of $N_l(i)$), the within-class scatter matrix is:

$$\mathbf{S}_B = \sum_{i=1}^{N_p} \sum_{j=1}^{N_l(i)} \sum_{k=1}^{N_f(i,j)} (\mathbf{x}_{i,j}^k - \bar{\mathbf{x}}_i)(\mathbf{x}_{i,j}^k - \bar{\mathbf{x}}_i)^T, \quad (8.9)$$

where N_p is the total number of training individuals and $\bar{\mathbf{x}}_i$ is the mean face of the person

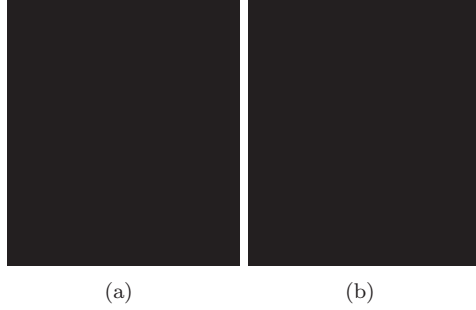


Figure 8.7: (a) Seamless output of the proposed smooth region-based GIC. Boundary artefacts are removed without blurring of the image. Contrast this with output of a original region-based GIC, after Gaussian smoothing (b). Image quality is significantly reduced, with boundary edges still clearly visible.

in the range of considered poses:

$$\bar{\mathbf{x}}_i = \frac{\sum_{j=1}^{N_l(i)} \sum_{k=1}^{N_f(i,j)} \mathbf{x}_{i,j}^k}{\sum_j N_f(i,j)}. \quad (8.10)$$

The pose-specific illumination subspace basis \mathbf{B}_I is then computed by eigendecomposition of \mathbf{S}_B as the principal subspace explaining 90% of data energy variation.

For offline learning of illumination subspaces we used 10s video sequences of 20 individuals, each in 5 illumination conditions, acquired at 10fps. The first few basis vectors learnt in the described manner are shown as images in Figure 8.8.

Employing the model. Let $\mathcal{C}_1 = \{\mathbf{x}_1^{(1)}, \dots, \mathbf{x}_{N_1}^{(1)}\}$ and $\mathcal{C}_2 = \{\mathbf{x}_1^{(2)}, \dots, \mathbf{x}_{N_2}^{(2)}\}$ be two corresponding pose clusters of different appearance manifolds, previously preprocessed using the region-based gamma correction algorithm described in Section 8.4.1. Cluster \mathcal{C}_1 is then illumination-normalized with respect to \mathcal{C}_2 (we will therefore refer to \mathcal{C}_2 as the *reference cluster*), under the null assumption that the identities of the two people they represent are the same. The normalization is performed on a frame-by-frame basis, by adding a vector $\mathbf{B}_I \mathbf{a}_i^*$ from the estimated pose-specific illumination subspace:

$$\forall i. \hat{\mathbf{x}}_i^{(1)} = \mathbf{B}_I \mathbf{a}_i^* + \mathbf{x}_i^{(1)} \quad (8.11)$$

where we define \mathbf{a}_i^* as:

$$\mathbf{a}_i^* = \arg \min_{\mathbf{a}_i} \|\mathbf{B}_I \mathbf{a}_i + \mathbf{x}_i^{(1)} - \langle \mathcal{C}_2 \rangle\|, \quad (8.12)$$



(a) Frontal



(b) Left



(c) Eigenvalues

Figure 8.8: *Shown as images are the first 5 bases of pose-specific illumination subspaces for the (a) frontal and (b) left head orientations. The distribution of energy for pose-specific illumination variation across principal directions is shown in (c).*

and $\|\dots\|$ is a vector norm and $\langle \mathcal{C}_2 \rangle$ the mean face of cluster \mathcal{C}_2 . We then define cluster \mathcal{C}_1 normalized to \mathcal{C}_2 to be $\hat{\mathcal{C}}_1 = \{\hat{\mathbf{x}}_i^{(1)}\}$. This form is directly motivated by the definition of a pose-specific subspace.

To understand the next step, which is the choice of the vector norm in (8.12), it is important to notice in the definition of the pose-specific illumination subspace, that the basis \mathbf{B}_I explains not only appearance variations caused by illumination: reflectance properties of faces used in training (e.g. their albedos), as well as subjects' pose changes also affect it.

This is especially the case as we do not make the common assumption that surfaces of faces are Lambertian, or that light sources are point lights at infinity.

The significance of this observation is that the subspace of a dimensionality sufficiently high to explain the modelled phenomenon (illumination changes) will, undesirably, also be able to explain ‘distracting’ phenomena, such as differing identity. The problem is therefore that of *constraining* the region of interest of the subspace to that which is most likely to be due to illumination changes for a particular individual. For this purpose we propose to exploit the local structure of appearance manifolds, which are smooth. We do this by employing the Mahalanobis distance (using the probability density corresponding to the reference cluster) when computing the illumination subspace correction for each novel frame using (8.12). Formally:

$$\mathbf{a}_i^* = \arg \min_{\mathbf{a}_i} \left(\mathbf{B}_I \mathbf{a}_i + \mathbf{x}_i^{(1)} - \langle \mathcal{C}_2 \rangle \right)^T \cdot \mathbf{B}_2 \mathbf{\Lambda}_2^{-1} \mathbf{B}_2^T \left(\mathbf{B}_I \mathbf{a}_i + \mathbf{x}_i^{(1)} - \langle \mathcal{C}_2 \rangle \right), \quad (8.13)$$

where \mathbf{B}_2 and $\mathbf{\Lambda}_2$ are, respectively, reference cluster’s orthonormal basis and the diagonalized covariance matrix. We found that the use of Mahalanobis distance, as opposed to the usual Euclidean distance, achieved better explanation of novel images when the person’s identity was the same, and worse when it was different, achieving better inter-to-intra class separation.

This quadratic minimization problem is solved by differentiation and the minimum is achieved for:

$$\mathbf{a}_i^* = \left(\mathbf{B}_I^T \mathbf{B}_2 \mathbf{\Lambda}_2^{-1} \mathbf{B}_2^T \mathbf{B}_I \right)^{-1} \cdot \mathbf{B}_I^T \mathbf{B}_2 \mathbf{\Lambda}_2^{-1} \mathbf{B}_2^T \left(\langle \mathcal{C}_2 \rangle - \mathbf{x} \right) \quad (8.14)$$

Examples of registered and cropped face images before and after illumination normalization can be seen in Figure 8.9 (a).

Practical considerations. The computation of the optimal value \mathbf{a}^* using (8.14) involves inversion and Principal Component Analysis (PCA) on matrices of size $D \times D$, where D is the number of pixels in a face image (in our case equal to 900, see Section 8.2). Both of these operations put high demands on computer resources. To reduce the computational overhead, we exploit the assumption that data modelled is of much lower dimensionality than D .

Formalizing the model of low-dimensional face manifolds, we assume that an image \mathbf{y} of subject i ’s face is drawn from the probability density $p_F^{(i)}(\mathbf{y})$ within the face space, and embedded in the image space by means of a mapping function $f^{(i)} : \mathbb{R}^d \rightarrow \mathbb{R}^D$. The resulting point in the D -dimensional space is further perturbed by noise drawn from a noise

distribution p_n (note that the noise operates in the image space) to form the observed image \mathbf{x} . Therefore the distribution of the observed face images of the subject i is given by the integral:

$$p^{(i)}(\mathbf{x}) = \int p_F^{(i)}(\mathbf{y}) p_n(f_i(\mathbf{y}) - \mathbf{x}) d\mathbf{y} \quad (8.15)$$

This model is then used in two stages:

1. Pose-specific PCA dimensionality reduction,
2. Exact computation of the linear principal and rapid estimation of the complementary subspace of a pose cluster.

Specifically, we first perform a linear projection of all images in a specific pose cluster to a *pose-specific face subspace* that explains 95% of data variation in a specific pose. This achieves data dimensionality reduction from 900 to 250.

Referring back to (8.15), to additionally speed up the process, we estimate the intrinsic dimensionality of face manifolds (defined as explaining 95% of within-cluster data variability) and assume that all other variation is due to isotropic Gaussian noise p_n . Hence, we can write the basis of the PCA subspace corresponding to the reference cluster as consisting of a principal and complementary subspaces [Tip99b] represented by orthonormal basis matrices, respectively \mathbf{V}_P and \mathbf{V}_C :

$$\mathbf{B}_2 = [\mathbf{V}_P \mathbf{V}_C] \quad (8.16)$$

where $\mathbf{V}_P \in \mathbb{R}^{250 \times 6}$ and $\mathbf{V}_C \in \mathbb{R}^{250 \times 244}$. The principal subspace and the associated eigenvectors $\mathbf{v}_1, \dots, \mathbf{v}_6$ are rapidly computed, e.g. using [Bag96]. The isotropic noise covariance and the complementary subspace basis are then estimated in the following manner:

$$\lambda_n = \omega \sum_{i=1}^6 \lambda_i \quad \mathbf{V}_C = \text{null}(\mathbf{V}_P) \quad (8.17)$$

where the nullspace of the principal subspace is computed using the QR-decomposition [Pre92] and the value of ω estimated from a small training corpus; we obtained $\omega \approx 2.2e-4$. The diagonalized covariance matrix is then simply:

$$\mathbf{\Lambda}_2 = \text{diag}(\lambda_1, \dots, \lambda_6, \overbrace{\lambda_n, \dots, \lambda_n}^{244}) \quad (8.18)$$

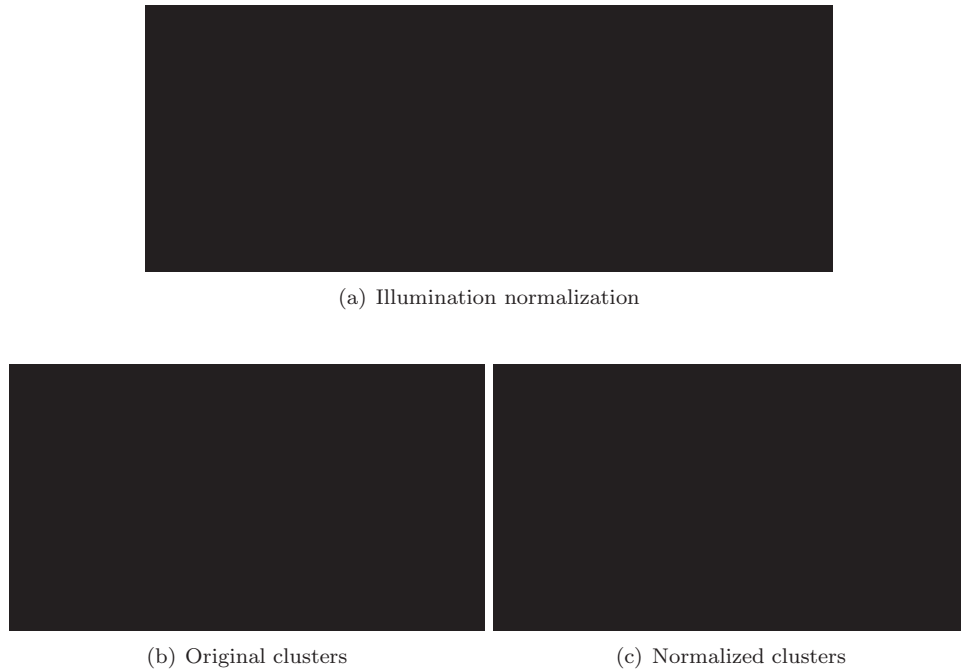


Figure 8.9: In (a) are respectively, top to bottom, shown the original registered and cropped face images from an input video sequence, the same faces after the proposed illumination normalization and a sample from the reference video sequence. The effects of strong side lighting have been greatly removed, while at the same time a high level of detail is retained. The corresponding data from the two sequences, before and after illumination compensation are shown under (b) and (c). Shown are their projections to the first two principal components. Notice that initially the clusters were completely non-overlapping. Illumination normalization has adjusted the location of centre of the blue cluster, but has also affected its spread. after normalization, while overlapping, the two sets of patterns are still distributed quite differently.

8.5 Comparing normalized pose clusters

Having illumination normalized one face cluster to match another, we want to compute a similarity measure between them, a *distance*, expressing our degree of belief that they belong to the same person.

At this point it is instructive to examine the effects of the described method for illumination normalization on the face patterns. Two clusters before, and after one has been normalized, are shown in Figure 8.9 (b,c). An interesting artefact can be observed: the spread of the normalized cluster is significantly reduced. This is easily understood by refer-

ring back to (8.11)-(8.12) and noticing that the normalization is performed frame-by-frame, trying to make each normalized face as close as possible to the reference cluster’s mean, i.e. a *single point*. For this reason, dissimilarity measures between probability densities common in the literature, such as the Bhattacharyya distance, the Kullback-Leibler divergence [Ara05b, Sha02a] or the Resistor-Average distance [Ara06e, Joh01], are not suitable choices. Instead, we propose to use the simple Euclidean distance between normalized cluster centres:

$$D(\mathcal{C}_1, \mathcal{C}_2) = \frac{\sum_{i=1}^{N_1} \hat{\mathbf{x}}_i^{(1)}}{N_1} - \frac{\sum_{j=1}^{N_2} \mathbf{x}_j^{(2)}}{N_2}. \quad (8.19)$$

Inter-manifold distance

The last stage in the proposed method is the computation of an inter-manifold distance, or an inter-manifold dissimilarity measure, based on the distances between corresponding pose clusters. There are two main challenges in this problem: (i) depending on the poses assumed by the subjects, one or more clusters, and hence the corresponding distances, may be void; (ii) different poses are not equally important, or discriminative, in terms of face recognition [Sim04].

Writing \mathbf{d} for the vector containing the three pose cluster distances, we want to classify a novel appearance manifold to the gallery class giving the highest probability of corresponding to it in identity, $P(s|\mathbf{d})$. Then, using the Bayes’ theorem:

$$P(s|\mathbf{d}) = \frac{p(\mathbf{d}|s)P(s)}{p(\mathbf{d})} \quad (8.20)$$

$$= \frac{p(\mathbf{d}|s)P(s)}{p(\mathbf{d}|s)P(s) + p(\mathbf{d}|\neg s)P(\neg s)} \quad (8.21)$$

$$= \frac{1}{1 + p(\mathbf{d}|\neg s)P(\neg s)/p(\mathbf{d}|s)P(s)} \quad (8.22)$$

Assuming that the ratio of same-identity to differing-identities priors $P(\neg s)/P(s)$ is a constant across individuals, it is clear than classifying to the class with the highest $P(s|\mathbf{d})$ is equivalent to classifying to the class with the highest *likelihood ratio*:

$$\mu(\mathbf{d}) = \frac{p(\mathbf{d}|s)}{p(\mathbf{d}|\neg s)} \quad (8.23)$$

Learning pose likelihood ratios. Understanding that $\mathbf{d} = [D_1, D_2, D_3]^T$ we assume statistical independence between pose cluster distances:

$$p(\mathbf{d}|s) = \prod_{i=1}^3 p(D_i|s) \quad (8.24)$$

$$p(\mathbf{d}|\neg s) = \prod_{i=1}^3 p(D_i|\neg s) \quad (8.25)$$

We propose to learn likelihood ratios $\mu(D_i) = p(\mathbf{d}|s)/p(\mathbf{d}|\neg s)$ offline, from a small data corpus, labelled by the identity, in two stages. First, (i) we obtain a Parzen window estimate of intra- and inter- personal pose distances by comparing all pairs of training appearance manifolds; then (ii) we refine the estimates using a Radial Basis Functions (RBF) artificial neural network trained for each pose.

A Parzen window-based [Dud00] estimate of $\mu(D)$ for the frontal head orientation, obtained by directly comparing appearance manifolds as described in Sections 8.2-8.5 is shown in Figure 8.10 (a). In the proposed method, this, and the similar likelihood ratio estimates for the other two head poses are not used directly for recognition as they suffer from an important limitation: the estimates are ill-defined in domain regions sparsely populated with training data. Specifically, an artefact caused by this problem can be observed by noting that the likelihood ratios are not monotonically decreasing. What this means is that *more distant* pose clusters can result in higher chance of classifying two sequences as originating from the *same individual*.

To overcome the problem of insufficient training data, we train a two-layer RBF-based neural network for each of the discrete poses used in approximating face appearance manifolds, see Figure 8.10 (c). In its basic form, this means that the estimate $\hat{\mu}(D_i)$ is given by the following expression:

$$\hat{\mu}(D_i) = \sum_j \alpha_j \mathcal{G}(D_i; \mu_j, \sigma_j), \quad (8.26)$$

where:

$$\mathcal{G}(D_i; \mu_j, \sigma_j) = \frac{1}{\sigma\sqrt{2\pi}} \exp - \frac{(D_i - \mu_j)^2}{2\sigma^2}. \quad (8.27)$$

In the proposed method, this is modified so as to enforce prior knowledge on the func-

tional form of $\mu(D_i)$ in the form of its monotonicity:

$$\hat{\mu}^*(D_i) = \max_{\delta > D_i} \left\{ \sum_j \alpha_j \mathcal{G}(D_i; \mu_j, \sigma_j), \hat{\mu}(\delta) \right\} \quad (8.28)$$

Finally, to ensure that the networks are trained using reliable data (in the context of training sample density in the training domain), we use only local peaks of Parzen window-based estimates. Results using six second-layer neurons, each with the spread of $\sigma_j = 60$, see (8.28), are summarized in Figures 8.10 and 8.11.

8.6 Empirical evaluation

Methods in this chapter were evaluated on the *ToshFace* data set. To establish baseline performance, we compared our recognition algorithm to:

- Mutual Subspace Method (MSM) of Fukui and Yamaguchi [Fuk03],
- KL divergence-based algorithm of Shakhnarovich *et al.* (KLD) [Sha02a],
- Majority vote across all pairs of frames using Eigenfaces of Turk and Pentland [Tur91a].

In the KL divergence-based method we used principal subspaces that explain 85% of data variation energy. In MSM we set the dimensionality of linear subspaces to 9 and used the first 3 principal angles for recognition, as suggested by the authors in [Fuk03]. For the Eigenfaces method, the 22-dimensional eigenspace used explained 90% of total training data energy.

Offline training, i.e. learning of the pose-specific illumination subspaces and likelihood ratios, was performed using 20 randomly chosen individuals in 5 illumination settings, for a total of 100 sequences. These were not used for neither gallery data nor test input for the evaluation reported in this section.

Recognition performance of the proposed system was assessed by training it with the remaining 40 individuals in a single illumination setting, and using the rest of the data as test input. In all tests, both training data for each person in the gallery, as well as test data, consisted of only a single sequence.

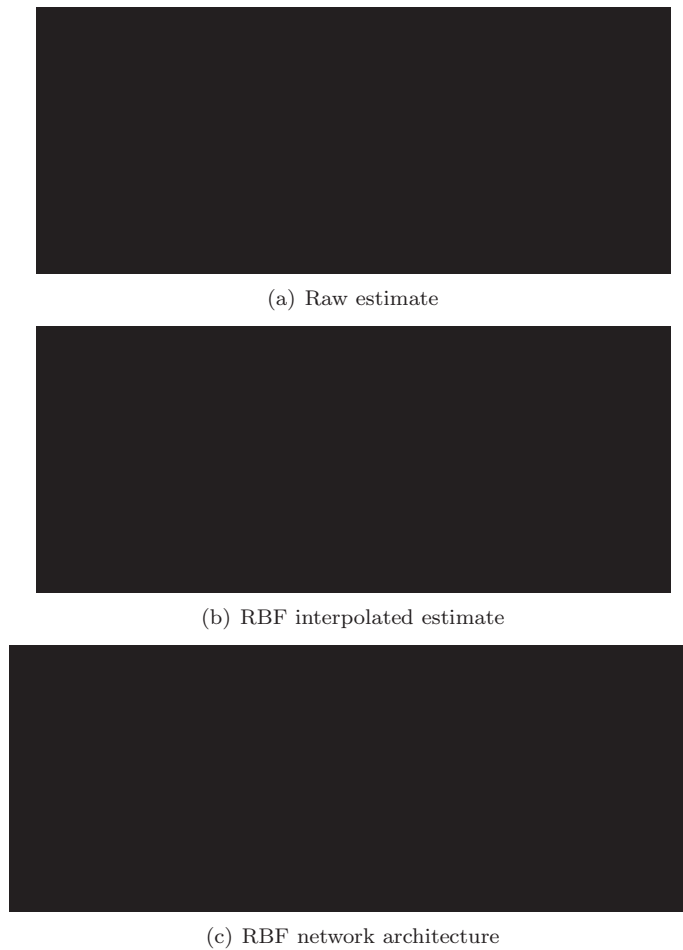


Figure 8.10: *Likelihood ratio corresponding to frontal head pose obtained from the training corpus using Parzen windows (a) and the RBF network-based likelihood ratio (b). The corresponding RBF network architecture is shown in (c). Note that the initial estimate (a) is not monotonically decreasing, while (b) is.*



Figure 8.11: *Joint RBF network-based likelihood ratio for the frontal and left head orientations.*

Table 8.1: *Recognition performance (%) of the proposed method using different illuminations for training and test input. Excellent results are demonstrated with little dependence of the recognition rate on the data acquisition conditions.*

	IL. 1	IL. 2	IL. 3	IL. 4	IL. 5	mean	std
IL. 1	100	90	95	95	90	94	4.2
IL. 2	95	95	95	95	90	94	2.2
IL. 3	95	95	100	95	100	97	2.7
IL. 4	95	90	100	100	95	96	4.2
IL. 5	100	80	100	95	100	95	8.7
mean	97	90	98	96	95	95.2	4.5

8.6.1 Results

The performance of the proposed method is summarized in Table 8.1. We tabulated the recognition rates achieved across different combinations of illuminations used for training and test input, so as to illustrate its degree of sensitivity to the particular choice of data acquisition conditions. An average rate of 95% was achieved, with a mean standard deviation of only 4.7%. Therefore, we conclude that the proposed method is successful in recognition across illumination, pose and motion pattern variation, with high robustness to the exact imaging setup used to provide a set of gallery videos.

This conclusion is further corroborated by Figure 8.12 (a), which shows cumulative distributions of inter- and intra-personal manifold distances (see Section 8.5) and Figure 8.12 (b) which plots the Receiver-Operator Characteristic of the proposed algorithm. Good class separation can be seen in both, illustrating the suitability of our method for verification



Figure 8.12: *Cumulative distributions of intra-personal (dashed line) and inter-personal (solid line) distances (a). Good separability is demonstrated. The corresponding ROC curve can be seen in (b) – less than 0.5% of false positive rate is attained for 91% true positive rate. The corresponding distance threshold choice is numerically well-conditioned, as witnessed by close-to-zero derivatives of the plots in (a) at the corresponding point.*

(one-against-one matching) applications: less than 0.5% false positive rate is attained for 91.2% true positive rate. Additionally, it is important to note that good separation is maintained across a wide range of distances, as can be seen in Figure 8.12 (a) from low gradients of inter- and intra- class distributions e.g. on the interval between 1.0 and 15.0. This is significant as it implies that the interclass threshold choice is not very numerically sensitive: by choosing a threshold in the middle of this range, we can expect the recognition performance to generalize well to different data sets.

Pose clusters

One of the main premises that this work rests on is the idea that illumination and pose robustness in recognition can be achieved by decomposing an appearance manifold into a set of pose ranges (see Section 8.3.1) which are, after being processed independently, probabilistically combined (see Section 8.5). We investigated the discriminating power of each of the three pose clusters used in the proposed context by performing recognition using the inter-cluster distance defined in Section 8.5. Table 8.2 show a summary of the results. High recognition rates were achieved even using only a single pose cluster. Furthermore, the proposed method for integrating cluster distance into a single inter-manifold distance can be seen to improve the average performance of the most discriminative pose. In the described recognition framework, side poses contributed more discriminative information to the distance than the frontal pose (in spite of a lower average number of side faces per sequence, see Figure 8.4 in Section 8.2), as witnessed by both a higher average recognition accuracy and lower standard deviation of recognition. It is interesting to observe that this

Table 8.2: A comparison of identification statistics for recognition using each of the pose-specific cluster distances separately and the proposed method for combining them using an RBF-based neural network. In addition to the expected performance improvement when using all over only some poses, it is interesting to note different contributions of side and frontal pose clusters, the latter being more discriminative in the context of the proposed method.

Measure	Manifold distance	Front clusters distance	Side clusters distance
mean	95	90	93
std	4.7	5.7	3.6

Table 8.3: Average recognition rates (%) of the compared methods across different illumination conditions used for training and test. The performance of the proposed method is by far the best, both in terms of the average recognition rate and its variance.

Method	Proposed method	Majority vote, Eigenfaces	KLD	MSM
mean	95	43	39	24
std	4.7	31.9	32.5	38.9

is in agreement with the finding that appearance in a roughly semi-profile head pose is inherently most discriminative for recognition [Sim04].

Other algorithms

The result of the comparison with the other evaluated methods is shown in Table 8.3. The proposed algorithm outperformed others by a significant margin. Majority vote using Eigenfaces and the KL divergence algorithm performed with statistically insignificant difference, while MSM showed least robustness to the extreme changes in illumination conditions. It is interesting to note that all three algorithms achieved perfect recognition when training and test sequences were acquired in the same illumination conditions. Considering the simplicity and computational efficiency of these methods, investigation of their behaviour when used on preprocessed data (e.g. high-pass filtered images [Ara05c, Fit02] or self-quotient images [Wan04a]) appears to be a promising research direction.

Failure modes

Finally, we investigated the main failure models of our algorithm. An inspection of failed recognitions suggests that the largest difficulty was caused by significant user motion to and

from the camera. During the data acquisition, for some of the illumination conditions the dominant light sources were relatively close to the user (from $\approx 0.5m$). This invalidated the implicit assumption that illumination conditions were unchanging within a single video sequence i.e. that the main cause of appearance changes in images was head rotation.

Another limitation of the method was observed in cases when only few faces were clustered to a particular pose, either because of facial feature detection failure or because the user did not spend enough time in a certain range of head poses. The noisy estimate of the corresponding cluster density in (8.16) propagated the estimation error to illumination normalized images and finally to the overall manifold distance, reducing the separation between classes.

8.7 Summary and conclusions

In this chapter we introduced a novel algorithm for face recognition from video, robust to changes in illumination, pose and the motion pattern of the user. This was achieved by combining person-specific face motion appearance manifolds with generic pose-specific illumination manifolds, which were assumed to be linear. Integrated into a fully automatic practical system, the method has demonstrated a high recognition rate in realistic, uncontrolled data acquisition conditions.

Related publications

The following publications resulted from the work presented in this chapter:

- O. Arandjelović and R. Cipolla. An illumination invariant face recognition system for access control using video. In *Proc. IAPR British Machine Vision Conference (BMVC)*, pages 537–546, September 2004. [Ara04c]

9

Generic Shape-Illumination Manifold



Maurits C. Escher. *Prententoonstelling*
1956, Lithograph

In the previous chapter it was shown how *a priori* domain-specific knowledge can be combined with data-driven learning to reliably recognize in the presence of illumination, pose and motion pattern variations. The main limitations of the proposed method are: (i) the assumption of linearity of pose-specific illumination subspaces, (ii) the coarse pose-based fusion of discriminative information from different frames, and (iii) the appearance distribution artifacts introduced during pose-specific illumination normalization.

This chapter finalizes the part of the thesis that deals with robustly comparing two face motion sequences. We describe the *Generic Shape-Illumination Manifold* recognition algorithm that in a principled manner handles all of the aforementioned limitations.

In particular there are three areas of novelty: (i) we show how a photometric model of image formation can be combined with a statistical model of generic face appearance variation to generalize in the presence of extreme illumination changes; (ii) we use the smoothness of geodesically local appearance manifold structure and a robust same-identity likelihood to achieve robustness to unseen head poses; and (iii) we introduce a precise video sequence “reillumination” algorithm to achieve robustness to face motion patterns in video.

The proposed algorithm consistently demonstrated a nearly perfect recognition rate (over 99.5% on *CamFace*, *ToshFace* and *Face Video* data sets), significantly outperforming state-of-the-art commercial software and methods from the literature.

9.1 Synthetic reillumination of face motion manifolds

One of the key ideas of this chapter is the algorithm for *reillumination* of video sequences. Our goal is to take two input sequences of faces and produces a third, synthetic one, that contains the same poses as the first in the illumination of the second one. For the proposed method, the crucial properties are the (i) continuity and (ii) smoothness of face motion manifolds, see Figure 9.1

The proposed method consists of two stages. First, each face from the first sequence is matched with the face from the second that corresponds to it best in terms of pose. Then, a number of faces close to the matched one are used to finely reconstruct the reilluminated version of the original face. Our algorithm is therefore global, unlike most of the previous methods which use a sparse set of detected salient points for registration, e.g. [Ara05c, Ber04, Fuk03]. We have found these to fail on our data set due to the severity of illumination conditions (see Section B.2). The two stages of the proposed algorithm are next described in detail.

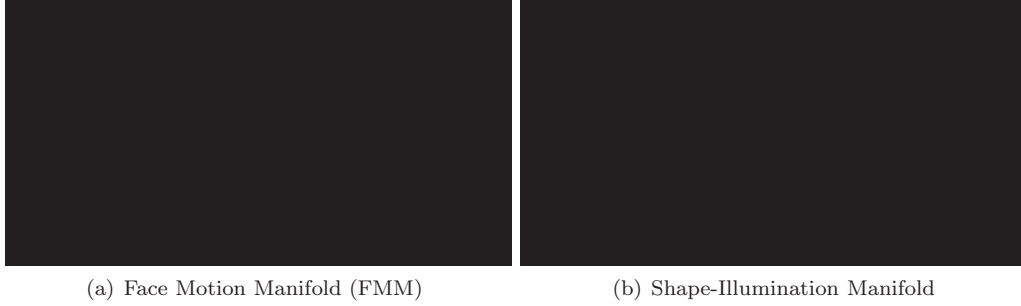


Figure 9.1: *Manifolds of (a) face appearance and (b) albedo-free appearance i.e. the effects of illumination and pose changes, in a single motion sequence. Shown are projections to the first 3 linear principal components, with a typical manifold sample on the top-right.*

9.1.1 Stage 1: pose matching

Let $\{\mathbf{X}_i\}^{(1)}$ and $\{\mathbf{X}_i\}^{(2)}$ be two motion sequences of a person’s face in two different illuminations. Then, for each $\mathbf{X}_i^{(1)}$ we are interested in finding $\mathbf{X}_{c(i)}^{(2)}$ that corresponds to it best in terms of head pose. Finding the unknown mapping c on a frame-by-frame basis is difficult in the presence of extreme illumination changes and when face images are of low resolution. Instead, we exploit the face manifold smoothness by formulating the problem as a minimization task with the fitness function taking on the form:

$$f(c) = f_{match}(c) + \omega f_{reg}(c) \quad (9.1)$$

$$= \underbrace{\sum_j d_E(\mathbf{X}_j^{(1)}, \mathbf{X}_{c(j)}^{(2)})^2}_{\text{Matching term}} + \omega \underbrace{\sum_j \sum_k \frac{d_G^{(2)}(\mathbf{X}_{c(j)}^{(2)}, \mathbf{X}_{c(n(j,k))}^{(2)}; \{\mathbf{X}_j\}^{(2)})}{d_G^{(1)}(\mathbf{X}_j^{(1)}, \mathbf{X}_{n(j,k)}^{(1)}; \{\mathbf{X}_j\}^{(1)})}}_{\text{Regularization term}} \quad (9.2)$$

where $n(i, j)$ is the j -th of K nearest neighbours of face i , d_E a pose dissimilarity function and $d_G^{(k)}$ a geodesic distance estimate along the FMM of sequence k . The first term is easily understood as a penalty for dissimilarity of matched pose-signatures. The latter is a regularizing term that enforces a *globally* good matching by favouring mappings that map geodesically close points from the domain manifold to geodesically close points on the codomain manifold.

Regularization. The manifold-oriented nature of the regularizing function $f_{reg}(c)$ in (9.2) has significant advantages over alternatives that use some form temporal smoothing. Firstly, it is unaffected by changes on the motion pattern of the user (i.e. sequential ordering of



Figure 9.2: *Manifold-to-manifold pose matching: geodesic distances between neighbouring faces on the domain manifold and the corresponding faces on the codomain manifold are used to regularize the solution.*



(a) Original



(b) Reilluminated

Figure 9.3: *(a) Original images from a novel video sequence and (b) the result of reillumination using the proposed genetic algorithm with nearest neighbour-based reconstruction.*

$\{\mathbf{X}_i\}^{(j)}$). On top of the inherent benefit (a person’s motion should not affect recognition), this is important for several practical reasons, e.g.

- face images need not originate from a single sequence - multiple sequences are easily combined together by computing the union of their frame sets, and
- regularization works even if there are bursts of missed or incorrect face detections (see Section B.2).

To understand the form of the regularizing function note that the mapping function c only affects the numerator of each summation term in $f_{reg}(c)$. Its effect is then to penalize cases in which neighbouring faces of the domain manifold map to geodesically distant faces on the codomain manifold. The penalty is further weighted by the inverse of the original geodesic distance $d_G^{(1)}(\mathbf{X}_j^{(1)}, \mathbf{X}_{n(j,k)}^{(1)}; \{\mathbf{X}_j\}^{(1)})$ to place more emphasis on local pose agreement.

Pose-matching function. The performance of function d_E in (9.2) at estimating the goodness of a frame match is crucial for making the overall optimization scheme work well. Our approach consists of filtering the original face image to produce a quasi illumination-invariant *pose-signature*, which is then compared with other pose-signatures using the Euclidean distance:

$$d_E(\mathbf{X}_j^{(1)}, \mathbf{X}_{c(j)}^{(2)}) = \left\| \mathbf{X}_j^{(1)} - \mathbf{X}_{c(j)}^{(2)} \right\|_2 \quad (9.3)$$

Note that the signatures are *only* used for frame matching and thus need not retain any power of discrimination between individuals – all that is needed is sufficient pose information. We use a distance-transformed edge map of the face image as a pose-signature, motivated by the success of this representation in object-configuration matching across other computer vision applications, e.g. [Gav00, Ste03].

Minimizing the fitness function. Exact minimization of the fitness function (9.2) over all functions c is an NP-complete problem. However, since the final synthesis of novel faces (Stage 2) involves an entire geodesic neighbourhood of the paired faces, it is inherently robust to some non-optimality of this matching. Therefore, in practice, it is sufficient to find a good match, not necessarily the optimal one.

We propose to use a genetic algorithm (GA) [Dud00] as a particularly suitable approach to minimization for our problem. GAs rely on the property of many optimization problems that sub-solutions of good solutions are good themselves. Specifically, this means that if we have a globally good manifold match, then local matching can be expected to be good too. Hence, combining two good matches is a reasonable attempt at improving the solution. This

Property	Population size	Elite survival no.	Mutation (%)	Migration (%)	Crossover (%)	Max. generations
Value	20	2	5	20	80	200



Figure 9.4: (a) The parameters of the proposed GA optimization, (b) the corresponding chromosome structure and (c) the population fitness (see (9.2)) in a typical evolution. Maximal generation count of 200 was chosen as a trade-off between accuracy and matching speed.

motivates the chromosome structure we use, depicted in Figure 9.4 (a), with the i -th gene in a chromosome being the value of $c(i)$. GA parameters were determined experimentally from a small training set and are summarized in Figure 9.4 (b,c).

Estimating geodesic distances. The definition of the fitness function in (9.2) involves estimates of geodesic distances along manifolds. Due to the nonlinearity of FMMS [Ara05b, Lee03] it is not well approximated by the Euclidean distance. We estimate the geodesic distance between every two faces from a manifold using the Floyd’s algorithm [Cor90] on a constructed undirected graph whose nodes correspond to face images (also see [Ten00]). Then, if \mathbf{X}_i is one of the K nearest neighbours of \mathbf{X}_j ¹:

$$d_G(\mathbf{X}_i, \mathbf{X}_j) = \|\mathbf{X}_i - \mathbf{X}_j\|_2. \quad (9.4)$$

Otherwise:

$$d_G(\mathbf{X}_i, \mathbf{X}_j) = \min_k [d_G(\mathbf{X}_i, \mathbf{X}_k) + d_G(\mathbf{X}_k, \mathbf{X}_j)]. \quad (9.5)$$

¹Note that the converse does not hold as \mathbf{X}_i being one of the K nearest neighbours of \mathbf{X}_j does not imply that \mathbf{X}_j is one of the K nearest neighbours of \mathbf{X}_i . Therefore the edge relation of this graph is a superset of the “in K -nearest neighbours” relation on \mathbf{X} s.

9.1.2 Stage 2: fine reillumination

Having computed a pose-matching function c^* , we turn to the problem of reilluminating frames $\mathbf{X}_i^{(1)}$. We exploit the smoothness of pose-signature manifolds (which was ensured by distance-transforming face edge maps), illustrated in Figure 9.5, by computing $\mathbf{Y}_i^{(1)}$, the reilluminated frame $\mathbf{X}_i^{(1)}$, as a linear combination of K nearest-neighbour frames of $\mathbf{X}_{c^*(i)}^{(2)}$. Linear combining coefficients $\alpha_1, \dots, \alpha_K$ are found from the corresponding pose-signatures by solving the following constrained minimization problem:

$$\{\alpha_j\} = \arg \min_{\{\alpha_j\}} \left\| \mathbf{x}_i^{(1)} - \sum_{k=1}^K \alpha_k \mathbf{x}_{n(c^*(i),k)}^{(2)} \right\|_2 \quad (9.6)$$

subject to $\sum_{k=1}^K \alpha_k = 1.0$, where $\mathbf{x}_i^{(j)}$ is the pose-signature corresponding to $\mathbf{X}_i^{(j)}$. In other words, the pose-signature of a novel face is first reconstructed using the pose-signatures of K training faces (in the target illumination), which are then combined in the same fashion to synthesize a reilluminated face, see Figure 9.3 and 9.6. We restrict the set of frames used for reillumination to the K -nearest neighbours for two reasons. Firstly, the computational time of using all faces would make this highly unpractical. Secondly, the nonlinearity of both face appearance manifolds and pose-signature manifolds, demands that only the faces in the local, Euclidean-like neighbourhood are used.

Optimization of (9.6) is readily performed by differentiation giving:

$$\begin{bmatrix} \alpha_2 \\ \alpha_3 \\ \vdots \\ \alpha_K \end{bmatrix} = \mathbf{R}^{-1} \mathbf{t}, \quad (9.7)$$

where:

$$R(j, k) = \left(\mathbf{x}_{n(c^*(i),1)}^{(2)} - \mathbf{x}_{n(c^*(i),j)}^{(2)} \right) \cdot \left(\mathbf{x}_{n(c^*(i),1)}^{(2)} - \mathbf{x}_{n(c^*(i),k)}^{(2)} \right), \quad (9.8)$$

$$t(j) = \left(\mathbf{x}_{n(c^*(i),1)}^{(2)} - \mathbf{x}_{n(c^*(i),j)}^{(2)} \right) \cdot \left(\mathbf{x}_{n(c^*(i),1)}^{(2)} - \mathbf{x}_i^{(1)} \right). \quad (9.9)$$

9.2 The shape-illumination manifold

In most practical applications, specularities, multiple or non-point light sources significantly affect the appearance of faces. We believe that the difficulty of dealing with these effects is



Figure 9.5: *A face motion manifold in the input image space and the corresponding pose-signature manifold (both shown in their respective 3D principal subspaces). Much like the original appearance manifold, the latter is continuous and smooth, as ensured by distance transforming the face edge maps. While not necessarily similar globally, the two manifolds retain the same local structure, which is crucial for the proposed fine illumination algorithm.*



Figure 9.6: *Face reillumination: the coefficients for linearly combining face appearance images (bottom row) are computed using the corresponding pose-signatures (top row). Also see Figure 9.5.*

one of the main reasons for poor performance of most face recognition systems when put to use in a realistic environment. In this work we make a very weak assumption on the process of image formation: the only assumption made is that the intensity of each pixel is a linear function of the albedo $a(j)$ of the corresponding 3D point:

$$X(j) = a(j) \cdot s(j) \quad (9.10)$$

where \mathbf{s} is a function of illumination, shape and other parameters not modelled explicitly. This is similar to the reflectance-lighting model used in Retinex-based algorithms [Kim03], the main difference being that we make no further assumptions on the functional form of \mathbf{s} . Note that the commonly-used (e.g. see [Bla03, Geo98, RR01]) Lambertian reflectance model is a special case of (9.10) [Bel98]:

$$s(j) = \sum_i \max(\mathbf{n}_j \cdot \mathbf{L}_i, 0) \quad (9.11)$$

where \mathbf{n}_i is the corresponding surface normal and $\{\mathbf{L}_i\}$ the intensity-scaled illumination directions at the point.

The image formation model introduced in (9.10) leaves the image pixel intensity as an unspecified function of face shape or illumination parameters. Instead of formulating a complex model of the geometry and photometry behind this function (and then needing to recover a large number of model parameters), we propose to learn it implicitly. Consider two images, \mathbf{X}_1 and \mathbf{X}_2 of the same person, in the same pose, but different illuminations. Then from (9.10):

$$\Delta \log X(j) = \log s_2(j) - \log s_1(j) \equiv d_s(j) \quad (9.12)$$

In other words, the difference between these logarithm-transformed images is not a function of face albedo. As before, due to the smoothness of faces, as the pose of the subject varies the difference-of-logs vector \mathbf{d}_s describes a manifold in the corresponding embedding vector space. These is the Shape-Illumination manifold (SIM) corresponding to a particular pair of video sequences, refer back to Figure 9.1 (b).

The generic SIM. A crucial assumption of our work is that the Shape-Illumination Manifold of all possible illuminations and head poses is *generic for human faces* (gSIM). This is motivated by a number of independent results reported in the literature that have shown face shape to be less discriminating than albedo across different models [Cra99, Gro04] or have reported good results in synthetic reillumination of faces using the constant-shape assumption [RR01]. In the context of face manifolds this means that the effects of

illumination and shape can be learnt offline from a training corpus containing typical modes of pose and illumination variation.

It is worth emphasizing the key difference in the proposed offline learning from previous approaches in the literature which try to learn the *albedo* of human faces. Since offline training is performed on persons not in the online gallery, in the case when albedo is learnt it is necessary to have means of generalization i.e. learning what *possible* albedos human faces can have from a small subset. In [RR01], for example, the authors demonstrate generalization to albedos in the rational span of those in the offline training set. This approach is not only unintuitive, but also without a meaningful theoretical justification. On the other hand, previous research indicates that illumination effects can be learnt *directly* without the need for generalization [Ara05b].

Training data organization. The proposed method consists of two training stages – a one-time offline learning performed using *offline training data* and a stage when *gallery data* of known individuals with associated identities is collected. The former (explained next) is used for learning the generic face shape contribution to face appearance under varying illumination, while the latter is used for subject-specific learning.

9.2.1 Offline stage: learning the generic SIM (gSIM)

Let $\mathbf{X}_i^{(j,k)}$ be the i -th face of the j -th person in the k -th illumination, same indexes corresponding in pose, as ensured by the proposed reillumination algorithm in Section 9.1. Then from (9.12), samples from the generic Shape-Illumination manifold can be computed by logarithm-transforming all images and subtracting those corresponding in identity and pose:

$$\mathbf{d} = \log \mathbf{X}_i^{(j,p)} - \log \mathbf{X}_i^{(j,q)} \quad (9.13)$$

Provided that training data contains typical variations in pose and illumination (i.e. that the p.d.f. confined to the generic SIM is well sampled), this becomes a standard statistical problem of high-dimensional density estimation. We employ the Gaussian Mixture Model (GMM). In the proposed framework, this representation is motivated by: (i) the assumed low-dimensional manifold model (3.1), (ii) its compactness and (iii) the existence of incremental model parameter estimation algorithms (e.g. [Ara05a, Hal00]).

Briefly, we estimate multivariate Gaussian components using the Expectation Maximization (EM) algorithm [Dud00], initialized by k -means clustering. Automatic model order selection is performed using the well-known Minimum Description Length criterion



Figure 9.7: *Learning complex illumination effects: Shown is the variation along the 1st mode of a single PPCA space in our SIM mixture model. Cast shadows (e.g. from the nose) and the locations of specularities (on the nose and above the eyes) are learnt as the illumination source moves from directly overhead to side-overhead.*

[Dud00] while the principal subspace dimensionality of PPCA components was estimated from eigenspectra of covariance matrices of a diagonal GMM fit, performed first. Fitting was then repeated using a PPCA mixture. From 6123 gSIM samples computed from 100 video sequences, we obtained 12 mixture components, each with a 6D principal subspace. Figure 9.7 shows an example of subtle illumination effects learnt with this model.

9.3 Novel sequence classification

The discussion so far has concentrated on offline training and building an illumination model for faces - the Generic Shape-Illumination manifold. Central to the proposed algorithm was a method for reilluminating a face motion sequence of a person with another sequence of the *same* person (see Section 9.1). We now show how the same method can be used to compute a similarity between two unknown individuals, given a single training sequence for each and the Generic SIM.

Let gallery data consist of sequences $\{\mathbf{X}_i\}^{(1)}, \dots, \{\mathbf{X}_i\}^{(N)}$, corresponding to N individuals, $\{\mathbf{X}_i\}^{(0)}$ be a novel sequence of one of these individuals and $\mathcal{G}(\mathbf{x}; \Theta)$ a Mixture of Probabilistic PCA corresponding to the generic SIM. Using the reillumination algorithm of Section 9.1, the novel sequence can be reilluminated with each $\{\mathbf{X}_i\}^{(j)}$ from the gallery, producing samples $\{\mathbf{d}_i\}^{(j)}$. We assume these to be identically and independently distributed according to a density corresponding to a *postulated* subject-specific SIM. We then compute the probability of these under $\mathcal{G}(\mathbf{x}; \Theta)$:

$$p_i^{(j)} = \mathcal{G}(\mathbf{d}_i^{(j)}; \Theta) \quad (9.14)$$

When $\{\mathbf{X}_i\}^{(0)}$ and $\{\mathbf{X}_i\}^{(j)}$ correspond in identity, from the way the Generic SIM is learnt, it can be seen that the probabilities $p_i^{(j)}$ will be large. The more interesting question arises when the two compared sequences do not correspond to the same person. In this case, the reillumination algorithm will typically fail to produce a meaningful result - the output frames will not correspond in pose to the target sequence, see Figure 9.8. Consequently, the observed appearance difference will have a low probability under the hypothesis that it is caused purely by an illumination change. A similar result is obtained if the two individuals share sufficiently similar facial lines and poses are correctly matched. In this case it is the differences in face surface albedo that are not explained well by the Generic SIM, producing low $p_i^{(j)}$ in (9.14).

Varying pose and robust likelihood. Instead of basing the classification of $\{\mathbf{X}_i\}^{(0)}$ on the likelihood of observing the *entire* set $\{\mathbf{d}_i\}^{(j)}$ in (9.14), we propose a more robust measure. To appreciate the need for robustness, consider the histograms in Figure 9.9 (a). It can be observed that the likelihood of the most similar faces in an inter-personal comparison, in terms of (9.14), approaches that of the most *dissimilar* faces in an *intra-personal* comparison (sometimes even exceeding it). This occurs when the correct gallery sequence contains poses that are very dissimilar to even the most similar ones in the novel sequence, or vice versa (note that small dissimilarities are extrapolated well from local manifold structure using (9.6)). In our method, the robustness to these, unseen modes of pose variation is achieved by considering the mean log-likelihood of only the most likely faces. In our experiments we used the top 15% of the faces, but we found the algorithm to exhibit little sensitivity to the exact choice of this number, see Figure 9.9 (b). A summary of the proposed algorithms is shown in Figure 9.10 and 9.11.

9.4 Empirical evaluation

We compared the performance of our recognition algorithm with and without the robust likelihood of Section 9.3 (i.e. using only the most reliable vs. all detected and reilluminated faces) on *CamFace*, *ToshFace* and *Face Video* data sets to that of:

- State-of-the-art commercial system FaceIt[®] by Identix [Ide03] (the best performing software in the most recent Face Recognition Vendor Test [Phi03]),
- Constrained MSM (CMSM) [Fuk03] used in Toshiba’s state-of-the-art commercial system FacePass[®] [Tos06]²,

²The algorithm was reimplemented through consultation with the authors.



Figure 9.8: An example of “reillumination” results when the two compared sequences do not correspond to the same individual: the target sequence is shown on the left, the output of our algorithm on the right. Most of the frames do not contain faces which correspond in pose.



Figure 9.9: (a) Histograms of intra-personal likelihoods across frames of a sequence when two sequences compared correspond to the same (red) and different (blue) people. (b) Recognition rate as a function of the number of frames deemed ‘reliable’.

Input: database of sequences $\{\mathbf{X}_i\}^{(j)}$.
Output: model of gSIM $\mathcal{G}(\mathbf{d}; \Theta)$.

1: gSIM iteration

for all persons i and illuminations j, k

2: Reilluminate using $\{\mathbf{X}_i\}^{(k)}$
 $\{\mathbf{Y}_i\}^{(j)} = \text{reilluminate}(\{\mathbf{X}_i\}^{(j)}; \{\mathbf{X}_i\}^{(k)})$

3: Add gSIM samples

$$\mathbb{D} = \mathbb{D} \cup \left\{ \mathbf{Y}_i^{(j)} - \mathbf{X}_i^{(j)} : i = 1 \dots \right\}$$

4: Fit GMM \mathcal{G} from gSIM samples

$$\mathcal{G}(\mathbf{d}; \Theta) = \text{EM_GMM}(\mathbb{D})$$

Figure 9.10: A summary of the proposed offline learning algorithm. Illumination effects on the appearance of faces are learnt as a probability density, in the proposed method approximated with a Gaussian mixture $\mathcal{G}(\mathbf{d}; \Theta)$.

Input: sequences $\{\mathbf{X}_i\}^{(G)}, \{\mathbf{X}_i\}^{(N)}$.
Output: same-identity likelihood ρ .

1: Reilluminate using $\{\mathbf{X}_i\}^{(G)}$
 $\{\mathbf{Y}_i\}^{(N)} = \text{reilluminate}(\{\mathbf{X}_i\}^{(N)}; \{\mathbf{X}_i\}^{(G)})$

2: Postulate SIM samples

$$\mathbf{d}_i = \log \mathbf{X}_i^{(N)} - \log \mathbf{Y}_i^{(N)}$$

3: Compute likelihoods of $\{\mathbf{d}_i\}$

$$p_i = \mathcal{G}(\mathbf{d}_i; \Theta)$$

4: Order $\{\mathbf{d}_i\}$ by likelihood

$$p_{s(1)} \geq \dots \geq p_{s(N)} \geq \dots$$

5: Inter-manifold similarity ρ

$$\rho = \sum_{i=1}^N \log p_{s(i)} / N$$

Figure 9.11: A summary of the proposed online recognition algorithm.

- Mutual Subspace Method (MSM) [Fuk03, Mae04]²,
- Kernel Principal Angles (KPA) of Wolf and Shashua [Wol03]³, and
- KL divergence-based algorithm of Shakhnarovich *et al.* (KLD) [Sha02a]³.

In all tests, both training data for each person in the gallery, as well as test data, consisted of only a single sequence. Offline training of the proposed algorithm was performed using 20 individuals in 5 illuminations from the *CamFace* data set – we emphasize that these were not used as test input for the evaluations reported in this section. The methods were evaluated using 3 face representations:

- raw appearance images \mathbf{X} ,
- Gaussian high-pass filtered images – used for face recognition in [Ara05c, Fit02]:

$$\mathbf{X}_H = \mathbf{X} - (\mathbf{X} * \mathbf{G}_{\sigma=1.5}), \quad (9.15)$$

- local intensity-normalized high-pass filtered images – similar to the Self Quotient Image [Wan04a] (also see [Ara06f]):

$$\mathbf{X}_Q = \mathbf{X}_H ./ (\mathbf{X} - \mathbf{X}_H), \quad (9.16)$$

the division being element-wise.

Background clutter was suppressed using a weighting mask \mathbf{M}_F , produced by feathering the mean face outline \mathbf{M} in a manner similar to [Ara05c] and as shown in Figure 9.12:

$$\mathbf{M}_F = \mathbf{M} * \exp - \left\{ \frac{r^2(x, y)}{8} \right\} \quad (9.17)$$

9.4.1 Results

A summary of experimental results is shown in Table 9.1. The proposed algorithm greatly outperformed other methods, achieving a nearly perfect recognition (99.3+%) on all 3 databases. This is an extremely high recognition rate for such unconstrained conditions (see Figure 2.16), small amount of training data per gallery individual and the degree of

³We used the original authors' implementation.



Figure 9.12: (a) The weighting mask used to suppress background clutter. (b) The three face representations used in evaluation, shown as images, before (top row) and after (bottom row) the weighting mask was applied.

illumination, pose and motion pattern variation between different sequences. This is witnessed by the performance of Simple KLD method which can be considered a proxy for gauging the difficulty of the task, seeing that it is expected to perform well if imaging conditions are not greatly different between training and test [Sha02a]. Additionally, it is important to note the excellent performance of our algorithm on the Japanese database, even though offline training was performed using Caucasian individuals only.

As expected, when plain likelihood was used instead of the robust version proposed in Section 9.3, the recognition rate was lower, but still significantly higher than that of other methods. The high performance of non-robust gSIM is important as an estimate of the expected recognition rate in the “still-to-video” scenario of the proposed method. We conclude that our algorithm’s performance seems very promising in this setup as well. An inspection of the Receiver-Operator Characteristics Figure 9.13 (a) of the two methods shows an ever more drastic improvement. This is an insightful observation: it shows that the use of the proposed robust likelihood yields less variation in the estimated similarity between individuals across different sequences.

Finally, note that the standard deviation of our algorithm’s performance across different training and test illuminations is much lower than that of other methods, showing less dependency on the exact imaging conditions used for data acquisition.

Representations. Both the high-pass and even further Self Quotient Image representations produced an improvement in recognition for all methods over the raw grayscale. This is consistent with previous findings in the literature [Adi97, Ara05c, Fit02, Wan04a].

However, unlike in previous reports of performance evaluation of these filters, we also ask the question of *when* they help and how much in *each case*. To quantify this, consider “per-

Table 9.1: Average recognition rates (%) and their standard deviations (if applicable).

	gSIM, rob.	gSIM	FaceIt	CMSM	KPA	MSM	KLD
<i>CamFace</i>							
X	99.7/0.8	97.7/2.3	64.1/9.2	73.6/22.5	63.1/21.2	58.3/24.3	17.0/8.8
X_H	–	–	–	85.0/12.0	83.1/14.0	82.8/14.3	35.4/14.2
X_Q	–	–	–	87.0/11.4	87.1/9.0	83.4/8.4	42.8/16.8
<i>ToshFace</i>							
X	99.9/0.5	96.7/5.5	81.8/9.6	79.3/18.6	49.3/25.0	46.6/28.3	23.0/15.7
X_H	–	–	–	83.2/17.1	61.0/18.9	56.5/20.2	30.5/13.3
X_Q	–	–	–	91.1/8.3	87.7/11.2	83.3/10.8	39.7/15.7
<i>Face Video</i>							
X	100.0	91.9	91.9	91.9	91.9	81.8	59.1
X_H	–	–	–	100.0	91.9	81.8	63.6
X_Q	–	–	–	91.9	91.9	81.8	63.6



Figure 9.13: (a) The Receiver-Operator Characteristic (ROC) curves of the gSIM method, with and without the robust likelihood proposed in Section 9.3 estimated from CamFace and ToshFace data sets.

formance vectors” \mathbf{s}_R and \mathbf{s}_F , corresponding to respectively raw and filtered input, whose each component is equal to the recognition rate of a method on a particular training/test data combination. Then the vector $\Delta\mathbf{s}_R \equiv \mathbf{s}_R - \bar{\mathbf{s}}_R$ contains relative recognition rates to its average on raw input, and $\Delta\mathbf{s} \equiv \mathbf{s}_F - \mathbf{s}_R$ the improvement with the filtered representation. We then considered the *angle* ϕ between vectors $\Delta\mathbf{s}_R$ and $\Delta\mathbf{s}$, using both the high-pass and Self Quotient Image representations. In both cases, we found the angle to be $\phi \approx 136^\circ$.

This is an interesting result: it means that while on average both representations increase the recognition rate, they actually *worsen* it in “easy” recognition conditions. The observed phenomenon is well understood in the context of energy of intrinsic and extrinsic image differences and noise (see [Wan03a] for a thorough discussion). Higher than average recognition rates for raw input correspond to small changes in imaging conditions between training and test, and hence lower energy of extrinsic variation. In this case the training and test data sets are already normalized to have the same illumination and the two filters can only decrease the signal-to-noise ratio, thereby worsening the recognition performance. On the other hand, when the imaging conditions between training and test are very different, normalization of extrinsic variation is the dominant factor and the performance is improved.

This is an important observation, as it suggests that the performance of a method that uses either of the representations can be increased further in a very straightforward manner by detecting the difficulty of recognition conditions. This is exploited in [Ara06f].

Imaging conditions. We were interested if the evaluation results on our database support the observation in the literature that some illumination conditions are intrinsically more difficult for recognition than others [Sim04]. An inspection of the performance of the evaluated methods has shown a remarkable correlation in relative performance across illuminations, despite the very different models used for recognition. We found that relative recognition rates across illuminations correlate on average with $\rho = 0.96$.

Faces and individuals. Finally, in the similar manner as previously for different illumination conditions, we were interested to see if certain individuals were more difficult for recognition than others. In other words, are incorrect recognitions roughly equally distributed across the database, or does a relatively small number of people account for most? Our robust algorithm failed in too few cases to make a statistically significant observation, so we instead looked at the performance of the non-robust gSIM which failed at about an order of magnitude greater frequency.

A histogram of recognition errors across individuals in *ToshFace* data set is shown Figure 9.14 (a), showing that most errors were indeed repeated. It is difficult to ascertain if this is a consequence of an inherent similarity between these individuals or a modelling limita-



Figure 9.14: (a) A histogram of non-robust *gSIM* recognition failures across individuals in the ToshFace data set. The majority of errors are repeated, of which two of the most common ones are shown in (b). Visual inspection of these suggests that these individuals are indeed inherently similar in appearance.

tion of our algorithm. A subjective qualitative inspection of the individuals most commonly confused, shown in Figure 9.14 (b), tends to suggest that the former is the dominant cause.

Computational complexity. We conclude this section with an analysis of the computational demands of our algorithm. We focus on the online, novel sequence recognition (see Section 9.3), as this is of most practical interest. It consists of the following stages (at this point the reader may find it useful to refer back to the summary in Figures 9.10 and 9.11):

1. K -nearest neighbour computation for each face,
2. geodesic distance estimation for all pairs of faces,
3. genetic algorithm optimization,
4. fine reillumination of all faces, and
5. robust likelihood computation.

We use the following notation: N is the number of frames in a sequence, D the number of face pixels, K the number of frames used in fine reillumination, N_{gen} the number of genetic

Algorithm stage	Asymptotic complexity
K -nearest neighbours (see Section 9.1.1)	$N(ND + N \log N)$
geodesic distances (see Section 9.1.1)	$N^3 + NK$
genetic algorithm (see Section 9.1.1)	$N_{gen}N_{chr}(ND + NK)$
fine reillumination (see Section 9.1.1)	NK^3
robust likelihood (see Section 9.3)	$NN_{comp}D^2 + N \log N$

(a) Asymptotic



(b) Measured

Figure 9.15: (a) *Asymptotic complexity of different stages of the proposed online, novel sequence recognition algorithm and (b) the actual measured times for our Matlab implementation.*

algorithm generations, N_{chr} the number of chromosomes in each generation and N_{comp} the number of Gaussian components in the Generic SIM GMM.

For each face, the K -nearest neighbour computation consists of computing its distances to all other faces, $O(DN)$, and ordering them to find the nearest K , $O(N \log N)$. The estimation of geodesic distances involves initialization, $O(NK)$, and an application of Floyd's algorithm, $O(N^3)$. In a generation of the genetic algorithm, for each chromosome we compute the similarity of all pose-signatures, $O(ND)$, and look-up geodesic distances in all K -neighbourhoods, $O(NK)$. Finally, robust likelihoods are computed for all faces, $O(N_{comp}D^2)$, which are then ordered, $O(N \log N)$. Treating everything but N as a constant, the overall asymptotic complexity of the algorithm is $O(N^3)$. A summary is presented in Figure 9.15 (a).

We next profiled our implementation of the algorithm. It should be stressed that this code was written in Matlab and consequently the running times reported are not indicative of its actual practicability. In all experiments only the number of faces per sequence was varied: we used $N = 25, 50, 100, 200, 400$ and 800 faces. Mean computation times for different

stages of the algorithm are plotted in Fig 9.15 (b). In this range of N , the measured asymptote slopes were typically lower than predicted, which was especially noticeable for the most demanding computations (e.g. of geodesic distances). The most likely reason for this phenomenon are large constants associated with Matlab's *for*-loops and data allocation routines.

9.5 Summary and conclusions

In this chapter we described a novel algorithm for face recognition that uses video to achieve invariance to illumination, pose and user motion pattern variation. We introduced the concept of the Generic Shape-Illumination manifold as a model of illumination effects on faces and showed how it can be learnt offline from a small training corpus. This was made possible by the proposed “reillumination” algorithm which is used extensively both in the offline and online stages of the method.

Our method was demonstrated to achieve a nearly perfect recognition on 3 databases containing extreme variation in acquisition conditions. It was compared to and has significantly outperformed state-of-the-art commercial software and methods in the literature. Furthermore, an analysis of a large-scale performance evaluation (i) showed that the method is promising for image-to-sequence matching, (ii) suggested a direction of research to improve image filtering for illumination invariance, and (iii) confirmed that certain illuminations and individuals are inherently particularly challenging for recognition.

There are several avenues for future work that we would like to explore. Firstly, we would like to make further use of offline training data, by constructing the gSIM while taking into account probabilities of both intra- and inter-personal differences. Additionally, we would like to improve the computational efficiency of the method, e.g. by representing each FMM by a strategically chosen set of sparse samples. Finally, we are evaluating the performance of image-to-sequence matching and looking into increasing its robustness, in particular to pose.

Related publications

The following publications resulted from the work presented in this chapter:

- O. Arandjelović and R. Cipolla. Face recognition from video using the generic shape-illumination manifold. In *Proc. IEEE European Conference on Computer Vision*, 4:pages 27–40, May 2006. [Ara06b]

- O. Arandjelović and R. Cipolla. Achieving robust face recognition from video by combining a weak photometric model and a learnt generic face invariant. *Pattern Recognition*, **46**(1):9–23, January 2013. [Ara13]

III

**Multimedia Organization and
Retrieval**

10

Film Character Retrieval



Charlie Chaplin. *The Gold Rush*
1925, screen capture

The preceding chapters concentrated on the user authentication paradigm of face recognition. The aim was to reliably compare two video sequences of random head motion performed by the users. In contrast, the objective of this work is to recognize all faces of a character in the closed world of a movie or situation comedy.

This is challenging because faces in a feature-length film are relatively uncontrolled with a wide variability of scale, pose, illumination, and expressions, and also may be partially occluded. Furthermore, unlike in the previous chapters, a continuous video stream does not contain a face of only a single person, which increases the difficulty of data extraction. In this chapter recognition is performed given a small number of query faces, all of which are specified by the user.

We develop and describe a recognition method based on a cascade of processing steps that normalize for the effects of the changing imaging environment. In particular there are three areas of novelty: (i) we suppress the background surrounding the face, enabling the maximum area of the face to be retained for recognition rather than a subset; (ii) we include a pose refinement step to optimize the registration between the test image and face exemplar; and (iii) we use robust distance to a sub-space to allow for partial occlusion and expression change.

The method is applied and evaluated on several feature length films. It is demonstrated that high recall rates (over 92%) can be achieved whilst maintaining good precision (over 93%).

10.1 Introduction

We consider face recognition for content-based multimedia retrieval: our aim is to retrieve, and *rank* by confidence, film shots based on the presence of specific actors. A query to the system consists of the user choosing the person of interest in one or more keyframes. Possible applications include:

1. **DVD browsing:** Current DVD technology allows users to quickly jump to the chosen part of a film using an on-screen index. However, the available locations are predefined. Face recognition technology could allow the user to rapidly browse scenes by formulating queries based on the presence of specific actors.
2. **Content-based web search:** Many web search engines have very popular image search features (e.g. <http://www.google.co.uk/imghp>). Currently, the search is performed based on the keywords that appear in picture filenames or in the surrounding web page content. Face recognition can make the retrieval much more accurate by focusing on the content of images.



Figure 10.1: *Automatically detected faces in a typical frame from the feature-length film “Groundhog day”. The background is cluttered, pose, expression and illumination very variable.*

As before, we proceed from the face detection stage, assuming localized faces. We use a local implementation of the method of Schneiderman and Kanade [Sch00] and consider a face to be correctly detected if both eyes and the mouth are visible, see Figure 10.1. In a typical feature-length film, using every 10th frame, we obtain 2000-5000 face detections which result from a cast of 10-20 primary and secondary characters (see Section 10.3).

Method overview. Our approach consists of computing a numerical value, a distance, expressing the degree of belief that two face images belong to the same person. Low distance, ideally zero, signifies that images are of the same person, whilst a large one signifies that they are of different people.

The method involves computing a series of transformations of the original image, each aimed at removing the effects of a particular extrinsic imaging factor. The end result is a *signature image* of a person, which depends mainly on the person’s identity (and expression, see Section 10.2.5) and can be readily classified. The preprocessing stages of our algorithm are summarized in Figure 10.4 and Figure A.2.

10.1.1 Previous work

Most previous work on face recognition focuses on user authentication applications, few authors addressing it in a setup similar to ours. Fitzgibbon and Zisserman [Fit02] investigated face clustering in feature films, though without explicitly using facial features for registration. Berg *et al.* [Ber04] consider the problem of clustering detected frontal faces extracted from web news pages. In a similar manner to us, affine registration with an underlying SVM-based facial feature detector is used for face rectification. The classification is then performed in a Kernel PCA space using combined image and contextual text-based features. The problem we consider is more difficult in two respects: (i) the variation in

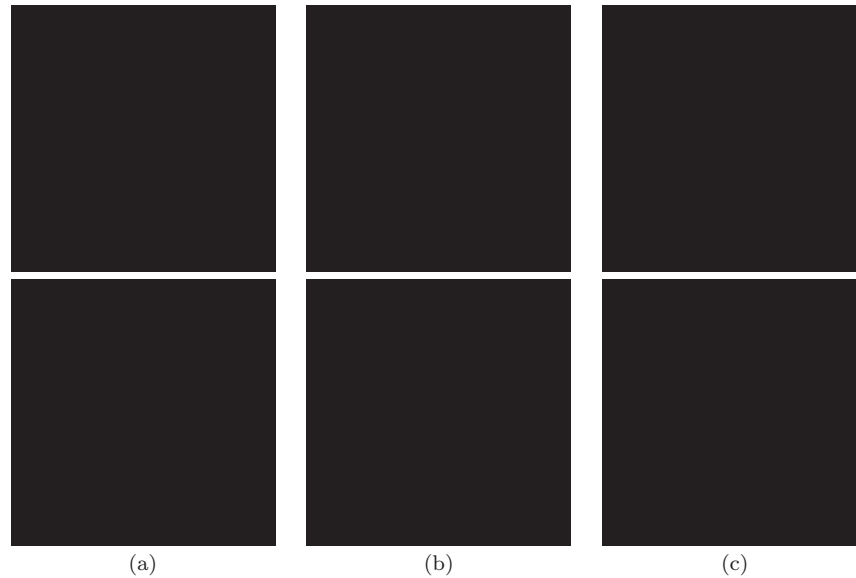


Figure 10.2: *The effects of imaging conditions – illumination (a), pose (b) and expression (c) – on the appearance of a face are dramatic and present the main difficulty to automatic face recognition.*

imaging conditions in films is typically greater than in newspaper photographs, and (ii) we do not use any type of information other than visual cues (i.e. no text). The difference in the difficulty is apparent by comparing the examples in [Ber04] with those used for evaluation in Section 10.3. For example, in [Ber04] the face image size is restricted to be at least 86×86 pixels, whilst a significant number of faces we use are of lower resolution.

Everingham and Zisserman [Eve04] consider face recognition in situation comedies. However, rather than using facial feature detection, a quasi-3D model of the head is used to correct for varying pose. Temporal information via shot tracking is exploited for enriching the training corpus. In contrast, we do not use any temporal information, and the use of local features (Section 10.2.1) allows us to compare two face images in spite of partial occlusions (Section 10.2.5).

10.2 Method details

In the proposed framework, the first step in processing a face image is the normalization of the subject’s pose i.e. registration. After the face detection stage, faces are only roughly localized and aligned – more sophisticated registration methods are needed to correct for the

Input: novel face image \mathbf{I} ,
training signature image \mathbf{S}_r .
Output: distance $d(\mathbf{I}, \mathbf{S}_r)$.

1: Facial feature localization

$$\{\mathbf{x}_i\} = \text{features}(\mathbf{I})$$

2: Pose effects – registration by affine warping

$$\mathbf{I}_R = \text{affine_warp}(\mathbf{I}, \{\mathbf{x}_i\})$$

3: Background clutter – face outline detection

$$\mathbf{I}_F = \mathbf{I}_R \cdot \text{mask}(\mathbf{I}_R)$$

4: Illumination effects – band-pass filtering

$$\mathbf{S} = \mathbf{I}_F * \mathbf{B}$$

5: Pose effects – registration refinement

$$\mathbf{S}_f = \text{warp_using_appearance}(\mathbf{I}_F, \mathbf{S}_r)$$

6: Occlusion effects – robust distance measure

$$d(\mathbf{I}, \mathbf{S}_r) = \text{distance}(\mathbf{S}_r, \mathbf{S}_f)$$

Figure 10.3: A summary of the main steps of the proposed algorithm. A novel, ‘input’ image \mathbf{I} is first preprocessed to produce a signature image \mathbf{S}_f , which is then compared with signatures of each ‘reference’ image \mathbf{S}_r . The intermediate results of preprocessing are also shown in Figure 10.4.

appearance effects of varying pose. One way of doing this is to “lock onto” characteristic facial points and warp images to align them. In our method, these facial points are the locations of the mouth and the eyes.

10.2.1 Facial feature detection

In the proposed algorithm Support Vector Machines¹ (SVMs) [Bur98, Sch02] are used for facial feature detection. A related approach was described in [Ber04]; alternative methods include pictorial structures [Fel05], shape+appearance cascaded classifiers [Fuk98] and the method of Cristinacce *et al.* [Cri04].

We represent each facial feature, i.e. the image patch surrounding it, by a feature vector. An SVM with a set of parameters (kernel type, its bandwidth and a regularization constant)

¹We used the LibSVM implementation freely available at <http://www.csie.ntu.edu.tw/~cjlin/libsvm/>



Figure 10.4: *Each step in the proposed preprocessing cascade produces a result invariant to a specific extrinsic imaging factor. The result is a ‘signature’ image of a person’s face.*

is then trained on a part of the training data and its performance iteratively optimized on the remainder. The final detector is evaluated by a one-time run on unseen data.

Training

For training we use manually localized facial features in a set of 300 randomly chosen faces from the feature-length film “Groundhog day” and the situation comedy “Fawlty Towers”. Examples are extracted by taking rectangular image patches centred at feature locations (see Figures 10.5 and 10.6). We represent each patch $\mathbf{I} \in \mathbb{R}^{H \times W}$ with a feature vector $\mathbf{v} \in \mathbb{R}^{2H \times W}$ containing appearance and gradient information (we used $H = 17$ and $W = 21$ for a face image of the size 81×81 - the units being pixels):

$$v_A(Wy + x) = I(x, y) \quad (10.1)$$

$$v_G(Wy + x) = |\nabla I(x, y)| \quad (10.2)$$

$$\mathbf{v} = \begin{bmatrix} \mathbf{v}_A \\ \mathbf{v}_G \end{bmatrix} \quad (10.3)$$

Local information. In the proposed method, implicit local information is included for increased robustness. This is done by complementing the image appearance vector \mathbf{v}_A with the grayscale intensity gradient vector \mathbf{v}_G , as in equation (10.3).

Synthetic data. For robust classification, it is important that training data sets are representative of the whole spaces that are discriminated between. In uncontrolled imaging conditions, the appearance of facial features exhibits a lot of variation, requiring an appropriately large training corpus. This makes the approach with manual feature extraction impractical. In our method, a large portion of training data (1500 out of 1800 training



Figure 10.5: *Without surrounding image context, distinguishing features in low resolution and severe illumination conditions is a hard task even for a human. Shown are a mouth and an eye that although easily recognized within the context of the whole image, are very similar in isolation.*



Figure 10.6: *A subset of the data (1800 features were used in total) used to train the SVM-based eye detector. Notice the low resolution and the importance of the surrounding image context for precise localization (see Figure 10.5).*



Figure 10.7: *A summary of the efficient SVM-based eye detection: 1: Prior on feature location restricts the search region. 2: Only $\sim 25\%$ of the locations are initially classified. 3: Morphological dilation is used to approximate the dense classification result from a sparse output. 4: The largest prior-weighted cluster is chosen as containing the feature of interest.*

examples) was synthetically generated. Seeing that the surface of the face is smooth and roughly fronto-parallel, its 3D motion produces locally affine-like effects in the image plane. Therefore, we synthesize training examples by applying random affine perturbations to the manually detected set (for similar approaches to generalization from a small amount of training data see [Ara06e, Mar02, Sun98]).

SVM-based feature detector

SVMs only provide classification decision for individual feature vectors, but no associated probabilistic information. Therefore, performing classification on all image patches produces as a result a binary image (a feature is either present or not in a particular location) from which only a single feature location is to be selected.

Our method is based on the observation that due to the robustness to noise of SVMs, the binary image output consists of connected components of positive classifications (we will refer to these as *clusters*), see Figure 10.7. We use a prior on feature locations to focus on the cluster of interest. Priors, corresponding to the three features are assumed to be independent and Gaussian (2D, with full covariance matrices) and are learnt from the training corpus of 300 manually localized features described in Section 10.2.1. We then consider the total ‘evidence’ for a feature within each cluster:

$$e(\mathcal{S}) = \int_{\mathbf{x} \in \mathcal{S}} P(\mathbf{x}) d\mathbf{x} \quad (10.4)$$

where \mathcal{S} is a cluster and $P(\mathbf{x})$ the Gaussian prior on the facial feature location. An unbiased feature location estimate with $\sigma \approx 1.5$ pixels was obtained by choosing the mean of the cluster with largest evidence as the final feature location. Intermediate results of the method

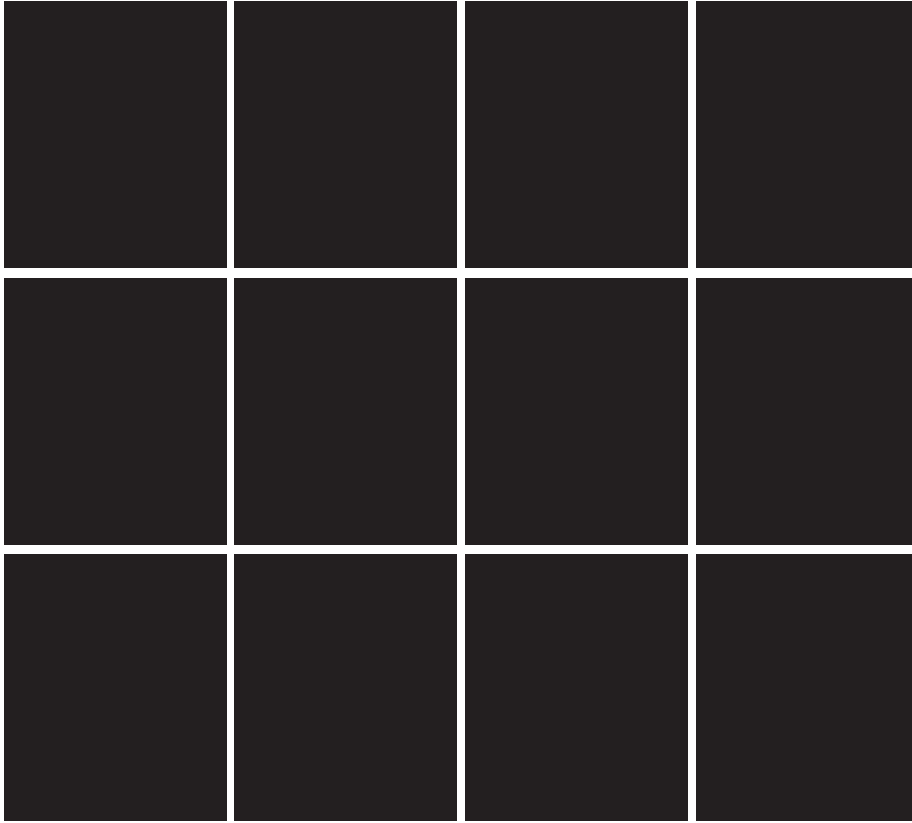


Figure 10.8: *High accuracy in automatic detection of facial features is achieved in spite of wide variation in facial expression, pose, illumination and the presence of facial wear (e.g. glasses and makeup).*

are shown in Figure 10.7, while Figure 10.8 shows examples of detected features.

10.2.2 Registration

In the proposed method dense point correspondences are implicitly or explicitly used in several stages: for background clutter removal, partial occlusion detection and signature image comparison (Section 10.2.3–10.2.5). To this end, images of faces are affine warped to have salient facial features aligned with their mean, canonical locations. The six transformation parameters are uniquely determined from three pairs of point correspondences – between detected facial features (the eyes and the mouth) and this canonical frame. In contrast to global appearance-based methods (e.g. [Bla99, Edw98a]) our approach is more robust to partial occlusion. It is summarized in Figure 10.9 with typical results shown in Figure 10.10.

Input: canonical facial feature locations \mathbf{x}_{can} ,
face image \mathbf{I} ,
facial feature locations \mathbf{x}_{in} .
Output: registered image \mathbf{I}_{reg} .

1: Estimate the affine warp matrix
 $\mathbf{A} = \text{affine_from_correspondences}(\mathbf{x}_{can}, \mathbf{x}_{in})$

2: Compute eigenvalues of \mathbf{A}
 $\{\lambda_1, \lambda_2\} = \text{eig}(\mathbf{A})$

3: Impose prior on shear and rescaling by \mathbf{A}
if ($|\mathbf{A}| \in [0.9, 1.1] \wedge \lambda_1/\lambda_2 \in [0.6, 1.3]$) **then**

4: Warp the image
 $\mathbf{I}_{reg} = \text{affine_warp}(\mathbf{I}; \mathbf{A})$

else

5: Face detector false +ve

Figure 10.9: A summary of the proposed facial feature-based registration of faces and removal of face detector false positives.



Figure 10.10: *Original (top) and corresponding registered images (bottom). The eyes and the mouth in all registered images are at the same, canonical locations. The effects of affine transformations are significant.*

10.2.3 Background removal

The bounding box of a face, supplied by the face detector, typically contains significant background clutter and affine registration boundary artefacts, see Figure 10.10. To realize a reliable comparison of two faces, segmentation to foreground (i.e. face) and background regions has to be performed. We show that the face outline can be robustly detected by combining a prior on the face shape, learnt offline, and a set of measurements of intensity discontinuity in an image of a face. The proposed method requires only grey level information, performing equally well for colour and greyscale input, unlike previous approaches which typically use skin colour for segmentation (e.g. [Ara05b]).

In detecting the face outline, we only consider points confined to a discrete mesh corresponding to angles equally spaced at $\Delta\alpha$ and radii at Δr , see Figure 10.11 (a); in our implementation we use $\Delta\alpha = 2\pi/100$ and $\Delta r = 1$. At each mesh point we measure the image intensity gradient in the radial direction – if its magnitude is locally maximal and greater than a threshold t , we assign it a constant high-probability and a constant low probability otherwise, see Figure 10.11 (a,b). Let \mathbf{m}_i be a vector of probabilities corresponding to discrete radius values at angle $\alpha_i = i\Delta\alpha$, and r_i the boundary location at the same angle.



Figure 10.11: *Markov chain observations: (a) A discrete mesh in radial coordinates (only 10% of the points are shown for clarity) to which the boundary is confined. Also shown is a single measurement of image intensity in the radial direction and the detected high probability points. The plot of image intensity along this direction is shown in (b) along with the gradient magnitude used to select the high probability locations.*

We seek the maximum *a posteriori* estimate of the boundary radii:

$$\{r_i\} = \arg \max_{\{r_i\}} P(r_1, \dots, r_N | \mathbf{m}_1, \dots, \mathbf{m}_N) = \quad (10.5)$$

$$\arg \max_{\{r_i\}} P(\mathbf{m}_1, \dots, \mathbf{m}_N | r_1, \dots, r_N) P(r_1, \dots, r_N), \text{ where } N = 2\pi/\Delta\alpha. \quad (10.6)$$

We make the Naïve Bayes assumption for the first term in equation (10.5), whereas, exploiting the observation that surfaces of faces are mostly smooth, for the second term we assume to be a first-order Markov chain. Formally:

$$P(\mathbf{m}_1, \dots, \mathbf{m}_N | r_1, \dots, r_N) = \prod_{i=1}^N P(\mathbf{m}_i | r_i) = \prod_{i=1}^N m_i(r_j) \quad (10.7)$$

$$P(r_1, \dots, r_N) = P(r_1) \prod_{i=2}^N P(r_i | r_{i-1}) \quad (10.8)$$

In our method model parameters (priors and likelihoods) are learnt from 500 manually delineated face outlines. The application of the model by maximizing expression in (10.5) is efficiently realized using dynamic programming i.e. the well-known Viterbi algorithm [Gri92].

Feathering. The described method of segmentation of face images to foreground and background produces as a result a binary mask image \mathbf{M} . As well as masking the corresponding registered face image \mathbf{I}_R (see Figure 10.12), we smoothly suppress image information around the boundary to achieve robustness to small errors in its localization. This is



Figure 10.12: *Original image, image with detected face outline, and the resulting image with the background masked.*



Figure 10.13: *Original images of detected and affine-registered faces and the result of the proposed segmentation algorithm. Subtle variations of the face outline caused by different poses and head shapes are handled with high precision.*

often referred to as *feathering*:

$$\mathbf{M}_F = \mathbf{M} * \exp - \left(\frac{r(x, y)}{4} \right)^2 \quad (10.9)$$

$$I_F(x, y) = I_R(x, y)M_F(x, y) \quad (10.10)$$

Examples of segmented and feathered faces are shown in Figure 10.13.

10.2.4 Compensating for changes in illumination

The last step in processing of a face image to produce its signature is the removal of illumination effects. As the most significant modes of illumination changes are rather coarse – ambient light varies in intensity, while the dominant illumination source is either frontal, illuminating from the left, right, top or bottom (seldom) – and noting that these produce mostly slowly varying, low spatial frequency variations [Fit02] (also see Section 2.3.2), we

normalize for their effects by band-pass filtering, see Figure 10.4:

$$\mathbf{S} = \mathbf{I}_F * \mathbf{G}_{\sigma=0.5} - \mathbf{I}_F * \mathbf{G}_{\sigma=8} \quad (10.11)$$

This defines the signature image \mathbf{S} .

10.2.5 Comparing signature images

In Section 10.2.1–10.2.4 a cascade of transformations applied to face images was described, producing a signature image insensitive to illumination, pose and background clutter. We now show how the accuracy of facial feature alignment and the robustness to partial occlusion can be increased further when two signature images are compared.

Improving registration

In the registration method proposed in Section 10.2.2, the optimal affine warp parameters were estimated from three point correspondences in 2D. Therefore, the 6 degrees of freedom of the affine transformation were uniquely determined, making the estimate sensitive to facial feature localization errors. To increase the accuracy of registration, we propose a dense, appearance-based affine correction to the already computed feature correspondence-based registration.

In our algorithm, the corresponding characteristic regions of two faces, see Figure 10.14 (a), are perturbed by small translations to find the optimal *residual shift* (i.e. that which gives the highest normalized cross-correlation score between the two overlapping regions). These new point correspondences now overdetermine the residual affine transformation (which we estimate in the least L_2 norm of the error sense) that is applied to the image. Some results are shown in Figure 10.14.

Distance

Single query image. Given two signature images in precise correspondence (see above), \mathbf{S}_1 and \mathbf{S}_2 , we compute the following distance between them:

$$d_S(\mathbf{S}_1, \mathbf{S}_2) = \sum_x \sum_y h(S_1(x, y) - S_2(x, y)) \quad (10.12)$$

where $h(\Delta S) = (\Delta S)^2$ if the probability of occlusion at (x, y) is low and a constant value k otherwise. This is effectively the L_2 norm with added outlier (e.g. occlusion) robustness, similar to [Bla98]. We now describe how this threshold is determined.

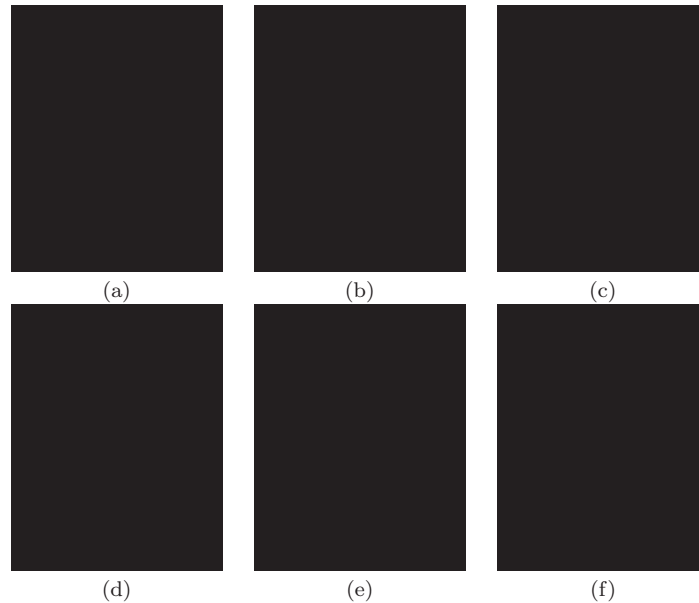


Figure 10.14: *Pose refinement summary: (a) Salient regions of the face used for appearance-based computation of the residual affine registration. (b)(c) Images aligned using feature correspondences alone. (d) The salient regions shown in (a) are used to refine the pose of (b) so that it is more closely aligned with (c). The residual rotation between (b) and (c) is removed. This correction can be seen clearly in the difference images: (e) is $|\mathbf{S}_c - \mathbf{S}_b|$, and (f) is $|\mathbf{S}_c - \mathbf{S}_d|$.*

Partial occlusions. Occlusions of imaged faces in films are common. Whilst some research has addressed detecting and removing specific artefacts only, such as glasses [Jin00], here we give an alternative non-parametric approach, and use a simple appearance-based statistical method for occlusion detection. Given that the error contribution at (x, y) is $\varepsilon = \Delta S(x, y)$, we detect occlusion if the probability $P_s(\varepsilon)$ that ε is due to inter- or intra-personal differences is less than 0.05. Pixels are classified as occluded or not on an independent basis. $P_s(\varepsilon)$ is learnt in a non-parametric fashion from a face corpus with no occlusion.

The proposed approach achieved a reduction of 33% in the expected within-class signature image distance, while the effect on between-class distances was found to be statistically insignificant.

Multiple query images. The distance introduced in equation (10.12) gives the confidence measure that two signature images correspond to the same person. Often, however,

more than a single image of a person is available as a query: these may be supplied by the user or can be automatically added to the query corpus as the highest ranking matches of a single image-based retrieval. In either case we want to be able to quantify the confidence that the person in the novel image is the same as in the query set.

Seeing that the processing stages described so far greatly normalize for the effects of changing pose, illumination and background clutter, the dominant mode of variation across a query corpus of signature images $\{\mathbf{S}_i\}$ can be expected to be due to facial expression. We assume that the corresponding manifold of expression is linear, making the problem that of point-to-subspace matching [Bla98]. Given a novel signature image \mathbf{S}_N we compute a robust distance:

$$d_G(\{\mathbf{S}_i\}, \mathbf{S}_N) = d_S(\mathbf{F}\mathbf{F}^T\mathbf{S}_N, \mathbf{S}_N) \quad (10.13)$$

where \mathbf{F} is orthonormal basis matrix corresponding to the linear subspace that explains 95% of energy of variation within the set $\{\mathbf{S}_i\}$.

10.3 Empirical evaluation

The proposed algorithm was evaluated on automatically detected faces from the situation comedy “Fawlty Towers” (“A touch of class” episode), and feature-length films “Groundhog Day” and “Pretty Woman”². Detection was performed on every 10th frame, producing respectively 330, 5500, and 3000 detected faces (including incorrect detections). Face images (frame regions within bounding boxes determined by the face detector) were automatically resized to 80×80 pixels, see Figure 10.17 (a).

10.3.1 Evaluation methodology

Empirical evaluation consisted of querying the algorithm with each image in turn (or image set for multiple query images) and ranking the data in order of similarity to it. Two ways of assessing the results were employed – using Receiver Operator Characteristics (ROC) and the rank ordering score introduced in Section 2.4.

10.3.2 Results

Typical Receiver Operator Characteristic curves obtained with the proposed method are shown in Figure 10.15 (a, b). These show that excellent results are obtained using as little as 1-2 query images, typically correctly recalling 92% of the faces of the query person with only 7% of false retrievals. As expected, more query images produced better retrieval

²Available at <http://www.robots.ox.ac.uk/~vgg/data/>

accuracy, also illustrated in Figure 10.15 (e, f). Note that as the number of query images is increased, not only is the ranking better on average but also more robust, as demonstrated by a decreased standard deviation of rank order scores. This is very important in practice, as it implies that less care needs to be taken by the user in the choice of query images. For the case of multiple query images, we compared the proposed subspace-based matching with the k-nearest neighbours approach, which was found to consistently produce worse results. The improvement of recognition with each stage of the proposed algorithm is shown in Figure 10.16.

Example retrievals are shown in Figures 10.17-10.19. Only a single incorrect face is retrieved in the first 50, and this is with a low matching confidence (i.e. ranked amongst the last in the retrieved set). Notice the robustness of our method to pose, expression, illumination and background clutter.

10.4 Summary and conclusions

In this chapter we introduced a content-based film-shot retrieval system driven by a novel face recognition algorithm. The proposed approach of systematically removing particular imaging distortions – pose, background clutter, illumination and partial occlusion has been demonstrated to consistently achieve high recall and precision rates on several well-known feature-length films and situation comedies.

Related publications

The following publications resulted from the work presented in this chapter:

- O. Arandjelović and A. Zisserman. Automatic face recognition for film character retrieval in feature-length films. In *Proc. IEEE Conference on Computer Vision and Pattern Recognition*, 1:pages 860–867, June 2005. [Ara05c]
- O. Arandjelović and A. Zisserman. *Interactive video: Algorithms and Technologies.*, chapter On Film Character Rretrieval in Feature-Length Films., pages 89–103. Springer-Verlag, 2006. ISBN 978-3-540-33214-5. [Ara06i]

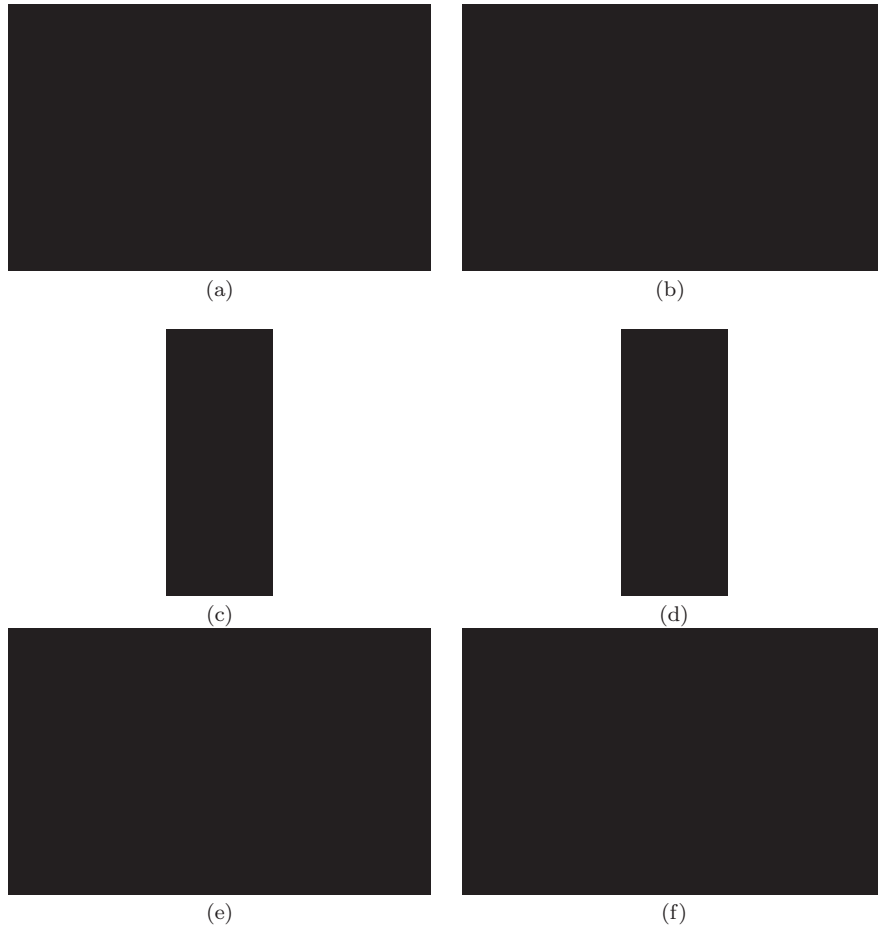


Figure 10.15: (a, b) ROC curves for the retrieval of Basil (c) and Sybil (d) in “Faulty Towers”. The corresponding rank ordering scores across 35 retrievals are shown in (e) and (f), sorted for the ease of visualization.



Figure 10.16: *The average rank ordering score of the baseline algorithm and its improvement as each of the proposed processing stages is added. The improvement is demonstrated both in the increase of the average score, and also in the decrease of its standard deviation averaged over different queries. Finally, note that the averages are brought down by few very difficult queries, which is illustrated well in Figure 10.15 (e,f).*



Figure 10.17: *(a) The “Pretty Woman” data set – every 50th detected face is shown for compactness. Typical retrieval result is shown in (b) – query images are outlined by a solid line, the incorrectly retrieved face by a dashed line. The performance of our algorithm is very good in spite of the small number of query images used and the extremely difficult data set – this character frequently changes wigs, makeup and facial expressions.*



Figure 10.18: *(a) The “Fawlty Towers” data set – every 30th detected face is shown for compactness. Typical retrieval result is shown in (b) – query images are outlined. There are no incorrectly retrieved faces in the top 50.*

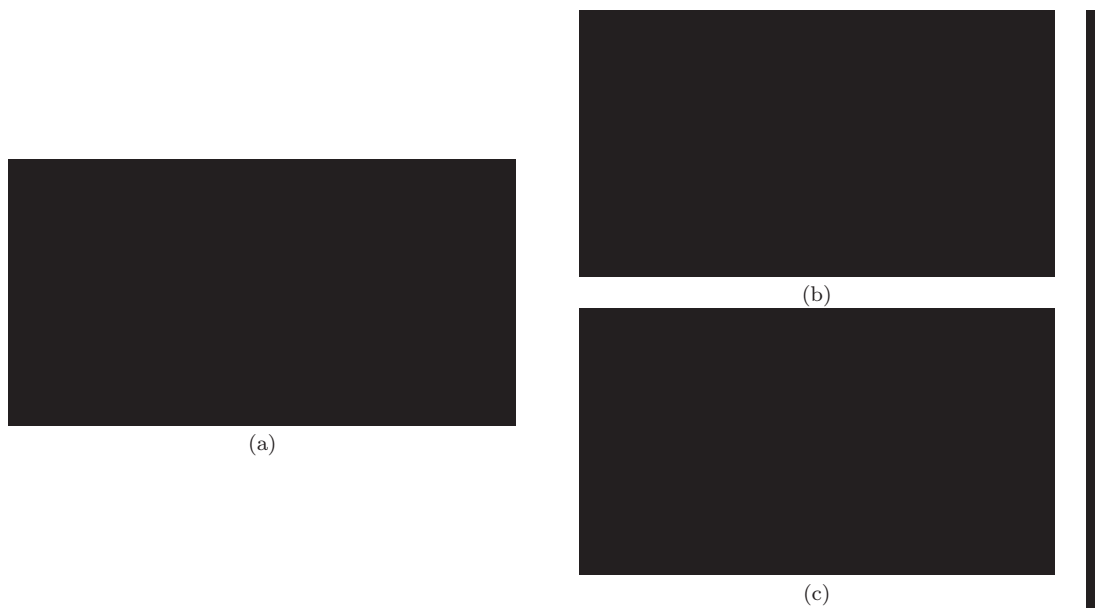


Figure 10.19: (a) The “Groundhog Day” data set – every 30th detected face is shown for compactness. Typical retrieval results are shown in (b) and (c) – query images are outlined. There are no incorrectly retrieved faces in the top 50.

11

Automatic Cast Listing in Films



Auguste Renoir. *Moulin de la Galette*
1876, Oil on canvas, 131 x 175 cm
Musée d'Orsay, Paris

In this chapter we continue looking at faces in feature-length films. We consider the most difficult recognition setting of all – fully automatic (i.e. without any dataset-specific training information) listing of the individuals present in a video. In other words, our goal is to automatically determine the cast of a feature-length film without any user intervention.

The main contribution of this chapter is an algorithm for clustering over face appearance manifolds themselves. Specifically: (i) we develop a novel algorithm for exploiting *coherence* of dissimilarities between manifolds, (ii) we show how to estimate the optimal *dataset-specific* discriminant manifold starting from a *generic* one, and (iii) we describe a fully automatic, practical system based on the proposed algorithm.

We present the results of preliminary empirical evaluation which show a vast improvement over traditional pattern clustering methods in the literature.

11.1 Introduction

The problem that we address in this chapter is that of automatically determining the cast of a feature-length film. This is a far more difficult problem than that of character retrieval. However, it is also more appealing from a practical standpoint: the method we will describe can be used to pre-compute and compactly store identity information for an entire film, rendering *any* retrieval equivalent to indexing a look-up table and, consequently, extremely fast.

The first idea of this chapter concerns the observation that some people are inherently more similar looking to each other than others. As an example from our data set, in certain imaging conditions Sir Hacker may be difficult to distinguish from his secretary, Sir Humphrey, see respectively Figures 11.1 and 11.10 in Section 11.2.3). However, regardless of the imaging setup he is unlikely to be mistaken, say, for his wife, see Figure 11.5 in Section 11.2.1. The question is then how to automatically extract and represent the structure of these inter-personal similarities from unlabelled sets of video sequences. We show that this can be done by working in what we term the *manifold space* – a vector space in which *each point* is an appearance manifold.

The second major contribution of this chapter is a method for unsupervised extraction of inter-class data for discriminative learning on an unlabelled set of video sequences. In spirit, this approach is similar to the work of Lee and Kriegman [Lee05] in which a generic appearance manifold is progressively updated with new data to converge to a person-specific one. In contrast, we start from a generic *discriminative* manifold and converge to a data-specific one, *automatically* collecting within-class data.

An overview of the entire system is shown in Figure A.2.



Figure 11.1: *The appearance of faces in films exhibits great variability depending on the extrinsic imaging conditions. Shown are the most common sources of intra-personal appearance variations (all faces are from the same episode of the situation comedy “Yes, Minister”).*

11.2 Method details

In this section we describe each of the steps in the algorithmic cascade of the proposed method: (i) automatic data acquisition and preprocessing, (ii) unsupervised discriminative learning and (iii) clustering over appearance manifolds.

11.2.1 Automatic data acquisition

Our cast clustering algorithm is based on pair-wise comparisons of face manifolds [Ara05b, Lee03, Mog02] that correspond to sequences of moving faces. Hence, the first stage of the proposed method is automatic acquisition of face data from a continuous feature-length film. We (i) temporally segment the video into *shots*, (ii) detect faces in each and, finally, (iii) collect detections through time by tracking in the (X, Y, scale) space.

Shot transition detection. A number of reliable methods for shot transition detection have been proposed in the literature [Ham95, Ots93, Zab95, Zha93]. We used the Edge Change Ratio (ECR) [Zab95] algorithm as it is able in a unified manner to detect all 3 standard types of shot transitions: (i) hard cuts, (ii) fades and (iii) dissolves. The ECR is defined as:

$$ECR_n = \max(X_n^{in}/\sigma_n, X_{n-1}^{out}/\sigma_{n-1}) \quad (11.1)$$

where σ_n is the number of edge pixels computed using the Canny edge detector [Can86], and X_n^{in} and X_n^{out} the number of entering and existing edge pixels in frame n . Shot changes are then recognized by considering local peaks of ECR_n , exceeding a threshold, see [Lie98,

Input: film frames $\{f_t\}$,
generic discrimination subspace \mathbf{B}_G .
Output: cast classes \mathbb{C} .

1: Data extraction – face manifolds

$\mathbf{T} = \text{get_manifolds}(\{f_t\})$

2: Synthetically repopulate manifolds

$\mathbf{T} = \text{repopulate}(\mathbf{T})$

3: Adaptive discriminative learning – distance matrix

$\mathbf{D}_S = \text{distance}(\mathbf{T}, \mathbf{B}_G)$

4: Manifold space

$\mathbb{M} = \text{MDS}(\mathbf{D}_S)$

5: Initial classes

$\mathbb{C} = \text{classes}(\mathbf{D}_S)$

6: Anisotropic boundaries in manifold space

for $\mathbf{C}_i, \mathbf{C}_j \in \mathbb{C}$

7: PPCA models

$(\mathcal{G}_i, \mathcal{G}_j) = \text{PPCA}(\mathbf{C}_i, \mathbf{C}_j, \mathbb{M})$

8: Merge clusters using Weighted Description Length

$\Delta\text{DL}(i, j) < \text{threshold} ? \text{merge}(i, j, \mathbb{C})$

Figure 11.2: *A summary of the main steps of the proposed algorithm.*

Zab95] for details and Figure 11.3 for an example.

Face tracking through shots. We detect faces in cluttered scenes on an independent, frame-by-frame basis with the Viola-Jones [Vio04] cascaded algorithm¹. For each detected face, the detector provides a triplet of the X and Y locations of its centre and scale s . In the proposed method, face detections are connected by tracks using a simple tracking algorithm in the 3D space $\mathbf{x} = (X, Y, s)$. We employ a form of the Kalman filter in which observations are deemed completely reliable (i.e. noise-free) and the dynamic model is that of zero mean velocity $[\dot{\mathbf{x}}] = 0$ with a diagonal noise covariance matrix. A typical tracking result is illustrated in Figure 11.4 with a single face track obtained shown in Figure 11.5.

¹We used the freely available code, part of the Intel® OpenCV library.



Figure 11.3: *The unsmoothed Edge Change Ratio for a 20s segment from the situation comedy “Yes, Minister”.*



Figure 11.4: *The X coordinate of detected faces (red dots) through time in a single shot and the resulting tracks connecting them (blue lines) as determined by our algorithm.*

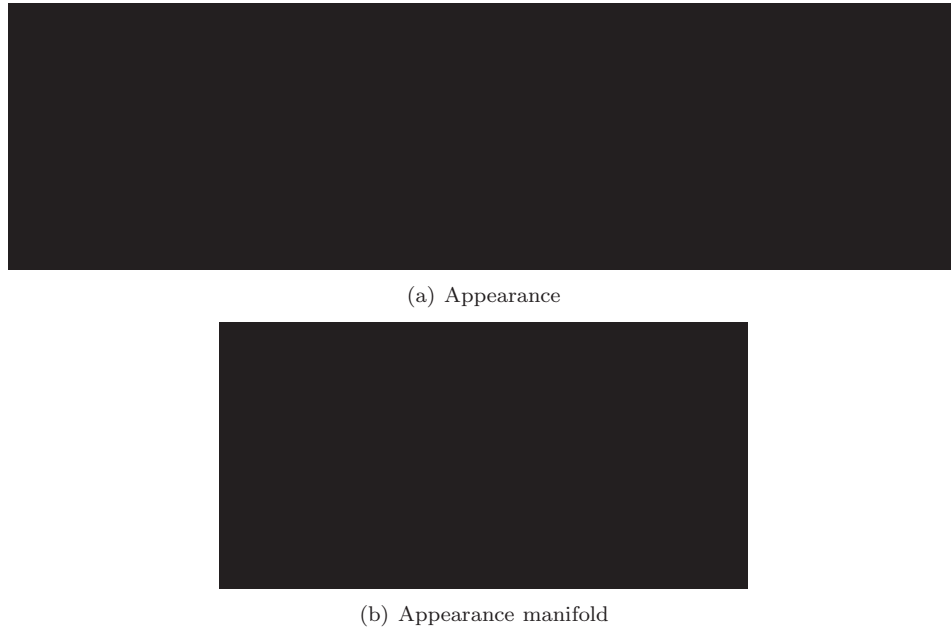


Figure 11.5: *A typical face track obtained using our algorithm. Shown are (a) the original images are detected by the face detector (rescaled to the uniform scale of 50×50 pixels) and (b) as points in the 3D principal component space with temporal connections.*

11.2.2 Appearance manifold discrimination

Having collected face tracks from a film, we turn to the problem of clustering these subsequences by corresponding identity. Due to the smoothness of faces, each track corresponds to an appearance manifold [Ara05b, Lee03, Mog02], as illustrated in Figure 11.5. We want to compare these manifolds and use the structure of the variation of dissimilarity between them to deduce which ones describe the same person.

Data preprocessing. As in the previous chapter, as the first step in the comparison of two appearance manifolds we employ simple preprocessing on a frame-by-frame basis that normalizes for the majority of illumination effects and suppresses the background. If \mathbf{X} is an image of a face, in the usual form of a raster-ordered pixel vector, we first normalize for the effects of illumination using a high-pass filter (previously used in [Ara05c, Fit02]) scaled

Input: manifolds $\mathbf{T} = \{T_i\}$.
generic discrimination subspace \mathbf{B}_G .
Output: distance matrix \mathbf{D}_S .

1: Distance matrix using generic discrimination

$$\mathbf{D}_G = \text{distance}(T, \mathbf{B}_G)$$

2: Provisional classes

$$\mathbb{C}_T = \text{classes}(\mathbf{D}_G)$$

3: Data-specific discrimination space

$$\mathbf{B}_S = \text{constraint_sspace}(\mathbb{C}_T)$$

4: Mixed discrimination space

$$\mathbf{B}_C = \text{combine_eigenspaces}(\mathbf{B}_S, \mathbf{B}_G)$$

5: Distance matrix using data-specific discrimination

$$\mathbf{D}_S = \text{distance}(\mathbf{T}, \mathbf{B}_C)$$

Figure 11.6: *From generic to data-specific discrimination – algorithm summary.*

by local image intensity:

$$\mathbf{X}_L = \mathbf{X} * \mathbf{G}_{\sigma=1.5} \quad (11.2)$$

$$\mathbf{X}_H = \mathbf{X} - \mathbf{X}_L \quad (11.3)$$

$$X_I(x, y) = X_H(x, y) / X_L(x, y). \quad (11.4)$$

This is similar to the Self-Quotient Image of Wang *et al.* [Wan04a]. The purpose of local scaling is to equalize edge strengths in shadowed (weak) and well-illuminated (strong) regions of the face.

Background is suppressed with a weighting mask \mathbf{M}_F , produced by feathering (similar to [Ara05c]) the mean face outline \mathbf{M} , as shown in Figure 11.7:

$$\mathbf{M}_F = \mathbf{M} * \exp - \left(\frac{r(x, y)}{4} \right)^2 \quad (11.5)$$

$$X_F(x, y) = X_I(x, y) M_F(x, y). \quad (11.6)$$



Figure 11.7: (a) The mask used to suppress cluttered background in images of automatically detected faces, and (b) an example of a detected, unprocessed face and the result of illumination normalization and background suppression.

Synthetic data augmentation. Many of the collected face tracks in films are short and contain little pose variation. For this reason, we automatically enrich the training data corpus by stochastically repopulating geodesic neighbourhoods of randomly drawn manifold samples. This is the same approach we used in Chapter 4 so here we only briefly summarize it for continuity.

Under the assumption that the face to image space embedding function is smooth, geodesically close images correspond to small changes in imaging parameters (e.g. yaw or pitch). Hence, using the first-order Taylor approximation of the effects of a projective camera, the face motion manifold is locally topologically similar to the affine warp manifold. The proposed algorithm then consists of random draws of a face image \mathbf{x} from the data, stochastic perturbation of \mathbf{x} by a set of affine warps $\{\mathbf{A}_j\}$ and finally, the augmentation of data by the warped images.

Comparing normalized appearance manifolds

For pair-wise comparisons of manifolds we employ the Constraint Mutual Subspace method (CMSM) [Fuk03], based on principal angles between subspaces [Hot36, Oja83]. This choice is motivated by: (i) CMSM’s good performance reports in the literature [Ara05b, Fuk03], (ii) its computational efficiency [Bjö73] and compact data representation, and (iii) its ability to extract the most similar modes of variation between two subspaces, see Chapter 5 for more detail.

As in [Fuk03], we represent each appearance manifold by a minimal linear subspace it is embedded in – estimated using Probabilistic PCA [Tip99b]. The similarity of two such subspaces is then computed as the mean of their first 3 canonical correlations, after



Figure 11.8: A visualization of the basis of the linear constraint subspace, the most descriptive linear subspace (eigenspace using PCA [Tur91a]) and the most discriminative linear subspace in terms of within and between class scatter (LDA [Bel97]).

the projection onto the *constraint subspace* – a linear manifold that attempts to maximize the separation (in terms of canonical correlations) between different class subspaces, see Figure 11.8.

Computing the constraint subspace. Let $\{\mathbf{B}_i\} = \mathbf{B}_1, \dots, \mathbf{B}_N$ be orthonormal basis matrices representing subspaces corresponding to N different classes (cast members, in our case). Fukui and Yamaguchi [Fuk03] compute the orthonormal basis matrix \mathbf{B}_C corresponding to the constraint subspace using PCA from:

$$(\mathbf{B}_R \ \mathbf{B}_C) \begin{pmatrix} \Lambda_L & \mathbf{0} \\ \mathbf{0} & \Lambda_S \end{pmatrix} \begin{pmatrix} \mathbf{B}_R^T \\ \mathbf{B}_C^T \end{pmatrix} = \sum_{i=1}^N \mathbf{B}_i \mathbf{B}_i^T, \mathbf{B}_R^T \mathbf{B}_C = \mathbf{0} \quad (11.7)$$

where Λ_L and Λ_S are diagonal matrices with diagonal entries, respectively, greater or equal than 1 and less than 1. We modify this approach by weighting the contribution of the projection matrix \mathbf{B}_i by the number of samples used to compute it. This way, a more robust estimate is obtained as subspaces computed from smaller amounts of data (i.e. with lower Signal-to-Noise Ratio) are de-emphasized:

$$(\mathbf{B}_R \ \mathbf{B}_C) \begin{pmatrix} \Lambda_L & \mathbf{0} \\ \mathbf{0} & \Lambda_S \end{pmatrix} \begin{pmatrix} \mathbf{B}_R^T \\ \mathbf{B}_C^T \end{pmatrix} = N \sum_{i=1}^N N_i \mathbf{B}_i \mathbf{B}_i^T / \sum_{i=1}^N N_i \quad (11.8)$$

From generic to data-specific discrimination. The problem of estimating \mathbf{B}_C lies in the fact that we do not know which appearance manifolds belong to the same class and which to different classes i.e. $\{\mathbf{B}_i\}$ are unknown. We therefore start from a *generic* constraint subspace \mathbf{B}_C^g , computed offline from a large data corpus. For example, for the evaluation

reported in Section 11.3 we estimated \mathbf{B}_i , $i = 1, \dots, 100$ using the *CamFace* data set (see Appendix C).

Now, consider the Receiver-Operator Characteristic (ROC) curve of CMSM in Figure 11.9, also estimated offline. The inherent tradeoff between recall and precision is clear, making it impossible to immediately draw class boundaries using the inter-manifold distance only. Instead, we propose to exploit the two marked salient points of the curve merely to collect data for the construction of the constraint subspace. Starting from an arbitrary manifold, the “high recall” point allows to confidently partition a *part* of the data into different classes. Then, using manifolds in each of the classes we can gather intra-class data using the “high precision” point. The collected class information can then be used to compute the basis \mathbf{B}_C^s of the *data-specific* constraint subspace.

The problem in using the above defined data-specific constraint subspace \mathbf{B}_C^s is that it is constructed using only the easiest to classify data. Hence, it cannot be expected to discriminate well in difficult cases, corresponding to the points on the ROC curve between “high precision” and “high recall”. To solve this problem, we do not *substitute* the data-specific for the generic constraint subspace, but iteratively *combine* the two based on our confidence $0.0 \leq \alpha \leq 1.0$ in the former:

$$\mathbf{B}_C = \text{mix}(\alpha, 1 - \alpha, \mathbf{B}_C^s, \mathbf{B}_C^g) \quad (11.9)$$

where α and $(1 - \alpha)$ are mixing weights. We used an eigenspace mixing algorithm similar to Hall *et al.* [Hal00]. The mixing confidence parameter α is determined as follows. Consider clustering appearance manifolds using each of the two salient points. The “high precision” point will give an overestimate $N_h \geq N$ of the number of classes N , while the “high recall” one an underestimate $N_l \leq N$. The closer N_h and N_l are, the more confident we can be that the constraint subspace estimate is good. Hence, we compute α as their normalized difference (which ensures that the condition $0.0 \leq \alpha \leq 1.0$ is satisfied):

$$\alpha = 1 - \frac{N_h - N_l}{M - 1} \quad (11.10)$$

where M is the number of appearance manifolds.

11.2.3 The manifold space

In Section 11.2.2 we described how to preprocess and pairwise compare appearance manifolds, optimally exploiting generic information for discriminating between human faces and automatically extracted data-specific information. One of the main premises of the proposed clustering method is that there is a structure to inter- and intra-personal distances between



Figure 11.9: *The ROC curve of the Constraint Mutual Subspace Method, estimated offline. Shown are two salient points of the curve, corresponding to high precision and high recall.*

appearance manifolds. To discover and exploit this structure, we consider a *manifold space* – a vector space in which each *point* represents an appearance manifold. In the proposed method, manifold representations in this space are constructed implicitly.

We start by computing a symmetric $N \times N$ distance matrix \mathbf{D} between all pairs of appearance manifolds using the method described in the previous section:

$$D(i, j) = \text{CMSM_dist}(i, j). \quad (11.11)$$

Note that the entries of \mathbf{D} do not obey the triangle inequality, i.e. in general: $D(i, j) \not\leq D(i, k) + D(k, j)$. For this reason, we next compute the normalized distance matrix $\hat{\mathbf{D}}$ using Floyd’s algorithm [Cor90]:

$$\forall k. \hat{D}(i, j) = \min[D(i, j), \hat{D}(i, k) + \hat{D}(k, j)]. \quad (11.12)$$

Finally, we employ a Multi-Dimensional Scaling (MDS) algorithm (similarly as Tenenbaum *et al.* [Ten00]) on $\hat{\mathbf{D}}$ to compute the natural embedding of appearance manifolds under the derived metric. A typical result of embedding is shown in Figure 11.10.

Anisotropically evolving class boundaries. Consider previously mentioned clustering of appearance manifolds using a particular point on the ROC curve, corresponding to a distance threshold d_t . It is now easy to see that in the constructed manifold space this corresponds to hyper-spherical class boundaries of radius d_t centred at each manifold, see Figure 11.11. We now show how to construct anisotropic class boundaries by considering the distributions of manifolds. First, (i) simple, isotropic clustering in the manifold space is performed using the “high precision” point on the ROC curve, then (ii) a single parametric, Gaussian model is fit to each provisional same-class cluster of manifolds, and finally (iii) Gaussian models corresponding to the provisional classes are merged in a pair-wise manner,

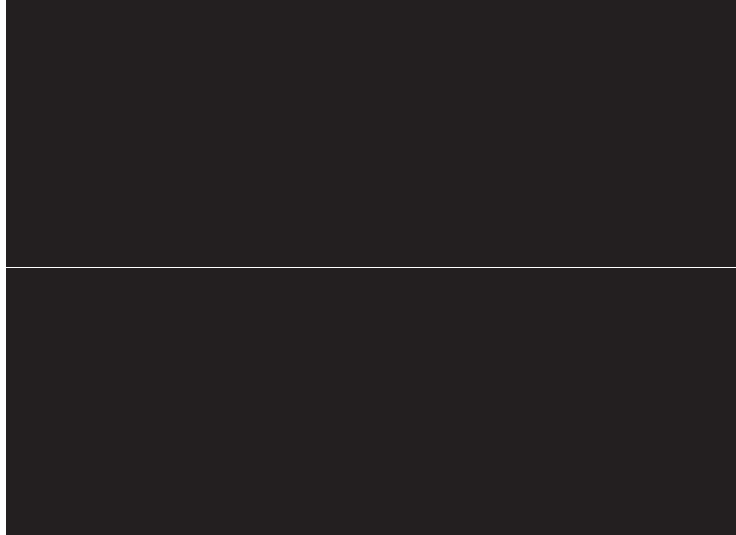


Figure 11.10: *Manifolds in the manifold space (shown are its first 3 principal components), corresponding to preprocessed tracks of faces of the two main characters in the situation comedy “Yes, Minister”. Each red dot corresponds to a single appearance manifold of Jim Hacker and black star to a manifold of Sir Humphrey (samples from two typical manifolds are shown below the plot). The distribution of manifolds in the space shows a clear structure. In particular, note that intra-class manifold distances are often greater than inter-manifold ones. Learning distributions of manifolds provides a much more accurate way of classification.*



Figure 11.11: *In the manifold space, the usual form of clustering – where manifolds within a certain distance (chosen from the ROC curve) from each other are grouped under the same class – corresponds to placing a hyper-spherical kernel at each manifold.*

using a criterion based on the model+data Description Length [Dud00]. The criterion for class-cluster merging is explained in detail next.

Class-cluster merging. In the proposed method, classes are represented by Gaussian clusters in the implicitly computed manifold space. Initially, the number of clusters is overestimated, each including only those appearance manifolds for which the same-class confidence is very high, using the manifold distance corresponding to the “high precision” point on the CMSM’s ROC curve. Then, clusters are pair-wise merged. Intuitively, if two Gaussian components are quite distant and have little overlap, not much evidence for each is needed to decide they represent different classes. The closer they get and the more they overlap, more supporting manifolds are needed to prevent merging. We quantify this using what we call the *weighted Description Length* DL_w and merge tentative classes if $\Delta DL_w < threshold$ (we used $threshold = -20$).

Let j -th of C appearance manifolds be \mathbf{m}_j and let it consist of $n(j)$ face images. Then we compute the log-likelihood of \mathbf{m}_j given the Gaussian model $\mathcal{G}(\mathbf{m}; \Theta)$ in the manifold space, weighted by the number of supporting-samples $n(j)$:

$$C \sum_{j=1}^C n(j) \log P(\mathbf{m}_j | \Theta) / \sum_{j=1}^C n(j) \quad (11.13)$$

The weighted Description Length of class data under the same model then becomes:

$$DL_w(\Theta, \{\mathbf{m}_j\}) = \frac{1}{2} N_E \log_2(n(j)) - \left[\prod_{j=1}^C P(\mathbf{m}_j | \Theta)^{n(j)} \right]^{C / \sum n(j)} \quad (11.14)$$

11.3 Empirical evaluation

In this section we report the empirical results of evaluating the proposed algorithm on the “Open Government” episode of the situation comedy “Yes, Minister”². Face detection was performed on every 5th out of 42,800 frames, producing 7,965 detections, see Figure B.3 (a). A large number of non-face images is included in this number, see Figure B.3 (b). Using the method for collecting face motion sequences described in Section 11.2.1 and discarding all tracks that contain less than 10 samples removes most of these. We end up with approximately 300 appearance manifolds to cluster. The primary and secondary cast consisted of 7

²Available at <http://mi.eng.cam.ac.uk/~oa214/academic/>



(a)



(b)

Figure 11.12: (a) The “Yes, Minister” data set – every 70th detection is shown for compactness. A large number of non-faces is present, typical of which are shown in (b).

characters: Sir Hacker, Miss Hacker, Frank, Sir Humphrey, Bernard, a BBC employee and the PM’s secretary.

Baseline clustering performance was established using the CMSM-based isotropic method with thresholds corresponding to the “high recall” and “high precision” points on the ROC curve. Formally, two manifolds are classified to the same class if the distance $D(i, j)$ between them is less than the chosen threshold, see (11.11) and Figure 11.11. Note that the converse is not true due to the transitivity of the in-class relation.

11.3.1 Results

The cast listing results using the two baseline isotropic algorithms are shown in Figure 11.13 (a) and 11.13 (b) – for each class we displayed a 10 image sample from its most likely manifold (under the assumption of normal distribution, see Section 11.2.2). As expected, the “high precision” method produced a gross overestimate of the number of different individuals e.g. suggesting three classes both for Sir Hacker and Sir Humphrey, and two for Bernard. Conversely, the “high recall” method underestimates the true number of classes. However, rather more interestingly, while grouping different individuals under the same class, this re-

sult still contains two classes for Sir Hacker. This is a good illustration of the main premise of this chapter, showing that the in-class distance threshold has to be chosen *locally* in the manifold space, if high clustering accuracy is to be achieved. That is what the proposed method implicitly does.

The cast listing obtained with anisotropic clustering is shown in Figure 11.14. For each class we displayed 10 images from the highest likelihood sequence. It can be seen that our method correctly identified the main cast of the film. No characters are ‘repeated’, unlike in both Figure 11.13 (a) and Figure 11.13 (b). This shows that the proposed algorithm for growing class boundaries in the manifold space has implicitly learnt to distinguish between intrinsic and extrinsic variations *between appearance manifolds*. Figure 11.15 corroborates this conclusion.

An inspection of the results revealed a particular failure mode of the algorithm, also predicted from the theory presented in previous sections. Appearance manifolds corresponding to the “BBC employee” were classified to the class dominated by Sir Humphrey, see Figure 11.15. The reason for this is a relatively short appearance of this character, producing a small number of corresponding face tracks. Consequently, with reference to (11.13) and (11.14), not enough evidence was present to maintain them as a separate class. It is important to note, however, that qualitatively speaking this is a tradeoff inherent to the problem in question. Under an assumption of isotropic noise in image space, *any* class in the film’s cast can generate *any* possible appearance manifold – it is enough evidence for each class that makes good clustering possible.

11.4 Summary and conclusions

A novel clustering algorithm was proposed to automatically determine the cast of a feature-length film, without any dataset-specific training information. The coherence of inter- and intra-personal dissimilarities between appearance manifolds was exploited by mapping each manifold into a single point in the manifold space. Hence, clustering was performed on actual appearance manifolds. A mixture-based generative model was used to anisotropically grow class boundaries corresponding to different individuals. Preliminary evaluation results showed a dramatic improvement over traditional clustering approaches.

Related publications

The following publications resulted from the work presented in this chapter:

- O. Arandjelović and R. Cipolla. Automatic cast listing in feature-length films with

Class 01:

Class 02:

Class 03:

Class 04:

Class 05:

Class 06:

Class 07:

Sir Hacker:

Miss Hacker:

Humphrey:

Secretary:

Bernard:

Frank:



Figure 11.14: *Anisotropic clustering results – shown are 10 frame sequences from appearance manifolds most “representative” of the obtained classes (i.e. the highest likelihood ones in the manifold space). Our method has correctly identified 6 out of 7 primary and secondary cast members, without suffering from the problems of the two isotropic algorithms (see Figure 11.12 and Figure 11.15).*



Figure 11.15: *Examples from the “Sir Humphrey” cluster – each horizontal strip is a 10 frame sample from a single face track. Notice a wide range of appearance changes between different tracks: extreme illumination conditions, pose and facial expression variation. The bottom-most strip corresponds to an incorrectly clustered track of “BBC employee”.*

anisotropic manifold space. In *Proc. IEEE Conference on Computer Vision Pattern Recognition (CVPR)*, **2**:pages 1513–1520, June 2006. [Ara06a]

IV

Conclusions, Appendices and Bibliography

12

Conclusion



Pieter P. Rubens. *The Last Judgement*

1617, Oil on canvas, 606 x 460 cm

Alte Pinakothek, Munich

This chapter summarizes the thesis. Firstly, we briefly highlight the main contributions of the presented research. We then focus on the two major conceptual and algorithmic novelties – the *Generic Shape-Illumination Manifold* recognition and the *Anisotropic Manifold Space Clustering* method. The significance of the contributions of these two algorithms to the face recognition field are considered in more detail. Finally, we discuss the limitations of the proposed methods and conclude the chapter with an outline of promising directions for future research.

12.1 Contributions

Each of the chapters 3 to 11 and appendices A to C was the topic of a particular contribution to the field of face recognition. For clarity, these are briefly summarized in Figure 12.1.

We now describe the two main contributions of the thesis in more detail, namely the *Generic Shape-Illumination Manifold* method of Chapter 9 and the *Anisotropic Manifold Space* clustering algorithm of Chapter 11.

Generic Shape-Illumination Manifold algorithm

Starting with Chapter 3 and concluding with Chapter 8 we considered the problem of matching video sequences of faces, gradually decreasing restrictions on the data acquisition process and recognizing using less training data. This ended in our proposing the *Generic Shape-Illumination Manifold* algorithm, in detail described in Chapter 9. The algorithm was shown to be extremely successful (nearly perfectly recognizing all individuals) on a large data set of over 1300 video sequences in realistic imaging conditions. Repeated explicitly, by this we mean that recognition is performed in the presence of: (i) large pose variations, (ii) extreme illumination conditions (significant non-Lambertian effects), (iii) large illumination changes, (iv) uncontrolled head motion pattern, and (v) low video resolution.

Our algorithm was shown to greatly outperform current state-of-the-art face recognition methods in the literature and the best performing commercial software. This is the result of the following main novel features:

1. Combination of data-driven machine learning and prior knowledge-based photometric model,
2. Concept of the Generic Shape-Illumination Manifold as a way of compactly representing complex illumination effects across all human faces (illumination robustness),
3. Video sequence re-illumination algorithm, used to learn the Generic Shape-Illumination Manifold (low resolution robustness), and

-
- Chapter 3** Statistical recognition algorithm suitable in the case when training data contains typical appearance variations.
 - Chapter 4** Appearance matching by nonlinear manifold unfolding, in the presence of varying pose, noise contamination, face detector outliers and mild illumination changes.
 - Chapter 5** Illumination invariant recognition by decision-level fusion of optical and infrared thermal imagery.
 - Chapter 6** Illumination invariant recognition by decision-level fusion of raw grayscale and image filter preprocessed visual data.
 - Chapter 7** Derivation of a local appearance manifold illumination invariant, exploited in the proposed learning-based nonlinear extension of canonical correlations between subspaces.
 - Chapter 8** Person identification system based on combining appearance manifolds with a simple illumination and pose model.
 - Chapter 9** Unified framework for data-driven learning and model-based appearance manifold matching in the presence of large pose, illumination and motion pattern variations.
 - Chapter 10** Content-based video retrieval based on face recognition; fine-tuned facial registration, accurate background clutter removal and robust distance for partial face occlusion.
 - Chapter 11** Automatic identity-based clustering of tracked people in feature-length videos; the manifold space concept.
 - Appendix A** Concept of Temporally-Coherent Gaussian mixtures and algorithm for their incremental fitting.
 - Appendix B** Probabilistic extension of canonical correlation-based pattern recognition by subspace matching.
 - Appendix C** Algorithm for automatic extraction of faces and background removal from cluttered video scenes.

Figure 12.1: *A summary of the contributions of this thesis.*

- 4. Automatic selection of the most reliable faces on which to base the recognition decision (pose and outlier robustness).

Anisotropic Manifold Space clustering

The last two chapters of this thesis considered face recognition in feature-length films, for the purpose of content-based retrieval and organization. The *Anisotropic Manifold Space* clustering algorithm was proposed to automatically determine the cast of a feature-length film, without any dataset-specific training information.

Preliminary evaluation results on an episode of the situation comedy “Yes, Minister” were vastly superior to those of conventional clustering methods. The power of the proposed approach was demonstrated by showing that the correct cast list was produced even using a very simple algorithm for normalizing images of faces and comparing individual manifolds. The key novelties are:

1. Clustering over appearance manifolds themselves, which were automatically extracted from a continuous video stream,
2. Concept of the *manifold space* – a vector space in which each point is an appearance manifold,
3. Iterative algorithm for estimating the optimal discriminative subspace for an unlabelled dataset, given the *generic* discriminative subspace, and
4. A hierarchical manifold space clustering algorithm based on the proposed appearance manifold-driven *weighted description length* and an underlying generative mixture model.

12.2 Future work

We conclude the thesis with a discussion on the most promising avenues for further research that the work presented has opened up. We will again focus on the two major contributions of this work, the *Generic Shape-Illumination Manifold* method of Chapter 9 and the *Anisotropic Manifold Space* clustering algorithm of Chapter 11.

Generic Shape-Illumination Manifold algorithm

The proposed *Generic Shape-Illumination Manifold* method has immediate potential for improvement in the following three areas:

- i Computational efficiency,
- ii Manifold representation, and

- iii Partial occlusion and facial expression changes.

In Section 9.4.1 we analyzed the computational complexity and the running time of our implementation of the algorithm. Empirical results show a computational increase that is dominated by a term roughly quadratic in the number of detected faces in a video sequence. The most expensive stages of the method are the computation of geodesic distances and K -nearest neighbours. While neither of these can be made more asymptotically efficient (they correspond to the all-pairs shortest path problem [Cor90]), they can be potentially avoided if a different manifold representation is employed. Possible candidates are some of the representations used in this thesis: Chapters 3 and 8 showed that Gaussian mixtures are suitable for modelling face appearance manifolds, while piece-wise linear models were employed in Chapter 3. Either of these would have the benefit of (i) constant storage requirements (in our current method, memory needed to represent a manifold is linear in the number of faces) and (ii) avoidance of the two most computationally expensive stages in the proposed method. Additionally, a novel incremental learning approach of such representations is described in Appendix A.

A more fundamental limitation of the *Generic Shape-Illumination Manifold* algorithm is its sensitivity to partial occlusions and facial expression changes. The former is likely an easier problem to tackle. Specifically, several recent methods for partial face occlusion detection (e.g. [Lee05, Wil04]) may prove useful in this regard: by detecting the occluded region of the face, pose matching and then robust likelihood estimation can be performed using only the non-occluded regions by marginalization of the density corresponding to the Generic SIM. Extending the algorithm to successfully deal with expression changes is a more challenging problem and a worthwhile aim for future research.

Anisotropic Manifold Space clustering

The *Anisotropic Manifold Space* algorithm for clustering of face appearance manifolds can be extended in the following directions:

- i More sophisticated appearance matching,
- ii The use of local manifold space projection, and
- iii Discriminative model fitting.

We now summarize these.

With the purpose of decreasing the computational load of empirical evaluation, as well as demonstrating the power of the introduced Manifold Space clustering, our implementation of the algorithm in Chapter 11 used a very simple, linear manifold model with per-frame image

filtering-based illumination normalization. The limitations of both the linear manifold model and the filtering approach to achieving illumination robustness were discussed throughout the thesis (e.g. see Chapter 2). A more sophisticated approach, such as one based on the proposed *Generic Shape-Illumination Manifold* of Chapter 9 would be the most immediate direction for improvement.

The proposed *Anisotropic Manifold Space* algorithm applies MDS to construct an embedding of all appearance manifolds in a feature-length video. This has the unappealing consequences of (i) rapidly growing computational load and (ii) decreased accuracy of the embedding with the increase in the number of manifolds. Both of these limitations can be overcome by recognizing that very distant manifolds should not affect mutual clustering membership. Hence, in the future we intend to investigate ways of automatically *a priori* partitioning the Manifold Space and unfolding it only a part at a time i.e. locally.

Finally, the clustering algorithm in the Manifold Space is based on a generative approach with the underlying Gaussian model of class data. Clustering methods better tuned for discrimination are likely to prove as more suitable for the task at hand.

A

Incremental Learning of Temporally-Coherent GMMs



Vincent Van Gogh. *Basket of Potatoes*
1885, Oil on canvas, 45.0 x 60.5 cm
Van Gogh Museum, Amsterdam

In this appendix we address the problem of learning Gaussian Mixture Models (GMMs) *incrementally*. Unlike previous approaches which universally assume that new data comes in blocks representable by GMMs which are then merged with the current model estimate, our method works for the case when novel data points arrive *one-by-one*, while requiring little additional memory. We keep only two GMMs in memory and no historical data. The current fit is updated with the assumption that the number of components is fixed, which is increased (or reduced) when enough evidence for a new component is seen. This is deduced from the change from the oldest fit of the same complexity, termed the *Historical GMM*, the concept of which is central to our method. The performance of the proposed method is demonstrated qualitatively and quantitatively on several synthetic data sets and video sequences of faces acquired in realistic imaging conditions.

A.1 Introduction

The Gaussian Mixture Model (GMM) is a semi-parametric method for high-dimensional density estimation. It is used widely across different research fields, with applications to computer vision ranging from object recognition [Dah01], shape [Coo99a] and face appearance modelling [Gro00] to colour-based tracking and segmentation [Raj98], to name just a few. It is worth emphasizing the key reasons for its practical appeal: (i) its flexibility allows for the modelling of complex and nonlinear pattern variations [Gro00], (ii) it is simple and efficient in terms of memory, (iii) a principled model complexity selection is possible, and (iv) there are theoretically guaranteed to converge algorithms for model parameter estimation.

Virtually all previous work with GMMs has concentrated on non time critical applications, typically in which model fitting (i.e. model parameter estimation) is performed offline, or using a relatively small training corpus. On the other hand, the recent trend in computer vision is oriented towards real-time applications (for example for human-computer interaction and on-the-fly model building) and modelling of increasingly complex patterns which inherently involves large amounts of data. In both cases, the usual batch fitting becomes impractical and an incremental learning approach is necessary.

Problem challenges. Incremental learning of GMMs is a surprisingly difficult task. One of the main challenges of this problem is the model complexity selection which is required to be dynamic by the very nature of the incremental learning framework. Intuitively, if all information that is available at any time is the current GMM estimate, a single novel point *never* carries enough information to cause an increase in the number of Gaussian components. Another closely related difficulty lies in the *order* in which new data arrives

[Hal04]. If successive data points are always badly correlated, then a large amount of data has to be kept in memory if accurate model order update is to be achieved.

A.1.1 Related previous work

The most common way of fitting a GMM is using the Expectation-Maximization (EM) algorithm [Dem77]. Starting from an estimate of model parameters, soft membership of data is computed (the *Expectation* step) which is then used to update the parameters in the maximal likelihood (ML) manner (the *Maximization* step). This is repeated until convergence, which is theoretically guaranteed. In practice, initialization is frequently performed using the K -means clustering algorithm [Bis95, Dud00].

Incremental approaches. Incremental fitting of GMMs has already been addressed in the machine learning literature. Unlike the proposed method, most of the existing methods assume that novel data arrives in *blocks* as opposed to a single datum at a time. Hall *et al.* [Hal00] merge Gaussian components in a pair-wise manner by considering volumes of the corresponding hyperellipsoids. A more principled method was recently proposed by Song and Wang [Son05] who use the W statistic for covariance and the Hotelling's T^2 statistic for mean equivalence. However, they do not fully exploit the available probabilistic information by failing to take into account the *evidence* for each component at the time of merging. Common to both [Hal00] and [Son05] is the failure to make use of the existing model when the GMM corresponding to new data is fitted. What this means is that even if some of the new data is already explained well by the current model, the EM fitting will try to explain it in the context of other novel data, affecting the accuracy of the fit as well as the subsequent component merging. The method of Hicks *et al.* [Hic03] (also see [Hal04]) does not suffer from the same drawback. The authors propose to first “concatenate” two GMMs and then determine the optimal model order by considering models of *all* low complexities and choosing the one that gives the largest penalized log-likelihood. A similar approach of combining Gaussian components was also described by Vasconcelos and Lippman [Vas98].

Model order selection. Broadly speaking, there are three classes of approaches for GMM model order selection: (i) EM-based using validation data, (ii) EM-based using model validity criteria, and (iii) dynamic algorithms. The first approach involves random partitioning of the data to training and validation sets. Model parameters are then iteratively estimated from training data and the complexity that maximizes the posterior of the validation set is sought. This method is typically less preferred than methods of the other two groups, being wasteful both of the data and computation time. The most popular group of methods is

EM-based and uses the posterior of all data, penalized with model complexity. Amongst the most popular are the Minimal Description Length (MDL) [Ris78], Bayesian Information (BIC) [Sch78] and Minimal Message Length (MML) [Wal99a] criteria. Finally, there are methods which combine the fitting procedure with dynamic model order selection. Briefly, Zwolinski and Yang [Zwo01], and Figueredo and Jain [Fig02] overestimate the complexity of the model and reduce it by discarding “improbable” components. Vlassis and Likas [Vla99] use a weighted sample kurtoses of Gaussian kernels, while Verbeek *et al.* introduce a heuristic greedy approach in which mixture components are added one at the time [Ver03].

A.2 Incremental GMM estimation

A GMM with M components in a D -dimensional embedding space is defined as:

$$\mathcal{G}(\mathbf{x}; \theta) = \sum_{j=1}^M \alpha_j \mathcal{N}(\mathbf{x}; \mu_j, \mathbf{C}_j) \quad (\text{A.1})$$

where $\theta = (\{\alpha_i\}, \{\mu_i\}, \{\mathbf{C}_i\})$ is the set of model parameters, α_i being the prior of the i -th Gaussian component with the mean μ_i and covariance \mathbf{C}_i :

$$\mathcal{N}(\mathbf{x}; \mu, \mathbf{C}) = \frac{1}{(2\pi)^{D/2} \sqrt{|\mathbf{C}|}} \exp\left(-\frac{1}{2}(\mathbf{x} - \mu)^T \mathbf{C}^{-1}(\mathbf{x} - \mu)\right) \quad (\text{A.2})$$

A.2.1 Temporally-coherent GMMs

We assume *temporal coherence* on the order in which data points are seen. Let $\{\mathbf{x}_t\} \equiv \{\mathbf{x}_0, \dots, \mathbf{x}_T\}$ be a stream of data, its temporal ordering implied by the subscript. The assumption of an underlying Temporally-Coherent GMM (TC-GMM) on $\{\mathbf{x}_t\}$ is:

$$\begin{aligned} \mathbf{x}_0 &\sim \mathcal{G}(\mathbf{x}; \theta) \\ \mathbf{x}_{t+1} &\sim p_S(\|\mathbf{x}_{t+1} - \mathbf{x}_t\|) \cdot \mathcal{G}(\mathbf{x}; \theta) \end{aligned}$$

where p_S is a unimodal density. Intuitively, while data is distributed according to an underlying Gaussian mixture, it is also expected to vary smoothly with time, see Figure A.1.

A.2.2 Method overview

The proposed method consists of a three-stage model update each time a new data point becomes available, see Figure A.2. At each time step: (i) model parameters are updated

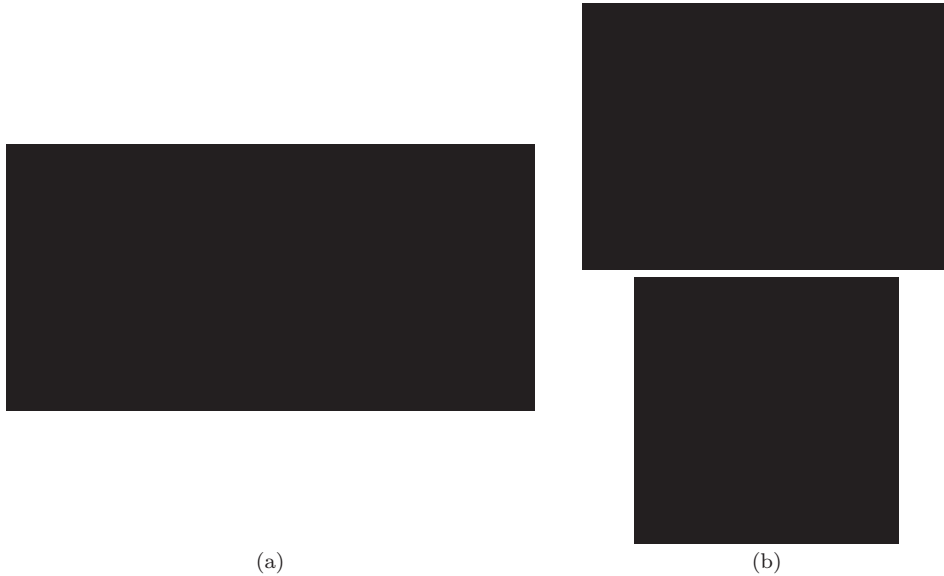


Figure A.1: (a) Average distribution of Euclidean distance between temporally consecutive faces across video sequences of faces in unconstrained motion. The distribution peaks at a low, but greater-than-zero distance, which is typical of Temporally-Coherent GMMs analyzed in this appendix. Both too low and too large distances are infrequent, in this case the former due to the time gap between the acquisition of consecutive video frames, the latter due to the smoothness of face shape and texture. (b) A typical sequence projected to the first three principal components estimated from the data, the corresponding MDL EM fit and the component centres visualized as images. On average, we found that over 80% of pairs of successive faces have the highest likelihood of having been generated by the same Gaussian component.

under the constraint of fixed complexity, (ii) new Gaussian components are postulated by model splitting and (iii) components are merged to minimize the expected model description length. We keep in memory only two GMMs and *no historical data*. One is the current GMM estimate, while the other is the oldest model of the same complexity after which no permanent new cluster creation took place – we term this the *Historical GMM*.

A.2.3 GMM update for fixed complexity

In the first stage of our algorithm, the current GMM $\mathcal{G}(\mathbf{x}; \theta)$ is updated under the *constraint of fixed model complexity*, i.e. fixed number of Gaussian components. We start with the assumption that the current model parameters are estimated in the ML fashion in a local

Input: set of observations $\{\mathbf{x}_i\}$,
KPCA space dimensionality D .
Output: kernel principal components $\{\mathbf{u}_i\}$.

1: Fixed-complexity update:
update($\mathcal{G}_N, \mathbf{x}$)

2: Model splitting:
 $\mathcal{G}_M = \text{split-all}(\mathcal{G}_N, \mathcal{G}_N^{(h)})$

3: Pair-wise component merging:
for all $(i, j) \in (1..N, 1..N)$

4: Expected description length:
 $[L_1, L_2] = \text{DL}\{\text{merge}(\mathcal{G}_M, i, j), \text{split}(\mathcal{G}_M, i, j)\}$

5: Complexity update
 $\mathcal{G}_M = L_1 < L_2 ? \text{merge}(\mathcal{G}_M, i, j) : \text{split}(\mathcal{G}_M, i, j)$

Figure A.2: A summary of the proposed Incremental TC-GMM algorithm.



Figure A.3: Fixed complexity update: the mean and the covariance of each Gaussian component are updated according to the probability that it generated the novel observation (red circle). Old covariances are shown as dashed, the updated ones as solid ellipses corresponding to component parameters, while historical data points are displayed as blue dots.

minimum of the EM algorithm:

$$\alpha_i = \frac{\sum_j p(i|\mathbf{x}_j)}{N} \quad \mu_i = \frac{\sum_j \mathbf{x}_j p(i|\mathbf{x}_j)}{\sum_j p(i|\mathbf{x}_j)} \quad \mathbf{C}_i = \frac{\sum_j (\mathbf{x}_j - \mu_i)(\mathbf{x}_j - \mu_i)^T p(i|\mathbf{x}_j)}{\sum_j p(i|\mathbf{x}_j)} \quad (\text{A.3})$$

where $p(i|\mathbf{x}_j)$ is the probability of the i -th component conditioned on data point \mathbf{x}_j . Similarly, for the updated set of GMM parameters θ^* it holds:

$$\alpha_i^* = \frac{\sum_j p^*(i|\mathbf{x}_j) + p^*(i|\mathbf{x})}{N + 1} \quad \mu_i^* = \frac{\sum_j \mathbf{x}_j p^*(i|\mathbf{x}_j) + \mathbf{x} p^*(i|\mathbf{x})}{\sum_j p^*(i|\mathbf{x}_j) + p^*(i|\mathbf{x})} \quad (\text{A.4})$$

$$\mathbf{C}_i^* = \frac{\sum_j (\mathbf{x}_j - \mu_i^*)(\mathbf{x}_j - \mu_i^*)^T p^*(i|\mathbf{x}_j) + (\mathbf{x} - \mu_i^*)(\mathbf{x} - \mu_i^*)^T p^*(i|\mathbf{x})}{\sum_j p^*(i|\mathbf{x}_j) + p^*(i|\mathbf{x})} \quad (\text{A.5})$$

The key problem is that the probability of each component conditioned on the data changes *even for historical data* $\{\mathbf{x}_j\}$. In general, the change in conditional probabilities can be arbitrarily large as the novel observation \mathbf{x} can lie anywhere in the \mathbb{R}^D space. However, the expected correlation between temporally close points, governed by the underlying TC-GMM model allows us to make the assumption that component likelihoods do not change much with the inclusion of novel information in the model:

$$p^*(i|\mathbf{x}_j) = p(i|\mathbf{x}_j) \quad (\text{A.6})$$

This assumption is further justified by the two stages of our algorithm that follow (Sections A.2.4 and A.2.5) – a large change in probabilities $p(i|\mathbf{x}_j)$ occurs only when novel data is not well explained by the current model. When enough evidence for a new Gaussian components is seen, model complexity is increased, while old component parameters switch back to their original value. Using (A.6), a simple algebraic manipulation of (A.3)-(A.4), omitted for clarity, and writing $\sum_j p(i|\mathbf{x}_j) \equiv E_i$, leads to the following:

$$\alpha_i^* = \frac{E_i + p(i|\mathbf{x})}{N + 1} \quad \mu_i^* = \frac{\mu_i E_i + \mathbf{x} p(i|\mathbf{x})}{E_i + p(i|\mathbf{x})} \quad (\text{A.7})$$

$$\mathbf{C}_i^* = \frac{(\mathbf{C}_i + \mu_i \mu_i^T - \mu_i \mu_i^{*T} - \mu_i^* \mu_i^T + \mu_i^* \mu_i^{*T}) E_i + (\mathbf{x} - \mu_i^*)(\mathbf{x} - \mu_i^*)^T p(i|\mathbf{x})}{E_i + p(i|\mathbf{x})} \quad (\text{A.8})$$

It can be seen that the update equations depend only on the parameters of the old model and the sum of component likelihoods, but *no historical data*. Therefore the additional memory requirements are of the order $O(M)$, where M is the number of Gaussian components. Constant-complexity model parameter update is illustrated in Figure A.3.

A.2.4 Model splitting

One of the greatest challenges of incremental GMM learning is the dynamic model order selection. In the second stage of our algorithm, new Gaussian clusters are postulated based

on the parameters of the current parameter model estimate \mathcal{G} and the *Historical GMM* $\mathcal{G}^{(h)}$, which is central to our idea. As, by definition, no permanent model order changes occurred between the Historical and the current GMMs, they have the same number of components and, importantly, the 1-1 correspondence between them is known (the current GMM is merely the Historical GMM that was updated under the constraint of fixed model complexity). Therefore, for each pair of corresponding components (μ_i, \mathbf{C}_i) and $(\mu_i^{(h)}, \mathbf{C}_i^{(h)})$ we compute the ‘difference’ component, see Figure A.4 (a-c). Writing (A.3) for the Historical and the current GMMs, and using the assumption in (A.6) the i -th difference component parameters become:

$$\alpha_i^{(n)} = \frac{E_i - E_i^{(h)}}{N - N^{(h)}} \quad \mu_i^{(n)} = \frac{\mu_i E_i - \mu_i^{(h)} E_i^{(h)}}{E_i - E_i^{(h)}} \quad (\text{A.9})$$

$$\mathbf{C}_i^{(n)} = \frac{\mathbf{C}_i E_i - (\mathbf{C}_i^{(h)} + \mu_i^{(h)} \mu_i^{(h)T}) E_i^{(h)} + (\mu_i^{(h)} \mu_i^T + \mu_i \mu_i^{(h)T}) E_i^{(h)} - \mu_i \mu_i^T E_i + \mu_i^{(n)} \mu_i^{(n)T} + \mu_i \mu_i^{(n)T} - \mu_i^{(n)} \mu_i^{(n)T}}{E_i - E_i^{(h)}} \quad (\text{A.10})$$

A.2.5 Component merging

In the proposed method, dynamic model complexity estimation is based on the MDL criterion. Briefly, MDL assigns to a model a cost related to the amount of information necessary to encode the model and the data *given* the model. This cost, known as the description length $L(\theta|\{\mathbf{x}_i\})$, is equal to the log-likelihood of the data under that model penalized by the model complexity, measured as the number of free parameters N_E :

$$L(\theta|\{\mathbf{x}_i\}) = \frac{1}{2} N_E \log_2(N) - \log_2 P(\{\mathbf{x}_i\}|\theta) \quad (\text{A.11})$$

In the case of an M -component GMM with full covariance matrices in \mathbb{R}^D space, free parameters are $(M - 1)$ for priors, MD for means and $MD(D + 1)/2$ for covariances:

$$N_E = M - 1 + MD + M \frac{D(D + 1)}{2} \quad (\text{A.12})$$

The problem is that for the computation of $P(\{\mathbf{x}_i\}|\theta)$ historical data $\{\mathbf{x}_i\}$ is needed – which is unavailable. Instead of $P(\{\mathbf{x}_i\}|\theta)$, we propose to compute the *expected* likelihood of the same number of data points and, hence, use the expected description length as the model order selection criterion. Consider two components with the corresponding multivariate

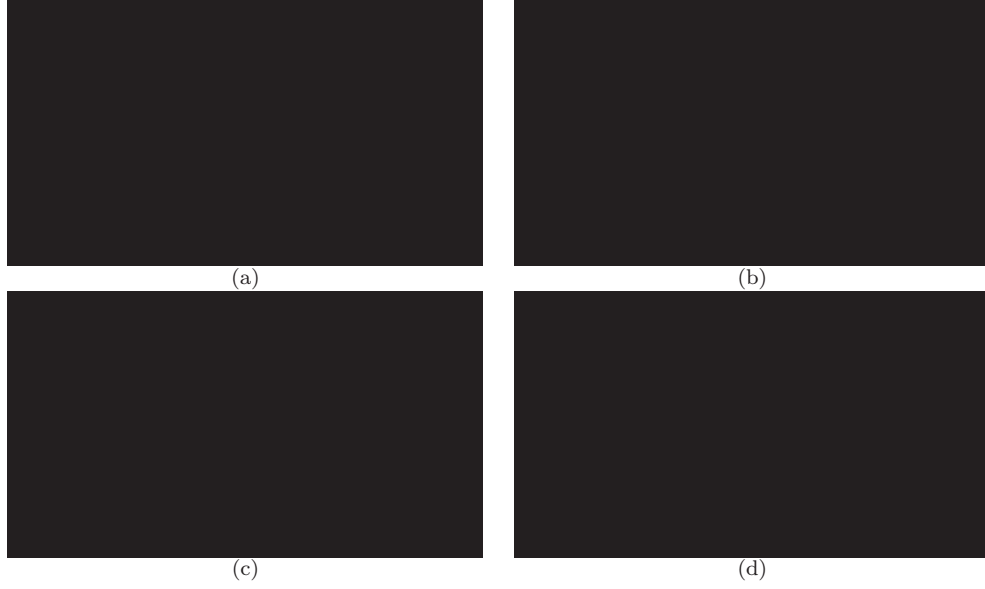


Figure A.4: *Dynamic model order selection: (a) Historical GMM. (b) Current GMM before the arrival of novel data. (c) New data point (red circle) causes the splitting of a Gaussian component, resulting in a 3-component mixture. (d) The contribution to the expected model description length for merging and splitting of the component, as the number of novel data points is increased.*

Gaussian densities $p_1(\mathbf{x}) \sim \mathcal{N}(\mathbf{x}; \mu_1, \mathbf{C}_1)$ and $p_2(\mathbf{x}) \sim \mathcal{N}(\mathbf{x}; \mu_2, \mathbf{C}_2)$. The expected likelihood of N_1 points drawn from the former and N_2 from the latter given model $\alpha_1 p_1(\mathbf{x}) + \alpha_2 p_2(\mathbf{x})$ is:

$$E [P(\{\mathbf{x}_j\}|\theta_S)] = \left(\int p_1(\mathbf{x})(\alpha_1 p_1(\mathbf{x}) + \alpha_2 p_2(\mathbf{x})) d\mathbf{x} \right)^{N_1} \left(\int p_2(\mathbf{x})(\alpha_1 p_1(\mathbf{x}) + \alpha_2 p_2(\mathbf{x})) d\mathbf{x} \right)^{N_2} \quad (\text{A.13})$$

where integrals of the type $\int p_i(\mathbf{x})p_j(\mathbf{x})d\mathbf{x}$ are recognized as related to the Bhattacharyya distance, and are for Gaussian distributions easily computed as:

$$d_B(p_i, p_j) = \int p_i(\mathbf{x})p_j(\mathbf{x})d\mathbf{x} = \frac{\exp(-K/2)}{(2\pi)^{D/2}|\mathbf{C}_i\mathbf{C}_j\mathbf{C}|^{1/2}} \quad (\text{A.14})$$

where:

$$\mathbf{C} = (\mathbf{C}_i^{-1} + \mathbf{C}_j^{-1})^{-1} \quad (\text{A.15})$$

$$\boldsymbol{\mu} = \mathbf{C}(\mathbf{C}_i^{-1}\boldsymbol{\mu}_i + \mathbf{C}_j^{-1}\boldsymbol{\mu}_j) \quad (\text{A.16})$$

$$\mathbf{K} = \boldsymbol{\mu}_i\mathbf{C}_i^{-1}\boldsymbol{\mu}_i^T + \boldsymbol{\mu}_j\mathbf{C}_j^{-1}\boldsymbol{\mu}_j^T - \boldsymbol{\mu}\mathbf{C}^{-1}\boldsymbol{\mu}^T \quad (\text{A.17})$$

On the other hand, consider the case when the two components are merged i.e. replaced by a single Gaussian component with the corresponding density $p(\mathbf{x})$. Then we compute the expected likelihood of N_1 points drawn from $p_1(\mathbf{x})$ and N_2 points drawn from $p_2(\mathbf{x})$, given model $p(\mathbf{x})$:

$$E[P(\{\mathbf{x}_j\}|\theta_M)] = \left(\int p(\mathbf{x})p_1(\mathbf{x})d\mathbf{x}\right)^{N_1} \cdot \left(\int p(\mathbf{x})p_2(\mathbf{x})d\mathbf{x}\right)^{N_2} \quad (\text{A.18})$$

Substituting the expected evidence and model complexity in (A.11) we get:

$$\begin{aligned} \Delta E[L] = E[L_S] - E[L_M] = & \frac{1}{4}D(D+1)\log_2(N_1 + N_2) - \\ & \log_2 E[P(\{\mathbf{x}_j\}|\theta_S)] + \log_2 E[P(\{\mathbf{x}_j\}|\theta_M)] \end{aligned} \quad (\text{A.19})$$

Then the condition for merging is simply $\Delta E[L] > 0$, see Figure A.4 (d). Merging equations are virtually the same as (A.9) and (A.10) for model splitting, so we do not repeat them.

A.3 Empirical evaluation

The proposed method was evaluated on several synthetic data sets and video sequences of faces in unconstrained motion, acquired in realistic imaging conditions and localized using the Viola-Jones face detector [Vio04], see Figure A.1 (b). Two synthetic data sets that we illustrate its performance on are:

1. 100 points generated from a Gaussian with a diagonal covariance matrix in radial coordinates: $r \sim \mathcal{N}(\bar{r} = 5, \sigma_r = 0.1)$, $\phi \sim \mathcal{N}(\bar{\phi} = 0, \sigma_\phi = 0.7)$
2. 80 points generated from a uniform distribution in x and a Gaussian noise perturbed sinusoid in y coordinate: $x \sim \mathcal{U}(\min x = 0, \max x = 10)$, $y \sim \mathcal{N}(\bar{y} = \sin x, \sigma_y = 0.1)$

Temporal ordering was imposed by starting from the data point with the minimal x coordinate and then iteratively choosing as the successor the nearest neighbour out of yet unused points. The initial GMM parameters, the final fitting results and the comparison with the

MDL-EM fitting are shown in Figure A.5. In the case of face motion video sequences, temporal ordering of data is inherent in the acquisition process. An interesting fitting example is shown and compared with the MDL-EM batch approach in Figure A.6.

Qualitatively, both in the case of synthetic and face data it can be seen that our algorithm consistently produces meaningful GMM estimates. Quantitatively, the results are comparable with the widely accepted EM fitting with the underlying MDL criterion, as witnessed by the description lengths of the obtained models.

Failure modes. On our data sets two types phenomena in data sometimes caused unsatisfactory fitting results. The first, one inherently problematic to our algorithm, is when newly available data is well explained by the Historical GMM. Referring back to Section A.2.4, it can be seen in (A.9) and (A.10) that this data contributes to the confidence of creating a *new* GMM component whereas it should not. The second failure mode was observed when the assumption of temporal coherence (Section A.2.1) was violated, e.g. when our face detector failed to detect faces in several consecutive video frames. While this cannot be considered an inherent fault of our algorithm, it does point out that ensuring temporal coherence of data is not always a trivial task in practice.

In conclusion, while promising, a more comprehensive evaluation on different sets of real data is needed to fully understand the behaviour of the proposed method.

A.4 Summary and conclusions

A novel algorithm for incremental learning of Temporally-Coherent Gaussian mixtures was introduced. Promising performance was empirically demonstrated on synthetic data and face appearance streams extracted from realistic video, and qualitatively and quantitatively compared with the standard EM-based fitting.

Related publications

The following publications resulted from the work presented in this appendix:

- O. Arandjelović and R. Cipolla. Incremental learning of temporally-coherent Gaussian mixture models. In *Proc. IAPR British Machine Vision Conference (BMVC)*, 2:pages 759–768, September 2005. [Ara05a]
- O. Arandjelovic' and R. Cipolla. Incremental learning of temporally-coherent Gaussian mixture models. *Society of Manufacturing Engineers (SME) Technical Papers*, May 2006. [Ara06d]

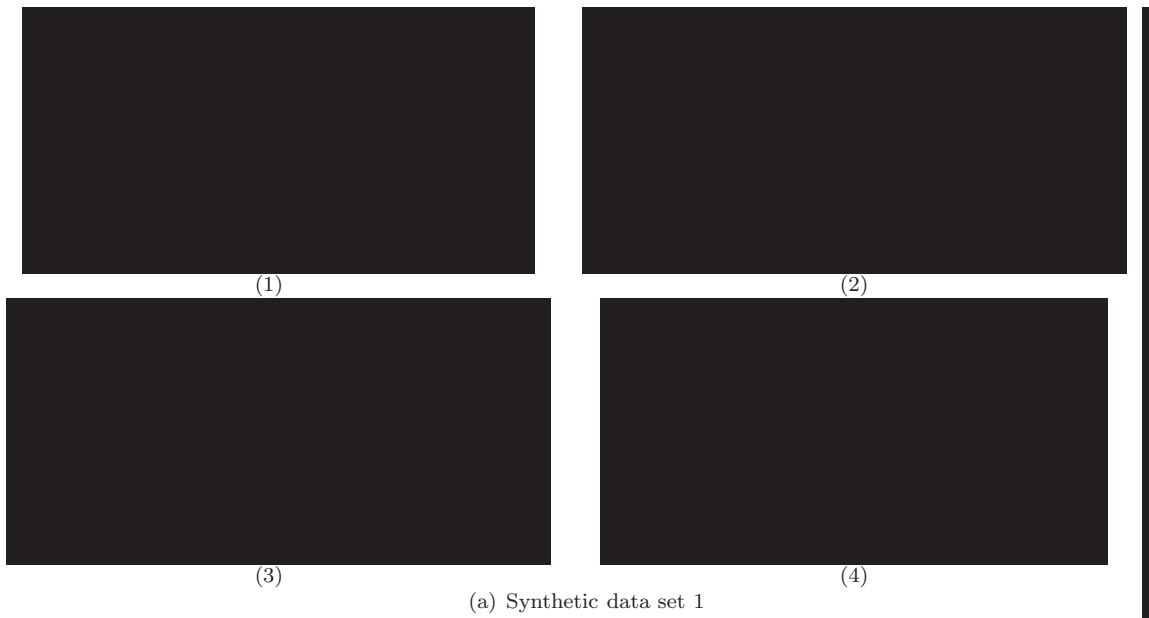


Figure A.5: *Synthetic data: (1) data (dots) and the initial model (visualized as ellipses corresponding to the parameters of the Gaussian components). (2) MDL-EM GMM fit. (3) Incremental GMM fit. (4) Description length of GMMs fitted using EM and the proposed incremental algorithm (shown is the description length of the final GMM estimate). Our method produces qualitatively meaningful results which are also qualitatively comparable with the best fits obtained using the usual batch method.*

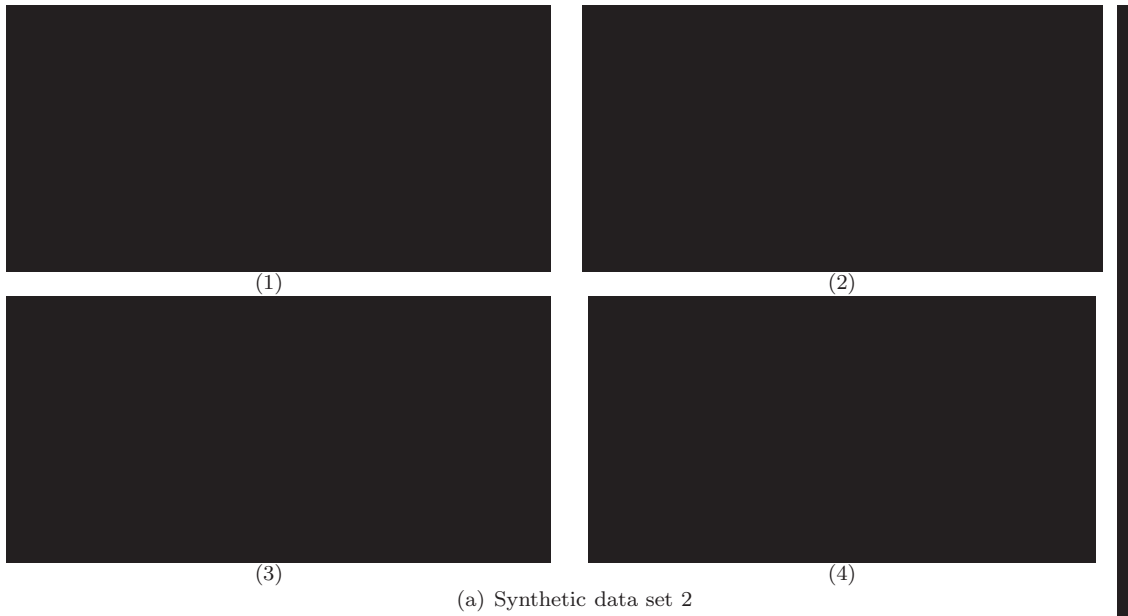


Figure A.5: *Synthetic data: (1) data (dots) and the initial model (visualized as ellipses corresponding to the parameters of the Gaussian components). (2) MDL-EM GMM fit. (3) Incremental GMM fit. (4) Description length of GMMs fitted using EM and the proposed incremental algorithm (shown is the description length of the final GMM estimate). Our method produces qualitatively meaningful results which are also qualitatively comparable with the best fits obtained using the usual batch method.*

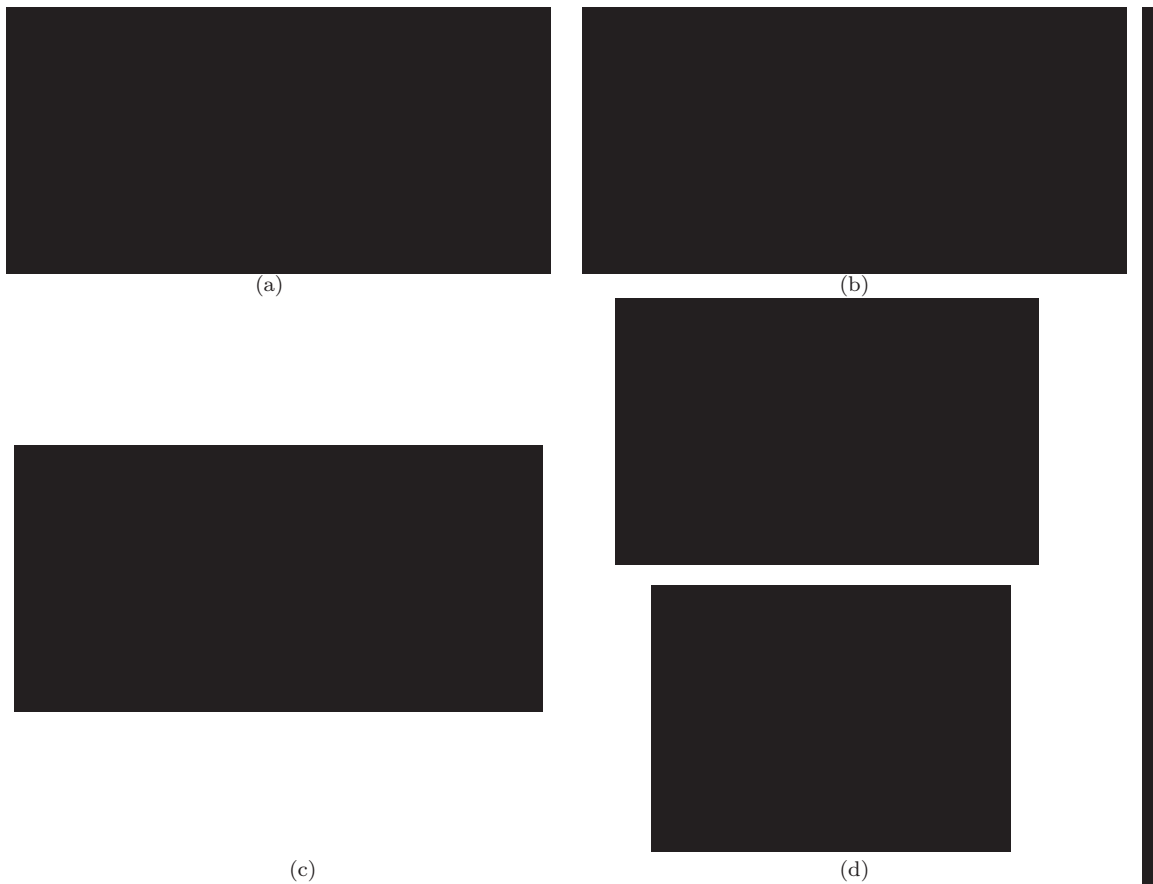


Figure A.6: Face motion data: data (dots) and (a) MDL-EM GMM fit. (b) Incremental GMM fit. (c) Description length of GMMs fitted using EM and the proposed incremental algorithm (shown is the description length of the final GMM estimate). (d) GMM component centres visualized as images for the MDL-EM fit (top) and the incremental algorithm (bottom).

B

Maximally Probable Mutual Modes



Salvador Dali. *Archeological Reminiscence of Millet's Angelus*

1933-5, Oil on panel, 31.7 x 39.3 cm

Salvador Dali Museum, St. Petersburg, Florida



Figure B.1: *Piece-wise representations of nonlinear manifolds: as a collection of (a) infinite-extent linear subspaces vs. (b) Gaussian densities.*

In this appendix we consider discrimination between linear patches corresponding to local appearance variations within face image sets. We propose the *Maximally Probable Mutual Modes* (MMPM) algorithm, a probabilistic extension of the Mutual Subspace Method (MSM). Specifically we show how the local manifold illumination invariant introduced in Section 7.1 naturally leads to a formulation of “common modes” of two face appearance distributions. Recognition is then performed by finding the most probable mode, which is shown to be an eigenvalue problem. The effectiveness of the proposed method is demonstrated empirically on the *CamFace* dataset.

B.1 Introduction

In Section 7.1 we proposed a piece-wise linear representation of face appearance variation as suitable for exploiting the identified local manifold illumination invariant. Recognition by comparing nonlinear appearance manifolds was thus reduced to the problem of comparing linear patches, which was performed using canonical correlations. Here we address the problem of comparing linear patches in more detail and propose a probabilistic extension to the concept of canonical correlations.

B.1.1 Maximally probably mutual modes

In Chapter 7, linear patches used to piece-wise approximate an appearance manifold were represented by linear subspaces, much like in the Mutual Subspace Method (MSM) of Fukui and Yamaguchi [Fuk03]. The patches themselves, however, are finite in extent and are hence better characterized by probability density functions, such as Gaussian densities. This is the approach we adopt here, see Figure B.1.

Unlike in the case when dealing with subspaces, in general both of the compared distributions can generate *any* point in the D -dimensional embedding space. Hence, the concept of the most-correlated patterns (c.f. canonical correlations) from the two classes is not meaningful in this context. Instead, we are looking for a mode – i.e. a linear direction in the pattern space – along which both distributions corresponding to the two classes are most likely to “generate” observations.

We define the mutual probability $p_m(\mathbf{x})$ to be the product of two densities at \mathbf{x} :

$$p_m(\mathbf{x}) = p_1(\mathbf{x})p_2(\mathbf{x}). \quad (\text{B.1})$$

Generalizing this, the mutual probability $S_{\mathbf{v}}$ of an entire linear mode \mathbf{v} is then:

$$S_{\mathbf{v}} = \int_{-\infty}^{+\infty} p_1(x\mathbf{v})p_2(x\mathbf{v})dx. \quad (\text{B.2})$$

Substituting $\frac{1}{(2\pi)^{D/2}|\mathbf{C}_i|^{1/2}} \exp\left[-\frac{1}{2}\mathbf{x}^T\mathbf{C}_i^{-1}\mathbf{x}\right]$ for $p_i(\mathbf{x})$, we obtain:

$$S_{\mathbf{v}} = \int_{-\infty}^{+\infty} \frac{1}{(2\pi)^{D/2}|\mathbf{C}_1|^{1/2}} \exp\left[-\frac{1}{2}x\mathbf{v}^T\mathbf{C}_1^{-1}\mathbf{v}x\right] \frac{1}{(2\pi)^{D/2}|\mathbf{C}_2|^{1/2}} \exp\left[-\frac{1}{2}x\mathbf{v}^T\mathbf{C}_2^{-1}\mathbf{v}x\right] dx = \quad (\text{B.3})$$

$$\frac{1}{(2\pi)^D|\mathbf{C}_1\mathbf{C}_2|^{1/2}} \int_{-\infty}^{+\infty} \exp\left[-\frac{1}{2}x^2\mathbf{v}^T(\mathbf{C}_1^{-1} + \mathbf{C}_2^{-1})\mathbf{v}\right] dx. \quad (\text{B.4})$$

Noting that the integral is now over a 1D Gaussian distribution (up to a constant):

$$S_{\mathbf{v}} = \frac{1}{(2\pi)^D|\mathbf{C}_1\mathbf{C}_2|^{1/2}} (2\pi)^{1/2} [\mathbf{v}^T(\mathbf{C}_1^{-1} + \mathbf{C}_2^{-1})\mathbf{v}]^{-1/2} = \quad (\text{B.5})$$

$$(2\pi)^{1/2-D}|\mathbf{C}_1\mathbf{C}_2|^{-1/2} [\mathbf{v}^T(\mathbf{C}_1^{-1} + \mathbf{C}_2^{-1})\mathbf{v}]^{-1/2} \quad (\text{B.6})$$

The expression above favours directions in which both densities have large variances, i.e. in which Signal-to-Noise ratio is the highest, as one may intuitively expect, see Figure B.4.

The mode that maximizes the mutual probability $S_{\mathbf{v}}$ can be found by considering eigenvalue decomposition of $\mathbf{C}_1^{-1} + \mathbf{C}_2^{-1}$. Writing:

$$\mathbf{C}_1^{-1} + \mathbf{C}_2^{-1} = \sum_{i=1}^D \lambda_i \mathbf{u}_i \mathbf{u}_i^T, \quad (\text{B.7})$$



Figure B.2: *Conceptual drawing of the Maximally Probable Mutual Mode concept for 2D Gaussian densities.*



Figure B.3: *Conceptual drawing of the Maximally Probable Mutual Mode concept for 2D Gaussian densities. A range of illumination and pose changes is present.*

where $0 \leq \lambda_1 \leq \lambda_2 \leq \dots \leq \lambda_D$ and

$$\begin{aligned} \mathbf{u}_i \cdot \mathbf{u}_j &= 0, i \neq j \\ \mathbf{u}_i \cdot \mathbf{u}_i &= 1. \end{aligned} \tag{B.8}$$

and since $\{\mathbf{u}_i\}$ span \mathbb{R}^D :

$$\mathbf{v} = \sum_{i=1}^D \alpha_i \mathbf{u}_i, \tag{B.9}$$

it is then easy to show that the maximal value of (B.6) is:

$$\max_{\mathbf{v}} S_{\mathbf{v}} = (2\pi)^{1/2-D} |\mathbf{C}_1 \mathbf{C}_2|^{-1/2} \lambda_D^{-1/2}. \tag{B.10}$$

This defines the class similarity score ν . It is achieved for $\alpha_1, \dots, \alpha_{D-1} = 0$, $\alpha_D = 1$ or $\mathbf{v} = \mathbf{u}_D$, i.e. the direction of the eigenvector corresponding to the smallest eigenvalue of $\mathbf{C}_1^{-1} + \mathbf{C}_2^{-1}$. A visualization of the most probable mode between two face sets of Figure B.3 is shown in Figure B.4.

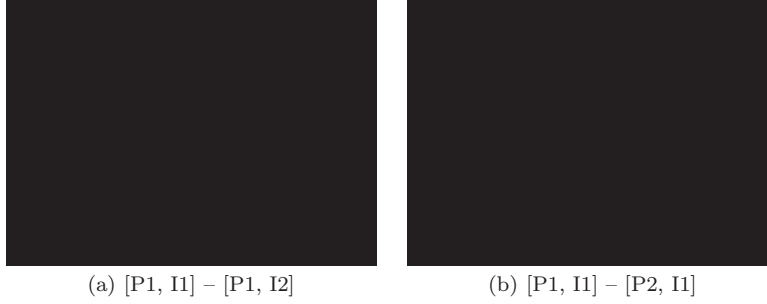


Figure B.4: *The maximally probable mutual mode, shown as an image, when two compared face sets belong to the (a) same and (b) different individuals (also see Figure B.3).*

B.1.2 Numerical and implementation issues

The expression for the similarity score $\nu = \max_{\mathbf{v}} S_{\mathbf{v}}$ in (B.10) involves the computation of $|\mathbf{C}_1 \mathbf{C}_2|^{-1/2}$. This is problematic as $\mathbf{C}_1 \mathbf{C}_2$ may be a singular, or a nearly singular, matrix (e.g. because the number of face images is much lower than the image space dimensionality D).

We solve this problem by assuming that the dimensionality of the principal linear subspaces corresponding to \mathbf{C}_1 and \mathbf{C}_2 is $M \ll D$, and that data is perturbed by isotropic Gaussian noise. If $\lambda_1^{(i)} \leq \lambda_2^{(i)} \leq \dots \leq \lambda_D^{(i)}$ are the eigenvalues of \mathbf{C}_i :

$$\forall j > M. \lambda_{D-j}^{(1)} = \lambda_{D-j}^{(2)}. \quad (\text{B.11})$$

Then, writing

$$|\mathbf{C}_i| = \prod_{j=1}^D \lambda_j^{(i)}, \quad (\text{B.12})$$

we get:

$$\nu = (2\pi)^{1/2-D} |\mathbf{C}_1 \mathbf{C}_2|^{-1/2} \lambda_D^{-1/2} = \quad (\text{B.13})$$

$$= \text{const} \times \left(\lambda_D \prod_{i=D-M+1}^D \lambda_i^{(1)} \lambda_i^{(2)} \right)^{-1/2}. \quad (\text{B.14})$$

Table B.1: *Recognition performance statistics (%)*.

Method		MPMM	MSM
Recognition rate	average	92.0	58.3
	std	7.8	24.3

Figure B.5: *Receiver-Operator Characteristic of MPMM*.

B.2 Experimental evaluation

We demonstrate the superiority of the Maximally Probable Mutual Modes to the Mutual Subspace Method [Fuk03] on the *CamFace* data set using the Manifold Principal Angles algorithm of Chapter 7. With the purpose of focusing on the underlying comparison of linear subspaces we omit the contribution of global appearance in the overall manifold similarity score by setting $\alpha = 0$ in (7.8).

A summary of the results is shown in Table B.1 with the Receiver-Operator Characteristics (ROC) curve for the MPMM method in Figure B.5. The proposed method achieved a significantly higher average recognition rate than the original MSM algorithm.

B.3 Summary and conclusions

We described a probabilistic extension to the concept of canonical correlations which has been widely used in the pattern recognition literature. The resulting method was demonstrated suitable for matching local appearance variations between face sets, exploiting a manifold illumination invariant.

Related publications

The following publications resulted from the work presented in this appendix:

- O. Arandjelović and R. Cipolla. Face set classification using maximally probable mutual modes. In *Proc. IEEE International Conference on Pattern Recognition (ICPR)*, pages 511–514, August 2006. [Ara06c]

C

The *CamFace* data set



Camille Pissarro. *Boulevard Montmartre*
1897, Oil on canvas, 74 x 92.8 cm
The State Hermitage Museum, Leningrad

Table C.1: *The proportion of the two genders in the CamFace dataset.*

Gender	Male	Female
Number	67	33

Figure C.1: *The distribution of people's ages across the CamFace data set.*

The University of Cambridge Face database (*CamFace* database) is a collection of video sequences of largely unconstrained, random head movement in different illumination conditions, acquired for the purpose of developing and evaluating face recognition algorithms. This appendix describes (i) the database and its acquisition, and (ii) a novel method for automatic extraction of face images from videos of head motion in a cluttered environment, suitable as a preprocessing step to recognition algorithms. The database and the preprocessing described are used extensively in this thesis.

C.1 Description

The *CamFace* data set is a database of face motion video sequences acquired in the Department of Engineering, University of Cambridge. It contains 100 individuals of varying age, ethnicity and gender, see Figure C.1 and Table C.1.

For each person in the database we collected 14 video sequences of the person in quasi-random motion. We used 7 different illumination configurations and acquired 2 sequences with each for a given person, see Figure C.2. The individuals were instructed to approach the camera and move freely, with the loosely enforced constraint of being able to see their eyes on the screen providing visual feedback in front of them, see Figure C.3 (a). Most sequences contain significant yaw and pitch variation, some translatory motion and negligible roll. Mild facial expression changes are present in some sequences (e.g. when the user was smiling or talking to the person supervising the acquisition), see Figure C.4.



(a)



(b)

Figure C.2: (a) Illuminations 1–7 from the CamFace data set. (b) Five different individuals in the illumination setting number 6. In spite of the same spatial arrangement of light sources, their effect on the appearance of faces changes significantly due to variations in people’s heights and the ad lib chosen position relative to the camera.



(a)



(b)

Figure C.3: (a) Visual feedback displayed to the user during data acquisition. (b) The pin-hole camera used to collect the CamFace data set.



Figure C.4: A 100 frame, 10 fps video sequence typical for the CamFace data set. The user positions himself ad lib and performs quasi-random head motion. Although instructed to keep head pose variations within the range in which the eyes are clearly visible, note that a significant number of poses does not meet this requirement.

Table C.2: An overview of CamFace data set statistics.

	Individuals	Illuminations	Sequences per illumination per person	Frames per second (fps)
Number	100	7	2	10

Acquisition hardware. Video sequences were acquired using a simple pin-hole camera with automatic gain control, mounted at 1.2m above the ground and pointing upwards at 30 degrees to the horizontal, see Figure C.3. Data was acquired at 10fps, giving 100 frames for each 10s sequence, in 320 by 240 pixel resolution, see Figure C.4 for an example and Table C.2 for a summary. On average, the face occupies an area of 60 by 60 pixels.

C.2 Automatic extraction of faces

We used the Viola-Jones cascaded detector [Vio04] in order to localize faces in cluttered images. Figure C.4 shows examples of input frames, Figure C.5 (b) an example of a correctly detected face and Figure C.6 all detected faces in a typical sequence. A histogram of the number of detections we get across the entire data set is shown in Figure C.7.

Rejection of false positives. The face detector achieves high true positive rates for our database. A larger problem is caused by false alarms, even a small number of which can affect the density estimates. We use a coarse skin colour classifier to reject many of the false detections. The classifier is based on 3-dimensional colour histograms built for two classes:

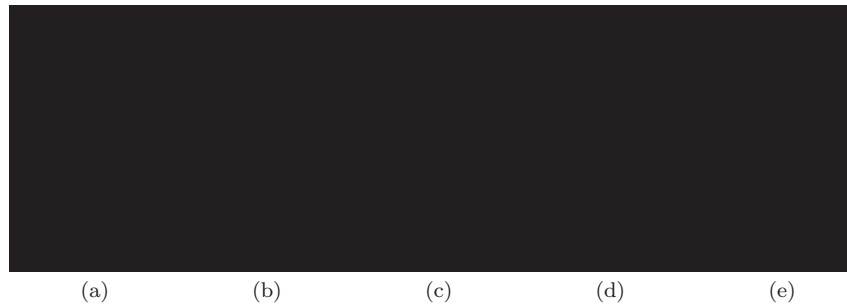


Figure C.5: *Illustration of the described preprocessing pipeline. (a) Original input frame with resolution of 320×240 pixels. (b) Face detection with average bounding box size of 75×75 pixels. (c) Resizing to the uniform scale of 40×40 pixels. (d) Background removal and feathering. (e) The final image after histogram equalization.*



Figure C.6: *Per-frame face detector output from a typical 100 frame, 10 fps video sequence (also see Figure C.4). The detector is robust to a rather large range of pose changes.*



Figure C.7: *A histogram of the number of face detections per sequence across the CamFace data set.*



Figure C.8: *Typical false face detections identified by our algorithm.*

skin and non-skin pixels [Jon99]. A pixel can then be classified by applying the likelihood ratio test. We apply this classifier and reject detections in which too few ($< 60\%$) or too many ($> 99\%$) pixels are labelled as skin. This step removes the vast majority of non-faces as well as faces with grossly incorrect scales – see Figure C.8 for examples of successfully removed false positives.

Background clutter removal. The bounding box of a detected face typically contains a portion of the background. The removal of the background is beneficial because it can contain significant clutter and also because of the danger of learning to discriminate based on the background, rather than face appearance. This is achieved by *set-specific* skin colour segmentation: Given a set of images from the same subject, we construct colour histograms for that subject’s face pixels and for the near-face background pixels in that set. Note that the classifier here is tuned for the given subject *and* the given background environment, and thus is more “refined” than the coarse classifier used to remove false positives. The face pixels are collected by taking the central portion of the few most symmetric images in the set (assumed to correspond to frontal face images); the background pixels are collected from the 10 pixel-wide strip around the face bounding box provided by the face detector,

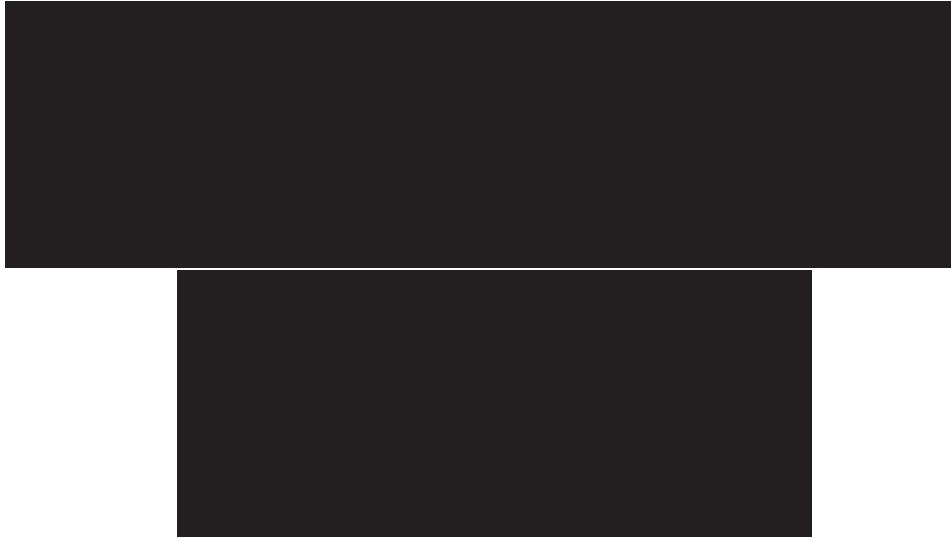


Figure C.9: *The response of our vertical symmetry-based measure of the “frontality” of a face, used to select the most reliable faces for extraction of background and foreground colour models. Also see Figures C.10 and C.11.*

see Figure C.10. After classifying each pixel within the bounding box independently, we smooth the result using a simple 2-pass algorithm that enforces the connectivity constraint on the face and boundary regions, see Figure C.5 (d). A summary of the cascade in its entirety is shown in Figure C.11.

Related publications

The following publications contain portions of work presented in this appendix:

- O. Arandjelović, G. Shakhnarovich, J. Fisher, R. Cipolla, and T. Darrell. Face recognition with image sets using manifold density divergence. In *Proc. IEEE Conference on Computer Vision and Pattern Recognition (CVPR)*, **1**:pages 581–588, June 2005. [Ara05b]
- O. Arandjelović and R. Cipolla. An information-theoretic approach to face recognition from face motion manifolds. *Image and Vision Computing (special issue on Face Processing in Video Sequences)*, **24**(6):pages 639–647, June 2006. [Ara06e]

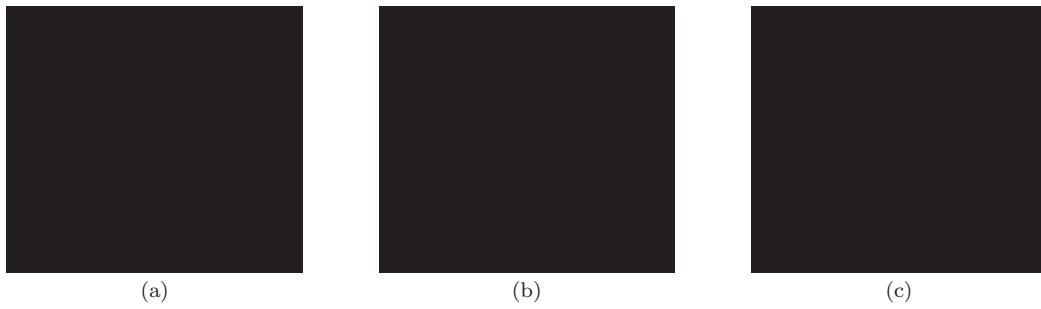


Figure C.10: (a) Areas used to sample face and background colours, and the corresponding (b) face and (b) background histograms in RGB space used for ML skin-colour detection. Larger blobs correspond to higher densities and are colour-coded.



Figure C.11: *A schematic representation of the face localization and normalization cascade.*

Bibliography

- []Abd98 H. Abdi, D. Valentin and B. E. Edelman. Eigenfeatures as intermediate level representations: The case for PCA models. *Brain and Behavioral Sciences*, **21**:pages 17–18, 1998.

- []Adi97 Y. Adini, Y. Moses and S. Ullman. Face recognition: The problem of compensating for changes in illumination direction. *IEEE Transactions on Pattern Analysis and Machine Intelligence (TPAMI)*, **19**(7):pages 721–732, 1997.

- []Aka91 S. Akamatsu, T. Sasaki, H. Fukumachi and Y. Suenaga. A robust face identification scheme - KL expansion of an invariant feature space. *Intelligent Robots and Computer Vision*, **1607**(10):pages 71–84, 1991.

- []Ara04a O. Arandjelović. Face recognition from face motion manifolds. First year Ph.D. report, University of Cambridge, Cambridge, UK, 2004.

- []Ara04b O. Arandjelović and R. Cipolla. Face recognition from face motion manifolds using robust kernel resistor-average distance. *In Proc. IEEE Workshop on Face Processing in Video Sequence*, **5**:page 88, 2004.

- []Ara04c O. Arandjelović and R. Cipolla. An illumination invariant face recognition system for access control using video. *In Proc. British Machine Vision Conference (BMVC)*, pages 537–546, 2004.
- []Ara05a O. Arandjelović and R. Cipolla. Incremental learning of temporally-coherent Gaussian mixture models. *In Proc. British Machine Vision Conference (BMVC)*, **2**:pages 759–768, 2005.
- []Ara05b O. Arandjelović, G. Shakhnarovich, J. Fisher, R. Cipolla and T. Darrell. Face recognition with image sets using manifold density divergence. *In Proc. IEEE Conference on Computer Vision and Pattern Recognition (CVPR)*, **1**:pages 581–588, 2005.
- []Ara05c O. Arandjelović and A. Zisserman. Automatic face recognition for film character retrieval in feature-length films. *In Proc. IEEE Conference on Computer Vision and Pattern Recognition (CVPR)*, **1**:pages 860–867, 2005.
- []Ara06a O. Arandjelović and R. Cipolla. Automatic cast listing in feature-length films with anisotropic manifold space. *In Proc. IEEE Conference on Computer Vision and Pattern Recognition (CVPR)*, **2**:pages 1513–1520, 2006.
- []Ara06b O. Arandjelović and R. Cipolla. Face recognition from video using the generic shape-illumination manifold. *In Proc. European Conference on Computer Vision (ECCV)*, **4**:pages 27–40, 2006.

- []Ara06c O. Arandjelović and R. Cipolla. Face set classification using maximally probable mutual modes. *In Proc. IAPR International Conference on Pattern Recognition (ICPR)*, pages 511–514, 2006.
- []Ara06d O. Arandjelović and R. Cipolla. Incremental learning of temporally-coherent Gaussian mixture models. *Society of Manufacturing Engineers (SME) Technical Papers*, **2**, 2006.
- []Ara06e O. Arandjelović and R. Cipolla. An information-theoretic approach to face recognition from face motion manifolds. *Image and Vision Computing (special issue on Face Processing in Video)*, **24**(6):pages 639–647, 2006.
- []Ara06f O. Arandjelović and R. Cipolla. A new look at filtering techniques for illumination invariance in automatic face recognition. *In Proc. IEEE International Conference on Automatic Face and Gesture Recognition (FG)*, pages 449–454, 2006.
- []Ara06g O. Arandjelović, R. Hammoud and R. Cipolla. On person authentication by fusing visual and thermal face biometrics. *In Proc. IEEE Conference on Advanced Video and Singal Based Surveillance (AVSS)*, pages 50–56, 2006.
- []Ara06h O. Arandjelović, R. I. Hammoud and R. Cipolla. Multi-sensory face biometric fusion (for personal identification). *In Proc. IEEE International Workshop on Object Tracking and Classification Beyond the Visible Spectrum (OTCBVS)*, pages 128–135, 2006.

- [Ara06i] O. Arandjelović and A. Zisserman. *Interactive Video: Algorithms and Technologies.*, chapter On Film Character Retrieval in Feature-Length Films., pages 89–103. Springer-Verlag, 2006. ISBN 978-3-540-33214-5.
- [Ara07a] O. Arandjelović and R. Cipolla. *Face recognition*, chapter Achieving illumination invariance using image filters., pages 15–30. I-Tech Education and Publishing, Vienna, Austria, 2007. ISBN 978-3-902613-03-5.
- [Ara07b] O. Arandjelović, R. I. Hammoud and R. Cipolla. *Face Biometrics for Personal Identification*, chapter Towards Person Authentication by Fusing Visual and Thermal Face Biometrics, pages 75–90. Springer-Verlag, 2007. ISBN 978-3-540-49344-0.
- [Ara09a] O. Arandjelović and R. Cipolla. A methodology for rapid illumination-invariant face recognition using image processing filters. *Computer Vision and Image Understanding (CVIU)*, **113**(2):pages 159–171, 2009.
- [Ara09b] O. Arandjelović and R. Cipolla. A pose-wise linear illumination manifold model for face recognition using video. *Computer Vision and Image Understanding (CVIU)*, **113**(1):pages 113–125, 2009.
- [Ara10] O. Arandjelović, R. I. Hammoud and R. Cipolla. Thermal and reflectance based personal identification methodology in challenging variable illuminations. *Pattern Recognition (PR)*, **43**(5):pages 1801–1813, 2010.

- [Ara13] O. Arandjelović and R. Cipolla. Achieving robust face recognition from video by combining a weak photometric model and a learnt generic face invariant. *Pattern Recognition (PR)*, **46**(1):pages 9–23, 2013.
- [Arc03] S. Arca, P. Campadelli and R. Lanzarotti. A face recognition system based on local feature analysis. *Lecture Notes in Computer Science (LNCS)*, **2688**:pages 182–189, 2003.
- [Bae02] A. D. Baek, B. A. Draper, J. R. Beveridge and K. She. PCA vs. ICA: A comparison on FERET data set. *In Proc. International Conference on Computer Vision, Pattern Recognition and Image Processing*, pages 824–827, 2002.
- [Bag96] J. Baglama, D. Calvetti and L. Reichel. Iterative methods for the computation of a few eigenvalues of a large symmetric matrix. *BIT*, **36**(3):pages 400–440, 1996.
- [Bai05] X. Bai, B. Yin, Q. Shi and Y. Sun. Face recognition based on supervised locally linear embedding method. *Journal of Information and Computational Science*, **2**(4):pages 641–646, 2005.
- [Bar98a] W. A. Barrett. A survey of face recognition algorithms and testing results. *Systems and Computers*, **1**:pages 301–305, 1998.
- [Bar98b] A. R. Barron, J. Rissanen and B. Yu. The minimum description length principle in coding and modeling. *IEEE Transactions on Information Theory*, **44**(6):pages 2743–2772, 1998.

- [Bar98c] M. S. Bartlett, H. M. Lades and T. J. Sejnowski. Independent component representations for face recognition. *In Proc. SPIE Symposium on Electronic Imaging: Science and Technology; Conference on Human Vision and Electronic Imaging III*, **3299**:pages 528–539, 1998.
- [Bar02] M. S. Bartlett, J. R. Movellan and T. J. Sejnowski. Face recognition by independent component analysis. *IEEE Transactions on Neural Networks (TNN)*, **13**(6):pages 1450–1464, 2002.
- [Bel96] P. N. Belhumeur and D. J. Kriegman. What is the set of images of an object under all possible lighting conditions? *In Proc. IEEE Conference on Computer Vision and Pattern Recognition (CVPR)*, pages 270–277, 1996.
- [Bel97] P. N. Belhumeur, J. P. Hespanha and D. J. Kriegman. Eigenfaces vs. fisherfaces: Recognition using class specific linear projection. *IEEE Transactions on Pattern Analysis and Machine Intelligence (TPAMI)*, **19**(7):pages 711–720, 1997.
- [Bel98] P. N. Belhumeur and D. J. Kriegman. What is the set of images of an object under all possible illumination conditions? *International Journal of Computer Vision (IJCV)*, **28**(3):pages 245–260, 1998.
- [Ber04] T. L. Berg, A. C. Berg, J. Edwards, M. Maire, R. White, Y. W. Teh, E. Learned-Miller and D. A. Forsyth. Names and faces in the news. *In Proc. IEEE Conference on Computer Vision and Pattern Recognition (CVPR)*, **2**:pages 848–854, 2004.

- [Bev01] J. R. Beveridge, K. She and B. A. Draper. A nonparametric statistical comparison of principal component and linear discriminant subspaces for face recognition. *In Proc. IEEE Conference on Computer Vision and Pattern Recognition (CVPR)*, **1**:pages 535–542, 2001.
- [Bic94] M. Bichsel and A. P. Pentland. Human face recognition and the face image set’s topology. *Computer Vision, Graphics and Image Processing: Image Understanding*, **59**(2):pages 254–261, 1994.
- [Big97] E. S. Bigun, J. Bigun, B. Duc and S. Fischer. Expert conciliation for multi-modal person authentication systems using Bayesian statistics. *In Proc. International Conference on Audio- and Video-based Biometric Person Authentication (AVBPA)*, pages 291–300, 1997.
- [Bis95] C. M. Bishop. *Neural Networks for Pattern Recognition*. Oxford University Press, Oxford, England, 1995.
- [Bjö73] Å. Björck and G. H. Golub. Numerical methods for computing angles between linear subspaces. *Mathematics of Computation*, **27**(123):pages 579–594, 1973.
- [Bla98] M. J. Black and A. D. Jepson. Recognizing facial expressions in image sequences using local parameterized models of image motion. *International Journal of Computer Vision (IJCV)*, **26**(1):pages 63–84, 1998.
- [Bla99] V. Blanz and T. Vetter. A morphable model for the synthesis of 3D faces. *In Proc. Conference on Computer Graphics (SIGGRAPH)*, pages 187–194, 1999.

- [Bla03] V. Blanz and T. Vetter. Face recognition based on fitting a 3D morphable model. *IEEE Transactions on Pattern Analysis and Machine Intelligence (TPAMI)*, **25**(9):pages 1063–1074, 2003.
- [Ble66] W. W. Bledsoe. Man-machine facial recognition. *Technical Report PRI:22*, Panoramic Research Inc., 1966.
- [Bol03] D. S. Bolme. Elastic bunch graph matching. Master’s thesis, Colorado State University, 2003.
- [Bos02] Boston Globe. Face recognition fails in Boston airport. July 2002.
- [Bri04] British Broadcasting Corporation. Doubts over passport face scans. *BBC News Online, UK Edition*, October 21, 2004. <http://news.bbc.co.uk/1/hi/uk/3762398.stm>.
- [Bro06] G. Brostow, M. Johnson, J. Shotton, O. Arandjelović, V. Kwatra and R. Cipolla. Semantic photo synthesis. *In Proc. Eurographics*, 2006.
- [Bru93] R. Brunelli and T. Poggio. Face recognition: Features vs. templates. *IEEE Transactions on Pattern Analysis and Machine Intelligence (TPAMI)*, **15**(10):pages 1042–1052, 1993.
- [Bru95a] R. Brunelli and D. Falavigna. Person recognition using multiple cues. *IEEE Transactions on Pattern Analysis and Machine Intelligence (TPAMI)*, **17**(10):pages 955–966, 1995.

- [Bru95b] R. Brunelli, D. Falavigna, T. Poggio and L. Stringa. Automatic person recognition by using acoustic and geometric features. *Machine Vision and Applications*, **8**(5):pages 317–325, 1995.
- [Bud04] P. Buddharaju, I. Pavlidis and I. Kakadiaris. Face recognition in the thermal infrared spectrum. *In Proc. IEEE International Workshop on Object Tracking and Classification Beyond the Visible Spectrum (OTCBVS)*, pages 133–138, 2004.
- [Bud05] P. Buddharaju, I. T. Pavlidis and P. Tsiamyrtzis. Physiology-based face recognition. *In Proc. IEEE Conference on Advanced Video and Singal Based Surveillance (AVSS)*, pages 354–359, 2005.
- [Buh94] J. M. Buhmann, M. Lades and F. Eeckmann. Illumination-invariant face recognition with a contrast sensitive silicon retina. *Advances in Neural Information Processing Systems (NIPS)*, pages 769–776, 1994.
- [Bur98] C. J. C. Burges. A tutorial on support vector machines for pattern recognition. *Data Mining and Knowledge Discovery*, **2**(2):pages 121–167, 1998.
- [BY98] S. Ben-Yacoub, Y. Abdeljaoued and E. Mayoraz. Fusion of face and speech data for person identity verification. *IEEE Transactions on Neural Networks (TNN)*, **10**(5):pages 1065–1075, 1998.
- [Cam00] T. E. de Campos, R. S. Feris and R. M. Cesar Junior. Eigenfaces versus eigeneyes: First steps toward performance assessment of representations for face recognition.

- In Proc. Mexican International Conference on Artificial Intelligence*, pages 193–201, 2000.
- []Can86 J. Canny. A computational approach to edge detection. *IEEE Transactions on Pattern Analysis and Machine Intelligence (TPAMI)*, **8**(6):pages 679–698, 1986.
- []Cap00 R. Cappelli, D. Maio and D. Maltoni. A computational approach to edge detection. *In Proc. International Workshop on Multiple Classifier Systems*, pages 351–361, 2000.
- []Cha65 H. Chan and W. W. Bledsoe. A man-machine facial recognition system: Some preliminary results. *Technical Report, Panoramic Research Inc.*, 1965.
- []Cha99 V. Chatzis, A. G. Bors and I. Pitas. Multimodal decision-level fusion for person authentication. *IEEE Transactions on Systems, Man, and Cybernetics, Part A: Systems and Humans*, **29**(6):pages 674–681, 1999.
- []Cha03 H. L. Chang, H. Seetzen, A. M. Burton and A. Chaudhuri. Face recognition is robust with incongruent image resolution: Relationship to security video images. *Journal of Experimental Psychology: Applied*, **9**:pages 33–41, 2003.
- []Che97 Z.-Y. Chen, M. Desai and X.-P. Zhang. Feedforward neural networks with multilevel hidden neurons for remotely sensed image classification. *In Proc. IEEE International Conference on Image Processing (ICIP)*, **2**:pages 653–656, 1997.
- []Che03 X. Chen, P. Flynn and K. Bowyer. Visible-light and infrared face recognition. *In Proc. Workshop on Multimodal User Authentication*, pages 48–55, 2003.

- [Che05] X. Chen, P. Flynn and K. Bowyer. IR and visible light face recognition. *Computer Vision and Image Understanding (CVIU)*, **99**(3):pages 332–358, 2005.
- [Coo95] T. Cootes, C. Taylor, D. Cooper and J. Graham. Active shape models - their training and application. *Computer Vision and Image Understanding*, **61**(1):pages 38–59, 1995.
- [Coo98] T. F. Cootes, G. J. Edwards and C. J. Taylor. Active appearance models. In *Proc. European Conference on Computer Vision (ECCV)*, **2**:pages 484–498, 1998.
- [Coo99a] T. Cootes and C. Taylor. A mixture model for representing shape. *Image and Vision Computing (IVC)*, **17**(8):pages 567–573, 1999.
- [Coo99b] T. F. Cootes, G. J. Edwards and C. J. Taylor. Comparing active shape models with active appearance models. In *Proc. British Machine Vision Conference (BMVC)*, pages 173–182, 1999.
- [Coo02] T. F. Cootes and P. Kittipanya-ngam. Comparing variations on the active appearance models. In *Proc. British Machine Vision Conference (BMVC)*, pages 837–846, 2002.
- [Cor90] T. H. Cormen, C. E. Leiserson and R. L. Rivest. *Introduction to Algorithms*. MIT Press, 1990. ISBN 978-0-262-03293-3.
- [Cov91] T. M. Cover and J. A. Thomas. *Elements of Information Theory*. Wiley, New York, 1991.

- [Cra99] I. Craw, N. P. Costen, T. Kato and S. Akamatsu. How should we represent faces for automatic recognition? *IEEE Transactions on Pattern Analysis and Machine Intelligence (TPAMI)*, **21**:pages 725–736, 1999.
- [Cri04] D. Cristinacce, C. T. F. and I. Scott. A multistage approach to facial feature detection. *In Proc. British Machine Vision Conference (BMVC)*, **1**:pages 277–286, 2004.
- [Dah01] J. Dahmen, D. Keysers, H. Ney and M. O. Güld. Statistical image object recognition using mixture densities. *Journal of Mathematical Imaging and Vision*, **14**(3):pages 285–296, 2001.
- [Dau80] J. Daugman. Two-dimensional spectral analysis of cortical receptive field profiles. *Vision Research*, **20**:pages 847–856, 1980.
- [Dau88] J. Daugman. Complete discrete 2-D Gabor transforms by neural networks for image analysis and compression. *IEEE Transactions on Acoustics, Speech and Signal Processing*, **36**:pages 1169–1179, 1988.
- [Dau92] J. Daugman. High confidence personal identification by rapid video analysis of iris texture. *In Proc. IEEE International Carnahan Conference on Security Technology*, pages 50–60, 1992.
- [DeC98] D. DeCarlos, D. Metaxas and M. Stone. An anthropometric face model using variational techniques. *In Proc. Conference on Computer Graphics (SIGGRAPH)*, pages 67–74, 1998.

- [Dem77] A. P. Dempster, N. M. Laird and D. B. Rubin. Maximum likelihood from incomplete data via the em algorithm. *Journal of the Royal Statistical Society*, **39**:pages 1–38, 1977.
- [deM93] D. deMers and G. Cottrell. Non-linear dimensionality reduction. *Advances in Neural Information Processing Systems*, **5**:pages 580–587, 1993.
- [DiP91] S. DiPaola. Extending the range of facial types. *The Journal of Visualization and Computer Animation*, **2**(4):pages 129–131, 1991.
- [Dor03] F. Dornaika and J. Ahlberg. Face model adaptation for tracking and active appearance model training. *In Proc. British Machine Vision Conference (BMVC)*, pages 559–568, 2003.
- [Dra03] B. A. Draper, K. Baek, M. S. Bartlett and J. R. Beveridge. Recognizing faces with PCA and ICA. *Computer Vision and Image Understanding*, **91**:pages 115–137, 2003.
- [Dud00] R. O. Duda, P. E. Hart and D. G. Stork. *Pattern Classification*. John Wiley & Sons, Inc., New York, 2nd edition, 2000. ISBN 0-471-05669-3.
- [Edw97] G. J. Edwards, C. J. Taylor and T. F. Cootes. Learning to identify and track faces in image sequences. *In Proc. British Machine Vision Conference (BMVC)*, pages 130–139, 1997.

- [Edw98a] G. Edwards, C. Taylor and T. Cootes. Interpreting face images using active appearance models. *In Proc. IEEE International Conference on Automatic Face and Gesture Recognition (FG)*, pages 300–305, 1998.
- [Edw98b] G. J. Edwards, T. F. Cootes and C. J. Taylor. Face recognition using active appearance models. *In Proc. European Conference on Computer Vision (ECCV)*, **2**:pages 581–595, 1998.
- [Edw99] G. Edwards, C. Taylor and T. Cootes. Improving identification performance by integrating evidence from sequences. *In Proc. IEEE Conference on Computer Vision and Pattern Recognition (CVPR)*, **1**:pages 486–491, 1999.
- [Eve04] M. Everingham and A. Zisserman. Automated person identification in video. *In Proc. IEEE International Conference on Image and Video Retrieval (CIVR)*, pages 289–298, 2004.
- [Fag06] N. Faggian, A. Paplinski and T.-J. Chin. Face recognition from video using active appearance model segmentation. *In Proc. IAPR International Conference on Pattern Recognition (ICPR)*, pages 287–290, 2006.
- [Fel05] P. F. Felzenszwalb and D. Huttenlocher. Pictorial structures for object recognition. *International Journal of Computer Vision (IJCV)*, **61**(1):pages 55–79, 2005.
- [Fer01] R. Feraud, O. Bernier, J.-E. Viallet and M. Collobert. A fast and accurate face detector based on neural networks. *International Journal of Computer Vision*

(*IJCV*), **23**(1):pages 42–53, 2001.

- []Fig02 M. Figueiredo and A. Jain. Unsupervised learning of finite mixture models. *IEEE Transactions on Pattern Analysis and Machine Intelligence (TPAMI)*, **24**(3):pages 381–396, 2002.
- []Fis81 M. A. Fischler and R. C. Bolles. Random sample consensus: A paradigm for model fitting with applications to image analysis and automated cartography. *IEEE Transactions on Computers*, **24**(6):pages 381–395, 1981.
- []Fit02 A. Fitzgibbon and A. Zisserman. On affine invariant clustering and automatic cast listing in movies. *In Proc. European Conference on Computer Vision (ECCV)*, pages 304–320, 2002.
- []Fre95 Y. Freund and R. E. Schapire. A decision-theoretic generalization of on-line learning and an application to boosting. *In Proc. European Conference on Computational Learning Theory*, pages 23–37, 1995.
- []Fri03 G. Friedrich and Y. Yeshurun. Seeing people in the dark: Face recognition in infrared images. *In Proc. British Machine Vision Conference (BMVC)*, pages 348–359, 2003.
- []Fuk98 K. Fukui and O. Yamaguchi. Facial feature point extraction method based on combination of shape extraction and pattern matching. *Systems and Computers in Japan*, **29**(6):pages 2170–2177, 1998.

- [Fuk03] K. Fukui and O. Yamaguchi. Face recognition using multi-viewpoint patterns for robot vision. *International Symposium of Robotics Research*, 2003.
- [Gab88] D. Gabor. Theory of communication. *Journal of the Institute of Electrical Engineers*, **93**(3):pages 429–457, 1888.
- [Gao02] Y. Gao and M. K. H. Leung. Face recognition using line edge map. *IEEE Transactions on Pattern Analysis and Machine Intelligence (TPAMI)*, **24**(6):pages 764–779, 2002.
- [Gar04] C. Garcia and M. Delakis. Convolutional face finder: A neural architecture for fast and robust face detection. *IEEE Transactions on Pattern Analysis and Machine Intelligence (TPAMI)*, **26**(11):pages 1408–1423, 2004.
- [Gav00] D. M. Gavrila. Pedestrian detection from a moving vehicle. *In Proc. European Conference on Computer Vision (ECCV)*, **2**:pages 37–49, 2000.
- [Geo98] A. S. Georghiades, D. J. Kriegman and P. N. Belhumeur. Illumination cones for recognition under variable lighting: Faces. *In Proc. IEEE Conference on Computer Vision and Pattern Recognition (CVPR)*, pages 52–58, 1998.
- [Git85] R. Gittins. *Canonical Analysis: A Review with Applications in Ecology*. Springer-Verlag, 1985.
- [Gol72] A. J. Goldstein, L. D. Harmon and A. B. Lesk. Man-machine interaction in human-face identification. *Bell System Technical Journal*, **51**(2):pages 399–427, 1972.

- [Gon92] R. Gonzalez and R. Woods. *Digital Image Processing*. Addison-Wesley Publishing Company, 1992.
- [Gor05] D. O. Gorodnichy. Associative neural networks as means for low-resolution video-based recognition. In *Proc. International Joint Conference on Neural Networks*, 2005.
- [Gra18] H. Gray. *Anatomy of the Human Body*. Philadelphia: Lea & Febiger, 20th edition, 1918.
- [Gra03] G. A. von Graevenitz. Biometrics in access control. *A&S International*, **50**:pages 102–104, 2003.
- [Gri92] G. R. Grimmett and D. R. Stirzaker. *Probability and Random Processes*. Clarendon Press, Oxford, 2nd edition, 1992.
- [Gro00] R. Gross, J. Yang and A. Waibel. Growing Gaussian mixture models for pose invariant face recognition. In *Proc. IAPR International Conference on Pattern Recognition (ICPR)*, **1**:pages 1088–1091, 2000.
- [Gro01] R. Gross, J. She and J. F. Cohn. Quo vadis face recognition. In *Proc. Workshop on Empirical Evaluation Methods in Computer Vision*, **1**:pages 119–132, 2001.
- [Gro04] R. Gross, I. Matthews and S. Baker. Generic vs. person specific active appearance models. In *Proc. British Machine Vision Conference (BMVC)*, pages 457–466, 2004.

- [Gro06] R. Gross, I. Matthews and S. Baker. Active appearance models with occlusion. *Image and Vision Computing (special issue on Face Processing in Video)*, **1**(6):pages 593–604, 2006.
- [Gya04] A. Gyaourova, G. Bebis and I. Pavlidis. Fusion of infrared and visible images for face recognition. *In Proc. European Conference on Computer Vision (ECCV)*, **4**:pages 456–468, 2004.
- [Hal00] P. Hall, D. Marshall and R. Martin. Merging and splitting eigenspace models. *IEEE Transactions on Pattern Analysis and Machine Intelligence (TPAMI)*, **22**(9):pages 1042–1048, 2000.
- [Hal04] P. M. Hall and Y. Hicks. A method to add Gaussian mixture models. *Tech. Report, University of Bath*, 2004.
- [Ham95] A. Hampapur, R. C. Jain and T. Weymouth. Production model based digital video segmentation. *Multimedia Tools and Applications*, **1**(1):pages 9–46, 1995.
- [Ham98a] G. Hamarneh, R. Abu-Gharbieh and T. Gustavsson. Active shape models - part I: Modeling shape and gray level variations. *In Proc. of the Swedish Symposium on Image Analysis*, pages 125–128, 1998.
- [Ham98b] G. Hamarneh, A.-G. R. and T. Gustavsson. Active shape models - part II: Image search and classification. *In Proc. of the Swedish Symposium on Image Analysis*, pages 129–132, 1998.

- [Hei00] B. Heisele, T. Poggio and M. Pontil. Face detection in still gray images. *A.I. Memo No. 1687, C.B.C.L. Paper No. 187 Center for Biological and Computational Learning, M.I.T.*, 2000.
- [Heo03a] J. Heo, B. Abidi, S. G. Kong and M. Abidi. Performance comparison of visual and thermal signatures for face recognition. *Biometric Consortium Conference*, 2003.
- [Heo03b] J. Heo, B. Abidi, J. Paik and M. A. Abidi. Face recognition: Evaluation report for FaceIt[®]. *In Proc. International Conference on Quality Control by Artificial Vision*, **5132**:pages 551–558, 2003.
- [Heo04] J. Heo, S. G. Kong, B. R. Abidi and M. A. Abidi. Fusion of visual and thermal signatures with eyeglass removal for robust face recognition. *In Proc. IEEE Conference on Computer Vision and Pattern Recognition Workshops (CVPRW)*, page 122, 2004.
- [Hic03] Y. A. Hicks, P. M. Hall and A. D. Marshall. A method to add Hidden Markov Models with application to learning articulated motion. *In Proc. British Machine Vision Conference (BMVC)*, pages 489–498, 2003.
- [Hin06] G. E. Hinton and R. R. Salakhutdinov. Reducing the dimensionality of data with neural networks. *Science*, **313**(5786):pages 504–507, 2006.
- [Hje01] E. Hjelmås. Face detection: A survey. *Computer Vision and Image Understanding*, (83):pages 236–274, 2001.

- [Hon04] P. S. Hong, L. M. Kaplan and M. J. T. Smith. A comparison of the octave-band directional filter bank and Gabor filters for texture classification. *In Proc. IEEE International Conference on Image Processing (ICIP)*, **3**:pages 1541–1544, 2004.
- [Hot36] H. Hotelling. Relations between two sets of variates. *Biometrika*, **28**:pages 321–372, 1936.
- [Hua05] C. Huang, H. Ai, Y. Li and S. Lao. Vector boosting for rotation invariant multi-view face detection. *In Proc. IEEE International Conference on Computer Vision (ICCV)*, **1**:pages 446–453, 2005.
- [Ide03] Identix Ltd. Faceit. <http://www.FaceIt.com/>, 2003.
- [Im03] S. K. Im, H. S. Choi and S. W. Kim. A direction-based vascular pattern extraction algorithm for hand vascular pattern verification. *ETRI Journal*, **25**(2):pages 101–108, 2003.
- [Int] International Biometric Group. <http://www.biometricgroup.com/>.
- [Isa98] M. Isard and A. Blake. CONDENSATION – conditional density propagation for visual tracking. *International Journal of Computer Vision (IJCV)*, **29**(1):pages 5–28, 1998.
- [Jai97] A. Jain, L. Hong, S. Pankanti and R. Bolle. An identity authentication system using fingerprints. *IEEE paper*, **85**(9):pages 1365–1388, 1997.

- [Jin00] Z. Jing and R. Mariani. Glasses detection and extraction by deformable contour. *In Proc. IAPR International Conference on Pattern Recognition (ICPR)*, **2**:pages 933–936, 2000.
- [Joh01] D. H. Johnson and S. Sinanović. Symmetrizing the Kullback-Leibler distance. *Technical report, Rice University*, 2001.
- [Joh06] M. Johnson, G. Brostow, J. Shotton, O. Arandjelović, V. Kwatra and R. Cipolla. Semantic photo synthesis. *Computer Graphics Forum*, **3**(25), 2006.
- [Jon87] J. P. Jones and L. A. Palmer. An evaluation of the two-dimensional Gabor filter model of simple receptive fields in cat striate cortex. *Neurophysiology*, **58**(6):pages 1233–1258, 1987.
- [Jon99] M. J. Jones and J. M. Rehg. Statistical color models with application to skin detection. In *In Proc. IEEE Conference on Computer Vision and Pattern Recognition (CVPR)*, pages 274–280. 1999.
- [Kai74] T. Kailath. A view of three decades of linear filtering theory. *IEEE Transactions on Information Theory*, **20**(2):pages 146–181, 1974.
- [Kan73] T. Kanade. Picture processing system by computer complex and recognition of human faces. Ph.D. thesis, Kyoto University, 1973.
- [Kan02] H. Kang, T. F. Cootes and C. J. Taylor. A comparison of face verification algorithms using appearance models. *In Proc. British Machine Vision Conference (BMVC)*, pages 477–486, 2002.

- []Kas87 M. Kass, A. Witkin and D. Terzopoulos. Snakes: Active contour models. *In Proc. IEEE International Conference on Computer Vision (ICCV)*, pages 259–268, 1987.
- []Kay72 Y. Kaya and K. Kobayashi. A basic study on human face recognition. *Frontiers of Pattern Recognition*, pages 265–289, 1972.
- []Kel70 M. Kelly. Visual identification of people by computer. *Technical Report AI-130, Stanford AI Project*, 1970.
- []Kim03 R. Kimmel, M. Elad, D. Shaked, R. Keshet and I. Sobel. A variational framework for retinex. *International Journal of Computer Vision (IJCV)*, **52**(1):pages 7–23, 2003.
- []Kim05a T. Kim, O. Arandjelović and R. Cipolla. Learning over sets using boosted manifold principal angles (BoMPA). *In Proc. British Machine Vision Conference (BMVC)*, **2**:pages 779–788, 2005.
- []Kim05b T.-K. Kim and J. V. Kittler. Locally linear discriminant analysis for multimodally distributed classes for face recognition with a single model image. *IEEE Transactions on Pattern Analysis and Machine Intelligence (TPAMI)*, **27**(3):pages 318–327, 2005.
- []Kim06 T.-K. Kim, J. V. Kittler and R. Cipolla. Learning discriminative canonical correlations for object recognition with image sets. *In Proc. European Conference on Computer Vision (ECCV)*, pages 251–262, 2006.

- []Kim07 T.-K. Kim, O. Arandjelović and R. Cipolla. Boosted manifold principal angles for image set-based recognition. *Pattern Recognition (PR)*, **40**(9):pages 2475–2484, 2007.
- []Kin97 I. King and L. Xu. Localized principal component analysis learning for face feature extraction and recognition. *In Proc. Workshop on 3D Computer Vision*, pages 124–128, 1997.
- []Kir90 M. Kirby and L. Sirovich. Application of the Karhunen-Love procedure for the characterization of human faces. *IEEE Transactions on Pattern Analysis and Machine Intelligence*, **12**(1):pages 103–108, 1990.
- []Kit98 J. Kittler, M. Hatef, R. Duin and J. Matas. On combining classifiers. *IEEE Transactions on Pattern Analysis and Machine Intelligence*, **20**(3):pages 226–239, 1998.
- []Koh77 T. Kohonen. *Associative Memory: A System Theoretical Approach*. Springer-Verlag, 1977.
- []Kon05 S. Kong, J. Heo, B. Abidi, J. Paik and M. Abidi. Recent advances in visual and infrared face recognition – a review. *Computer Vision and Image Understanding (CVIU)*, **97**(1):pages 103–135, 2005.
- []Kot98 C. Kotropoulos, A. Tefas and I. Pitas. Face authentication using variants of elastic graph matching based on mathematical morphology that incorporate local

- discriminant coefficients. *In Proc. IEEE Conference on Computer Vision and Pattern Recognition (CVPR)*, **1**:pages 814–819, 1998.
- [Kot00a] C. Kotropoulos, A. Tefas and I. Pitas. Frontal face authentication using discriminating grids with morphological feature vectors. *IEEE Transactions on Multimedia*, **2**(1):pages 14–26, 2000.
- [Kot00b] C. Kotropoulos, A. Tefas and I. Pitas. Frontal face authentication using morphological elastic graph matching. *IEEE Transactions on Image Processing (TIP)*, **9**(4):pages 555–560, 2000.
- [Kot00c] C. Kotropoulos, A. Tefas and I. Pitas. Morphological elastic graph matching applied to frontal face authentication under well-controlled and real conditions. *Pattern Recognition (PR)*, **33**(12):pages 31–43, 2000.
- [Krü00] V. Krüger, A. Happe and G. Sommer. Affine real-time face tracking using Gabor wavelet networks. *In Proc. IAPR International Conference on Pattern Recognition (ICPR)*, **1**:pages 127–130, 2000.
- [Krü02] V. Krüger and G. Sommer. Gabor wavelet networks for efficient head pose estimation. *Journal of the Optical Society of America*, **19**(6):pages 1112–1119, 2002.
- [Le06] D.-D. Le, S. Satoh and M. E. Houle. Face retrieval in broadcasting news video by fusing temporal and intensity information. *In Proc. IEEE International Conference on Image and Video Retrieval (CIVR)*, pages 391–400, 2006.

- []Lee96 S. Y. Lee, Y. K. Ham and R.-H. Park. Image representation using 2D Gabor wavelets. *IEEE Transactions on Pattern Analysis and Machine Intelligence (TPAMI)*, **18**(10):pages 1–13, 1996.
- []Lee03 K. Lee, J. Ho and D. Kriegman. Nine points of light: Acquiring subspaces for face recognition under variable lighting. *In Proc. IEEE Conference on Computer Vision and Pattern Recognition (CVPR)*, **1**:pages 519–526, 2003.
- []Lee04 J. Lee, B. Moghaddam, H. Pfister and R. Machiraju. Finding optimal views for 3D face shape modeling. *In Proc. IEEE International Conference on Automatic Face and Gesture Recognition (FG)*, pages 31–36, 2004.
- []Lee05 K. Lee and D. Kriegman. Online learning of probabilistic appearance manifolds for video-based recognition and tracking. *In Proc. IEEE Conference on Computer Vision and Pattern Recognition (CVPR)*, **1**:pages 852–859, 2005.
- []Li99 S. Li and J. Lu. Face recognition using the nearest feature line method. *IEEE Transactions on Neural Networks (TNN)*, **10**(2):pages 439–443, 1999.
- []Li02 S. Z. Li, L. Zhu, Z. Zhang, A. Blake, H. Zhang and H. Shum. Face recognition using the nearest feature line method. *In Proc. European Conference on Computer Vision (ECCV)*, **4**:pages 67–81, 2002.
- []Li04 S. Z. Li and A. K. Jain, editors. *Handbook of Face Recognition*. Springer-Verlag, 2004. ISBN 0-387-40595-x.

- [Li07] S. Z. Li, R. Chu, S. Liao and L. Zhang. Illumination invariant face recognition using near-infrared images. *IEEE Transactions on Pattern Analysis and Machine Intelligence (TPAMI)*, **29**(4):pages 627–639, 2007.
- [Lie98] R. Lienhart. Comparison of automatic shot boundary detection algorithms. *SPIE*, **3656**:pages 290–301, 1998.
- [Lin04] C. L. Lin and K. C. Fan. Biometric verification using thermal images of palm-dorsa vein patterns. *IEEE Transactions on Circuits and Systems for Video Technology*, **14**(2):pages 199–213, 2004.
- [Mac03] D. J. C. MacKay. *Information Theory, Inference and Learning Algorithms*. Cambridge University Press, Cambridge, 2003.
- [Mae04] K. Maeda, O. Yamaguchi and K. Fukui. Towards 3-dimensional pattern recognition. *Statistical Pattern Recognition*, **3138**:pages 1061–1068, 2004.
- [Mal98] E. C. Malthouse. Limitations of nonlinear PCA as performed with generic neural networks. *IEEE Transactions on Neural Networks (TNN)*, **9**(1):pages 165–173, 1998.
- [Mal03] D. Maloni, D. Maio, A. K. Jain and S. Prabhakar. *Handbook of Fingerprint Recognition*. Springer-Verlag, 2003.
- [Mar80] S. Marcelja. Mathematical description of the response of simple cortical cells.. *Journal of the American Optical Society*, **70**:pages 1297–1300, 1980.

- [Mar02] A. M. Martinez. Recognizing imprecisely localized, partially occluded and expression variant faces from a single sample per class. *IEEE Transactions on Pattern Analysis and Machine Intelligence (TPAMI)*, **24**(6):pages 748–763, 2002.
- [Mik01] K. Mikolajczyk, R. Choudhury and C. Schmid. Face detection in a video sequence – a temporal approach. *In Proc. IEEE Conference on Computer Vision and Pattern Recognition (CVPR)*, **2**:pages 96–101, 2001.
- [Mit05] T. Mita, T. Kaneko and O. Hori. Joint haar-like features for face detection. *In Proc. IEEE International Conference on Computer Vision (ICCV)*, **2**:pages 1619–1626, 2005.
- [Miu04] N. Miura, A. Nagasaka and T. Miyatake. Feature extraction of finger vein patterns based on iterative line tracking and its application to personal identification. *Systems and Computers in Japan*, **35**(7):pages 61–71, 2004.
- [Mog95] B. Moghaddam and A. Pentland. An automatic system for model-based coding of faces. *In Proc. IEEE Data Compression Conference*, pages 1–5, 1995.
- [Mog98] B. Moghaddam, W. Wahid and A. Pentland. Beyond eigenfaces - probabilistic matching for face recognition. *In Proc. IEEE International Conference on Automatic Face and Gesture Recognition (FG)*, pages 30–35, 1998.
- [Mog02] B. Moghaddam and A. Pentland. Principal manifolds and probabilistic subspaces for visual recognition. *IEEE Transactions on Pattern Analysis and Machine Intelligence (TPAMI)*, **24**(6):pages 780–788, 2002.

- [MT89] N. Magnenat-Thalmann, H. Minh, M. Angelis and D. Thalmann. Design, transformation and animation of human faces. *The Visual Computer*, **5**:pages 32–39, 1989.
- [Mun05] K. Muneeswaran, L. Ganesan, S. Arumugam and K. R. Soundar. Texture classification with combined rotation and scale invariant wavelet features. *Pattern Recognition (PR)*, **38**(10):pages 1495–1506, 2005.
- [Nat] National Center for State Courts (NCSC). Biometrics comparison chart. <http://ctl.ncsc.dni.us/biometweb/BMCompare.html>.
- [Nef96] A. V. Nefian. Statistical approaches to face recognition. Ph.D. thesis, Georgia Institute of Technology, 1996.
- [Nis06] M. Nishiyama and O. Yamaguchi. Face recognition using the classified appearance-based quotient image. In *Proc. IEEE International Conference on Automatic Face and Gesture Recognition (FG)*, pages 49–54, 2006.
- [Oja83] E. Oja. *Subspace Methods of Pattern Recognition*. Research Studies Press and J. Wiley, 1983.
- [Ots93] O. Otsuji and Y. Tonomura. Projection detecting filter for video cut detection. In *Proc. ACM International Conference on Multimedia*, pages 251–257, 1993.
- [Pan06] Y. Pang, Z. Liu and N. Yu. A new nonlinear feature extraction method for face recognition. *NeuroComputing*, **69**(7–9):pages 949–953, 2006.

- [Par75] F. I. Parke. A model for human faces that allows speech synchronized animation. *Computers and Graphics*, **1**:pages 3–4, 1975.
- [Par82] F. I. Parke. Parameterized models for facial animation. *IEEE Transactions on Computer Graphics and Applications*, **2**(9):pages 61–68., 1982.
- [Par96] F. I. Parke. *Computer Facial animation*. AKPeters, Wellesley, Massachusetts, 1996.
- [Pen94] A. Pentland, B. Moghaddam and T. Starner. View-based and modular eigenspaces for face recognition. *In Proc. IEEE Conference on Computer Vision and Pattern Recognition (CVPR)*, **84–91**, 1994.
- [Pen96] P. S. Penev and J. J. Atick. Local feature analysis: A general statistical theory for object representation. *Network: Computation in Neural Systems*, **7**(3):pages 477–500, 1996.
- [Phi95] P. J. Phillips and Y. Vardi. Data driven methods in face recognition. *In Proc. International Workshop on Automatic Face and Gesture Recognition*, pages 65–70, 1995.
- [Phi03] P. J. Phillips, P. Grother, R. J. Micheals, D. M. Blackburn, E. Tabassi and J. M. Bone. FRVT 2002: Overview and summary. *Technical report, National Institute of Justice*, 2003.

- []Pre92 W. H. Press, S. A. Teukolsky, W. T. Vetterling and B. P. Flannery. *Numerical Recipes in C : The Art of Scientific Computing*. Cambridge University Press, 2nd edition, 1992.
- []Pri01 J. R. Price and T. F. Gee. Towards robust face recognition from video. *In Proc. Applied Image Pattern Recognition Workshop, Analysis and Understanding of Time Varying Imagery*, pages 94–102, 2001.
- []Pro98 F. J. Prokoski and R. Riedel. *BIOMETRICS: Personal Identification in Networked Society*, chapter Infrared Identification of Faces and Body Parts. Kluwer Academic Publishers, 1998.
- []Pro00 F. Prokoski. History, current status, and future of infrared identification. *In Proc. IEEE International Workshop on Object Tracking and Classification Beyond the Visible Spectrum (OTCBVS)*, pages 5–14, 2000.
- []Pun04 C. M. Pun and M. C. Lee. Extraction of shift invariant wavelet features for classification of images with different sizes. *IEEE Transactions on Pattern Analysis and Machine Intelligence (TPAMI)*, **26**(9):pages 1228–1233, 2004.
- []Raj98 Y. Raja, S. J. McKenna and S. Gong. Segmentation and tracking using colour mixture models. *In Proc. Asian Conference on Computer Vision (ACCV)*, pages 607–614, 1998.
- []Ris78 J. Rissanen. Modeling by shortest data description. *Automatica*, **14**:pages 465–471, 1978.

- []Rom02 S. Romdhani, V. Blanz and T. Vetter. Face identification by fitting a 3D morphable model using linear shape and texture error functions. *In Proc. European Conference on Computer Vision (ECCV)*, pages 3–19, 2002.
- []Rom03a S. Romdhani, P. H. S. Torr, B. Schölkopf and A. Blake. Efficient face detection by a cascaded reduced support vector expansion. *Proceedings of the Royal Society, Series A*, **460**:pages 3283–3297, 2003.
- []Rom03b S. Romdhani and T. Vetter. Efficient, robust and accurate fitting of a 3D morphable model. *In Proc. IEEE International Conference on Computer Vision (ICCV)*, pages 59–66, 2003.
- []Ros03 A. Ross and A. K. Jain. Information fusion in biometrics. *Pattern Recognition Letters*, **24**(13):pages 2115–2125, 2003.
- []Ros05 A. Ross and R. Govindarajan. Feature level fusion using hand and face biometrics. *In Proc. SPIE Conference on Biometric Technology for Human Identification II*, **5779**:pages 196–204, 2005.
- []Ros06 A. Ross, K. Nandakumar and A. K. Jain. *Handbook of Multibiometrics*. Springer, New York, USA, 2006.
- []Row98 H. A. Rowley, S. Baluja and T. Kanade. Neural network-based face detection. *IEEE Transactions on Pattern Analysis and Machine Intelligence*, **20**(1):pages 23–38, 1998.

- [Row01] S. Roweis and L. K. Saul. Nonlinear dimensional reduction by locally linear embedding. *Science*, **290**, 2001.
- [RR01] T. Riklin-Raviv and A. Shashua. The quotient image: Class based re-rendering and recognition with varying illuminations. *IEEE Transactions on Pattern Analysis and Machine Intelligence (TPAMI)*, **23**(2):pages 219–139, 2001.
- [Saa06] Y. Saatci and C. Town. Cascaded classification of gender and facial expression using active appearance models. *In Proc. IEEE International Conference on Automatic Face and Gesture Recognition (FG)*, pages 393–400, 2006.
- [Sad04] M. T. Sadeghi and J. V. Kittler. Decision making in the lda space: Generalised gradient direction metric. *In Proc. IEEE International Conference on Automatic Face and Gesture Recognition (FG)*, pages 248–253, 2004.
- [Sal83] G. Salton and M. J. McGill. *Introduction to Modern Information Retrieval*. McGraw Hill, New York, 1983.
- [Sch78] G. Schwarz. Estimating the dimension of a model. *Annals of Statistics*, **6**:pages 461–464, 1978.
- [Sch99] B. Schölkopf, A. Smola and K. Müller. *Advances in Kernel Methods – SV Learning*, chapter Kernel principal component analysis., pages 327–352. MIT Press, Cambridge, MA, 1999.
- [Sch00] H. Schneiderman. A statistical approach to 3D object detection applied to faces and cars. Ph.D. thesis, Robotics Institute, Carnegie Mellon University, 2000.

- [Sch02] B. Schölkopf and A. Smola. *Learning with kernels*. MIT Press, Cambridge, MA, 2002.
- [ScI98] S. Sclaroff and J. Isidoro. Active blobs. *In Proc. IEEE International Conference on Computer Vision (ICCV)*, pages 1146–1153, 1998.
- [Sco03] I. M. Scott, T. F. Cootes and C. J. Taylor. Improving appearance model matching using local image structure. *In Proc. International Conference on Information Processing in Medical Imaging*, pages 258–269, 2003.
- [Sel02] A. Selinger and D. Socolinsky. Appearance-based facial recognition using visible and thermal imagery: A comparative study. Technical Report 02-01, Equinox Corporation, 2002.
- [Sen99] A. W. Senior. Face and feature finding for a face recognition system. *In Proc. International Conference on Audio and Video-based Biometric Person Authentication*, pages 154–159, 1999.
- [Sha02a] G. Shakhnarovich, J. W. Fisher and T. Darrel. Face recognition from long-term observations. *In Proc. European Conference on Computer Vision (ECCV)*, **3**:pages 851–868, 2002.
- [Sha02b] A. Shashua, A. Levin and S. Avidan. Manifold pursuit – a new approach to appearance based recognition. *In Proc. IAPR International Conference on Pattern Recognition (ICPR)*, pages 590–594, 2002.

- []Sha03 S. Shan, W. Gao, B. Cao and D. Zhao. Illumination normalization for robust face recognition against varying lighting conditions. *In Proc. IEEE International Workshop on Analysis and Modeling of Faces and Gestures*, pages 157–164, 2003.
- []Shi04 T. Shimooka and K. Shimizu. Artificial immune system for personal identification with finger vein pattern. *In Proc. International Conference on Knowledge-Based Intelligent Information and Engineering Systems*, pages 511–518, 2004.
- []Sim04 T. Sim and S. Zhang. Exploring face space. *In Proc. IEEE Workshop on Face Processing in Video*, page 84, 2004.
- []Sin04 S. Singha, A. Gyaourovaa, G. Bebisa and I. Pavlidis. Infrared and visible image fusion for face recognition. *In Proc. SPIE Defense and Security Symposium (Biometric Technology for Human Identification)*, 2004.
- []Sir87 L. Sirovich and M. Kirby. Low-dimensional procedure for the characterization of human faces. *Journal of Optical Society of America*, 4(3):pages 519–524, 1987.
- []Siv03 J. Sivic and A. Zisserman. Video Google: A text retrieval approach to object matching in videos. *In Proc. IEEE International Conference on Computer Vision (ICCV)*, 2:pages 1470–1477, 2003.
- []Siv05 J. Sivic, M. Everingham and A. Zisserman. Person spotting: video shot retrieval for face sets. *In Proc. IEEE International Conference on Image and Video Retrieval (CIVR)*, pages 226–236, 2005.

- [Sne89] G. W. Snedecor and W. G. Cochran. *Statistical Methods*. Iowa State University Press, Ames, Iowa, 8 edition, 1989.
- [Soc02] D. Socolinsky and A. Selinger. A comparative analysis of face recognition performance with visible and thermal infrared imagery. *In Proc. IAPR International Conference on Pattern Recognition (ICPR)*, **4**:pages 217–222, 2002.
- [Soc03] D. Socolinsky, A. Selinger and J. Neuheisel. Face recognition with visible and thermal infrared imagery. *Computer Vision and Image Understanding (CVIU)*, **91**(1–2):pages 72–114, 2003.
- [Soc04] D. A. Socolinsky and A. Selinger. Thermal face recognition over time. *In Proc. IAPR International Conference on Pattern Recognition (ICPR)*, **4**:pages 187–190, 2004.
- [Son05] M. Song and H. Wang. Highly efficient incremental estimation of Gaussian mixture models for online data stream clustering. *In Proc. SPIE Conference on Intelligent Computing: Theory And Applications*, 2005.
- [Sri03] A. Srivastana and X. Liu. Statistical hypothesis pruning for recognizing faces from infrared images. *Image and Vision Computing (IVC)*, **21**(7):pages 651–661, 2003.
- [Ste03] B. Stenger, A. Thayananthan, P. H. S. Torr and R. Cipolla. Filtering using a tree-based estimator. *In Proc. IEEE International Conference on Computer Vision (ICCV)*, **2**:pages 1063–1070, 2003.

- [Ste06] A. Stergiou, A. Pnevmatikakis and L. Polymenakos. EBGGM vs. subspace projection for face recognition. *In Proc. International Conference on Computer Vision Theory and Applications*, 2006.
- [Sun98] K. K. Sung and T. Poggio. Example-based learning for view-based human face detection. *IEEE Transactions on Pattern Analysis and Machine Intelligence (TPAMI)*, **20**(1):pages 39–51, 1998.
- [Sun05] Q.-S. Sun, P.-A. Heng, Z. Jin and D. Xia. Face recognition based on generalized canonical correlation analysis. *In Proc. IEEE International Conference on Intelligent Computing*, **2**:pages 958–967, 2005.
- [Tak98] B. Takács. Comparing face images using the modified Hausdorff distance. *Pattern Recognition (PR)*, **31**(12):pages 1873–1881, 1998.
- [Ten00] J. B. Tenenbaum, V. d. Silva and J. C. Langford. A global geometric framework for nonlinear dimensionality reduction. *Science*, **290**(5500):pages 2319–2323, 2000.
- [Tip99a] M. E. Tipping and C. M. Bishop. Mixtures of probabilistic principal component analyzers. *Neural Computation*, **11**(2):pages 443–482, 1999.
- [Tip99b] M. E. Tipping and C. M. Bishop. Probabilistic principal component analysis. *Journal of the Royal Statistical Society*, **61**(3):pages 611–622, 1999.

- [Tor00] L. Torres, L. Lorente and J. Vila. Automatic face recognition of video sequences using selfeigenfaces. *In Proc. IAPR International Symposium on Image/Video Communications over Fixed and Mobile Networks*, 2000.
- [Tos06] Toshiba. Facepass. www.toshiba.co.jp/mmlab/tech/w31e.htm, 2006.
- [Tru05] L. Trujillo, G. Olague, R. Hammoud and B. Hernandez. Automatic feature localization in thermal images for facial expression recognition. *In Proc. IEEE International Workshop on Object Tracking and Classification Beyond the Visible Spectrum (OTCBVS)*, **3**:page 14, 2005.
- [Tur91a] M. Turk and A. Pentland. Eigenfaces for recognition. *Journal of Cognitive Neuroscience*, **3**(1):pages 71–86, 1991.
- [Tur91b] M. Turk and A. Pentland. Face recognition using Eigenfaces. *In Proc. IAPR International Conference on Pattern Recognition (ICPR)*, pages 586–591, 1991.
- [Vas98] N. Vasconcelos and A. Lippman. Learning mixture hierarchies. *Advances in Neural Information Processing Systems (NIPS)*, pages 606–612, 1998.
- [Ver99] P. Verlinde and G. Cholet. Comparing decision fusion paradigms using k-NN based classifiers, decision trees and logistic regression in a multi-modal identity verification application. *In Proc. International Conference on Audio- and Video-Based Biometric Person Authentication (AVBPA)*, **5**(2):pages 188–193, 1999.
- [Ver03] J. J. Verbeek, N. Vlassis and B. Kröse. Efficient greedy learning of Gaussian mixture models. *Neural Computation*, **5**(2):pages 469–485, 2003.

- [Vet04] T. Vetter and S. Romdhani. Face modelling and recognition tutorial (part II). *Face Recognition Tutorial at IEEE European Conference on Computer Vision*, 2004.
- [Vio04] P. Viola and M. Jones. Robust real-time face detection. *International Journal of Computer Vision (IJCV)*, **57**(2):pages 137–154, 2004.
- [Vla99] N. Vlassis and A. Likas. A kurtosis-based dynamic approach to Gaussian mixture modeling. *IEEE Transactions on Systems, Man, and Cybernetics – Part A: Systems and Humans*, **24**(9):pages 393–399, 1999.
- [Wal99a] C. S. Wallace and D. L. Dowe. Minimum message length and kolmogorov complexity. *Computer Journal*, **42**(4):pages 270–283, 1999.
- [Wal99b] C. Wallraven, V. Blanz and T. Vetter. 3D reconstruction of faces - combining stereo with class-based knowledge. *In Proc. Deutsche Arbeitsgemeinschaft für Mustererkennung (DAGM) Symposium*, pages 405–412, 1999.
- [Wal01] T. C. Walker and R. K. Miller. *Health Care Business Market Research Handbook*. Norcross (GA): Richard K. Miller & Associates, Inc., 5th edition, 2001.
- [Wan03a] X. Wang and X. Tang. Unified subspace analysis for face recognition. *In Proc. IEEE International Conference on Computer Vision (ICCV)*, **1**:pages 679–686, 2003.

- [Wan03b] Y. Wang, T. Tan and A. K. Jain. Combining face and iris biometrics for identity verification. *In Proc. International Conference on Audio- and Video-based Biometric Person Authentication (AVBPA)*, pages 805–813, 2003.
- [Wan04a] H. Wang, S. Z. Li and Y. Wang. Face recognition under varying lighting conditions using self quotient image. *In Proc. IEEE International Conference on Automatic Face and Gesture Recognition (FG)*, pages 819–824, 2004.
- [Wan04b] J. Wang, E. Sung and R. Venkateswarlu. Registration of infrared and visible-spectrum imagery for face recognition. *In Proc. IEEE International Conference on Automatic Face and Gesture Recognition (FG)*, pages 638–644, 2004.
- [Wan04c] X. Wang and X. Tang. Random sampling LDA for face recognition. *In Proc. IEEE Conference on Computer Vision and Pattern Recognition (CVPR)*, pages 259–265, 2004.
- [Wan05] Y. Wang, Y. Jia, C. Hu and M. Turk. Non-negative matrix factorization framework for face recognition. *International Journal of Pattern Recognition and Artificial Intelligence*, **19**(4):pages 495–511, 2005.
- [Was89] A. I. Wasserman. *Neural Computing: Theory and Practice*. Van Nostrand Reinhold, New York, 1989.
- [Wen93] J. Weng, N. Ahuja and T. S. Huang. Learning recognition and segmentation of 3-D objects from 2-D images. *In Proc. IEEE International Conference on Computer Vision (ICCV)*, pages 121–128, 1993.

- [Wil94] R. P. Wildes, J. C. Asmuth, G. L. Green, S. C. Hsu, R. Kolczynski, J. Matey and S. McBride. A system for automated iris recognition. *In Proc. IEEE Workshop on Applications of Computer Vision*, pages 121–128, 1994.
- [Wil04] O. Williams, A. Blake and R. Cipolla. The variational ising classifier (VIC) algorithm for coherently contaminated data. *Advances in Neural Information Processing Systems (NIPS)*, pages 1497–1504, 2004.
- [Wis97] L. Wiskott, J.-M. Fellous, N. Krüger and C. von der Malsburg. Face recognition by elastic bunch graph matching. *IEEE Transactions on Pattern Analysis and Machine Intelligence*, **19**(7):pages 775–779, 1997.
- [Wis99a] L. Wiskott and J.-M. Fellous. *Intelligent Biometric Techniques in Fingerprint and Face Recognition*, chapter Face Recognition by Elastic Bunch Graph Matching., pages 355–396. 1999.
- [Wis99b] L. Wiskott, J.-M. Fellous, N. Krüger and C. von der Malsburg. Face recognition by elastic bunch graph matching. *Intelligent Biometric Techniques in Fingerprint and Face Recognition*, pages 355–396, 1999.
- [Wol01] L. B. Wolff, D. A. Socolinsky and C. K. Eveland. Quantitative measurement of illumination invariance for face recognition using thermal infrared imagery. *In Proc. IEEE International Workshop on Object Tracking and Classification Beyond the Visible Spectrum (OTCBVS)*, 2001.

- []Wol03 L. Wolf and A. Shashua. Learning over sets using kernel principal angles. *Journal of Machine Learning Research (JMLR)*, **4**(10):pages 913–931, 2003.
- []Wu04 B. Wu, H. Ai, C. Huang and S. Lao. Fast rotation invariant multi-view face detection based on real adaboost. *In Proc. IEEE International Conference on Automatic Face and Gesture Recognition (FG)*, pages 79–84, 2004.
- []Yam98 O. Yamaguchi, K. Fukui and K. Maeda. Face recognition using temporal image sequence. *In Proc. IEEE International Conference on Automatic Face and Gesture Recognition (FG)*, (10):pages 318–323, 1998.
- []Yam00 W. S. Yambor. Analysis of PCA-based and fisher discriminant-based image recognition algorithms. Master’s thesis, Colorado State University, 2000.
- []Yan00 M.-H. Yang, N. Ahuja and D. Kriegman. Face recognition using kernel eigenfaces. *In Proc. IEEE International Conference on Image Processing (ICIP)*, **1**:pages 37–40, 2000.
- []Yan02a M.-H. Yang. Face recognition using extended Isomap. *In Proc. IEEE International Conference on Image Processing (ICIP)*, **2**:pages 117–120, 2002.
- []Yan02b M.-H. Yang. Kernel eigenfaces vs. kernel fisherfaces: Face recognition using kernel methods. *In Proc. IEEE International Conference on Automatic Face and Gesture Recognition (FG)*, pages 215–220, 2002.

- [Yan02c] M.-H. Yang, N. Ahuja and D. Kriegman. A survey on face detection methods. *IEEE Transactions on Pattern Analysis and Machine Intelligence (TPAMI)*, **24**(1):pages 34–58, 2002.
- [Yan05] J. Yang, X. Gao, D. Zhang and J. Yang. Kernel ICA: An alternative formulation and its application to face recognition. *Pattern Recognition (PR)*, **38**(10):pages 1784–1787, 2005.
- [Yos99] S. Yoshizawa and K. Tanabe. Dual differential geometry associated with Kullback-Leibler information on the Gaussian distributions and its 2-parameter deformations. *Science University of Tokyo Journal of Mathematics*, **35**(1):pages 113–137, 1999.
- [Zab95] R. Zabih, J. Miller and K. Mai. A feature-based algorithm for detecting and classifying scene breaks. *In Proc. ACM International Conference on Multimedia*, pages 189–200, 1995.
- [Zha93] H. J. Zhang, A. Kankanhalli and S. Smoliar. Automatic partitioning of full-motion video. *Multimedia Systems*, **1**(1):pages 10–28, 1993.
- [Zha98] W. Zhao, R. Chellappa and A. Krishnaswamy. Discriminant analysis of principal components for face recognition. *In Proc. IEEE International Conference on Automatic Face and Gesture Recognition (FG)*, pages 336–341, 1998.
- [Zha00] W. Zhao, R. Chellappa, A. Rosenfeld and P. J. Phillips. Face recognition: A literature survey. *UMD CFAR Tech. Report CAR-TR-948*, 2000.

- [Zha04] W. Zhao, R. Chellappa, P. J. Phillips and A. Rosenfeld. Face recognition: A literature survey. *ACM Computing Surveys*, **35**(4):pages 399–458, 2004.
- [Zho03] S. Zhou, V. Krueger and R. Chellappa. Probabilistic recognition of human faces from video. *Computer Vision and Image Understanding*, **91**(1):pages 214–245, 2003.
- [Zwo01] M. Zwolinski and Z. R. Yang. Mutual information theory for adaptive mixture models. *IEEE Transactions on Pattern Analysis and Machine Intelligence (TPAMI)*, **23**(4):pages 396–403, 2001.